

**Bioinspired Light-Harvesting
Zinc Chlorin Rod Aggregates
Powered by Peripheral Chromophores**

Dissertation zur Erlangung des
naturwissenschaftlichen Doktorgrades
der Julius-Maximilians-Universität Würzburg

vorgelegt von
Cornelia Röger
aus Schwäbisch Hall

Würzburg 2007

Eingereicht am: 21.12.2007

bei der Fakultät für Chemie und Pharmazie

1. Gutachter: Prof. Dr. Frank Würthner

2. Gutachter: Prof. Dr. Alfred Holzwarth
der Dissertation

1. Prüfer: Prof. Dr. Frank Würthner

2. Prüfer: Prof. Dr. Alfred Holzwarth

3. Prüfer: Prof. Dr. Volker Engel
des Öffentlichen Promotionskolloquiums

Tag des Öffentlichen Promotionskolloquiums: 22. 02.2008

Doktorurkunde ausgehändigt am: _____

für meine Eltern

Acknowledgement / Danksagung

Meinem Doktorvater, Herrn Prof. Dr. Frank Würthner, danke ich zunächst für das Überlassen spannender Forschungsgebiete, seine fundierte und zuverlässige wissenschaftliche Betreuung sowie die exzellenten Arbeitsbedingungen in seinem Arbeitskreis. Weiterhin bin ich ihm sehr dankbar für all die mir zugebilligten Freiräume und das Vertrauen, das er mir beim Bearbeiten der Projekte entgegengebracht hat. Darüber hinaus habe ich mich sehr über seine Unterstützung bei der Beantragung eines Promotionsstipendiums und viele Möglichkeiten zum Besuch von Fachkonferenzen, Workshops und des BASF-Sommerkurses gefreut.

Bei Herrn Prof. Dr. Alfred Holzwarth, Frau Yuliya Miloslavina und Herrn Dr. Marc Müller möchte ich mich für die gute Zusammenarbeit im Rahmen einer Kooperation und zahlreiche wissenschaftliche Diskussionen bedanken, die am Max-Planck-Institut für Bioanorganische Chemie in Mülheim an der Ruhr stattfinden konnten.

Der Degussa Stiftung danke ich für die Gewährung eines Promotionsstipendiums.

Herrn Dr. Chantu Saha-Möller danke ich für seine exzellente und zuverlässige Überarbeitung von Manuskripten, Postern und Teilen der vorliegenden Doktorarbeit.

Ein großes Dankeschön gilt Herrn Prof. Dr. Stefan Matile von der Universität Genf für eine fruchtbare Kooperation.

Meiner wissenschaftlichen „Mitreiterin“ auf dem Gebiet der Chlorine, Frau Dr. Valerie Huber, danke ich für ihre Diskussionsbereitschaft und die stets ausgezeichnete Zusammenarbeit.

Mein Dank gilt weiterhin Frau Dipl.-Chem. Doris Brunner für ihre motivierte und kompetente Mitarbeit während eines Forschungspraktikums sowie für die schöne gemeinsame Zeit im Labor während ihrer Diplomarbeit.

Herrn Viktor Weber danke ich für seine zuverlässige und tatkräftige Unterstützung während seiner Ausbildungszeit als Chemielaborant.

Bei Frau Dr. Marina Knoll möchte ich mich für die Aufnahme von rasterkraftmikroskopischen Abbildungen sowie ihre Diskussionsbereitschaft bedanken.

Mein Dank gilt weiterhin Frau Ana-Maria Krause für Durchführung und Beratung bei cyclovoltammetrischen Messungen.

Bei Frau Christiana Toussaint bedanke ich mich für ihre schnelle und kompetente Hilfe bei Formalitäten und organisatorischen Angelegenheiten.

Mehrere große Dankeschöns gehen an Herrn Dipl.-Chem. Rüdiger Schmidt für seine rege Diskussionsbereitschaft und das tolle Teamwork im Labor.

Herrn Dipl.-Chem. Andreas Lohr sei für das Erstellen der Graphiken von Chlorin-Aggregaten gedankt.

Herrn Joachim Bialas danke ich für Unterstützung und Tipps im Laboralltag.

Bei Herrn Dr. Matthias Grüne und Frau Elfriede Ruckdeschel bedanke ich mich für die Aufnahme von COSY NMR-Spektren, bei Herrn Dr. Michael Büchner und Herrn Fritz Dadrich für die Anfertigung von Massenspektren und bei Frau Lieselotte Michels für die Durchführung der Elementaranalysen.

Herrn Dipl.-Ing. Bernd Brunner sei für die kompetente Hilfe bei allen Computerfragen gedankt.

All meinen ehemaligen Kollegen aus dem Arbeitskreis Würthner danke ich für ihre Unterstützung in vielfältigen Belangen und eine freundschaftliche Atmosphäre.

Ich bedanke mich bei meiner Familie sowie bei Rüdiger, Marina, Fabian, Kristina, Christian, Stefanie, Thomas, Valerie, Andreas, Daniel, Johann, Doris, Suhrit, Fritz, Sven, Petra, Alina, Michael und Ingrid dafür, dass auch meine Freizeit während der Promotionszeit sehr schön war.

Thorsten danke ich für seine Geduld und dafür, dass ich bei ihm immer Rückhalt gefunden habe.

Meinen Eltern, denen diese Arbeit gewidmet ist, gebührt großer Dank für all ihre Unterstützung.

List of Abbreviations

AFM	atomic force microscopy
BChl	bacteriochlorophyll
BOC	<i>tert</i> -butyloxycarbonyl
CD	circular dichroism
COSY	correlation spectroscopy
DAS	decay associated spectra
DCC	dicyclohexylcarbodiimide
DCM	4-dicyanomethylene-2-methyl-6- <i>p</i> -dimethylamino-styryl-4H-pyran
DMAP	4-(dimethylamino)pyridine
DPTS	4-(dimethylamino)pyridinium 4-toluenesulfonate
EI	electron impact ionization
eq	equation
ESI	electrospray ionization
FAB	fast atom bombardment
FRET	fluorescence resonance energy transfer
HATU	O-(7-azabenzotriazole-1-yl)- <i>N,N,N',N'</i> -tetramethyluronium hexafluorophosphate
HOMO	highest occupied molecular orbital
HOPG	highly ordered pyrolytic graphite
HPLC	high performance liquid chromatography
HR	high resolution
LH	light-harvesting
LUMO	lowest unoccupied molecular orbital
MALDI	matrix-assisted laser desorption injection
Me	methyl
NDI	naphthalene diimide
NMR	nuclear magnetic resonance
RC	reaction center
RP	reversed phase
rt	room temperature
SPT	single photon timing
TEM	transmission electron microscopy
THF	tetrahydrofuran
UV	ultraviolet
vis	visible
ZnChl	zinc chlorin

Table of Contents

Chapter 1: Aim of this Thesis	1
Chapter 2: State of Knowledge	5
2.1 Structural and Functional Features of Light-Harvesting Systems	5
2.1.1 <i>Requirements to Light-Harvesting Systems</i>	5
2.1.2 <i>Natural Antenna Chromophores</i>	7
2.1.3 <i>Energy Transport Mechanisms</i>	16
2.2 Structure and Function of Bacterial Antennae	24
2.2.1 <i>Purple Bacteria</i>	24
2.2.2 <i>Chlorosomes</i>	28
2.3 Circular Artificial Supramolecular Light-Harvesting Systems	38
2.3.1 <i>Zinc Chlorin Antennae</i>	38
2.3.2 <i>Porphyrin Assemblies</i>	43
2.3.3 <i>Cyanin Assemblies</i>	52
Chapter 3: Results and Discussion	55
3.1 Synthesis	55
3.1.1 <i>Synthesis of Chlorin and Naphthalene Diimide Precursors</i>	55
3.1.2 <i>Synthesis of Zinc Chlorin-Naphthalene Diimide Dyads</i>	58
3.1.3 <i>Synthesis of a ZnChl-NDI_{NN}-NDI_{NO} Triad</i>	62
3.2 Solvent-Dependent Self-Organization	65
3.2.1 <i>UV-vis Absorption and Steady State Emission Properties of Reference Chromophores</i>	65
3.2.2 <i>UV-vis Absorption and Steady State Emission Properties of Zinc Chlorin-Naphthalene Diimide Dyads</i>	68
3.2.3 <i>Temperature-Dependent UV-vis Absorption and CD Spectroscopy of Zinc Chlorin-Naphthalene Diimide Dyads</i>	71
3.2.4 <i>UV-vis Absorption, Steady State Emission, and CD Properties of the ZnChl-NDI_{NN}-NDI_{NO} Triad 3</i>	75

3.2.5	<i>AFM Studies</i>	77
3.3	Investigation of Light-Harvesting Properties	80
3.3.1	<i>Time-Resolved Fluorescence Spectroscopy Measurements – Instrumentation and Analysis</i>	80
3.3.2	<i>Excited State Decay of Zinc Chlorins and Naphthalene Diimides</i>	83
3.3.3	<i>Kinetics of Energy Transfer Processes in Dyad and Triad Monomers</i>	84
3.3.4	<i>Kinetics of Energy Transfer Processes in Self-Assembled Dyads and Triad</i>	90
3.3.5	<i>Calculation of Energy Transfer Efficiencies</i>	97
3.3.6	<i>Calculation of Light-Harvesting Efficiencies</i>	97
Chapter 4:	Summary	99
Chapter 5:	Zusammenfassung	102
Chapter 6:	Experimental Section	106
6.1	Materials and Methods	106
6.2	Synthesis and Analytical Data of Intermediates and Target Molecules	110
References		136
Curriculum Vitae		146
List of Publications		147

Chapter 1: Aim of this Thesis

Sunlight is the primary energy source for all life on Earth and it provides us with huge energy amounts. More precisely, solar radiation represents 99.978% of the total energy flux entering the Earth's atmosphere contributing a power of 1.74×10^{17} W.¹ For comparison, the average power consumption on Earth in 2004 equalled 1.5×10^{13} W.² Photosynthetic organisms have found a way to make an infinite energy source available. In the course of evolution, photosynthetic species have generated highly potential light-harvesting (LH) systems to absorb the solar irradiation efficiently and to fuel this excitation energy over often huge distances into the reaction centers (RCs), where the conversion into chemical energy takes place.³⁻¹⁰

In most natural photosynthetic light-harvesting (LH) complexes sunlight is not only collected by chlorophyll or bacteriochlorophyll (BChl) chromophores, which are powerful absorbers in the violet, blue, and red wavelength region, but they are supported by accessory LH dyes such as phycobiliproteins and carotenoids to make use of the intensive green region of the solar spectrum. In the majority of LH complexes, all chromophores are embedded in a rigid protein scaffold, providing a sophisticated geometrical arrangement in order to guarantee efficient excitation energy transport within the LH system. As an exception, the LH complexes of green sulfur bacteria and of the green filamentous bacterium *Chloroflexus aurantiacus*, the so-called chlorosomes, do not contain such a variety of LH chromophores, since they miss a protein matrix to keep a diverse dye assembly together.^{11,12} Chlorosomes show flattened sac-like structures, which mainly include, besides a few carotenoids, cylindrical self-assemblies of BChl *c*, *d*, and *e*, whose defined arrangement is governed by intermolecular forces between the BChl molecules only. However, chlorosomes take an advantage of their spartan constitution, since the tight packing of BChls within the self-assembled rods provides a high chromophore density and affords a large cross-section for red/NIR light absorption. Therefore, it is not astonishing that the best low-sunlight-adapted phototroph known to date is a population of green sulfur bacteria, inhabiting the Black Sea at depths of 100 m.¹³

In recent years it has been demonstrated that the self-assembly process of BChl *c*, *d*, and *e* into rod-like structures cannot only be achieved *in vivo* but as well *in vitro* by choosing nonpolar, aprotic solvents.^{11,12} Zinc chlorins (ZnChl), which are more easily available than BChl and which can be prepared by stepwise derivatization of Chl *a*, serve as appropriate model compounds for BChl by performing an analogous self-assembly process into rod-type aggregates.¹¹ BChl and ZnChl self-assemblies drew especially high attention, since they show extremely fast exciton mobilities,¹⁴ which recommend these aggregates for a possible application in supramolecular photonic and electronic devices. A first step towards the preparation of well-defined nanorods for the development of materials based on artificial ZnChl LH systems was gained by functionalization of ZnChl monomers with solubilizing alkyl chains, leading to well soluble ZnChl self-assemblies, which can be deposited on graphite surfaces.¹⁵ However, for an application of such supramolecular systems for LH and photovoltaics not only well-defined nanostructures but also optimal utilization of the terrestrial solar spectrum is required.¹⁶⁻²⁰ Since ZnChl aggregates are not well-suited for absorption of the dominant green-yellow-orange region of solar spectral irradiance due to the above mentioned lack of appropriate LH dyes (Figure 1), the aim of this thesis was to design multi-chromophoric LH systems consisting of the cylindrical ZnChl antenna and more, green light-absorbing LH chromophores in the periphery of the nanorod (Figure 2).

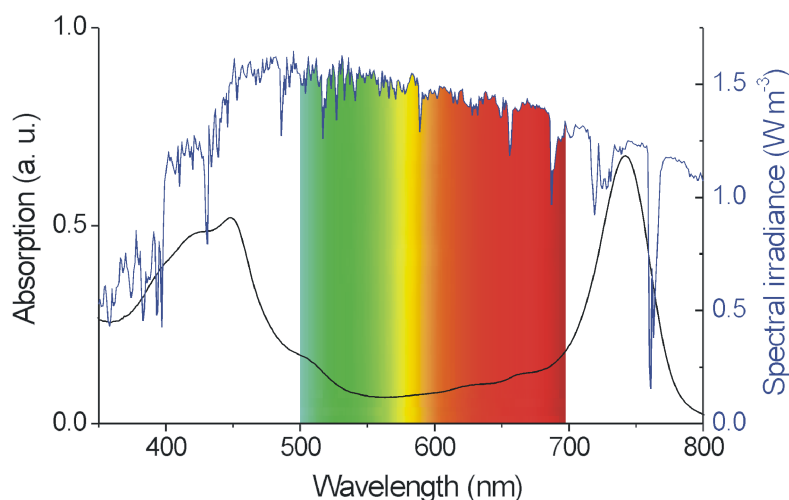


Figure 1. Absorption spectrum of BChl *c* *in vitro* aggregates in *n*-hexane/ THF (1%) (black line) and the ASTM G173-03 reference spectrum for the terrestrial solar irradiance (blue line). In the colored wavelength region (~500-700 nm) the absorption of BChl *c* aggregates is quite low. Data for preparation of the spectral irradiance graph were taken from <http://rredc.nrel.gov/solar/spectra/am1.5/>.

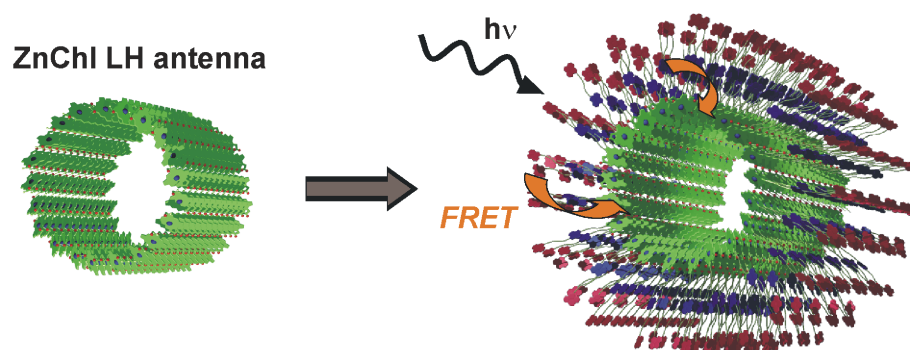


Figure 2. Concept for improvement of the natural BChl c LH antennae by means of additional peripheral chromophores that harvest the green fraction of solar light.

As additional LH chromophores 2,6-core-disubstituted naphthalene diimides (NDIs) were chosen in this thesis, since the absorption maxima of these strong fluorophores can be easily tuned within the whole range of the “green gap” by variation of the electron-donating character of the core-substituents.²¹⁻²³ For instance, the functionalization of NDI by one alkoxy and one alkylamino core-substituent results in a magenta colored dye, while two alkylamino substituents provide blue color. As an advantage over the natural green light absorbing antenna pigments, namely phycobiliproteins and carotenoids, NDIs show excellent photostability. Thus, in this work different NDI chromophores have been covalently attached to ZnChl monomers in order to achieve self-assembling multichromophoric antenna building blocks (Chart 1).

Chapter 2 gives a short overview on common structural and functional features of supramolecular LH complexes. Furthermore, the highly efficient antennae of the most investigated bacterial species are introduced. Since the latter systems owe their good performance not least to their circular geometry, various approaches to artificial cyclic LH systems are reviewed.

In *Chapter 3.1* the syntheses of NDI-functionalized ZnChl dyads **1,2** and triad **3** are presented (Chart 1). The electronic properties and the aggregation behavior of compounds **1-3** in dependence on the different peripheral NDI substituents have been examined by UV-vis absorption, circular dichroism (CD), and steady state fluorescence spectroscopy as well as atomic force microscopy (AFM) (*Chapter 3.2*). LH properties of **1-3** have been studied by investigation of energy transfer processes from peripheral NDIs to the ZnChl rod antenna using time-resolved fluorescence

spectroscopy (*Chapter 3.3*). The influence of the additional NDI chromophores on the LH efficiencies of **1-3** aggregates has been calculated.

The thesis concludes with summaries in English (*Chapter 4*) and German (*Chapter 5*), followed by the Experimental Section (*Chapter 6*).

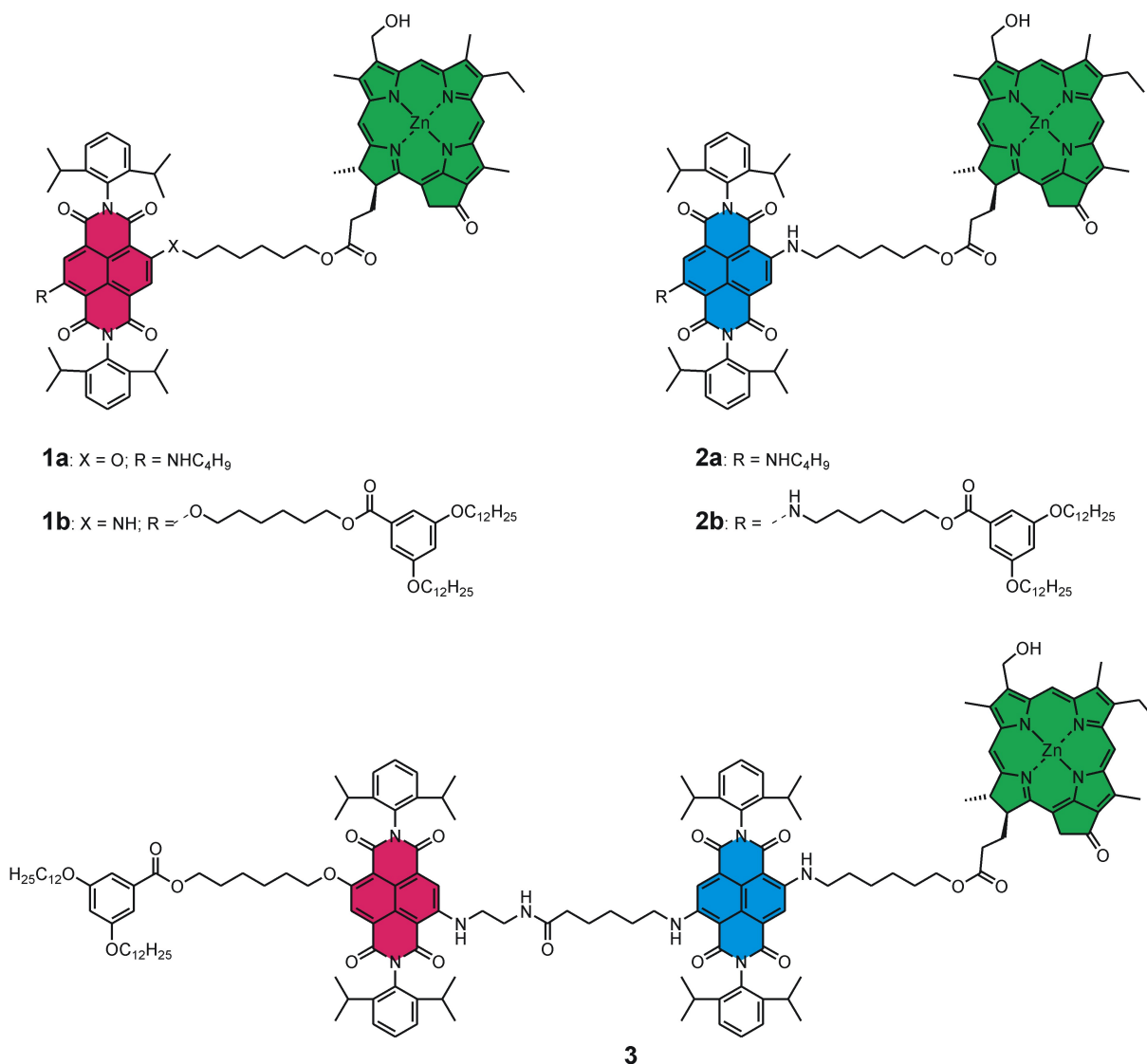


Chart 1. Chemical structures of dyads ZnChI-NDI_{NO} **1** and ZnChI-NDI_{NN} **2** and triad ZnChI-NDI_{NN}-NDI_{NO} **3**.

Chapter 2: State of Knowledge

2.1 Structural and Functional Features of Light-Harvesting Systems

2.1.1 Requirements to Light-Harvesting Systems

Although very different types of LH antennae have been developed by the various photosynthetic organisms in order to adapt to the particular lighting conditions, all LH systems have a few fundamental characteristics in common. First of all, a LH system consists of a **large amount of LH chromophores** to ensure the efficient energy supply for the more demanding electron transfer steps in the reaction centers and the secondary processes like reduction of CO₂ to carbohydrates.²⁴ At a lack of light the number of antenna pigments is increased, while under very bright conditions it is decreased. Also the **density of chromophores** can strongly differ for the diverse antennae to adjust the system to the respective light intensity.

Furthermore, LH systems provide a **huge variety of antenna chromophores** in order to absorb efficiently at various wavelengths of the solar spectrum. Figure 3 shows the solar irradiance spectra for extraterrestrial (black line) and terrestrial conditions (blue line) at an incidence angle of 37°. In both cases, the maximum intensity is observed for the green region of the solar spectrum. As light passes through the atmosphere, some wavelengths are absorbed by gases such as ozone and oxygen with specific absorption bands. Further, the terrestrial irradiance shows a remarkable gap in the range of 900-1000 nm, which equals the region of the first intensive absorption band of water.

In the various habitats of photosynthetic organisms, the solar irradiance spectrum differs drastically, depending on the environment and on the season.²⁵ For example, in pure water the solar spectrum is narrowed down and the intensity decreases due to reflection at the water surface, but its maximum intensity is still found in the blue-

green region. A large concentration of suspended sediments enlarges the degree of scattering and therefore additionally decreases the light intensity. Since Rayleigh scattering rises proportionally to the fourth power of frequency, the spectral maximum of solar irradiance in turbid water is bathochromically shifted to the red or even the infrared region. Furthermore, the radiation intensities in water can be reduced strongly by the cover of vegetation on top of the surface. Especially those photosynthetic species, which always have to cope with very low lighting conditions, were provoked to generate highly efficient LH antennae. Some organisms are even able to vary their antenna constellation in dependence on their particular location.²⁶

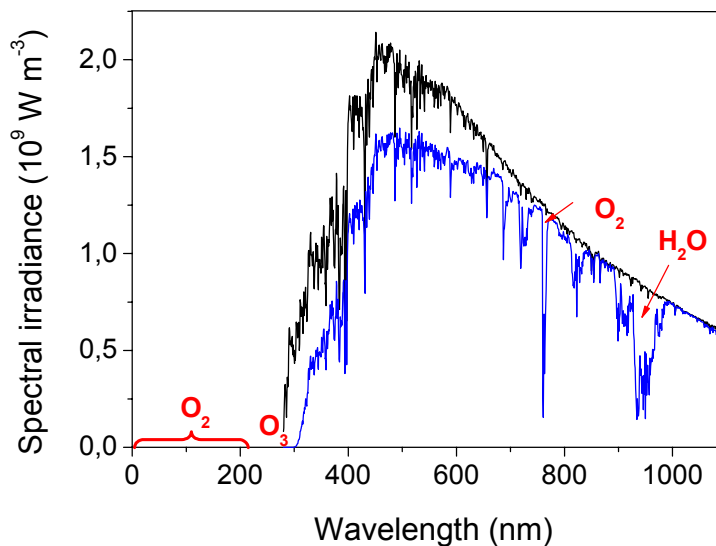


Figure 3. ASTM G173-03 reference spectra for the solar spectral irradiance: Extraterrestrial Solar Irradiance (black) and Global Total Spectral Irradiance on the 37° sun facing tilted surface for atmospheric conditions (blue). The data for preparation of the graph were taken from <http://rredc.nrel.gov/solar/spectra/am1.5/>.

As yet another requirement to LH complexes, the geometrical arrangement of LH chromophores should be addressed. A **defined arrangement of the dyes** is essential to enable fast and efficient energy transport between the different antenna chromophores to the reaction center and to avoid concurrence processes. In most photosynthetic species stabilization of the geometry is provided by a protein matrix embedding the antenna chromophores.

2.1.2 Natural Antenna Chromophores

Nature exhibits appropriate antenna chromophores for the whole wavelength range of the visible solar spectrum. There are three different classes of LH pigments, namely chlorophylls, phycobiliproteins, and carotenoids. Their absorption spectra are depicted in Figure 4.

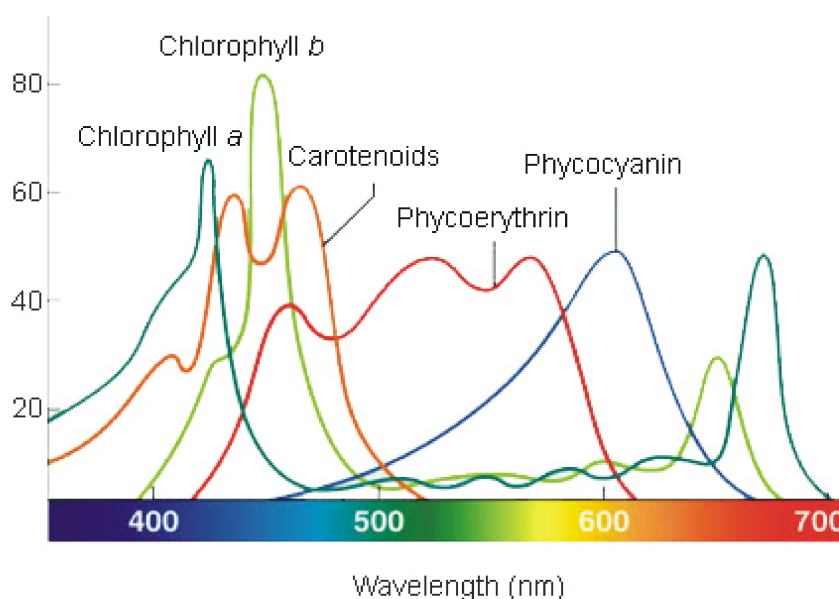


Figure 4. Absorption spectra of photosynthetic LH pigments (taken from http://www.citruscollege.edu/pic/46/c06_06.jpg).

Cyclic tetrapyrroles

The predominant pigments in photosynthetic LH systems are chlorophylls, whose structures are based on tetrapyrrole cycles of different hydrogenation states, i.e. porphyrins, chlorins (Chl; 17,18-dihydroporphyrin), or bacteriochlorins (7,8,17,18-tetrahydroporphyrin) (Chart 2).²⁷

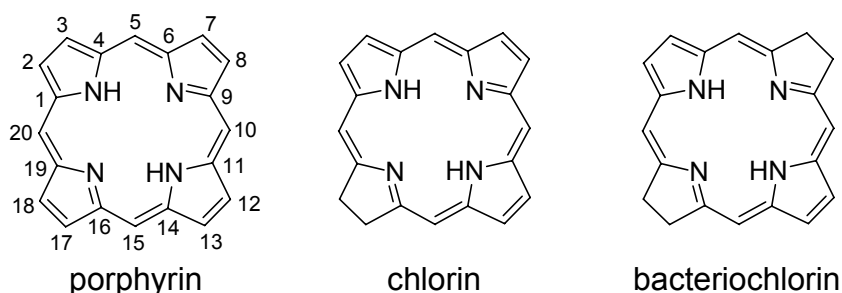


Chart 2. Basic tetrapyrrole cycles present in (bacterio-)chlorophylls.

Chlorophylls are characterized by a fifth, isocyclic ring and a central magnesium or, in rare cases, zinc ion (Chart 3). The most prevalent species is chlorophyll *a*, which is present in all oxygenic photosynthetic organisms. Some chlorophyll derivatives are named bacteriochlorophylls (BChls) due to the fact that they are the predominant chromophores in some photosynthetic bacteria. Notably, only BChl *a* and *b* contain a bacteriochlorin cycle, while BChl *c*, *d*, and *e* are based on a chlorin structure.

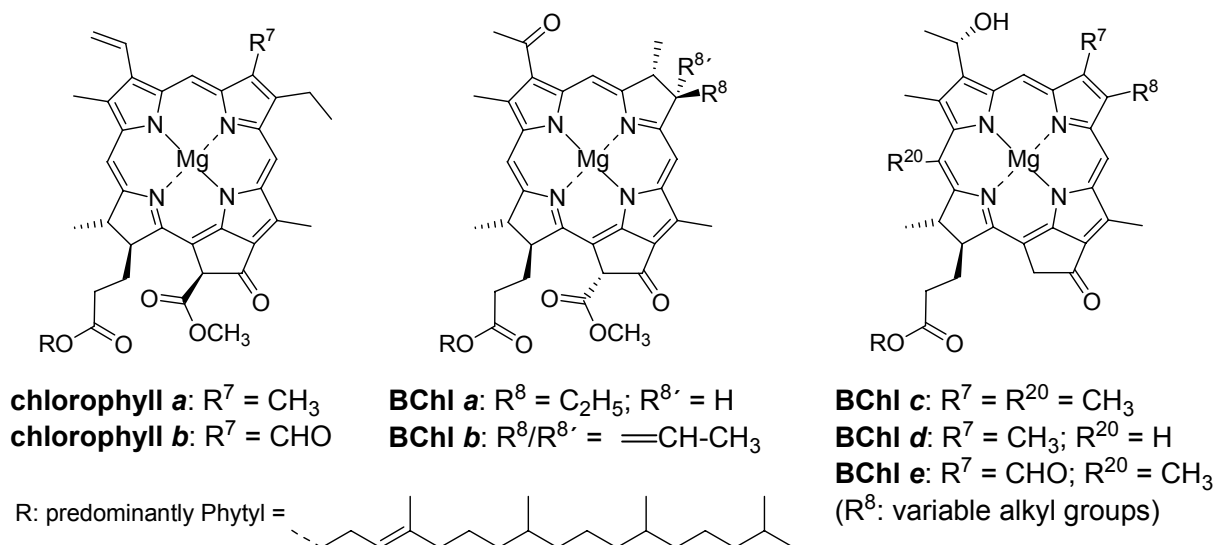


Chart 3. Molecular structures of the photosynthetic chromophores chlorophyll *a* and *b* and BChl *a-e*.

The absorption spectra of the cyclic tetrapyrrole dyes are influenced by the π perimeter of the chromophore and by the nature of the central metal ion and substituents. The UV-vis spectra of porphyrins are dominated by an intensive transition in the near UV region (~ 400 nm), which is referred to as B band or Soret band (Figure 5). Further, the free porphyrin base exhibits two less intensive electronic transitions in the range of 500-660 nm, the so-called Q_x and Q_y bands showing a defined vibronic fine structure. For porphyrin metal salts only one Q band is observed.²⁸

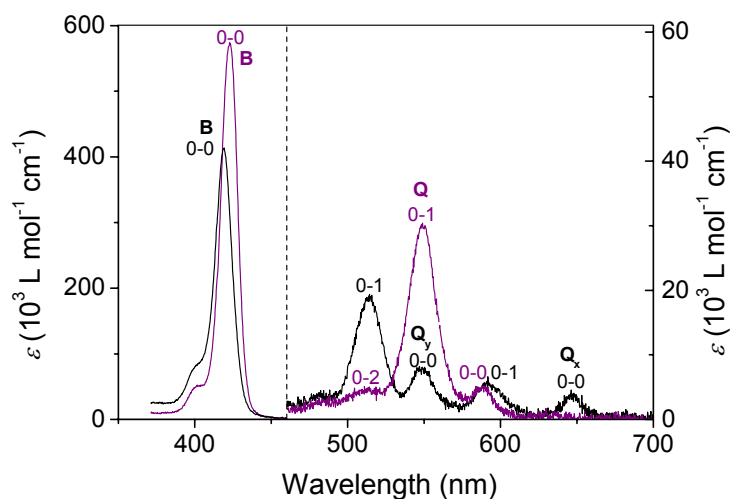


Figure 5. Absorption spectra of the free tetraphenyl porphyrin base (black line) and the tetraphenyl porphyrin zinc salt (purple line) in toluene.

The outstanding characteristic of chlorin absorption spectra is an intense red band (Figure 6). Unlike the porphyrins, the change from the free base to the metal salt does not simplify the structure of the visible bands.²⁹

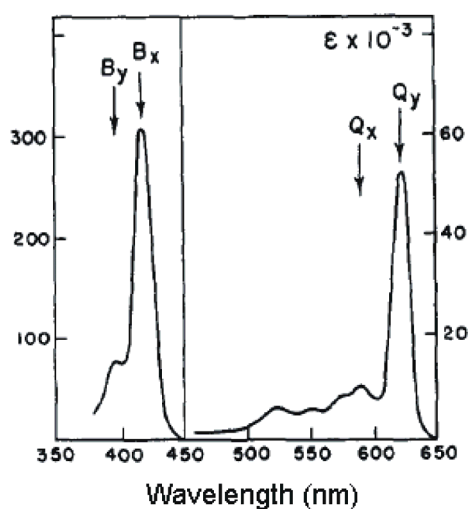


Figure 6. Absorption spectrum of the tetraphenyl chlorin zinc salt in benzene. Reprinted from ref. 30. Copyright (1963), with permission from Elsevier.

In early calculations of metalloporphyrin absorption spectra the molecules were regarded as a 16-membered cyclic polyene system with 18 π -electrons, showing a D_{4h} symmetry (Figure 7).³¹



Figure 7. General structure of metalloporphyrins. The 16-membered cyclic polyene system with 18 π -electrons is situated along the red line.

Shortly afterwards, from simple LCAO-MO calculations it was derived that metalloporphyrins exhibit a pair of HOMO orbitals showing the symmetries a_{2u} and a_{1u} and four nodes, respectively, and a degenerate pair of LUMO levels with the symmetry e_g and five nodes.³² Later, Gouterman developed the so-called four-orbital model on the basis of the free-electron model and the LCAO-MO calculations.^{30,33-35} The four-orbital model (Figure 8) is not only useful to give a relatively simple and lucid explanation of porphyrin absorption spectra, but can also be applied to chlorins and bacteriochlorins. Gouterman *et al* proposed that the optical spectra of cyclic tetrapyrroles result from linear combinations of one-electron promotions between the two HOMOs and the two LUMOs.

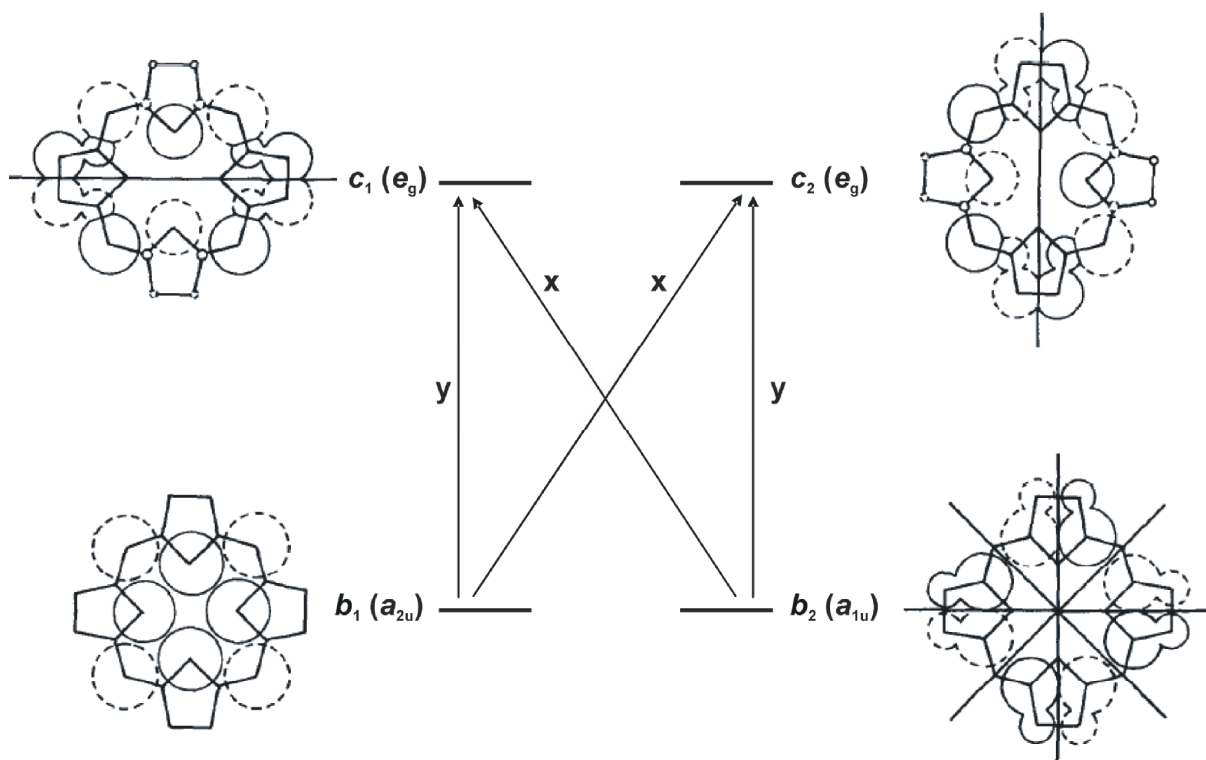


Figure 8. The two HOMOs and two LUMOs of metalloporphyrins. The atomic orbital coefficients are proportional to the size of the circles; solid or dashed lines indicate the sign. Reprinted from ref. 34. Copyright (1961), with permission from Elsevier.

The two HOMOs of cyclic tetrapyrroles were nominated b_1 and b_2 , while the two LUMOs are referred to as c_1 and c_2 . In the case of metalloporphyrins, the symmetry of the molecules is D_{4h} and the molecular π^* -orbitals c_1 and c_2 are degenerate, since the in-plane x- and y-axes are equivalent. The slight difference in energy of π -orbitals b_1 and b_2 is due to the conjugation of an empty p_z orbital of the respective central metal ion and b_1 . As the electropositivity of the metal rises, the energy of b_1 is increased.

Two out of the four possible promotions are x-polarized ($b_1 \rightarrow c_2$; $b_2 \rightarrow c_1$) and two promotions are y-polarized ($b_1 \rightarrow c_1$; $b_2 \rightarrow c_2$). The transition dipole moments of the promotions interact in pairs to give four possible combinations, in which they either reinforce or oppose each other. The plus combination of the two x-polarized promotions causes the B_x band and the minus combination gives rise to the Q_x band. B_y and Q_y bands, respectively, are observed in an analogous manner from the y-polarized promotions. For metalloporphyrins, x- and y-polarized electronic transitions are degenerate.

The intensities of Q_x and Q_y bands are proportional to λ_x^2 and λ_y^2 , respectively, which can be calculated from the initial energy gap Δ between the allowed B and Q bands and from the energies ε of the HOMO and LUMO orbitals:

$$\lambda_x = \frac{(\varepsilon(c_2) - \varepsilon(b_1)) - (\varepsilon(c_1) - \varepsilon(b_2))}{2\Delta} \quad (1)$$

$$\lambda_y = \frac{(\varepsilon(c_1) - \varepsilon(b_1)) - (\varepsilon(c_2) - \varepsilon(b_2))}{2\Delta} \quad (2)$$

It is obvious that the Q band intensity becomes very weak for a high degree of degeneration of the respective x and y transitions, as it is the case for metalloporphyrins.

In the case of chlorins, the degeneracy in x and y direction is removed. Orbitals b_2 and c_1 have electron density at the reduced positions, thus, their energy is increased. This effect is even more pronounced for bacteriochlorins showing two reduced positions (Figure 9). However, LUMO c_2 is not influenced by the pyrrole ring saturation and, indeed, homologous porphyrins, chlorins, and bacteriochlorins do have similar reduction potentials.

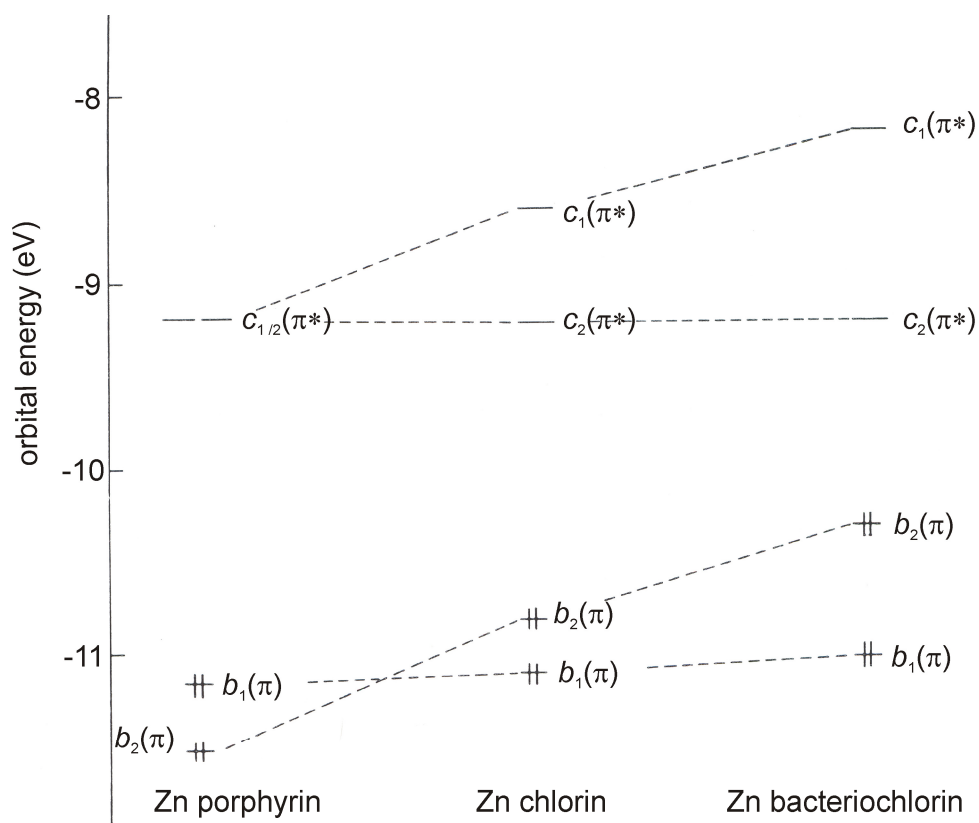


Figure 9. Calculated energies of the highest filled and lowest unoccupied MOs of Zn porphyrin, Zn chlorin, and Zn bacteriochlorin. The figure was prepared according to the orbital energies given in ref. 35.

The changes in orbital energies of porphyrins, chlorins, and bacteriochlorins have the following consequences for the four one-electron transition energies: $b_1 \rightarrow c_1$ (y-polarized) $>$ $b_1 \rightarrow c_2$ (x-polarized) $>$ $b_2 \rightarrow c_1$ (x-polarized) $>$ $b_2 \rightarrow c_2$ (y-polarized). For all tetrapyrroles, the two promotions that comprise the Q_x transition are very similar in energy, thus, the respective Q_x intensity is quite low. Further, these x-promotion energies are similar for porphyrins, chlorins, and bacteriochlorins. As a result, the Q_x bands are found at similar wavelengths. In contrast, the two promotions that comprise the Q_y transitions are very different in energy for chlorins and even more for bacteriochlorins. According to formula (2), the intensity of Q_y bands increases with the degree of saturation. Furthermore, a bathochromic shift is observed for Q_y bands going from porphyrins to chlorins and bacteriochlorins, since the energy of Q_y becomes increasingly dominated by the promotion with lower energy, the decreasing $b_2 \rightarrow c_2$ promotion.

Linear Tetrapyrroles

The second type of natural LH chromophores are linear, metal-free tetrapyrrole pigments, the bilins, which are covalently attached to proteins at a cystein site.³⁶⁻³⁸ These so-called phycobiliproteins are found in the LH complexes of cyanobacteria (blue-green algae), red algae, and cryptomonads. There are three abundant chromophores in phycobiliproteins: phycocyanobilins,³⁹ phycoerythrobilins,⁴⁰ and phycourobilins (Chart 4). In some cyanobacteria also phycobiliviolins are present. Photosynthetic bilins are very similar in structure and resemble the mammalian bile pigments, namely bilirubin and biliverdin.

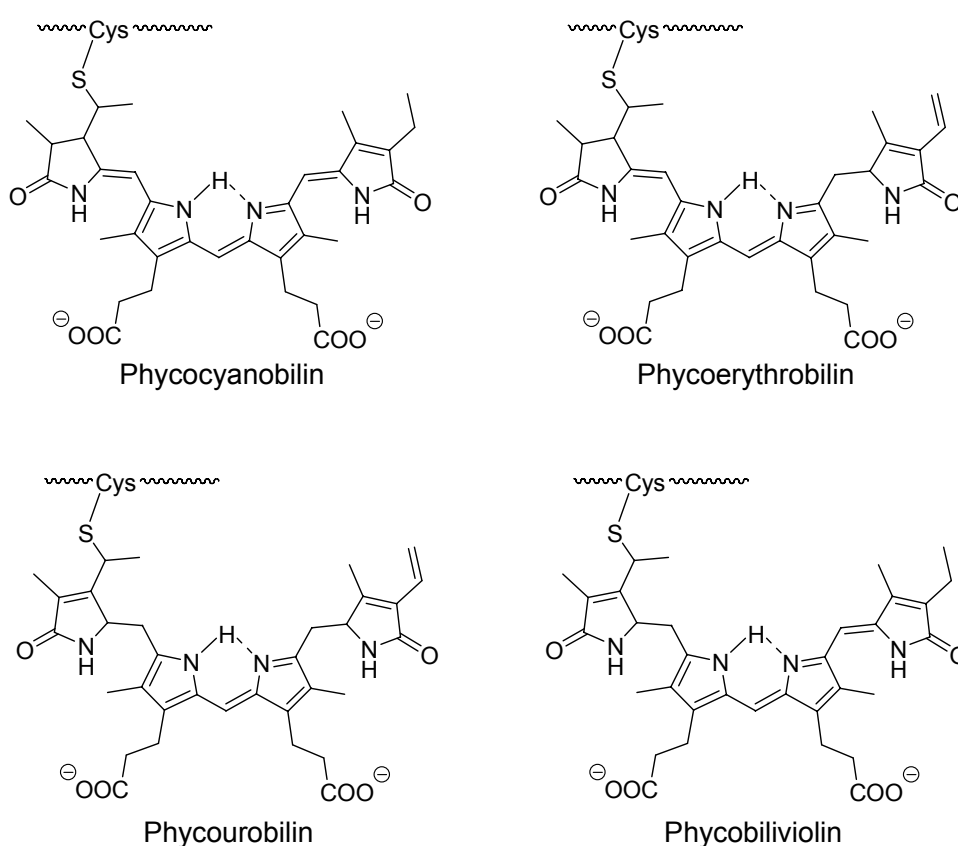


Chart 4. Chemical structures of the cystein-linked bilins found as prosthetic groups on phycobiliproteins.

The electronic properties of phycobiliproteins strongly depend on the surrounding protein structure. The extinction coefficients of native phycobiliproteins in the visible wavelength range exceed those of denatured species by a factor of five. The higher absorption is due to the conformationally fixed linear structure of the bilin chromophores in the protein matrix, for which the electronic transitions in the visible range are allowed. In contrast, free bilin dyes prefer a more flexible cyclic

conformation, exhibiting broad and weak visible absorption bands. The absorption bands of native phycobiliproteins are found in the range of 480-640 nm. While the blue phycocyanobilins show absorption maxima around 615 nm, the red phycoerythrins exhibit maxima at 540-565 nm. Furthermore and despite of the higher transition dipole moment, the excited state lifetimes of the native proteins ($\tau \approx 5$ ns) are about four orders of magnitude larger, since competing deactivation processes are avoided by the rigidification of the bilin dye. Thus, phycobiliproteins are very valuable antenna chromophores for natural LH systems, which transfer the absorbed energy to the reaction centres with quantum efficiencies of nearly 100%. However, due to the requirement of a protein matrix linear tetrapyrroles are not recommended for artificial supramolecular antenna systems.

Carotenoids

The third class of LH chromophores are carotenoids, which are, along with chlorophylls, the most abundant pigments found in nature. The chemical structures of carotenoids are based on diterpenes, which are generated by head-head condensation of two geranylgeranyl pyrophosphate units resulting in a linear polyene structure (Chart 5).⁴¹ In nature, there are over 600 known carotenoids, which are split into two classes, the oxygen-containing xanthophylls and the oxygen-free carotenes. The most abundant derivative is β -carotene.

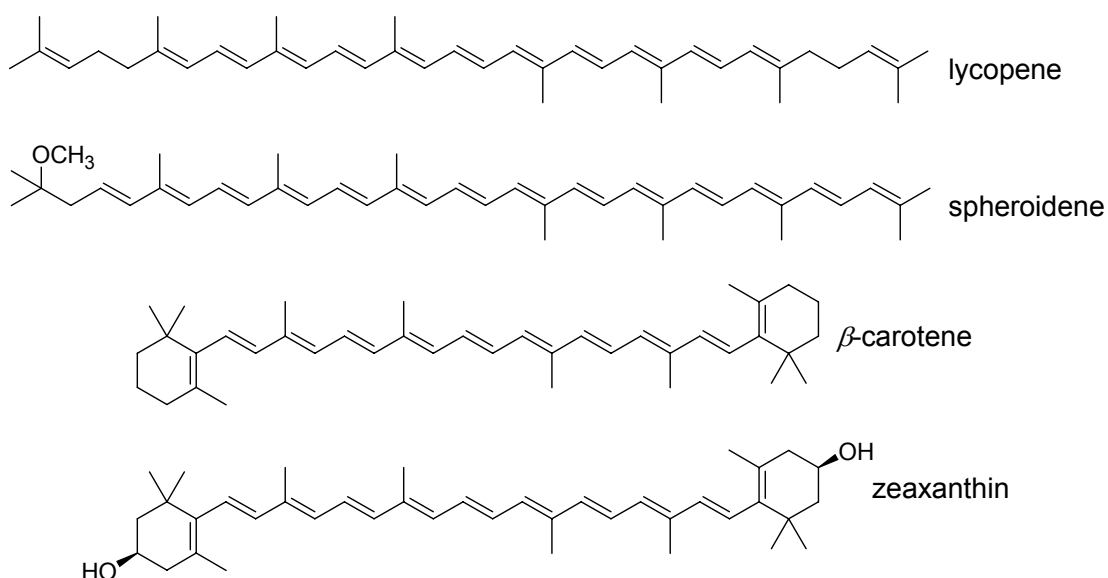


Chart 5. Structures of photosynthetic carotenoids lycopene, spheroidene, β -carotene, and zeaxanthin.

Carotenoids are not only implicated in the role of LH,⁴²⁻⁴⁵ but they serve as photoprotectors,⁴⁶ singlet oxygen scavengers,⁴⁷ excess energy dissipaters,⁴⁸⁻⁵¹ and structure stabilizers.⁵² The functional variety is directly related to their unique spectroscopic properties, resulting from the polyene structure of the carotenoid molecule. As a special feature, the absorbing state ($1^1B_u^+$ symmetry) of all-trans polyenes having conjugation lengths > 3 is not the lowest excited state but an additional, “dark” state ($2^1A_g^-$ symmetry) is located between the ground state (A_g^- symmetry) and the absorbing state. As a consequence, the strong absorption of carotenoid in the blue-green spectral region is caused by the S_0 - S_2 transition. The energy of this transition decreases with the conjugation length. For naturally occurring carotenoids having conjugation lengths in the range of 7-13 double bonds, the 0-0 band of the S_0 - S_2 transition is located between 475 and 525 nm, which gives the bright colors of carotenoids varying from yellow to red. Carotenoids showing conjugation lengths ≥ 8 double bonds violate Kasha’s rule as they exhibit emission from the S_2 state, having radiative lifetimes in the range of nanoseconds.⁵³ However, measured fluorescence quantum yields of the S_2 emission are on the order of 10^{-5} only, since the S_2 dynamics are governed by internal conversion on the subpicosecond time scale.⁵⁴ Nevertheless, carotenoids serve as efficient energy donors in natural as well as in small artificial photosynthetic units.^{42-45,55-58}

2.1.3 Energy Transport Mechanisms

When a photon of an appropriate energy reaches a LH complex at a certain position, it is absorbed and an exciton is created. Then the excitation energy has to traverse several chromophores until the exciton reaches the reaction center (Figure 10).

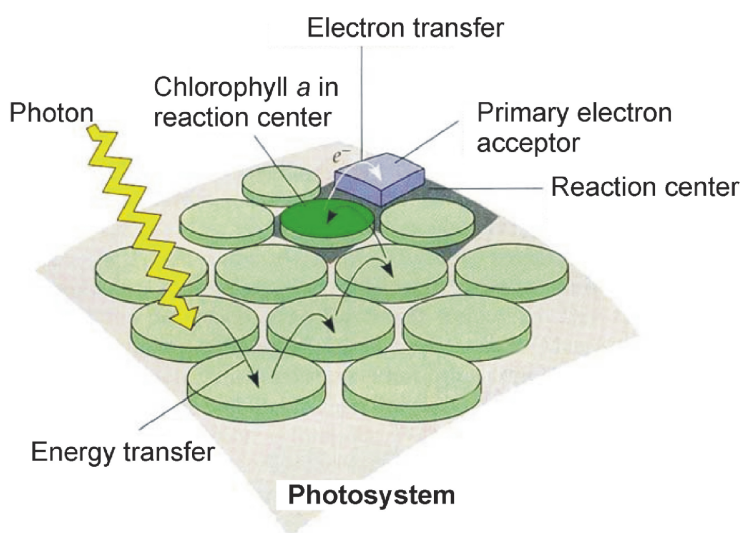


Figure 10. Schematic presentation of a LH system. Reprinted from ref. 59. Copyright (1997), with permission from Prentice Hall.

The excitation energy can either be transported over excitonically coupled, identical dye molecules sharing their excited states, or the energy transfer proceeds cascaded via different types of antenna chromophores according to the Förster (FRET, “fluorescence resonance energy transfer”) or Dexter mechanism. The different transfer mechanisms do not involve the appearance of a photon. Instead, Dexter energy transfer can take place via an overlap of orbitals and an exchange of electrons, while excitonic coupling and FRET are due to induced dipole-induced dipole interactions of the respective chromophores.

Excitonic Coupling: Kasha’s Theory

Excitonic coupling is a phenomenon, which can be observed for molecular dye aggregates.^{60,61} The most important characteristic of excitonically coupled chromophores are collective excited states and delocalization of excitation energy over many molecules, while the ground states do not differ from monomers. When aggregated chromophores are excited by one photon, coherence is created between them. This means that their transition dipole moments now oscillate with a constant

phase relation. The dipole-dipole interaction between them can either be repulsive or attractive. Therefore, the energies of the excited state are split, and joint energy states for the molecules in the aggregate exist. The number of these so-called exciton states equals the number of aggregating molecules. The exciton theory which has been developed by Kasha and McRae discusses the role of the geometrical arrangement of chromophores and the estimation of splitting energies for certain dimer aggregates. The exciton theory is a state interaction theory, implying that the interacting molecules preserve their individuality in the aggregate.

The relative arrangement of molecular transition dipole moments and their electrostatic interaction can be used to demonstrate the excited state interactions and to evaluate the selection rules for certain arrangements. Figure 11 shows exemplarily the energy schemes for a linear transition dipole moment arrangement. In this case, the out-of-phase dipole oscillation is repulsive. Thus it can be assigned to the upper energy state of the dimer. Since the sum of transition dipole moment vectors equals zero, the transition from the ground state to the upper energy state is forbidden. In contrast, the in-phase oscillation is attractive, thus, it belongs to the lower energy state, which is an allowed state due to its large transition dipole moment. As a consequence, the absorption spectrum of a linearly arranged dimer aggregate shows a bathochromic shift.

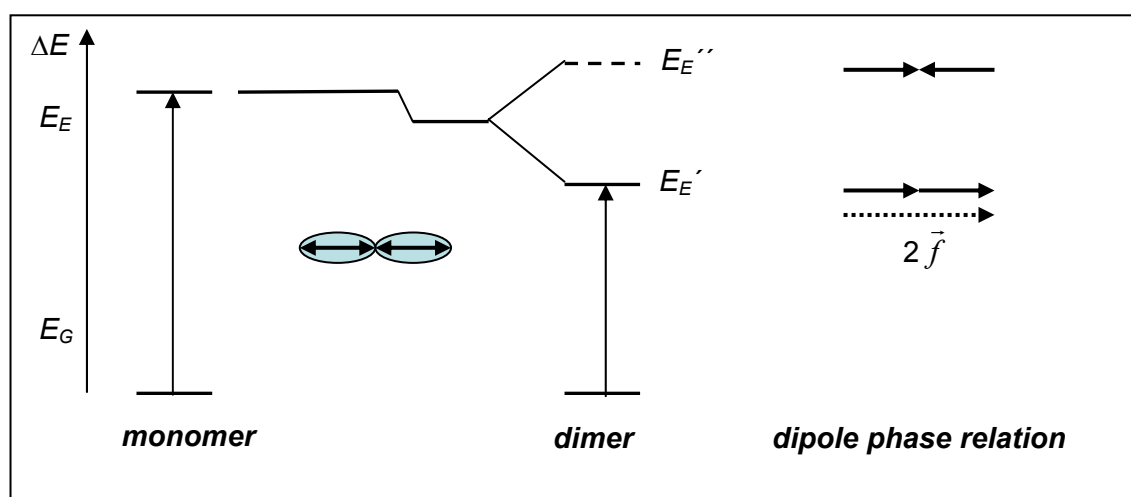


Figure 11. Energy scheme for a dimer aggregate exhibiting linearly arranged transition dipoles.

A different situation is given for parallel dipoles. Their interaction is repulsive if they oscillate in phase (Figure 12). Then the exciton splitting term is positive and the energy of this allowed exciton state is higher than the monomer excited state. Out-of-

phase oscillation implies attractive interaction forces and a negative exciton splitting term. Since the transition from the ground state to the lower exciton state shows an oscillator strength equal to zero, it is forbidden and the absorption band is shifted to lower wavelengths.

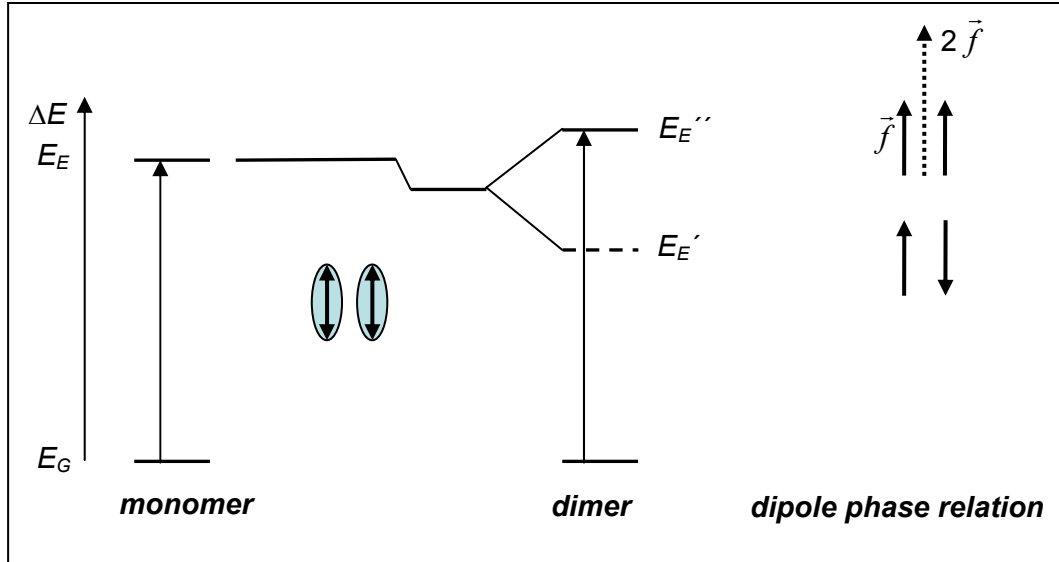
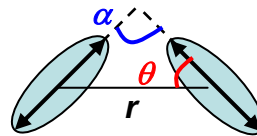


Figure 12. Energy scheme for a dimer aggregate exhibiting parallel arranged transition dipoles.

The exciton splitting energy $\Delta\varepsilon$ is often called “Davydov splitting”. $\Delta\varepsilon$ depends on angles α , θ and distances r between the molecules and on the norm of their transition dipole moment $\vec{\mu}_{mon}$. For a dimer aggregate, it is

$$\Delta\varepsilon = 2 \frac{|\vec{\mu}_{mon}|^2}{r^3} (\cos \alpha - 3 \cos^2 \theta) \quad (3)$$



The intensity of an absorption band can be described by integration of the absorption coefficient $\varepsilon(\nu)$ in the respective frequency range $\Delta\nu$.⁶²

$$A = \int_{band} \varepsilon(\nu) d\nu \quad (4)$$

The norm of the oscillator strength \vec{f} of a certain transition and of the transition dipole moment $\vec{\mu}$, respectively, are related to A by the following equation:

$$|\vec{f}| = \frac{4m_e c \varepsilon_0 \ln(10)}{10 N_A e^2} A = \frac{8\pi^2 m_e \nu}{3 h e^2} |\vec{\mu}|^2 \quad (5)$$

where m_e is the mass and c the charge of the electron, n is the refraction index of the medium and ν is the averaged frequency of the transition. Thus, for chromophores showing strong absorption bands, for example the Q_y bands of chlorins and bacteriochlorophylls, a large exciton splitting energy $\Delta\varepsilon$ is expected.

In the general case of a parallel chromophore arrangement as it is depicted in Figure 13, the exciton splitting energy depends on the angle θ only, while α equals zero. For $\theta = 54.7^\circ$ the exciton splitting energy becomes zero. For smaller values of θ , the situation is similar to the linear dipole moment arrangement. Such types of aggregates are called J -aggregates. If the value of θ exceeds 54.7° , the chromophore arrangement is named H -aggregate. However, in larger aggregates there are manifold ways to arrange chromophores. Thus, each aggregate geometry requires its own theoretical analysis.^{63,64}

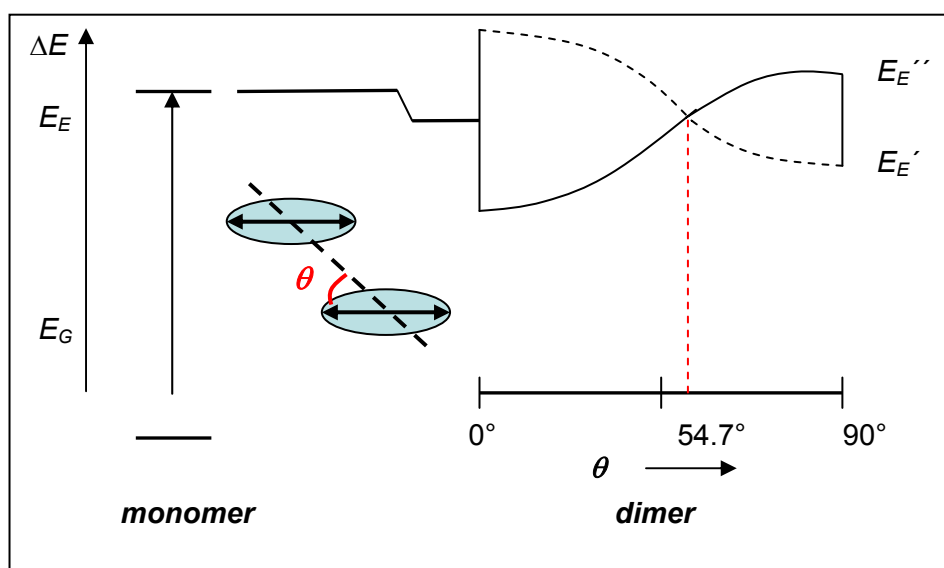


Figure 13. Energy scheme for parallel transition dipole moments in dependence on the angle θ .

FRET

FRET is an energy transfer process, which occurs in the case of weakly coupling transition dipole moments of an excited energy donor D^* and a mostly dissimilar acceptor A .⁶⁵ In contrast to excitonic coupling, the energy surfaces, which correspond to D^* and A^* are considered to be separate and distinct. Thus, the absorption spectra of D and A are not influenced by the Coulombic interactions and no band shift is

observed. When the molecule D is excited, a vertical $D^* \rightarrow D$ jump can trigger the $A \rightarrow A^*$ transition (Figure 14).

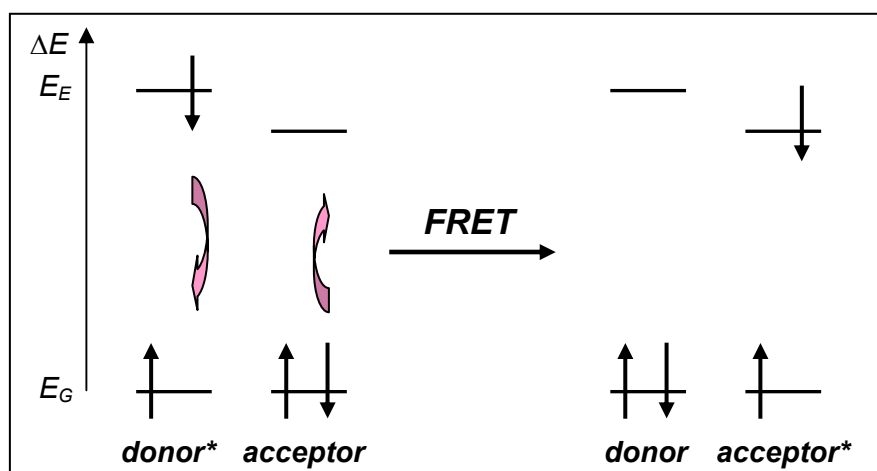


Figure 14. Schematic presentation of FRET.

The mechanism by which A is excited can be described as a perturbation from the excited electron oscillations of D^* on the HOMO electron oscillations of A, at which the resonance condition is $\Delta E(D^* \rightarrow D) = \Delta E(A \rightarrow A^*)$. For this perturbation, no physical contact of the interacting partners is required. Thus, FRET can proceed over chromophore distances up to 100 Å.

FRET transfer rates k_{FRET} show a r_{DA}^{-6} distance dependence:

$$k_{FRET} = \frac{1}{\tau_D} \left(\frac{R_0}{r_{DA}} \right)^6 \quad (6)$$

τ_D is the fluorescence lifetime of the energy donor in the absence of the acceptor and R_0 is the so-called Förster radius, which is defined as the distance between D and A, for which the probability of FRET equals 50%. A typical operational range for R_0 would be 10-80 Å. The Förster radius can be calculated from the simplified equation 7:

$$R_0 = 0.211 \frac{\kappa^2 \phi_D J(\lambda)}{n^4} \quad (7)$$

κ^2 is the so-called orientation factor, representing the relative arrangement of involved transition dipole moments with values in the range of 0 to 4. For statistical arrangement of donor and acceptor molecules $\kappa^2 = 2/3$. Further, n denotes the refraction index of the solvent and ϕ_D is the fluorescence quantum yield of the donor in the absence of the acceptor. The so-called overlap integral $J(\lambda)$ is defined as

$$J(\lambda) = \frac{\int_0^{\infty} I_D(\lambda) \varepsilon_A(\lambda) \lambda^4 d\lambda}{\int_0^{\infty} I_D(\lambda) d\lambda} \quad (8)$$

where $\varepsilon_A(\lambda)$ is the UV-vis absorption spectrum of the acceptor and $I_D(\lambda)$ is the emission spectrum of the energy donor, with the normalization condition

$$\int_0^{\infty} I_D(\lambda) d\lambda = 1 \quad (9)$$

The dependence of k_{FRET} on the extinction coefficients of $A \rightarrow A^*$, $\varepsilon_A(\nu)$, and the fluorescence quantum yield of the donor, ϕ_D , implies that FRET arises only when the transitions $D \rightarrow D^*$, $A \rightarrow A^*$ both are optically allowed.

In comparison to energy transfer between excitonically coupled chromophores, rates of FRET are much smaller (Figure 15). While the fastest FRET rates are in the range of a few picoseconds, energy transfer in strongly excitonically coupled aggregates can proceed on the femtosecond time scale.

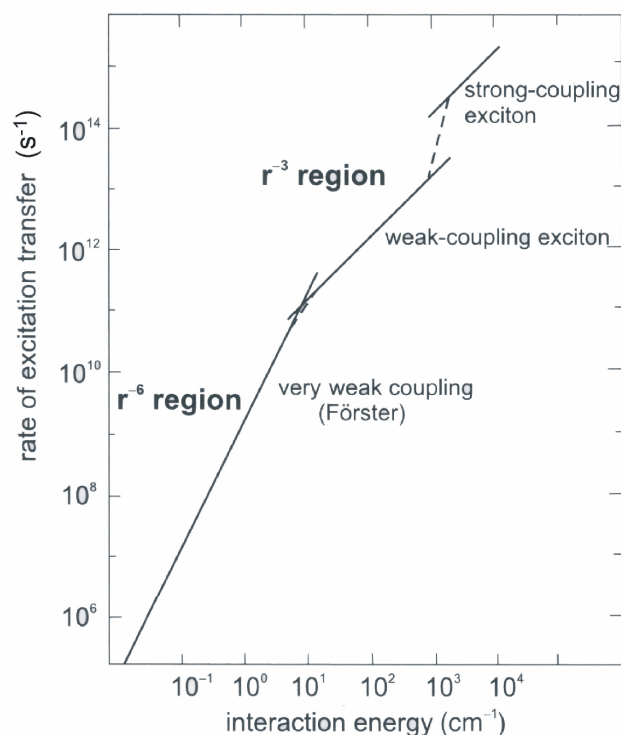


Figure 15. Values of energy transfer rates related to Coulombic interaction energies. Reprinted from ref. 66. Copyright (2002), with permission from Wiley-VCH Verlag GmbH & Co. KGaA.

Dexter Mechanism

Dexter energy transfer is likely to be the dominant mechanism in the case of an overlap of electron clouds, since it requires physical contact between the interaction partners.⁶⁵ This mechanism is caused by an exchange perturbation, which is represented in terms of firstly an overlap of the electron in the LUMO of D* and the LUMO of A and secondly an overlap of one electron in the HOMO of A with the HOMO of the excited donor D*. These overlaps result in a double electron exchange reaction (Figure 16).

The rate constant for energy transfer by electron exchange k_{Dexter} is expected to fall off exponentially as the distance r_{DA} increases, because electron densities usually decrease exponentially as the distance between electron and nucleus rises:

$$k_{Dexter} = KJ(\lambda)e^{-\frac{2r_{DA}}{L}} \quad (10)$$

where K is related to the specific orbital interactions and L is the sum of van der Waals radii of donor and acceptor.

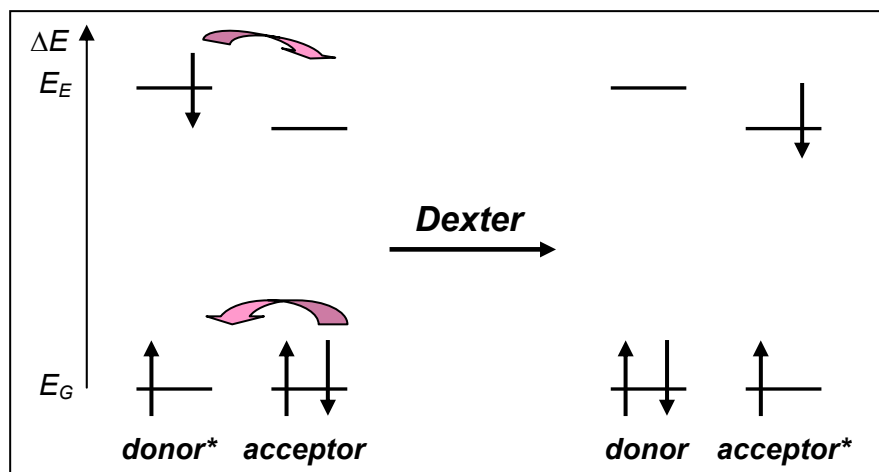


Figure 16. Schematic presentation of Dexter energy transfer.

2.2 Structure and Function of Bacterial Antennae

The most efficient LH systems are found in organisms, which have to live under very poor lighting conditions. The most extremely low-sunlight-adapted phototroph known to date is a population of green sulfur bacteria inhabiting the Black Sea chemocline at depths of 100 m.¹³ Recently another green sulfur bacterial species was found to live in a deep-sea hydrothermal vent at depths of even 2300 m, where the only source of light is geothermal radiation.⁶⁷ A further example of photosynthetic species living under extreme conditions are purple bacteria. They grow on the ground of waterbodies where the water surface is covered by higher plants, algae, and cyanobacteria.^{6,8} Composition and structural arrangement of LH systems of different green sulfur bacteria and purple bacteria have been subject to detailed research. Thus, relationships between the distinct structural features of their powerful LH complexes and their function could be elucidated.

2.2.1 Purple Bacteria

Photosynthetic Apparatus of Purple Bacteria

In contrast to higher plants or algae, the photosystems of purple bacteria are not located in chloroplasts, but they are directly embedded in the photosynthetic membrane.^{6,8} Photons are absorbed by the LH complexes and nearly all excitation energy is transferred to the RC initiating a charge separation. In most species of purple bacteria, there are two LH complexes, namely LH-I and LH-II. Only LH-I is tightly bound to the reaction centers (RC), while LH-II supplies energy via a FRET process to LH-I (Figure 17). The RC binds quinone QB, reduces it to hydroquinone QBH₂, and releases the latter. QBH₂ is oxidized by the bc₁ complex, which uses the exothermic reaction to pump protons across the membrane; electrons are shuttled back to the RC by the cytochrome c₂ complex from the ubiquinone-cytochrome bc₁ complex. The electron-transfer across the membrane produces a large proton gradient that drives the synthesis of ATP from ADP by the ATPase.

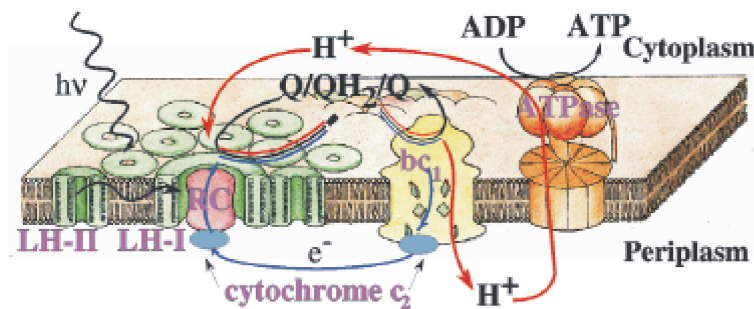


Figure 17. Schematic representation of the photosynthetic apparatus in the intracytoplasmic membrane of purple bacteria. Reprinted from ref. 6.

Structures of Purple Bacterial LH Systems

The evaluation of the architecture of LH-II of two species, namely *Rhodospseudomonas (Rps.) acidophila*⁶⁸ and *Rhodospirillum (Rs.) molischianum*,⁶⁹ by a combination of high-resolution X-ray diffraction and *ab initio* molecular modeling has opened the door to an understanding of the structure-function relationship in bacterial LH. LH-II of *Rps. acidophila* consists of two concentric cylinders of helical protein subunits, which enclose the pigment molecules (Figure 18). 18 BChl *a* molecules, the so-called B850 pigments, showing an absorption maximum at 850 nm form a continuous overlapped ring, which is embedded between the outer β - and the inner α -apoprotein cycle. A further nine BChl *a*, namely B800, are arranged in a second ring perpendicular to B850 and the transmembrane apoprotein helix axis.

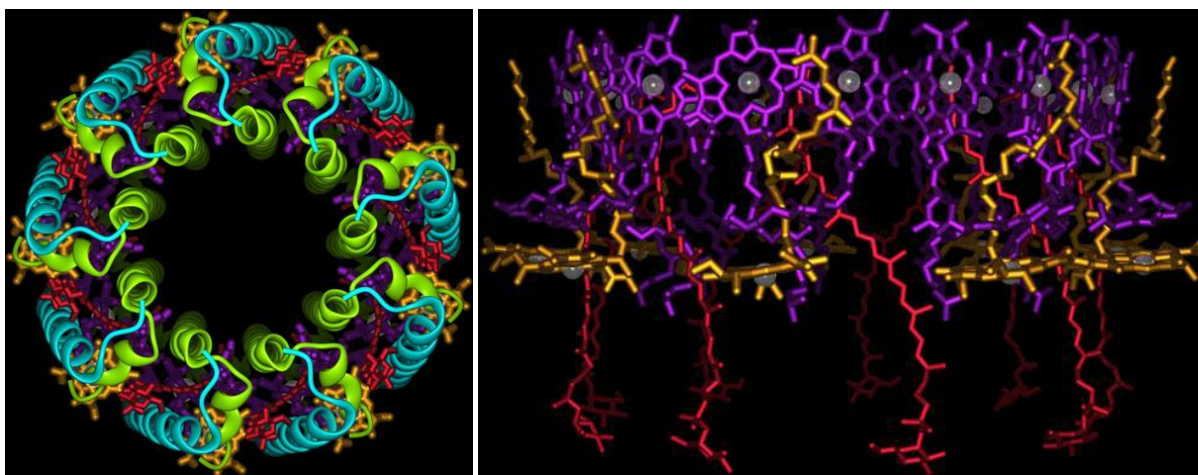


Figure 18. Geometrical arrangement of B850 (violet), B800 (yellow), and carotenoid (red) LH chromophores and nine α - (green) and β -apoproteins (blue), respectively, in the LH-II complex of *Rps. acidophila*, observed by crystal structure analysis. Left: top view from the cytoplasmic face; right: side view, periplasm at top, on LH-II. For better clarity, apoproteins are not depicted on the right side. Reprinted from ref. 70, with permission from R. Cogdell.

Nine carotenoids intertwine the BChl phytyl chains, spanning and stabilizing the complex. The carotenoids, rhodopin glucosides, have 12 double bonds, of which 11 are conjugated, and they are in the all-*trans* configuration. All together, LH-II of *Rps. acidophila* consists of nine identical subunits.

The absorption spectrum of the LH-II complex of *Rps. acidophila* is depicted in Figure 19. It shows the characteristic bands arising from the Q_x (green) and Q_y (red) transition dipoles of BChl B800 and B850. The absorption band of carotenoid is found in the range of 450-570 nm, and at lower wavelengths, the BChl Soret bands are observed. In contrast to plants, algae, or cyanobacteria, purple bacteria use light in the near IR and green spectral range, since the plant cover on top of purple bacteria consumes the blue and red light.

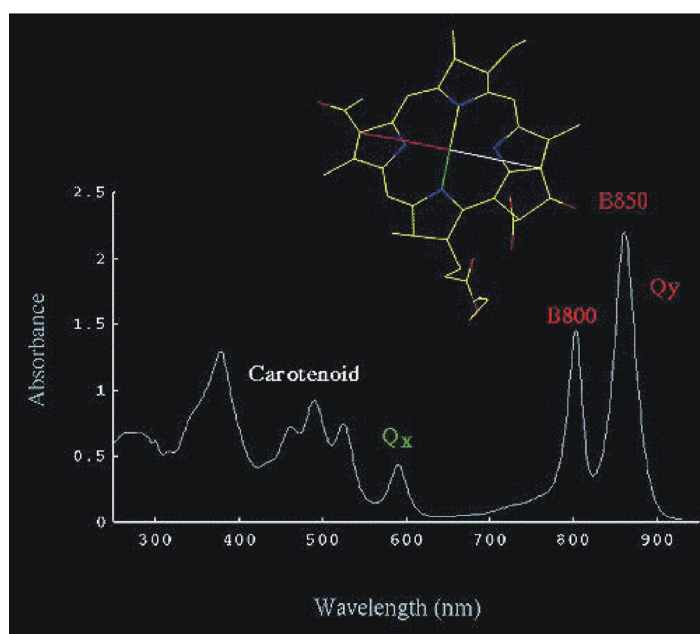


Figure 19. Absorption spectrum of the LH-II antenna complex from *Rps. Acidophila*. Reprinted from ref. 71. Copyright (1996), with permission from Elsevier.

The composition of the purple bacterium *Rs. molischianum* is quite similar to that of *Rps. acidophila*. The former exhibits only eight α - and eight β -protein subunits, which bind noncovalently to eight B800 and 16 B850 BChls and eight carotenoids (Figure 20).^{69,72,73}

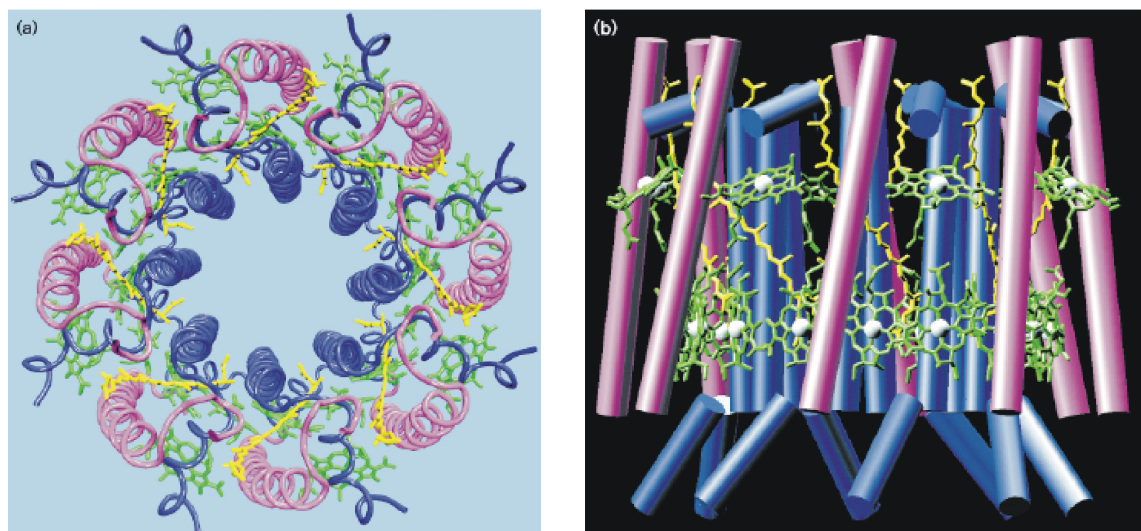


Figure 20. Top view (a) and side view (b) on the LH-II complex of *Rs. molischianum*. The α - and β -apoproteins are shown in blue and magenta, respectively; BChls are shown in green and carotenoids in blue. Reprinted from ref. 69. Copyright (1996), with permission from Elsevier.

Light-Harvesting Mechanisms in Purple Bacteria

The difference in absorption maxima between the chromophores of LH-II complexes of purple bacteria facilitates an excitation energy transfer cascade. As a result, energy absorbed by carotenoids or the B800 BChls is funnelled into the B850 ring. Then the B850 ring transfers the excitation energy into LH-I. The B800→B850 energy transfer proceeds according to the Förster mechanism within 700 fs in the case of *Rs. molischianum*. Carotenoids show an absorption maximum at 500 nm, which is attributed to the $S_0 \rightarrow S_2$ transition. S_2 decays by internal conversion within 200 fs into the optically forbidden S_1 state. The latter then couples to the lowest B850 Q_y transition through Coulombic interaction resulting in FRET within 260 fs. Unlike, the function of carotenoids as photoprotectors by quenching BChl triplet states follows the Dexter mechanism.

The perpendicular arrangement of B800 and B850 allows the absorption of incoming photons from all directions. The different absorption characteristics of the two BChl species, which structurally differ only in the lengths of their phytyl chain, are due to their differing ligation sites within the surrounding protein matrix⁷⁴ and excitonic coupling between the B850 Q_y transitions.⁷⁵ The complete oscillator strength of the excitonically coupled B850 ring is allocated to only two exciton states, the superradiant states $|2\rangle$ and $|3\rangle$. In contrast, the lowest exciton state $|1\rangle$ carries no oscillator strength and is optically forbidden. Thus, thermal relaxation from the higher exciton states to the lowest state $|1\rangle$ prevents the antenna from wasteful

fluorescence. The energy, which is trapped on the B850 ring, migrates between the different B850 molecules within the fs time scale. After arrival of the photon's excitation energy at the B850 ring it leaves LH-II and reaches the RC via the B875 BChl ring of LH-I in overall 100 ps and near unit efficiency.

2.2.2 Chlorosomes

Chlorosomes in the Photosynthetic Apparatus

The LH systems of green sulfur bacteria (*Chlorobi*) and some green filamentous anoxygenic phototrophs (*Chloroflexi*) are embedded in ellipsoidal, sac-like cell organelles, the so-called chlorosomes. Chlorosomes are surrounded by a lipid monolayer and contain, besides small amounts of carotenoids, a large concentration of BChl *c*. In the case of green sulfur bacteria, also BChl *d* and *e* are present. The size and thickness of chlorosomes depends on the species, the stage of development, and on the growth conditions. In the case of *Chloroflexus* they are approximately 100 nm long, 20-40 nm wide and 10-20 nm high,⁷⁶⁻⁷⁸ while chlorosomes of sulfur bacteria are larger showing lengths of 70-180 nm and widths of 30-60 nm.⁷⁹

In contrast to purple bacteria, chlorosomes are not integrated into the cytoplasmic membrane but are attached onto its surface. In *Chlorobi* the chlorosomes are connected to the membrane-embedded RCs through the BChl *a*-containing Fenna-Matthews-Olson (FMO) proteins. FMO complexes serve as additional LH complexes that direct light energy from the chlorosome membrane to the RCs. Before the excitation energy of the chlorosomal LH antennae reaches the FMO complexes, it is funnelled into the baseplate of chlorosomes, where BChl *a* molecules act as energy acceptors. *Chloroflexi* do not contain such FMO proteins; here baseplates of chlorosomes are directly attached to the membrane. The photosynthetic apparatus of the green sulfur bacterium *Chlorobium tepidum* is exemplarily shown in Figure 21.⁸⁰

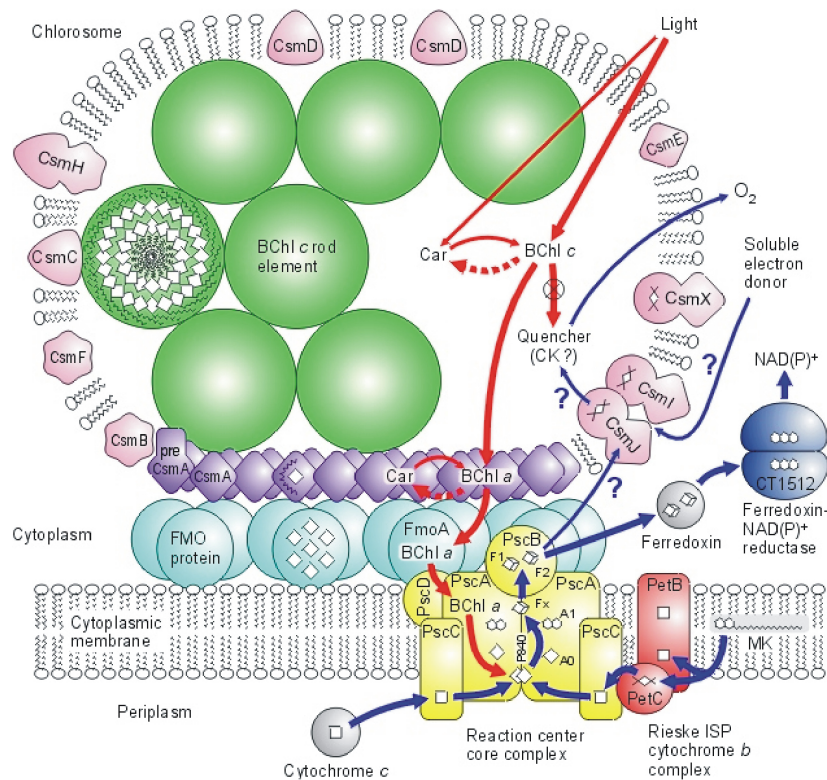


Figure 21. Cross-sectional view of an antenna system model for the photosynthetic apparatus in wild type *Chlorobium tepidum*. BChl aggregates (green) are surrounded by a lipid monolayer and connected to the FMO proteins (blue) via a BChl a containing base plate (violet). Reprinted from ref. 80. Copyright (2003), with permission from Elsevier.

Structures of Chlorosomal Antennae

The arrangement of the LH pigments in chlorosomes differs from all other photosynthetic species, since there is no protein matrix to stabilize the structure.⁸¹⁻⁸³ Instead, the LH systems consist of self-assembled BChl *c*, *d*, and *e*, whose defined arrangement is controlled by intermolecular forces between the BChl molecules only. One chlorosome contains about 1000-16000 BChl chromophores.⁸⁴ Thus, chlorosomes provide a high chromophore density and a huge cross section for solar light absorption in the wavelength range of chlorin aggregates. The chlorosomal BChl aggregates could be visualized by freeze-fracture electron microscopy of *Chloroflexus aurantiacus* and *Chlorobium limicola* (Figure 22). Chlorosomes of the former species were filled with elongated objects showing a diameter of 5.2 nm, while for the latter larger diameters in the range of 10 nm were observed.^{75,78,85}

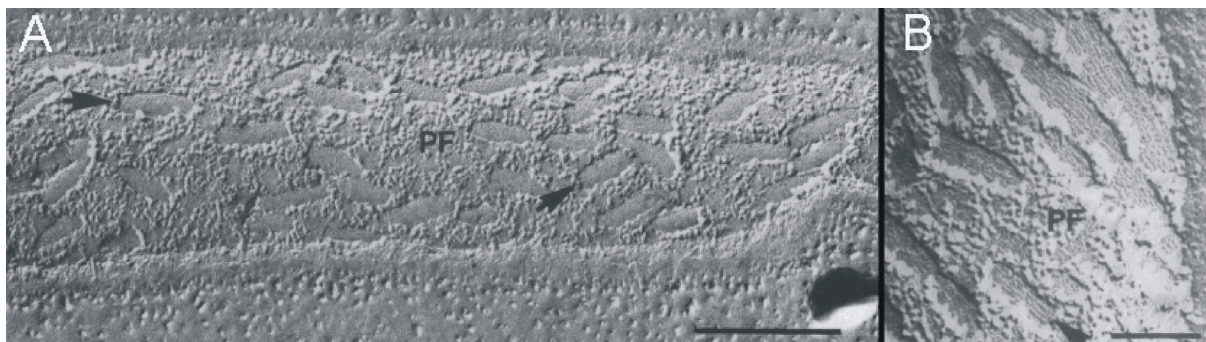


Figure 22. Electron microscopic picture of freeze-fractured cells of *Chloroflexus aurantiacus*. (A) Cigar-shaped chlorosomes are attached to the cytoplasmic membrane; scale bar: 0.2 μm (B) Rodlike elements are located in the interior of chlorosomes showing diameters of 5 to 6 nm; scale bar: 0.1 μm . Reprinted from ref. 85. Copyright (1981), with permission from the American Society for Microbiology.

The structure of these BChl self-assemblies has been intensively investigated and discussed controversially. In contrast to purple bacteria, no crystal structure could be determined for chlorosomes, which would have simplified the structural assignment. Nowadays, among the various proposed structure models of BChl self-assemblies, a tubular, protein-free aggregation model suggested by Katz, Holzwarth, Schaffner, Van Rossum, Steensgaard, and De Groot is the most accepted proposition.^{86,87} According to this model BChl *c*, *d*, and *e* form tubular aggregates by means of an interplay of three different types of interactions between the molecular units (Figure 23).

The combination of π - π stacking of the extended aromatic core and coordination of the central metal ion by the 3¹ hydroxy group of a neighboring molecule leads to the formation of one-dimensional stacks of slipped chromophores (*J*-aggregates). These stacks are held together by hydrogen bonding between the 3¹ hydroxy group and the 13¹ keto functionality resulting in so-called rod elements (Figure 24).

The tubular aggregation model was supported by solid state MAS (“Magic Angle Spinning”) ¹³C NMR,⁸⁸ resonance raman spectroscopy,⁸⁹⁻⁹¹ small angle neutron scattering,⁹² and molecular modeling.^{93,94} All polarized light experiments suggested that BChl aggregate structures are highly ordered. The Q_y band of chlorosomes of *Chloroflexus aurantiacus* shows highly polarized fluorescence and a strong linear dichroism. The analysis of these data resulted in an average angle between the Q_y transition dipole moment and the long aggregate axis of 15-20°.⁹⁵⁻⁹⁷ Circular dichroism spectra are strongly size-dependent, since the CD effect is caused by a

macroscopic chirality due to circular distribution of the transition dipole moments of BChl monomers within the aggregate.⁹⁸

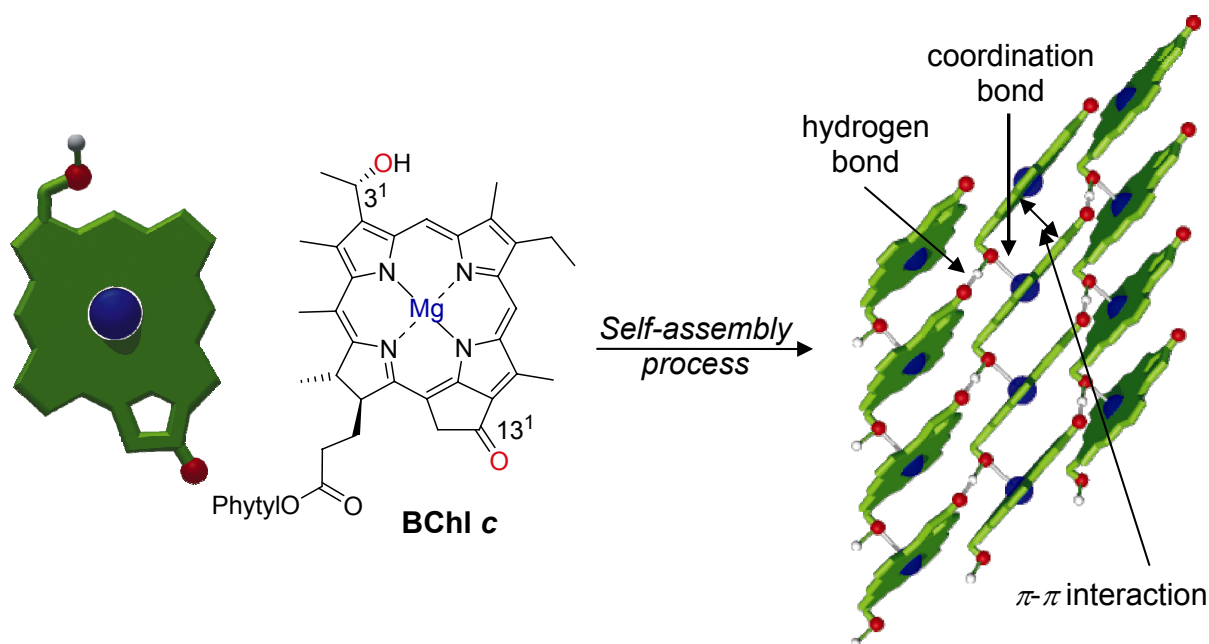


Figure 23. Interactions between BChl c leading to the formation of self-assembled dye aggregates.

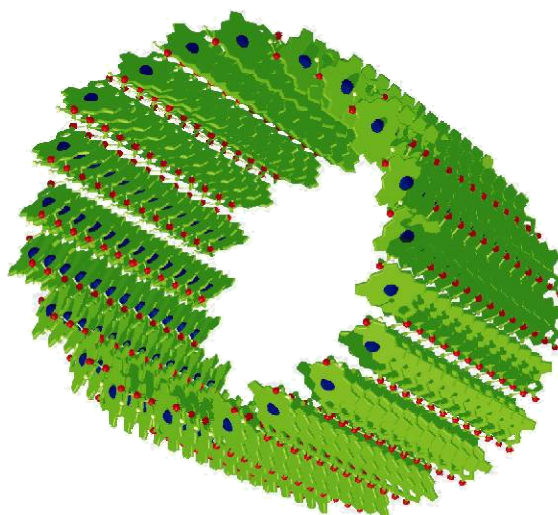


Figure 24. Model of supramolecular arrangement of BChl c chromophores into tubular rod aggregates.

Later, for the chlorosomes of *Chlorobi* a refined model was proposed suggesting a double-wall structure of the rod aggregates (Figure 25). The bilayer model fits well to the diameter of 10 nm observed for *Chlorobi*.^{99,100}

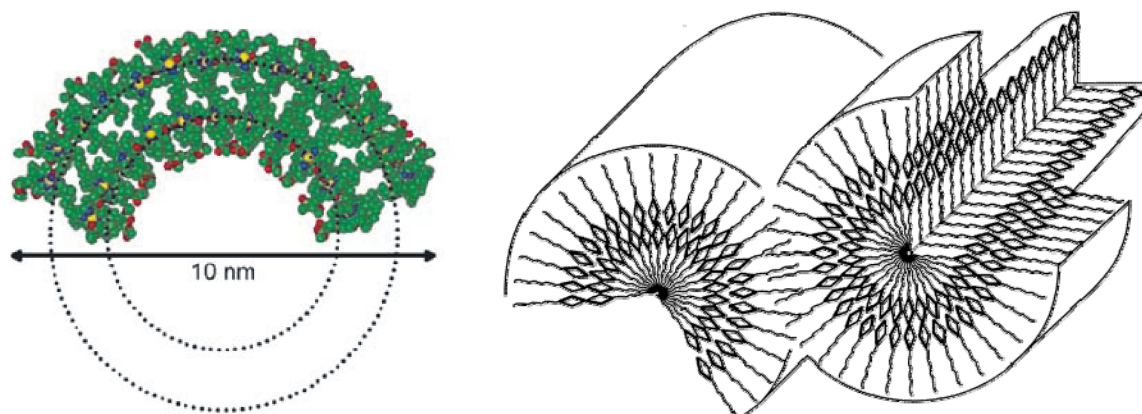


Figure 25. Refined model of the bilayer rod structure suggested for BChl aggregates in chlorosomes of *Chlorobi*. Two adjacent rods are shown. In each rod, the chlorin moieties of the inner and outer ring are located next to each other, whereas the ester side chains point in opposite directions. Reprinted from ref. 99. Copyright (2000), with permission from the American Chemical Society.

It has been demonstrated by various techniques that structures of *in vitro* BChl aggregates in water in the presence of a lipid or in nonpolar aprotic solvents, respectively, resemble those found in chlorosomes.^{11,12} Natural and *in vivo* aggregates both exhibit the same absorption and emission,^{11,12,81,101,102} linear dichroism,¹⁰¹ circular dichroism,¹⁰³ resonance raman,^{89,90,91} and solid-state NMR⁸⁸ spectra as well as analogous small angle neutron scattering characteristics⁹² suggesting analogous collinearity, helicity, and pigment interactions.

Light-Harvesting Properties of Chlorosomes

The characteristic feature of BChl *c*, *d*, and *e* rod aggregate absorption spectra is a pronounced bathochromic shift of the S_0 - S_1 transition band, namely the Q_y band, of about 80-90 nm compared to monomer spectra.^{81,104,105} This shift is due to the excitonic coupling of the chromophores, resulting in the formation of *J*-type aggregates. Figure 26 shows the absorption spectra of chlorosomes of *Chlorobium limicola* and *Chloroflexus aurantiacus*.

The main features of these spectra are the Q_y band with a maximum at 730-740 nm and the Soret band at about 450 nm. Additionally, a shoulder at about 500 nm is observed, which arises from a small amount of carotenoids, namely β - and γ -carotene, in chlorosomes. The absorption maximum around 792 nm for *Chloroflexus aurantiacus* is due to small amounts of BChl *a* (1-5%), which is embedded in the baseplate. Furthermore, the absorption spectrum of a solution of BChl *c* in *n*-hexane/ CH_2Cl_2 (0.5%) is depicted in Figure 26, resembling the absorption spectra of

chlorosomes. Under the gradual addition of methanol, the typical BChl *c* monomer spectrum is observed, exhibiting an absorption maximum at 662 nm for the Q_y band. This change of spectral properties is due to the disaggregation process of the *in vitro* self-assemblies.

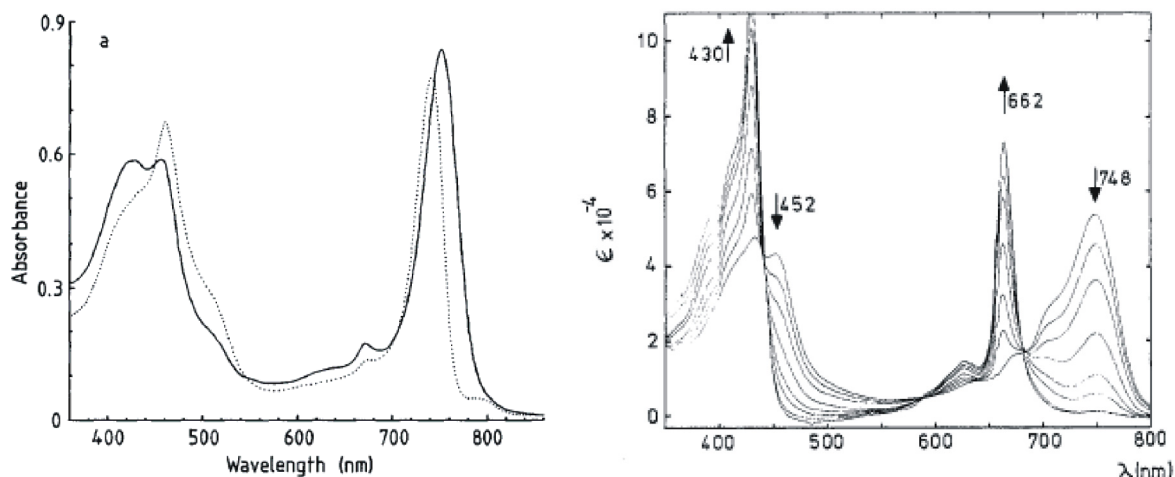
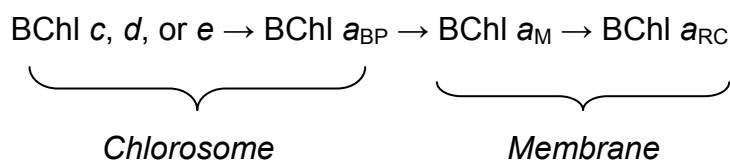


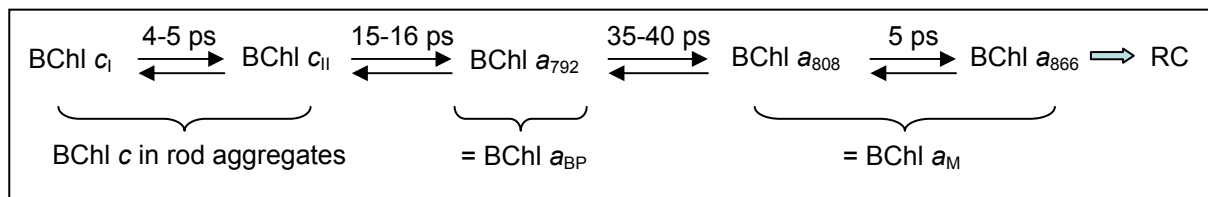
Figure 26. Left: Absorption spectra of chlorosomes from *Chlorobium limicola* (solid line) and *Chloroflexus aurantiacus* (dotted line). Chlorosomes were suspended in 10 mM Tris C1 buffer, pH 7.8. Reprinted from ref. 104. Copyright (1990), with permission from Elsevier. Right: Spectrophotometric titration of a 1.95×10^{-5} M solution of BChl *c* in hexane/ CH_2Cl_2 (0.5%). During the titration, methanol was added. Reprinted from ref. 82. Copyright (1983), with permission from the American Chemical Society.

LH by chlorosomes comprises a variety of different energy transfer processes.⁷⁸ Upon irradiation of the BChl *c*, *d*, and *e* aggregates, the excitation energy is delocalized between the chromophores of the same kind within one rod, then it is transferred between neighboring rods, and transmitted from the rods to the baseplate BChl a_{BP} . This is followed by energy transfer from the latter to BChl a_M of the membrane, the so-called B808-B866 LH complex, and, in the last step, to BChl a_{RC} in the RC. The energy transfer cascade to progressively red-shifted pigment pools and finally to the RC can be written as follows:



The energy transfer steps along this cascade usually proceed via the Förster mechanism, while the energy delocalization along the tubular BChl *c*, *d*, or *e* rod aggregates is due to excitonic interactions. The different energy transfer processes in chlorosomes and the subsequent transfer steps to the RC have been studied by various groups, whereas the most examined species is *Chloroflexus aurantiacus*.

Brune *et al* were the first to measure the energy transfer from BChl *c* rods to BChl *a*_{BP} and from there to the B808-866 BChl *a*_M protein in isolated and membrane-bound chlorosomes.¹⁰⁶ They observed a fast FRET process below the instrumental limit of temporal resolution (30-50 ps) for BChl *c* → BChl *a*_{BP}. Holzwarth and co-workers used time-resolved fluorescence detection and global analysis deconvolution methods with picosecond resolution to investigate the kinetics of energy transfer processes in whole cells of *Chloroflexus aurantiacus*.¹⁰⁷ The obtained decay-associated spectra (DAS) in the observation range 730-930 nm revealed a 15-16 ps transfer time for BChl *c* to BChl *a*_{BP} and a 35-40 ps time constant for BChl *a*_{BP} to BChl *a*_M (Scheme 1). These results were also confirmed by others on chlorosome preparations with membrane fractions attached.^{108,109}



Scheme 1. Kinetic scheme summarizing the results of intact cells and those of isolated complexes.¹¹⁰

Furthermore, time-resolved fluorescence measurements on BChl *a*-free chlorosomes revealed energy transfer with a time constant of 5 ps between two different types of BChl *c* pigment pools, namely BChl *c*_I and BChl *c*_{II}, which are shifted in energy relative to each other by about 10-20 nm.¹¹¹ However, it could not be excluded that the 5 ps lifetime component would alternatively be due to a relaxation process from upper exciton states to lower exciton states of the BChl *c* aggregate.

Savikhin *et al* performed transient absorption experiments with femtosecond resolution on isolated, BChl *a*_{BP}-containing chlorosomes of *Chloroflexus aurantiacus* at room temperature, finding energy transfer lifetimes of ~100 fs, ~2 ps, and ~10 ps.¹¹² They proposed a kinetic model, in which BChl *c* excitations equilibrate rapidly (~100 fs) with a BChl spectral form absorbing near 790 nm. Subsequent energy transfers occurred to a longer-wavelength BChl *a* species (~795-800 nm) with ~10 ps

kinetics. It could not be determined if the intermediate 790 nm BChl form was a BChl *c* or *a* species. Later, Savikhin and co-workers reinvestigated the kinetics of chlorosomes by two-color pump-probe experiments with improved sensitivity at room temperature.¹¹³ Now it was stated that it was not necessary to invoke the presence of a 790 nm BChl species. The BChl *c* → BChl *a* energy transfer kinetics appeared to be multiphasic with lifetimes of 2-3 ps and 8-11 ps and did not exhibit a sub-picosecond component. Furthermore, the same authors described analogous measurements at 19 K.¹¹⁴ In two-color absorption difference experiments chlorosomes were excited at 731 nm and probed at 758 nm revealing a 300 fs rise component, which was assigned to a downhill energy transfer among different spectral forms of BChl *c*.

The excitation delocalization in the BChl *c* rod aggregates of *Chloroflexus aurantiacus* was investigated at low temperature (1.27 K) by two-pulse photon echo and one-color transient absorption techniques with ~100 fs resolution.⁹⁴ At 745 nm four different dephasing times T_2 and four relaxation population times T_1 in the range from ~100 fs to ~100 ps were observed. Values of T_1 resembled about twice the values of T_2 implying that there is no pure dephasing without thermal phonons and thus proving the coherence of exciton delocalization in chlorosomes. The energy transfer was essentially divided into four steps (Figure 27): the shortest dephasing time was assigned to the loss of coherence of the initially coherent state due to interaction with the phonon bath. The next higher dephasing and depopulation times were attributed to complex relaxation processes over a wide time range from ~100 fs to ~5 ps. It was not possible to strictly separate energy relaxation processes within a single rod from energy exchange among neighboring rods in the framework of an exciton model. The longest energy transfer time (~40 ps for *Chloroflexus aurantiacus*) was observed for the transfer from the lower exciton states to the base plate. As a basis for this interpretation of excitation dephasing and energy transfer pathways a superlattice-like structural model for the closely packed rod aggregates was proposed based on experimental data and computer modelling.⁹⁴ This model predicted a fine structure of the aggregate Q_y absorption region due to splitting of the exciton band. In the calculated absorption spectrum of *Chloroflexus aurantiacus*, the main sub-bands are located at 739 and 755 nm. The large dipole strength of the aggregate is concentrated only in these few allowed exciton states.

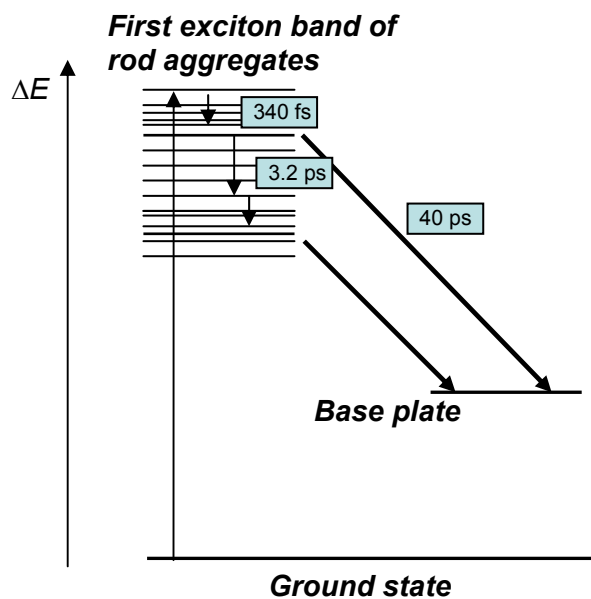


Figure 27. Proposed energetic and kinetic diagram for chlorosomes of *Chloroflexus aurantiacus*. The averaged energy transfer time constants are shown.⁹⁴

Later, Saga *et al* performed fluorescence spectroscopy on single chlorosomes at cryogenic temperature in order to investigate the BChl *c* \rightarrow BChl *a*_{BP} energy transfer process.¹¹⁵ They claimed that the efficiency of this step is different among individual chlorosomes, since the ratio of the fluorescence peak intensities of BChl *c* and BChl *a* was distributed between 0.09 and 0.72. The heterogeneity was explained by the concurrence of this process and the energy transfer from larger BChl *c* aggregates to smaller ones. As a further reason, the heterogeneity of microenvironments where individual chlorosomes were situated was given.

Blankenship and co-workers isolated the baseplate of *Chloroflexus aurantiacus* and demonstrated that it contains not only BChl *a*_{BP} but carotenoids as well.¹¹⁶ The baseplate consists of a ratio of 1.0 CsmA proteinⁱ/1.6 BChl *a*/4.2 β -carotenes. Within the baseplate, energy transfer efficiency from carotenoids to BChl *a* was 30% as measured by steady state and time-resolved fluorescence and absorption spectroscopies. In contrast to the chlorosomal LH systems, the baseplate does not contain pure pigment oligomers but pigment-protein complexes. Accordingly, CD spectroscopy showed no evidence for excitonic coupling of BChl *a* chromophores. The architecture of the baseplate pigment-protein complexes has not been determined yet.

ⁱ The CsmA protein is one out of the ten different types of proteins present in chlorosomes and it is the only protein which is found in the baseplate. The CsmA matrix is associated with BChl *a* chromophores.

The inner-membrane B808-866 BChl a_M complex is spectrally very similar to the purple bacterial LH-II complex, since it contains two types of BChl a absorbing at 808 and 866 nm, respectively, and a carotenoid species, namely γ -carotene. Blankenship and co-workers could show by ultrafast transient absorption and time-resolved fluorescence spectroscopy that FRET from the B808 to the B866 BChl a species proceeds within 1.6-3 ps.¹¹⁷ This is in good agreement with the results observed by Griebenow *et al* who observed ~5 ps for the same process (Scheme 1).¹¹⁸

Finally, energy transfer from the excited B808-866 BChl a_M complex to the special pair chromophores in the RC takes place, followed by a primary electron transfer to a bacteriopheophytin a acceptor molecule. A secondary electron transfer to a quinone molecule stabilizes the charge separation across the cytoplasmic membrane. The overall trapping process of the excitation energy from BChl a_M to the RC is determined by the rate of the primary electron transfer, which depends on the photochemical redox state of the RC. For energy trapping by open RCs (oxidized quinone) a time constant of 70-90 ps was observed, while for the closed RCs (reduced quinone) the time constant increased to 180-200 ps.¹¹⁰

2.3 Circular Artificial Supramolecular Light-Harvesting Systems

Since the highly efficient bacterial LH systems are based on circular supramolecular chromophore arrangements, this geometrical element was chosen by several groups for the development of artificial LH antennae. As LH chromophores not only chlorins but also porphyrins and cyanine dyes have been used.

2.3.1 Zinc Chlorin Antennae

Zinc chlorins (ZnChl) derived from natural Chl *a* have been applied as appropriate model systems for chlorosomal BChl aggregates, because they exhibit analogous absorption and aggregation characteristics.^{11,15,90,119-121} Chart 6 exemplarily shows the structures of such ZnChl derivatives **4** and **5** exhibiting the structural features which proved to be essential for the self-assembly process, i. e. the hydroxy group at the 3¹ position, a central metal ion, and the keto functionality at the 13¹ carbon atom.

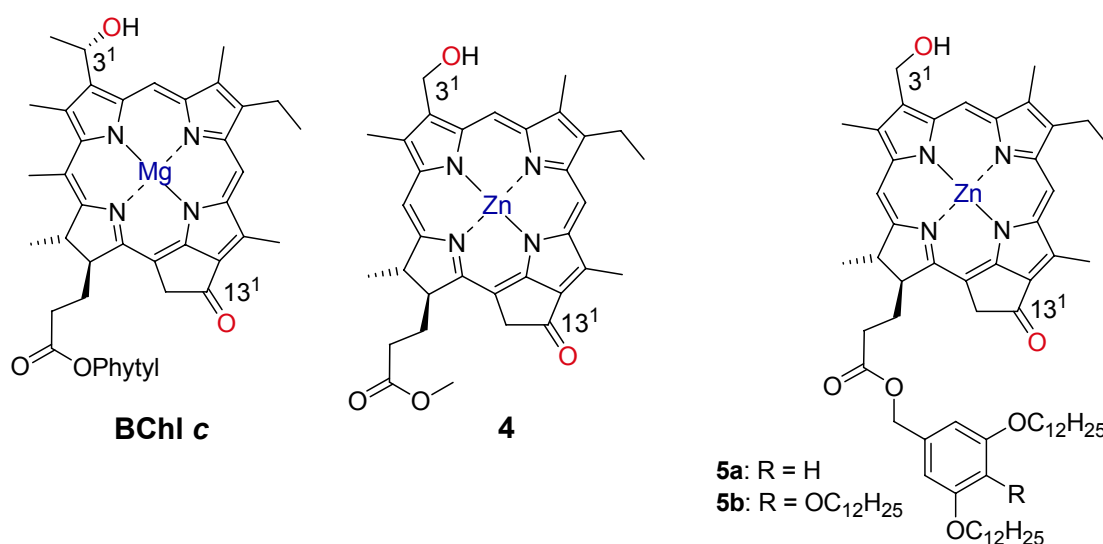


Chart 6. Chemical structures of (A) BChl *c*, (B) the first ZnChl model compound **4**,¹¹⁹ and (C) ZnChl model compound **5** forming soluble aggregates.¹⁵

The advantages of ZnChl model systems in comparison to BChl are firstly a better availability, since ZnChl can be derived from algae which are rich in Chl *a* via a semi-synthetic approach. Secondly, the coordination of the chlorin to a central zinc ion provides a better chemical stability than a magnesium ion, since the magnesium derivatives are easily demetallated in the presence of traces of acids. It is also advantageous that ZnChls can be easily functionalized in the 17³ position by long alkyl chains that provide a better solubility of the model aggregates in nonpolar aprotic solvents and prevent further aggregation to multi-rod structures.¹⁵

Light-Harvesting Properties of ZnChl Antennae

For the utilization of the absorbed light energy in a potential device the energy should be concentrated rapidly in an energy trap, to which an artificial RC might be attached. Tamiaki, Holzwarth, and co-workers succeeded to funnel the energy of the ZnChl rod antenna to a metal-free bacteriochlorin acceptor.¹²²⁻¹²³ The latter was covalently linked to the self-assembling ZnChl building block in the 17³ position. The acceptors are not capable of co-aggregating with the ZnChl moieties, because they lack both a central metal ion and a 3¹ hydroxy group. Aggregates were generated in *n*-hexane/THF (1%) using a 50:1 mixture of ZnChl **4** and the ZnChl-acceptor dyad **6** (Chart 7).

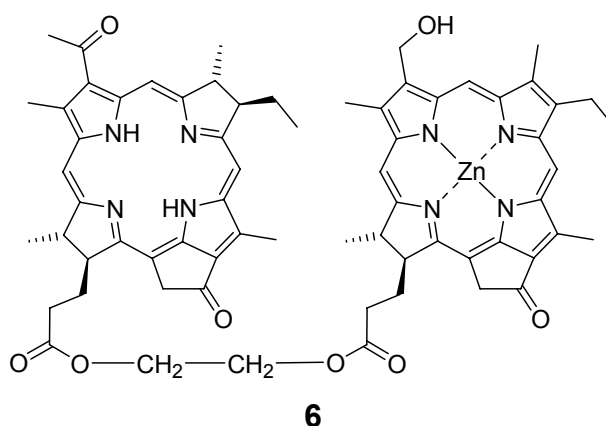


Chart 7. Dyad **6** consisting of a self-assembling ZnChl moiety and a metal-free bacteriochlorin unit.

The absorption maximum of the aggregate was located at 740 nm, remaining uninfluenced by the presence of the acceptor units (Figure 28). A shoulder appears at ~800 nm, reflecting the absorption of the metal-free bacteriochlorin trap that is substantially red-shifted compared to the absorption of the free monomers with a maximum around 750 nm. This red-shift was attributed to excitonic interaction with the aggregated pigments. The Stokes-shift of the Q_y band of ZnChl aggregates is

typically quite small (8-15 nm), which is a characteristic feature for excitonically coupled *J*-type aggregates. Energy transfer from the ZnChl aggregate to the acceptor moieties was observed by the emission and excitation spectra of **6** indicating a quenching effect of about 50%. In an aqueous solution of a mixture of **4** and **6** in the presence of α -lecithin as a lipid the transfer efficiency was increased up to >60%.¹²⁴

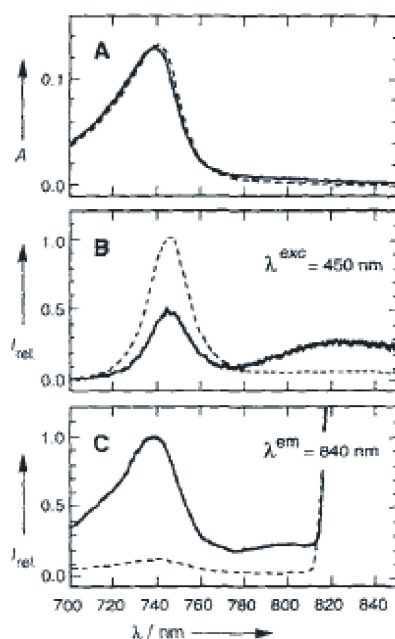
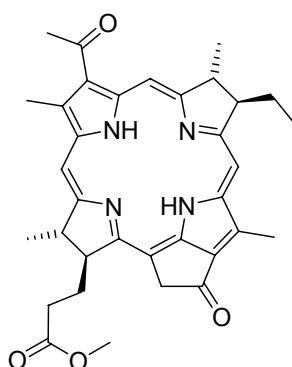


Figure 28. (A) Visible absorption, (B) corrected fluorescence, and (C) corrected fluorescence excitation spectra of **4** (dashed lines) and a 50:1 mixture of **4** and **6** (solid lines) in *n*-hexane/ THF (1%). Reprinted from ref. 123. Copyright (1996), with permission from Wiley-VCH Verlag GmbH & Co. KGaA.

However, the authors state that the presently measured transfer efficiency would represent only the lower limit to the possible maximal transfer efficiency if the energy arriving on the acceptor could be converted rapidly into some other form of energy. This could be achieved by coupling of the present energy acceptor with an energy user, e. g. in the form of photoinduced electron-transfer.

Furthermore, small amounts of isolated bacteriochlorins and metal-free chlorins such as compound **7** (Chart 8) can co-aggregate with **4** even though the former molecules lack the central metal atoms and the 3¹ hydroxy groups.¹²² In the co-aggregate bacteriochlorins or metal-free chlorins again act as excitation energy traps. The trapping process in co-aggregates of **4** and **7** is followed by radiationless deactivation of the energy acceptors. However, a functional antenna system requires that the acceptor energy is not wasted by radiationless dissipation but it should be available

in the form of light emission as in the above case of co-aggregates of compounds **4** and **7**.



7

Chart 8. Molecular structure of the metal-free energy trapping molecule **7**.

The energy transfer from the supramolecular ZnChl assemblies to the attached energy traps has been investigated in more detail by time-resolved fluorescence spectroscopy with a time resolution of ~ 2 ps.^{125,126} To observe reducing conditions, before the spectroscopic measurements sodium dithionite was added to the aggregate solution. With such reducing conditions, the attempt was made to eliminate the small amounts of ZnChl cations, which are formed by photoautooxidation upon illumination in the presence of molecular oxygen. Once formed, such cations remain in the aggregates and act as very efficient quenchers. These quenching processes are responsible for the generally low fluorescence quantum yields of ZnChl aggregates. A dependence of the fluorescence on redox conditions has as well been found for natural chlorosomes and might be caused by analogous quenching processes.¹²⁷

The excitation kinetics of the antenna aggregate of **4** without energy trap can be described by four exponentials ranging from 16 ps to ~ 1 ns (Figure 29). It has been reported that the shortest lifetime components of the multi-exponential decay are most likely due to energy transfer processes between different excitonic levels of **4** aggregates characterized by different radiative lifetimes.¹²⁵

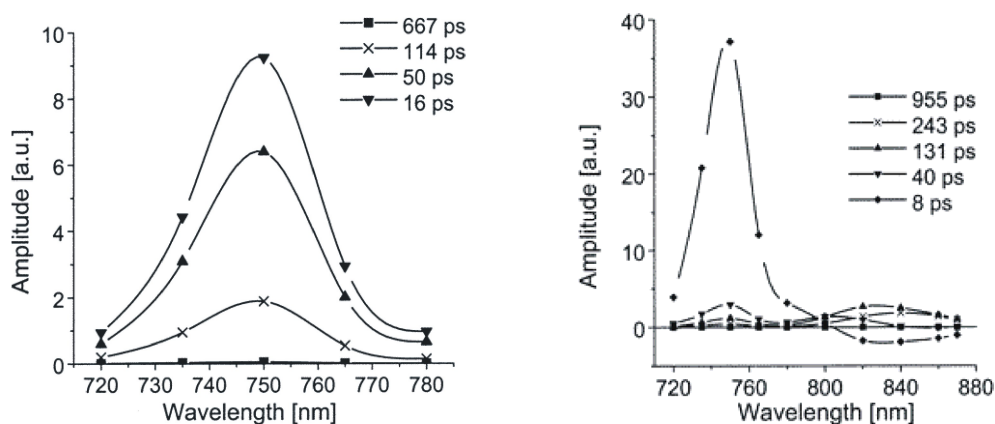


Figure 29. DAS of ZnChl **4** aggregates (left, $\lambda_{\text{ex}} = 713$ nm) and of co-aggregates of ZnChl **4** and metal-free energy trap **7** in the ratio 25:1 (right, $\lambda_{\text{ex}} = 710$ nm) in aqueous α -lecithin solution. Reprinted from ref. 125. Copyright (2002), with permission from the American Chemical Society.

In a further experiment, time-resolved fluorescence spectroscopy was carried out for a mixture of ZnChl **4** and metal-free compound **7** in the ratio 25:1. DAS of the co-aggregates revealed an energy transfer component with an 8 ps lifetime.¹²⁶ This component shows strongly positive amplitudes in the wavelength range of the ZnChl aggregate emission (~ 720 - 770 nm) and turns negative for the trap emission region (~ 810 - 870 nm). The efficiency of this energy transfer was calculated from the following relationship:

$$\phi_{ET} = \frac{k_{ET}}{k_{ET} + k_D}; k = \frac{1}{\tau} \quad (11)$$

where ϕ_{ET} is the energy transfer efficiency, k_{ET} is the energy transfer rate, and k_D is the donor fluorescence decay rate in the absence of the acceptor. For this calculation the average lifetime of the donor aggregate ($\tau_{av} = 17$ ps) was used giving an energy transfer efficiency of $\sim 70\%$. Average lifetimes were calculated as

$$\tau_{av} = \frac{\sum a_i \tau_i}{\sum a_i} \quad (12)$$

where τ_i are the lifetimes and a_i are the associated amplitudes at the respective observation wavelengths.

Time-resolved fluorescence studies on co-aggregates of ZnChl **4** and ZnChl-trap molecule dyads such as compound **6** have been performed as well.¹²⁵ The DAS of this measurement are depicted in Figure 30. The energy transfer from the ZnChl rod to the co-aggregate traps occurs with 7 ps lifetime and exhibits an efficiency of 68%.

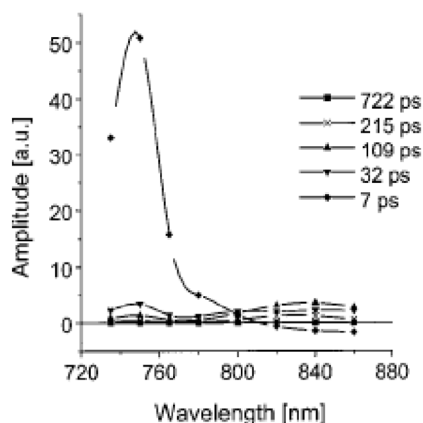


Figure 30. DAS of co-aggregates of ZnChl **4** and dyad **6** aqueous α -lecithin solution; $\lambda_{\text{ex}} = 710$ nm. Reprinted from ref. 125. Copyright (2002), with permission from the American Chemical Society.

The ratio between negative and positive amplitudes of the energy transfer components is in the range of 20:1 to 30:1. It was deduced quantitatively that this large ratio can only be explained if the excitation energy is delocalized over at least 10-15 molecules within the aggregate at room temperature.¹²⁵ This number actually resembles the delocalization length, which has been observed previously for chlorosomes of *Chloroflexus aurantiacus* at 1.27 K using transient absorption technique.⁹³ Thus, ZnChl rod aggregates are not only appropriate structural, but also very good functional model systems for the highly efficient LH systems of green and filamentous bacteria.

2.3.2 Porphyrin Assemblies

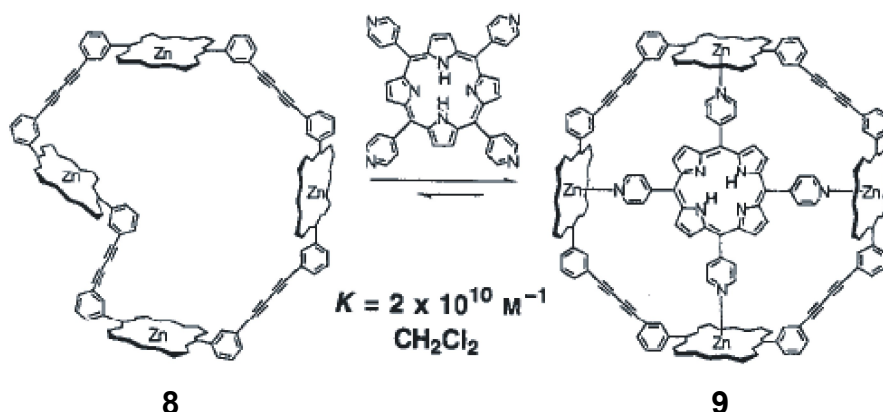
Inspired by the wheel-like architecture of photosynthetic pigments in purple bacterial LH complexes, in recent years various groups have started to develop artificial antennae consisting of circular porphyrin arrays, in order to mimic the natural LH systems and to find new applications as optoelectronic materials. The advantages of ring-shaped porphyrin arrays over linear analogues in intramolecular energy transfer

have been discussed in the literature.¹²⁸ The kinetics of energy migration in weakly coupled multipigment arrays has been modelled. As a result it was predicted that cyclic array architectures exhibit higher quantum efficiencies for energy transfer to an acceptor than linear architectures with equal numbers of pigments. Thus, different covalent¹²⁹ and metal-coordinated¹³⁰ porphyrin cycles¹³¹ were designed and several attempts have been undertaken to observe rod-like porphyrin assemblies.

However, one disadvantage of porphyrins as building blocks for supramolecular LH systems is the relatively low intensity of their Q_x and Q_y absorption bands in comparison to those of chlorins.³⁴ The lower intensities of porphyrin bands are responsible for weaker excitonic interactions between the chromophores.⁶¹

Covalent Porphyrin Cycles

The first challenge for the design of circular, covalent porphyrin LH systems was to achieve a rigid ring structure. Anderson, Sanders, and co-workers synthesized the cyclic tetramer **8**, which is existent in different conformations (Scheme 2).¹³²



Scheme 2. One possible conformer of cyclic tetramer **8** and the complex formed with a tetrapyrrolylporphyrin ligand. Reprinted from ref. 132. Copyright (1995), with permission from Wiley-VCH Verlag GmbH & Co. KGaA.

Complexation of a tetrapyrrolylporphyrin ligand locks the tetramer in a single symmetrical, square-type conformation. Complex **9** represents a model system for the LH-I-RC complex of purple bacteria, since photoexcitation of **9** at 411 nm results predominantly in electron-transfer from the zinc porphyrin units to the included free-base porphyrin as indicated by complete fluorescence quenching of **9**.

Lindsey and co-workers synthesized several shape-persistent cyclic porphyrin hexamers such as compound **10** consisting of an alternating arrangement of zinc and

free-base porphyrins (Chart 9).¹³³⁻¹³⁷ Time-resolved spectroscopy revealed energy transfer from zinc porphyrins to adjacent free-base porphyrins with a 34 ps time constant and a quantum efficiency of 99%. Various dipyrridyl-substituted porphyrin ligands were complexed as “spokes” by the porphyrin hexamers. Upon photoexcitation of the wheels energy transfer to the spokes was observed showing maximum efficiencies of 75%.

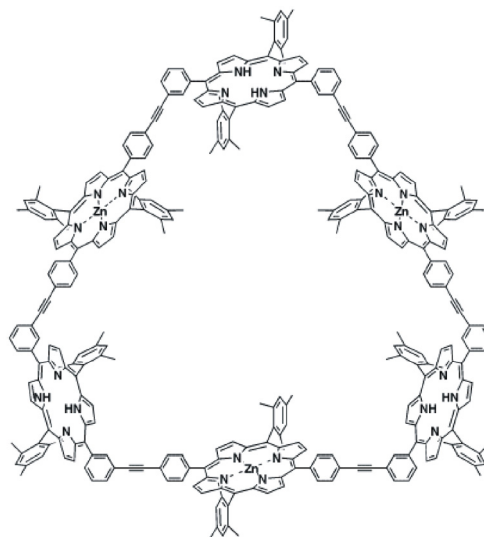
**10**

Chart 9. Cyclic hexamer **10**. Reprinted from ref. 129. Copyright (2004), with permission from Wiley-VCH Verlag GmbH & Co. KGaA.

For more efficient energy transfer between covalently linked porphyrin molecules a direct connection without any linkers was expected to be most promising. Thus, Osuka, Kim, and coworkers synthesized the dodecameric porphyrin wheel **11** and the tetracosameric cycle **12** (Figure 31) containing only six 1,3-phenylene linkers. Such linkers are required to provide the bending of the oligomers.¹³⁸⁻¹⁴⁰

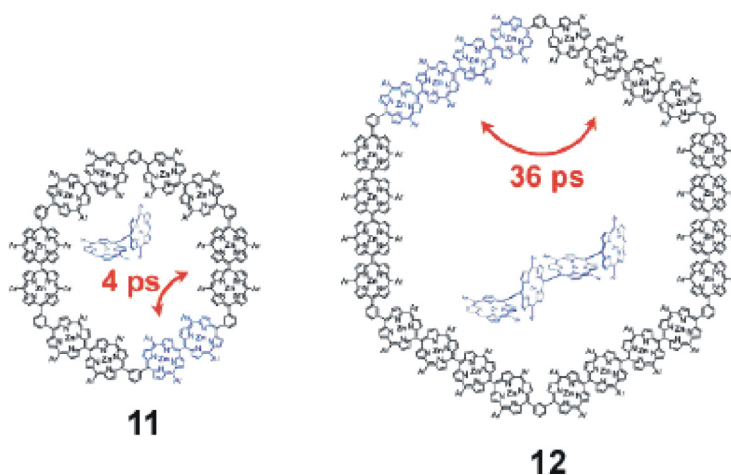


Figure 31. Covalent porphyrin cycles **11** and **12**. Reprinted from ref. 140. Copyright (2007), with permission from the American Chemical Society.

Oligoporphyrins **11** and **12** exhibit strong absorption bands in the blue and green wavelength region. The absorption spectra of **11** and **12** and the respective bis- or tetraporphyrin subunits are depicted in Figure 32. In these subunits the porphyrin dyes are excitonically coupled. The splitting energy due to exciton coupling becomes more pronounced in the absorption spectrum of **12**.

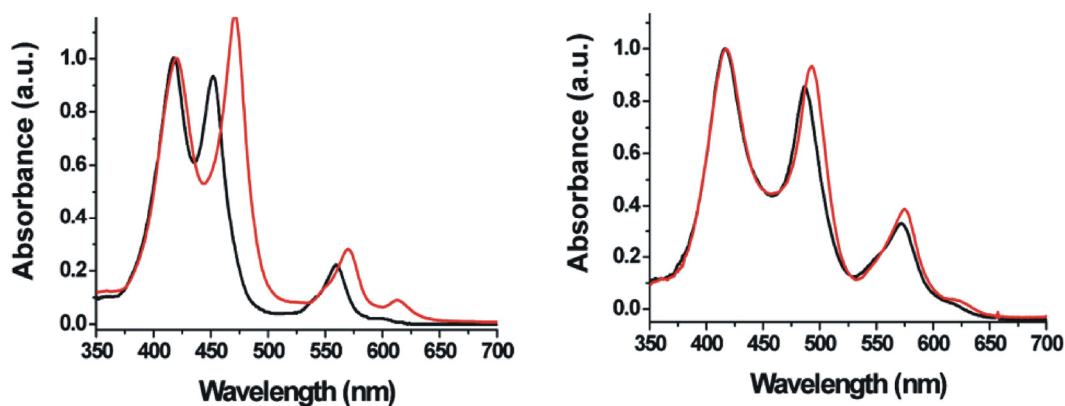
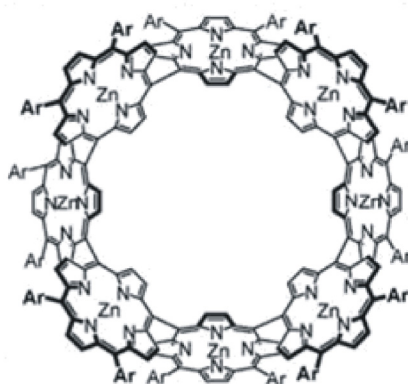


Figure 32. Absorption spectra of cycle **11** (black line) and its bisporphyrin subunit (red line) (left) and of cycle **12** (black line) and its tetraporphyrin building block (red line) (right). Reprinted from ref. 140. Copyright (2007), with permission from the American Chemical Society.

The excitation energy transfer along the rings has been confirmed by time-resolved fluorescence spectroscopy and transient absorption anisotropy measurements. For the smaller cycle **11** transfer rates of 4 ps between neighboring bisporphyrin subunits have been observed, while energy transfer between the tetraporphyrin subunits of **12** proceeds with a time constant of 36 ps. The energy transfer between the different

subunits proceeds via the Förster mechanism, since complete delocalization of excitation energy in **11** and **12** is impeded by the meta-phenylene linker molecules.

Recently, Osuka and coworkers synthesized porphyrin ring **13**, which does not exhibit any linker molecules (Chart 10).¹⁴¹ The absorption spectrum of **13** exhibits a broad non-split Soret absorption band at 460 nm. The excitation energy hopping time constant equals 236 fs, indicating strong electronic coupling between the neighboring porphyrins. Compound **13** shows the fastest excitation energy transfer within covalent porphyrin cycles so far.



13

Chart 10. Structure of directly linked porphyrin ring **13**. Reprinted from ref. 141. Copyright (2007), with permission from Elsevier.

Metallo Supramolecular Porphyrin Cycles

Metal-coordinated supramolecular porphyrin squares find applications in various research fields such as catalysis.¹⁴² However, in such an arrangement excitonic interaction between the four porphyrins has not been observed. Nevertheless, energy which is collected by square **14** is transmitted to a dipyrindyl-substituted free-base porphyrin guest with an efficiency of 90% (Chart 11).¹⁴³

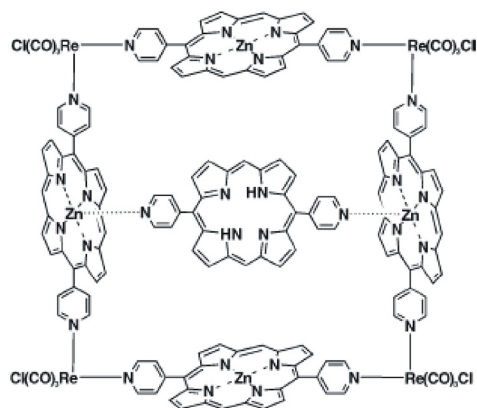
**14**

Chart 11. Host-guest complex **14** consisting of a supramolecular zinc porphyrin square and a dipyridyl-substituted free-base porphyrin ligand. Reprinted from ref. 143. Copyright (1997), with permission from Wiley-VCH Verlag GmbH & Co. KGaA.

Hunter and co-workers have synthesized the unsymmetrical cobalt porphyrin **15** bearing two pyridine ligands, which self-assembles to form a dodecameric macrocyclic array (Figure 33).¹⁴⁴ In this cycle, the chromophores are too far apart to show strong excitonic coupling in the absorption spectrum and, unfortunately, cobalt quenches the porphyrin fluorescence. Thus, any analysis of the energy transfer properties of this system is impeded.

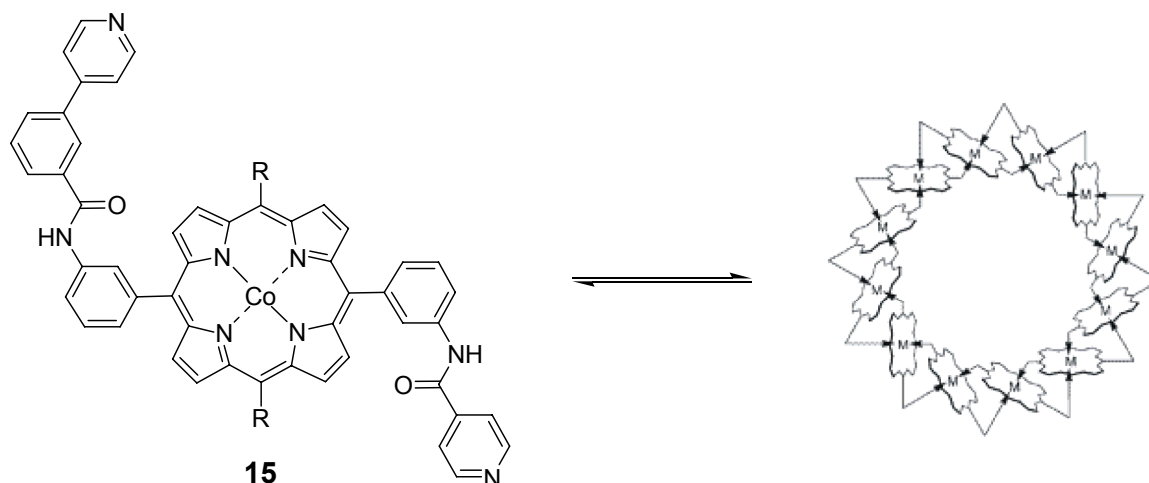
**15**

Figure 33. Cobalt porphyrin **15** self-assembles to form a macrocyclic dodecamer. Reprinted from ref. 144. Copyright (2000), with permission from the American Chemical Society.

Kobuke and co-workers used 1,3-phenylene-linked zinc porphyrin dimers as supramolecular building blocks for the cyclic hexamer **16** (Chart 12).¹⁴⁵ The absorption spectrum of **16** revealed a large split of the Soret bands, indicating

excitonic coupling which occurs for the slipped-cofacial as well as for the phenylene-bridged porphyrin neighbors.

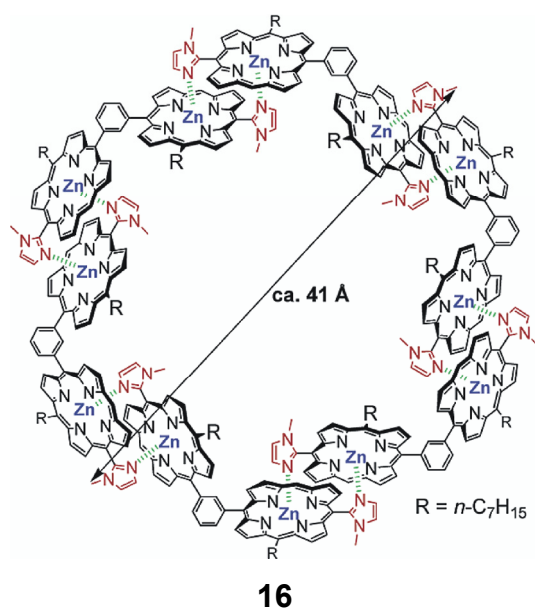


Chart 12. A structural model of the cyclic hexamer **16**. Reprinted from ref. 145. Copyright (2003), with permission from the American Chemical Society.

To increase the stability of these metallosupramolecular arrays, macrocycle **16** and the analogous pentamer were covalently fixed by olefin metathesis reactions, giving compounds **17** and **18** (Chart 13).^{146,147} The energy hopping time constants through the coordination dimer units were determined by the analysis of anisotropy depolarization of the transient absorption spectra after polarized light excitation. Furthermore, exciton-exciton annihilation rates were observed from the pump power dependence of the transient absorption. The resulting time constants for energy transfer between two phenylene-bridged porphyrins within the cycle equal 8.0 ps for the pentamer **17** and 5.3 ps for the hexamer **18**. Energy transfer between two slipped cofacial porphyrin units is faster proceeding with a time constant of 0.2 ps in both cases. The emission lifetime of **17** and **18** is 2.2 ns, thus, rapid energy transfer should take place 300-400 times within the cycle during its excited state lifetime. Accordingly, macrocycles **17** and **18** seem to be well-defined structural and functional antenna models for the cyclic LH systems of purple bacteria.

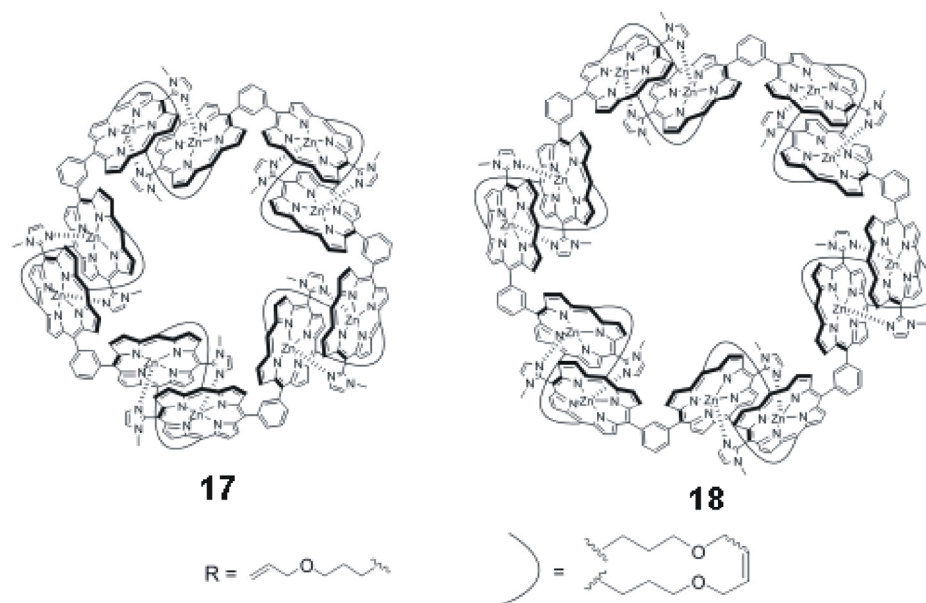
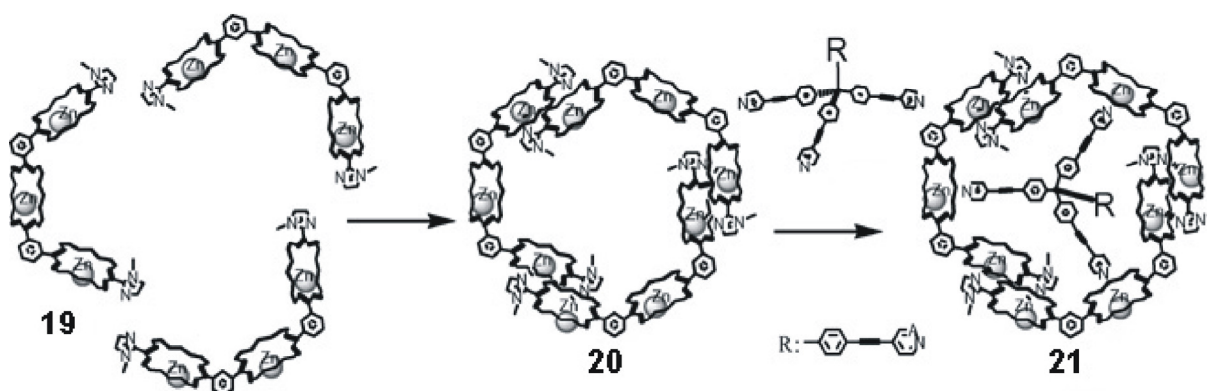


Chart 13. Molecular structures of cyclic zinc porphyrin arrays **17** and **18**. Reprinted from ref. 146. Copyright (2005), with permission from Wiley-VCH Verlag GmbH & Co. KGaA.

Compound **19** consists of three zinc porphyrin chromophores bridged by 1,3-substituted phenylene linkers and functionalized with imidazolyl groups at the molecular terminals (Scheme 3).¹⁴⁸ Only the two terminal porphyrins in **19** are used in the formation of the cyclic trimer **20** by complementary coordination. The three remaining free porphyrinato-Zn(II) sites in **20** can serve to bind a tetrapodal pyridine guest molecule. It is of great interest to adjust an electron acceptor to the fourth ligand arm in order to obtain a model of the LH-I-RC complex.¹⁴⁹



Scheme 3. Self-assembly of trisporphyrin **19** into macrocyclic trimer **20** accommodating a tripodal pyridyl ligand. Reprinted from ref. 130. Copyright (2006), with permission from Wiley-VCH Verlag GmbH & Co. KGaA.

Supramolecular Porphyrin Rods

Nanotubes which are entirely composed of porphyrins have been obtained by ionic self-assembly of the two oppositely charged synthetic porphyrin molecules **22** and **23** (Chart 14).¹⁵⁰

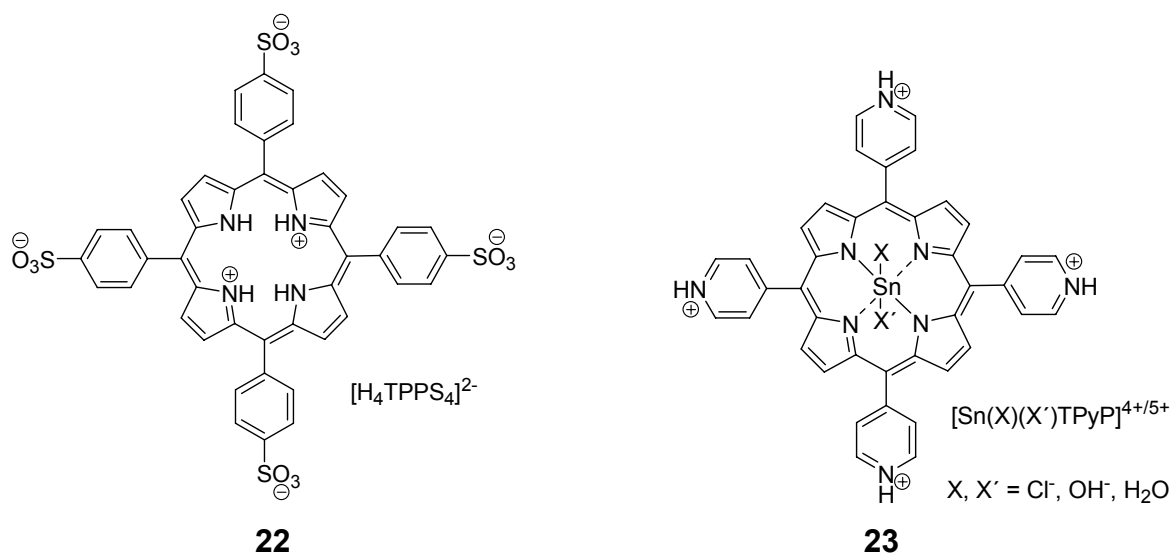


Chart 14. Porphyrins **22** and **23** used in making nanotubes.¹⁵⁰

Transmission electron microscope (TEM) images of the porphyrin nanotubes confirmed a hollow tubular structure and revealed that the cylinders are micrometers in length and have diameters in the range of 50-70 nm with approximately 20 nm thick walls (Figure 34).

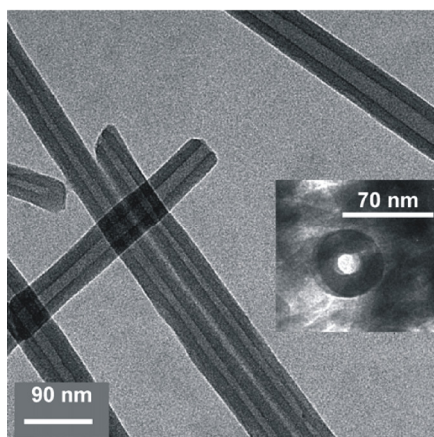


Figure 34. TEM image of porphyrin nanotubes consisting of co-aggregated compounds **22** and **23**. Reprinted from ref. 150. Copyright (2004), with permission from the American Chemical Society.

Absorption spectroscopy showed *J*-type aggregation behaviour as indicated by bathochromically shifted Q_y and Soret bands. However, no aggregation model has been proposed by Shelnut and co-workers so far and the examination of excitation energy transport has not yet been reported.

2.3.3 Cyanin Assemblies

Another tubular supramolecular LH system only consisting of chromophoric building-blocks has been investigated by Dähne and co-workers.¹⁵¹ In a 10^{-2} M aqueous NaOH solution the amphiphilic dye **24** forms rod-type, double-walled structures exhibiting a threefold split *J*-absorption band with maxima at 562, 583, and 600 nm (Figure 35).¹⁵²

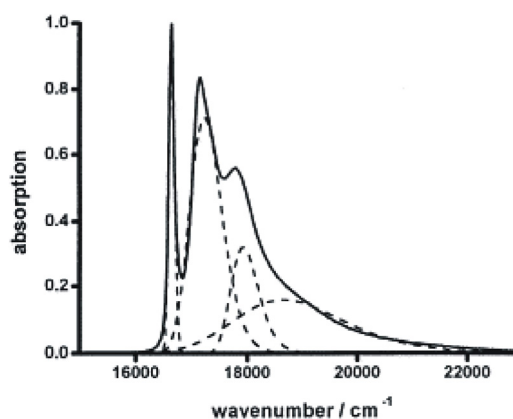
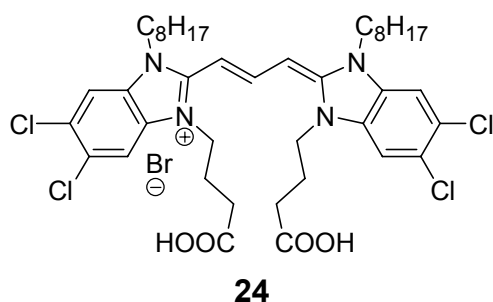


Figure 35. Left: Molecular structure of amphiphilic dye **24**. Right: Absorption spectrum of **24** aggregates in 10^{-2} M aqueous NaOH solution. Reprinted from ref. 152. Copyright (2002), with permission from Elsevier.

According to cryogenic TEM images 3-10 cylindrical strands form micrometer-sized, rope-like superhelices (Figure 36).¹⁵³ The diameter of a single cylinder is about 9-10 nm. The cylinders are composed of bilayers whose structure is held together by the hydrophobic interaction of octyl chains. The acidic carboxypropyl substituents of the inner layer point to the center of the cylinder and that of the outer layer interact with the surrounding water molecules.

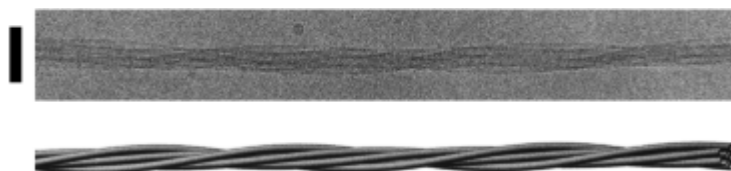


Figure 36. Top: Cryo-TEM picture of a **24** aggregate that consists of five single strands. Scale bar: 50 nm. Bottom: A simple model that consists of a bundle of tubules that are twisted around each other. Reprinted from ref. 153. Copyright (2000), with permission from Wiley-VCH Verlag GmbH & Co. KGaA.

The lowest exciton state is polarized along the cylinder axis, while the second state is polarized perpendicular to it. Since these exciton states cannot be explained by Kasha's theory for dimer aggregates,^{54,56} the exciton model was extended to cylindrical *J*-aggregates by Bendarz and Knoester.¹⁵⁴ On the basis of this model it was possible to derive the geometrical arrangement of chromophores within the aggregates of **24** (Figure 37).

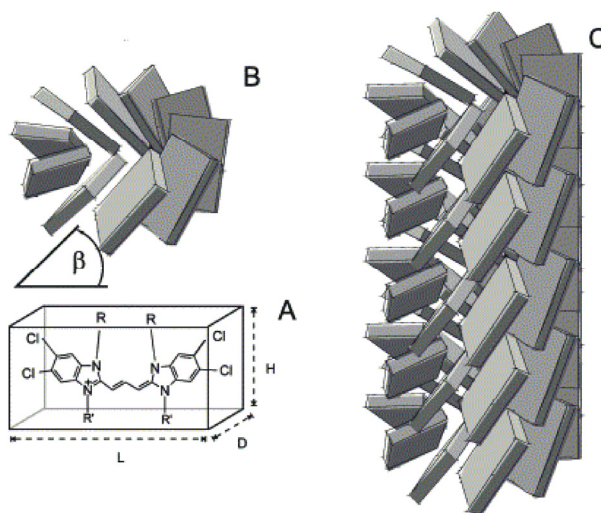


Figure 37. Model for the circular arrangement of the molecules in the **24** aggregates: (A) each dye molecule is represented by a box with the dimensions $L=1.9$ nm, $H=1.0$ nm, and $D=0.4$ nm. The molecular transition dipole moment lies in direction of the long edge of the box. (B) In this example a circle is built by $N_{\text{ring}} = 10$ molecules which are tilted by angle β with respect to the circle plane. (C) A cylinder consisting of a tenfold helix which is formed by putting five rings one upon another. Reprinted from ref. 152. Copyright (2002), with permission from Elsevier.

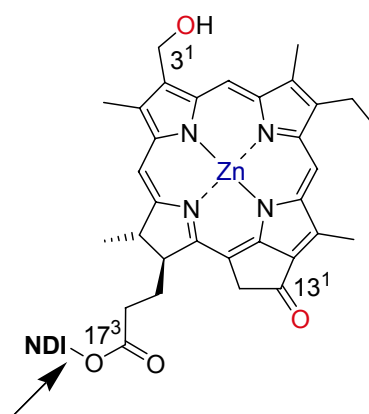
The inner layer of the double-walled cyanine cylinder is based on a 6-membered ring structure, while the outer layer contains 9-membered rings. The tilt angle β was calculated to be 31° and 18° for the inner and the outer cylinder, respectively. Furthermore, this exciton model was useful for the interpretation of the results

obtained by time-resolved fluorescence, transient absorption and ultrafast pump-probe spectroscopy. It was calculated that at 1.5 K the excitons are delocalized coherently over 16 ± 4 molecules along the long axis of the rod and over 6 ± 1 molecules along one ring.¹⁵⁵ Thus, at this temperature the delocalization length is about 95 ± 10 molecules. However, the delocalization length at room temperature has not been evaluated. But already at 81 K, this value decreases to ~ 70 molecules due to increasing static and dynamic disorder at increasing temperature.

Chapter 3: Results and Discussion

3.1 Synthesis

For the attachment of additional chromophores to a chlorin building block the 17³ position was chosen. Regarding Holzwarth's and Schaffner's aggregation model (vide supra),^{9,11} the ZnChl self-assembly process should be least impaired by functionalization at this site.



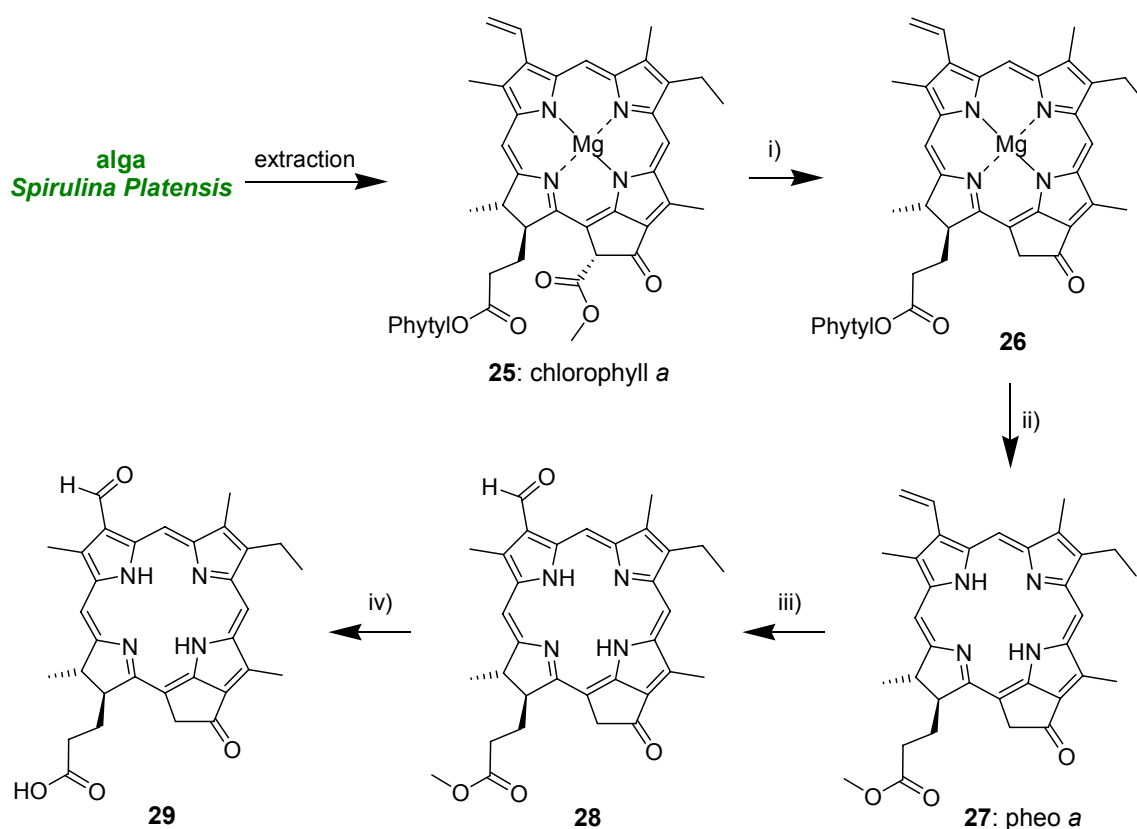
Thus, for the synthesis of target molecules **1-3** a carboxy-functionalized chlorin building block and either hydroxy- or amino-functionalized NDIs were required in order to connect the different moieties by esterification or amidation.

3.1.1 Synthesis of Chlorin and Naphthalene Diimide Precursors

Synthesis of the Literature-Known Chlorin Precursor

The carboxy-functionalized chlorin precursor **29** which was used for the synthesis of all target molecules **1-3** was obtained via a semi-synthetic approach starting from the blue alga *Spirulina Platensis* (Scheme 4). This alga provides an economic access to chlorophyll *a* (**25**), which can be gained by Soxhlet extraction of the dried algae with

acetone according to a slightly modified procedure described by Smith and co-workers.¹⁵⁶ Alternatively, the algae *Spirulina Maxima* or *Spirulina Geitleri* can serve as source for chlorophyll *a*.^{121,156} The raw algae extract was reacted with 2,4,6-trimethylpyridine at high temperature (reaction i), leading to the decarboxylated compound **26**. Subsequent reaction in the presence of concentrated sulphuric acid and methanol (reaction ii) led to demetallation of the central magnesium ion, giving the free-base chlorin. Concurrently, transesterification of the phytol ester group at the 17³ position into a methyl ester took place. The resulting 13²-demethoxycarbonyl pheophorbide *a* methylester (**27**; pheo *a*) was purified by column chromatography and, in contrast to the former compounds, it was storable for several months due to its higher chemical and photochemical stability. All together, extraction of ~800 g *Spirulina Platensis* resulted in ~4 g purified pheo *a* (**27**).

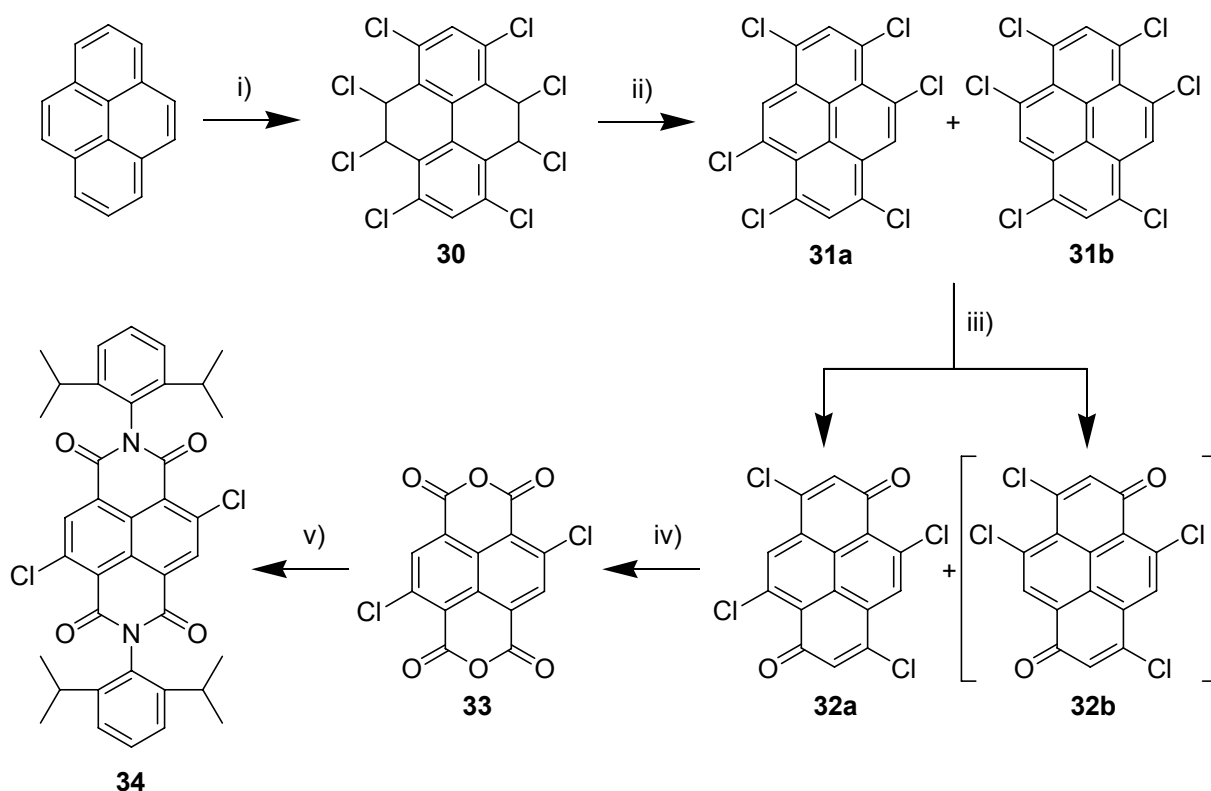


Scheme 4. Literature known synthesis of chlorin building block **29**.^{156,157,122} Reagents and conditions: i) 2,4,6-trimethylpyridine, 160 °C, 6 h; ii) conc. H₂SO₄, MeOH, rt, 16 h; iii) 1. OsO₄, HOAc, H₂O, THF, rt, 1 h; 2. NaIO₄, rt, 3.5 h, yield: 95% of **28**; v) conc. HCl, THF, rt, 3 h, yield: 81% of **29**.

In the next step (iii), the vinyl group at the 3¹ position of pheo *a* (**27**) was dihydroxylated using osmium tetroxide according to a procedure described earlier by Wasielewski and co-workers.¹⁵⁷ Subsequent oxidative cleavage of the diol *in situ* with sodium periodate gave aldehyde **28** in very good yield. In the last reaction (iv) the desired chlorin building block **29** was obtained by saponification of the methyl ester functionality of **28** under acidic conditions.¹²²

Synthesis of the Literature-Known NDI Precursor

Dichlorosubstituted NDI **34** was used as a precursor for all core-disubstituted NDI derivatives presented in this work. The synthesis of **34** starts from pyrene (Scheme 5).



Scheme 5. Literature known and slightly modified synthesis of 2,6-dichlorosubstituted NDI **34**.^{21,23} i) Cl₂ (g), I₂ (in catalytic amounts), 1,2,4-trichlorobenzene, 25-110 °C, 6 h, yield: 36-38% of **30**; ii) KOH, ethanol, 80 °C, 5 h, yield: 96-97% of **31a,b** as isomeric mixture; iii) fuming HNO₃, 0-5 °C, 15 min, yield: 32-45% of **32a** (isomer **32b** was not purified); iv) fuming HNO₃, conc. H₂SO₄, 100 °C, 5 min, yield: 45-49% of **33**; v) 2,6-diisopropylaniline, HOAc, 120 °C, 30 min, yield: 44% of **34**.

The first four steps, i. e. chlorination, HCl elimination, and oxidations, have been described previously by Vollmann and co-workers.¹⁵⁸ However, the procedure reported in this classical publication could not be reproduced satisfyingly. Modification of this procedure resulted in successful synthesis of **34**, which is described in detail in the Experimental Section. In the course of chlorination of pyrene (Scheme 5, reaction i), it is essential to adjust the reaction temperature in particular time intervals. The separation of 2,6- and 2,7-dichloro isomers was achieved at the quinone stage where the 2,6 isomer **32a** precipitated from the reaction mixture. For this reaction, fuming nitric acid was used, instead of concentrated nitric acid used in the previously reported procedure. The *trans* isomer **32a** was separated by filtration and purification could be achieved by sublimation. The ¹H NMR spectrum of **32a** in deuterated concentrated sulfuric acid showed only two signals at 7.96 and 6.76 ppm, which can be taken as an evidence for the isolated *trans* product.²³ Reaction of **33** with 2,6-diisopropylaniline in refluxing glacial acetic acid yielded the corresponding 2,6-dichloro-substituted NDI **34**.²¹ This highly protic solvent activates the carbonyl group whilst the reactivity of the amine is sufficiently low because most amino functions are protonated. Accordingly, imide formation is more favored over substitution of the chlorine atoms.

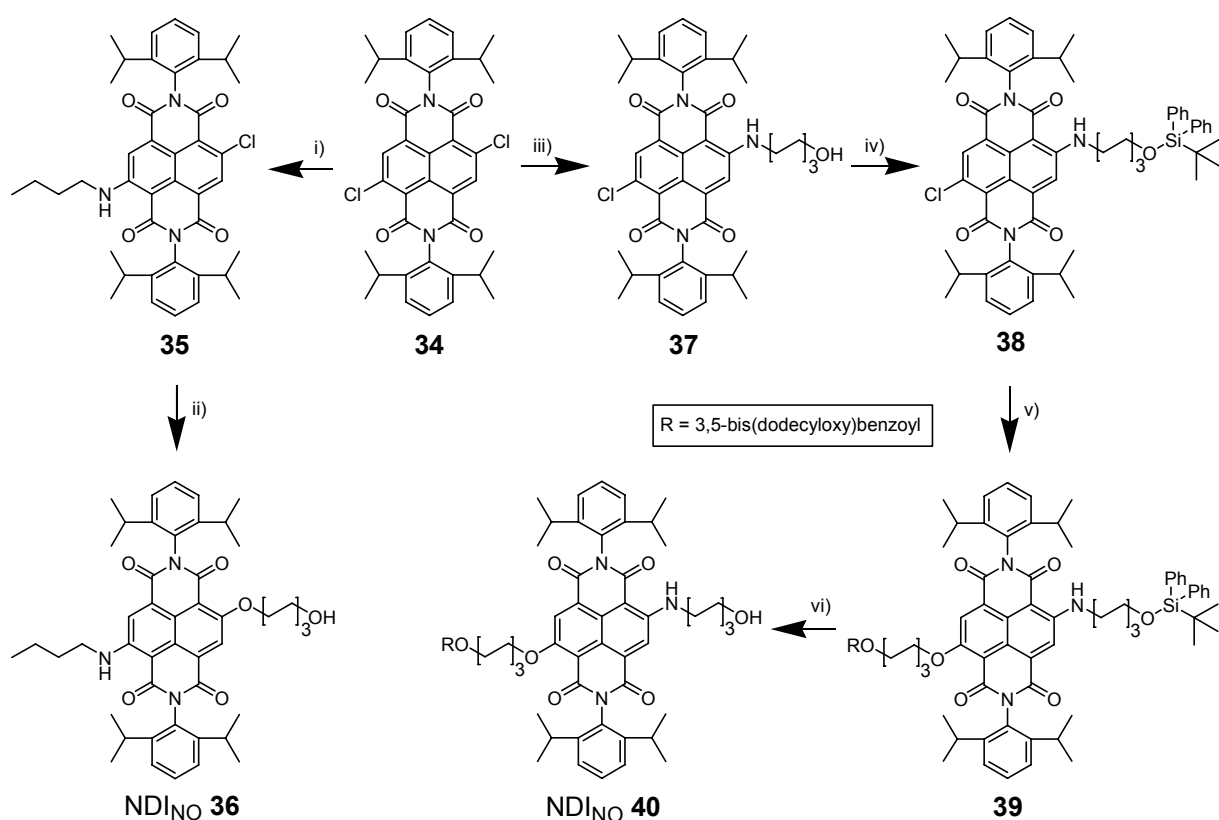
3.1.2 Synthesis of Zinc Chlorin-Naphthalene Diimide Dyads

Synthesis of ZnChl-NDI_{NO} Dyads 1a,b

It has been described in literature that pink colored NDI chromophores can be prepared by stepwise functionalization of the aromatic core with one alkylamino- and one alkyloxy-substituent.²¹ In Scheme 6 the synthetic routes to hydroxy-functionalized pink NDI_{NO} building blocks **36** and **40** starting from the 2,6-dichloro-substituted NDI **34** is depicted. Nucleophilic substitution of one chlorine atom of **34** with *n*-butylamine in dichloromethane was carried out as described in the literature to yield NDI **35** (reaction i).²¹ Subsequently, the remaining chlorine substituent could be replaced by reaction with melted 1,6-hexanediol in the presence of potassium carbonate giving the pink NDI_{NO} **36**.

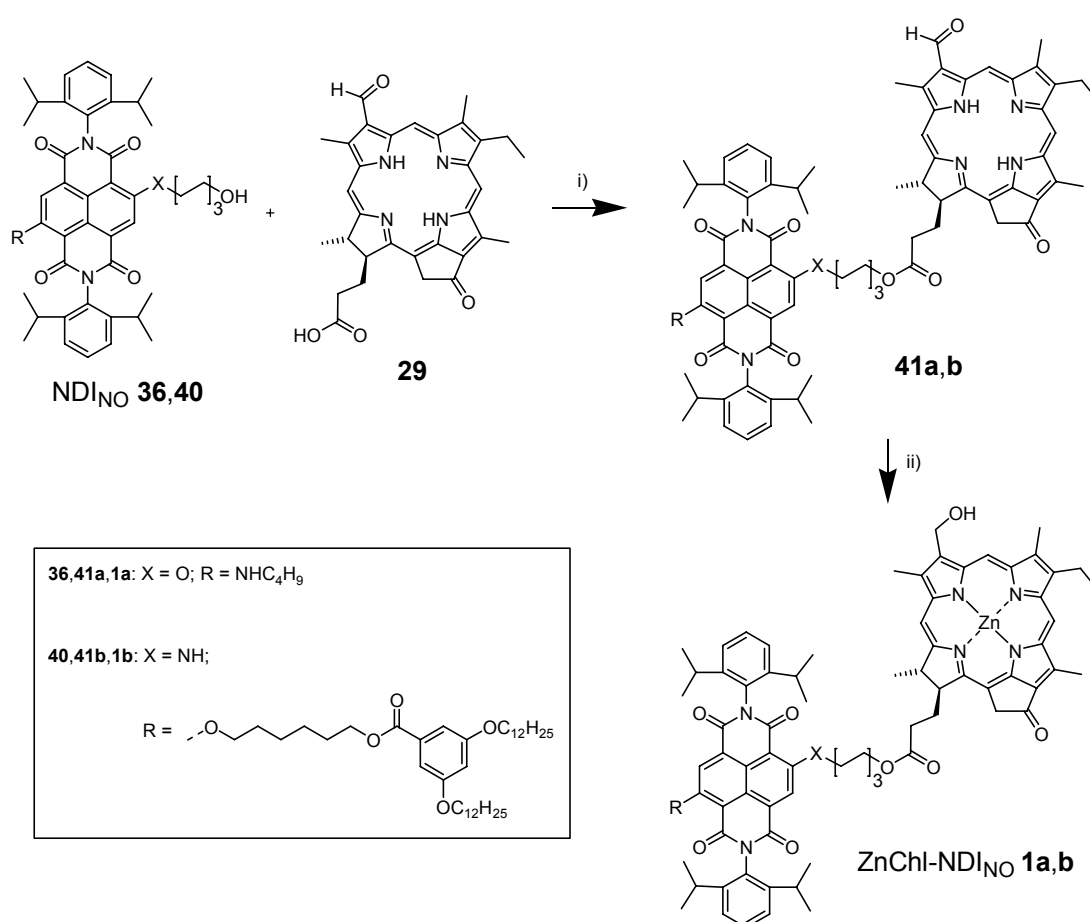
The synthesis of an alternative pink NDI_{NO} building block (**40**) started with nucleophilic substitution of one chlorine atom by 6-aminohexanol in chloroform

resulting in NDI **37** in good yield (reaction iii). Fortunately, the nucleophilic character of the hydroxy group of 6-aminohexanol is not strong enough to substitute a chlorine atom competitively. However, since the remaining chlorine atom of **37** was wished to be replaced by another alkoxy nucleophile, first the hydroxy group had to be protected by quantitative reaction with *tert*-butyldiphenylsilyl chloride (reaction iv). Then, NDI **38** was subjected to nucleophilic substitution with melted 1,6-hexanediol in the presence of potassium carbonate, followed by esterification of the new hydroxy group with 3,5-bis(dodecyloxy)benzoic acid. After cleavage of the silyl protecting group using tetra-*n*-butylammonium fluoride the pink NDI_{NO} **40** was obtained.



Scheme 6. Synthesis of pink NDI_{NO} building blocks **36** and **40**. Reagents and conditions: i) *n*-butylamine, CH₂Cl₂, rt, 2 h, yield: 41%;²¹ ii) 1,6-hexanediol, K₂CO₃, 120 °C, 4 h, yield: 42% of **36**; iii) 6-aminohexanol, CHCl₃, rt, 5 h, yield: 89% of **37**; iv) *tert*-butyldiphenylsilyl chloride, imidazol, DMAP, CH₂Cl₂, ar, rt, 30 min, yield: >99% of **38**; v) 1. 1,6-hexanediol, K₂CO₃, 100 °C, 12 h; 2. 3,5-bis(dodecyloxy)benzoic acid, DCC, DMAP, DPTS, CH₂Cl₂, rt, 3 h, yield: 68% of **39**; vi) tetra-*n*-butylammonium fluoride, THF, ar, rt, 4 h, yield: 64% of **40**.

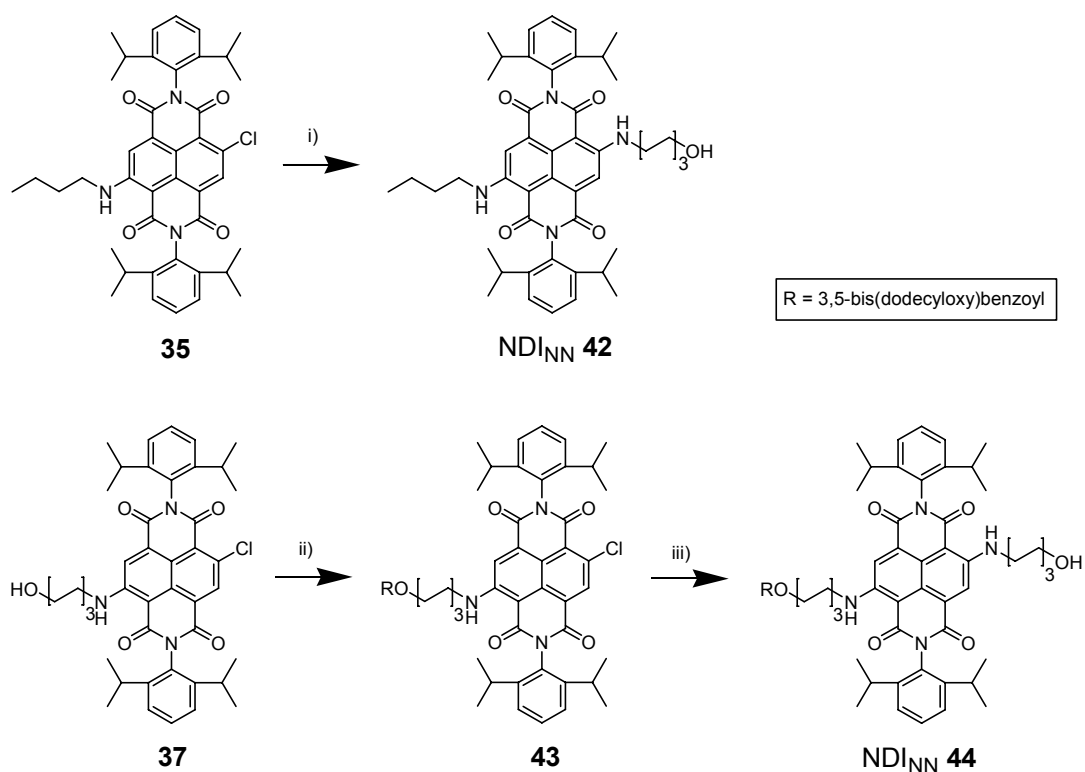
Esterification of chlorin building block **29** with NDI_{NO} chromophores **36** and **40**, respectively, yielded the dyads **41a** and **41b** (Scheme 7). For activation of the carboxylic acid **29** DCC, DMAP, and DPTS in the presence of *N*-ethyl-diisopropylamine and chloroform were applied. Subsequently, selective reduction of the aldehyde group at the 3¹ position of compounds **41a,b** was achieved by using borane-*tert*-butylamine complex. In the last step, reactions of **41a** and **41b**, respectively, with saturated methanolic zinc acetate solution led to zinc metallation of the chlorin chromophore. The resulting target molecules ZnChl-NDI_{NO} **1a** and **1b** both exhibit brownish violet color.



Scheme 7. Synthesis of ZnChl-NDI_{NO} dyads **1a** and **1b**. Reagents and conditions: i) DCC, DMAP, DPTS, *N*-ethyl-diisopropylamine, CH₂Cl₂, ar, rt, 24 h, yields: 40% of **41a** and 39% of **41b**; ii) 1. BH₃(*t*-BuNH₂), CH₂Cl₂, ar, 0 °C, 3-4 h; 2. Zn(OAc)₂ × 2 H₂O, MeOH, THF, ar, rt, 2-6 h, yields: 55% of ZnChl-NDI_{NO} **1a** and 50% of ZnChl-NDI_{NO} **1b**. DCC = dicyclohexylcarbodiimide, DMAP = 4-(dimethylamino)-pyridine, DPTS = 4-(dimethylamino)pyridinium 4-toluenesulfonate.

Synthesis of ZnChl-NDI_{NN} Dyads 2a,b

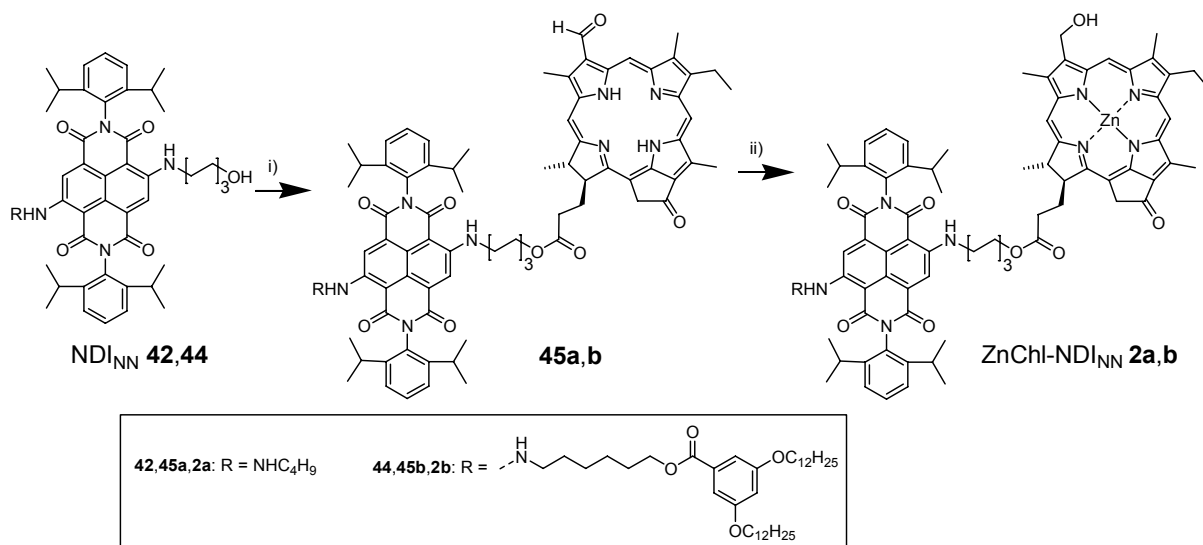
In order to obtain blue colored, fluorescent NDI chromophores, functionalization of the naphthalene core with two alkylamino core-substituents was required. Hydroxy-functionalized NDI_{NN} **42** was prepared from **35** by nucleophilic substitution of the chlorine atom by molten 6-aminohexanol in good yield (Scheme 8, reaction i). For the synthesis of another blue dye, the monoalkylamino-monochloro-substituted NDI **37** was used as a starting material. First esterification with 3,5-bis(dodecyloxy)benzoic acid was carried out to give NDI **43** (Scheme 8, reaction ii). The reaction of **43** with 6-aminohexanol facilitated the nucleophilic substitution of the remaining chlorine atom, resulting in the blue NDI_{NN} **44**.



Scheme 8. Synthesis of blue NDI_{NN} building blocks **42** and **44**. Reagents and conditions: i) 6-aminohexanol, 80 °C, 2 h, yield: 66% of **42**; ii) 3,5-bis(dodecyloxy)benzoic acid, DCC, DMAP, DPTS, CH₂Cl₂, rt, 2 h, yield: 54% of **43**; iii) 6-aminohexanol, 90 °C, 2 h, yield: 80% of **44**.

Esterification of the blue hydroxy-functionalized NDI_{NN} chromophores **42** and **44**, respectively, with chlorin **29** led to dyads **45a,b** (Scheme 9, reaction i). Subsequent reduction of the 3¹ aldehyd functionality to a primary hydroxy group followed by zinc metallation of the free-base chlorin moiety provided the greenish blue ZnChl-NDI_{NN} dyads **2a** and **2b**. Dyads **1** and **2** were all purified by preparative

HPLC and characterized by $^1\text{H-NMR}$ and H,H-COSY NMR spectroscopy, high-resolution ESI mass spectrometry, and UV-vis absorption spectroscopy.

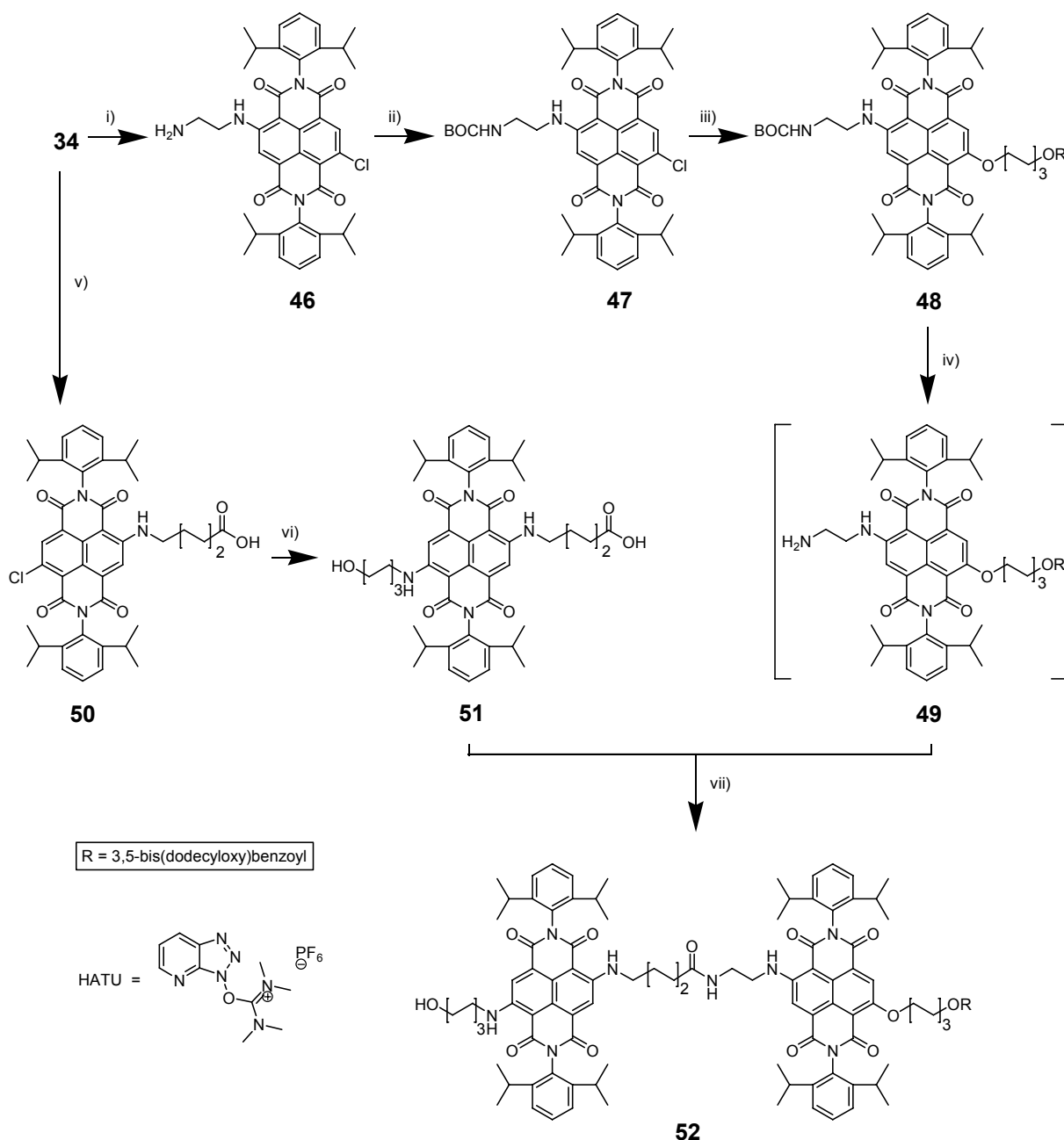


Scheme 9. Synthesis of ZnChl-NDI_{NN} dyads **2a** and **2b**. Reagents and conditions: i) **29**, DCC, DMAP, DPTS, *N*-ethyl-diisopropylamine, CHCl_3 , ar, rt, 24 h, yields: 43% of **45a** and 43% of **45b**; ii) 1. $\text{BH}_3(\text{t-BuNH}_2)$, CH_2Cl_2 , ar, 0°C , 4 h; 2. $\text{Zn}(\text{OAc})_2 \times 2 \text{H}_2\text{O}$, MeOH, THF, ar, rt, 2-6 h, yields: 59% of ZnChl-NDI_{NN} **2a** and 59% of ZnChl-NDI_{NN} **2b**.

3.1.3 Synthesis of a ZnChl-NDI_{NN}-NDI_{NO} Triad

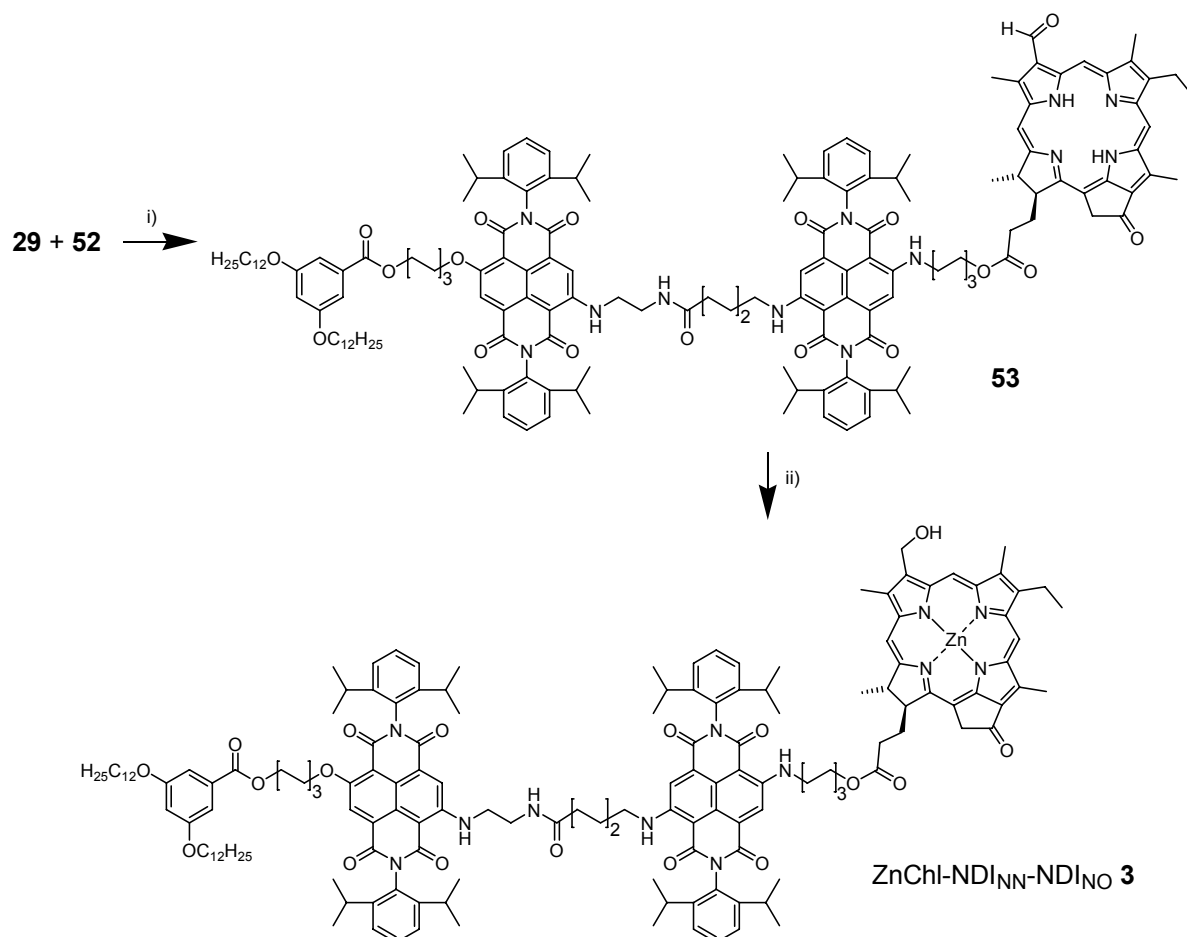
In this section, the preparation of a supramolecular building block containing three different chromophores is described. The synthetic route started with the connection of a pink NDI_{NO} and a blue NDI_{NN} unit (Scheme 10). In the first step of the synthetic pathway to the marginal NDI_{NO} moiety, NDI **46** was prepared using ethylene diamine as described in the literature (reaction i).²¹ Then, the amino group of **46** was protected by a *tert*-butyloxycarbonyl (BOC) group to obtain NDI **47** in good yield. The alkoxy-core-substituent was introduced by reaction of **47** with melted 1,6-hexanediol using potassium carbonate as a base. After subsequent esterification of the new hydroxy group with 3,5-bis(dodecyloxy)benzoic acid compound **48** was isolated. Cleavage of the BOC group yielded the pink colored NDI_{NO} building block **49** as a primary amine. For the synthesis of the middle blue NDI_{NN} chromophore, first the literature-known preparation of NDI **50** was applied.²¹ NDI_{NN} **51** was synthesized from NDI **50** by nucleophilic substitution with 6-aminohexanol. Coupling of amine **49** and

carboxylic acid **51** was achieved by amidation in the presence of HATU, giving the violet colored dyad $\text{NDI}_{\text{NN}}\text{-NDI}_{\text{NO}}$ **52**.



Scheme 10. Synthesis of hydroxy-functionalized $\text{NDI}_{\text{NN}}\text{-NDI}_{\text{NO}}$ building block **52**. Reagents and conditions: i) ethylene diamine, CH_2Cl_2 , rt, 24 h, yield: 48% of **46**;²¹ ii) BOC_2O , CH_2Cl_2 , rt, 30 min, yield: 87% of **47**; iii) 1. 1,6-hexanediol, K_2CO_3 , 80 °C, 6 h; 2. 3,5-bis(dodecyloxy)benzoic acid, DCC, DMAP, DPTS, *N*-ethyl-diisopropylamine, CH_2Cl_2 , rt, 3 h, yield: 55% of **48**; iv) CF_3COOH , CH_2Cl_2 , rt, 30 min, yield: 96% of **49**; v) 6-aminohexanoic acid, DBU, CH_2Cl_2 , rt, 16 h, yield: 63% of **50**;²¹ vi) 6-aminohexanol, 80 °C, 2 h, yield: 91% of **51**; vii) HATU, *N*-ethyl-diisopropylamine, CH_2Cl_2 , rt, 5 min, yield: 62% of **52**. HATU = O-(7-Azabenzotriazole-1-yl)-*N,N,N'*-tetramethyluronium hexafluorophosphate.

Finally, the pink-blue dyad **52** was esterified with chlorin acid **29** (Scheme 11). The aldehyde functionality of the resulting triad **53** was again reduced using borane-*tert*-butylamine complex at 0 °C. In the last step, zinc metallation of the chlorin unit resulted in the black colored triad ZnChI-NDI_{NN}-NDI_{NO} **3**.



Scheme 11. Synthesis of ZnChI-NDI_{NN}-NDI_{NO} triad **3**. Reagents and conditions: i) DCC, DMAP, DPTS, *N*-ethyl-diisopropylamine, CH₂Cl₂, ar, 35 °C, 24 h, yield: 26% of **53**; ii) BH₃(*t*-BuNH₂), CH₂Cl₂, ar, 0 °C, 3 h; Zn(OAc)₂ × 2H₂O, MeOH, THF, ar, rt, 16 h, yield: 66% of ZnChI-NDI_{NN}-NDI_{NO} **3**.

3.2 Solvent-Dependent Self-Organization

In Chapter 3.2, the examination of the aggregation process of dyads **1,2** and triad **3** into supramolecular LH systems is investigated. Thus, the UV-vis absorption, steady state emission, CD, and AFM properties of the multichromophoric supramolecular building blocks **1-3** are recorded and the results are discussed comparatively with those of the single NDI and ZnChl reference chromophores.

3.2.1 UV-vis Absorption and Steady State Emission Properties of Reference Chromophores

The self-assembly process of BChl *c*, *d*, *e* and ZnChl dyes into rod aggregates goes along with a pronounced bathochromic shift of the Q_y band of about 80-90 nm compared to monomer spectra, indicating the organization of ZnChl dyes as *J*-aggregates (see Chapters 2.2.2 and 2.3.1). These *J*-aggregates are observed in water or in nonpolar aprotic solvents such as *n*-hexane or cyclohexane already at low concentration ($\sim 10^{-6}$ M) due to an interplay of π - π interactions between the large aromatic systems, coordination of the central metal ion by the 3¹ hydroxy group of a neighboring molecule, and hydrogen bonding between the 3¹ hydroxy group and a neighboring 13¹ keto functionality.^{9,11,86,90,92,94}

In Figure 38A a typical rod aggregate absorption spectrum is depicted for ZnChl **5a** (green line). As a solvent mixture cyclohexane/ tetrachloromethane (1%)/ THF (0.1%) has been used. The small percentage of THF was required to prepare a highly concentrated stock solution, since ZnChl **5a** shows excellent solubility in this polar solvent. In addition, coordination of the THF oxygen as a fifth ligand of the zinc ion facilitates the formation of well-defined self-assembled nanorods by reducing the kinetic barriers for ligand exchange ("self-repair"). Accordingly, well soluble aggregates were obtained by dilution of the stock solution with a nonpolar-aprotic solvent to form well soluble aggregates. The absorption maximum of the Q_y band of **5a** aggregates is located at 739 nm and the Soret band is found at 447 nm. The emission spectrum is only slightly shifted with respect to the absorption band

showing a maximum at 742 nm. Such a small Stokes shift is a typical feature of *J*-aggregates, where thermal equilibration of excitation energy over the different exciton states is given.^{60,61,120}

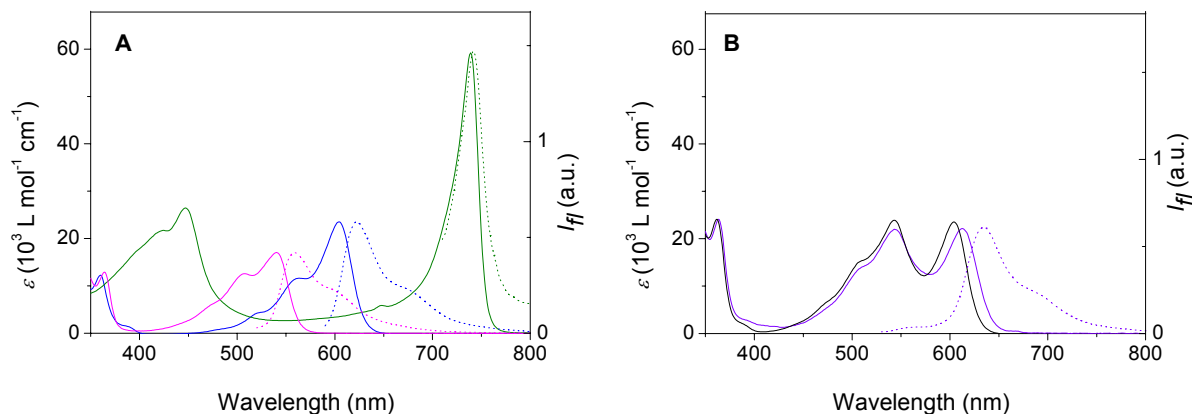
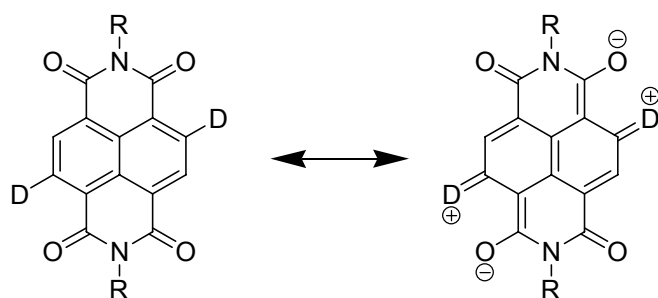


Figure 38. A) UV-vis (solid lines) and normalized fluorescence spectra (dotted lines) of ZnChl **5a** rod aggregate in cyclohexane (98.9%)/ tetrachloromethane (1%)/ THF (0.1%) (green lines, $\lambda_{\text{ex}} = 700 \text{ nm}$), NDI_{NO} **40** in cyclohexane/ tetrachloromethane (1%) (pink lines, $\lambda_{\text{ex}} = 510 \text{ nm}$), and NDI_{NN} **44** in cyclohexane/ tetrachloromethane (1%) (blue lines, $\lambda_{\text{ex}} = 575 \text{ nm}$). B) UV-vis (violet solid line) and normalized fluorescence spectrum (violet dotted line, $\lambda_{\text{ex}} = 520 \text{ nm}$) of NDI_{NN}-NDI_{NO} **52** and, for comparison, the calculated sum of the UV-vis absorption spectra of **40** and **44** (black line) in cyclohexane/ tetrachloromethane (1%).

The absorption and emission properties of 2,6-core-disubstituted NDIs are influenced by the nature of the respective core-functionalities.²¹ In comparison to core-unsubstituted NDIs, a “new” HOMO orbital is created from the interaction of the core-substituents with the π -conjugated naphthalene core, while the LUMO remains unchanged.²¹ Thus, the energy of the S_0 - S_1 transition of core-substituted NDIs is strongly dependent on the extent of this π -conjugation and the electron-donating strength of the substituents (Scheme 12).



Scheme 12. Resonance model for 2,6-core-disubstituted NDIs which explains the strong impact of electron donor substituents D on the absorption and emission wavelengths.²¹

The fluorescence quantum yields of 2,6-core-disubstituted NDIs are affected by the nature of the heteroatom in the 2,6-core positions as well. Furthermore, it has been observed that arylamino substituents provoke complete emission quenching, while alkylamino-disubstituted NDIs are fluorescent.²³ Unlike, substituents at the imide positions do not have a significant effect on the optical chromophore properties of NDIs.²³

NDI_{NO} **40**, NDI_{NN} **44**, and NDI_{NN}-NDI_{NO} **52** were chosen as reference compounds for the NDI building blocks of dyads **1,2** and triad **3**. The absorption and emission maxima of **40**, **44**, and **52** in THF and in cyclohexane/ tetrachloromethane (1%) are listed in Table 1. The absorption maximum of the S₀-S₁ transition of NDI_{NO} **40** is found at 547 nm in THF and it is hypsochromically shifted to 540 nm in the less polar cyclohexane-based solvent system. However, this observation should not be due to an aggregation process, since intermolecular π - π interactions between NDIs **40** are prevented by the bulky 2,6-diisopropylphenyl imide substituents. This assumption is supported by the fact that the shape of the absorption spectrum of **40** in cyclohexane/ tetrachloromethane (1%) strongly resembles the absorption spectrum of **40** in THF (Figure 38). Instead, the blue shift is caused by the strongly pronounced solvatochromism of core-substituted NDIs, which has been investigated previously for related NDI chromophores.²¹

Table 1. Absorption Maxima (λ_{abs}), Absorption Coefficients (ϵ), Emission Maxima (λ_{em}) and Fluorescence Quantum Yields (Φ_{fl}) of NDI Reference Chromophores **40**, **42**, and **52**.

	solvent	λ_{abs} (nm)	ϵ (M ⁻¹ cm ⁻¹)	λ_{em} (nm)	Φ_{fl}
40	THF	547	17100	575	0.58
40	cyclohexane/ CCl ₄ (1%)	540	17100	558	0.67
44	THF	614	23700	637	0.50
44	cyclohexane/ CCl ₄ (1%)	604	23500	622	0.70
52	THF	548	23900		
		613	20900	638	0.39
52	cyclohexane/ CCl ₄ (1%)	543	22000		
		612	22100	634	0.51

The blue color of NDI_{NN} **44** solutions is due to an absorption maximum of the S₀-S₁ band at 614 nm in THF and 604 nm in cyclohexane/ tetrachloromethane (1%), respectively (Table 1, Figure 38A). The absorption spectra of dyad NDI_{NN}-NDI_{NO} **52** in the same two different solvent systems closely resemble the sum of the absorption spectra of the single NDI_{NN} and NDI_{NO} chromophores, respectively (Figure 38B). Thus, it can be concluded that there are no ground state interactions between the two NDI building blocks of the bichromophoric compound **52**.

The emission spectra of NDI_{NO} **40** and NDI_{NN} **44** are both in mirror image relation to the respective absorption spectra (Figure 38A). NDI_{NO} **40** shows fluorescence quantum yields of 58% and 67% in THF and cyclohexane/ tetrachloromethane (1%), respectively. For NDI_{NN} **44** quantum yields of 50% and 70%, respectively, were observed. Upon selective excitation of the pink colored NDI_{NO} moiety in dyad **52** at a wavelength of 520 nm, emission predominantly from the blue NDI_{NN} was detected, indicating an efficient intramolecular FRET process (Figure 38B). The fluorescence quantum yields of 39% in THF and 51% in cyclohexane/ tetrachloromethane (1%) were slightly lower than those of the blue NDI_{NN} **44** (50% and 70%, respectively).

3.2.2 UV-vis Absorption and Steady State Emission Properties of Zinc Chlorin-Naphthalene Diimide Dyads

To access the self-assembly behavior of multi-chromophoric dyads **1** and **2** dilute solutions were prepared in the polar solvent THF and the unpolar solvent mixture cyclohexane/ tetrachloromethane (1%). Solutions of dyads **1a,b** in THF show violet color and turn into brown in the unpolar solvent, foretelling an aggregation process (Figure 39). Solutions of dyads **2a,b** undergo a color change as well, turning from blue in THF to dark green in cyclohexane/ tetrachloromethane (1%).

However, while compounds **1b** and **2b** bearing two long unpolar alkyl chains in the 17³ position show excellent solubility in both solvents, for the *n*-butylamino-substituted dyads **1a** and **2a** no appropriate unpolar aprotic solvent system could be found. This observation is in good agreement with the concept proposed by Huber *et al* for the solubility behaviour of ZnChl rod aggregates.^{15,86} It was shown that *in vitro* BChl *c* self-assembles as well as aggregates formed by artificial ZnChls bearing only one alkyl chain at the 17³ substituent tend to grow into larger agglomerates in

nonpolar aprotic solvents due to interpenetration of alkyl chains of nearby rods. Instead, functionalization of ZnChls by two or three alkyl chains at the 17³ position establishes an envelope that prevents this agglomeration and affords highly soluble cylindrical micelles.

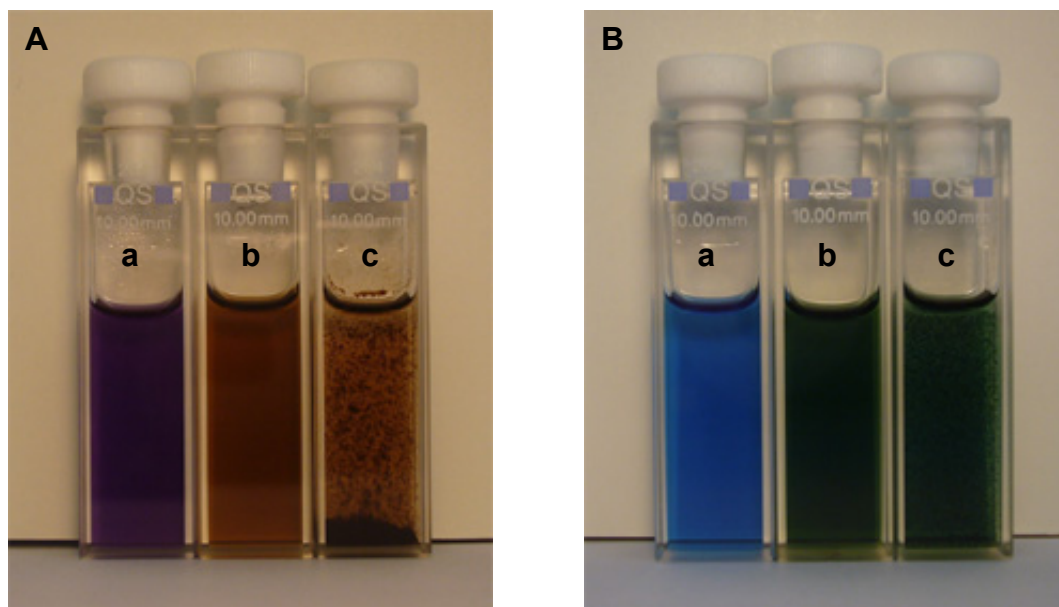


Figure 39. Left: Colors and solubility properties of (A) ZnChl-NDI_{NO} **1a,b** and (B) ZnChl-NDI_{NN} **2a,b**. A) a) Monomer solution of **1b** in THF; b) aggregate solution of **1b** and c) precipitated **1a** in cyclohexane/tetrachloromethane (1%). B) a) Monomer solution of **2b** in THF; b) aggregate solution of **2b** and c) precipitated **2a** in cyclohexane/tetrachloromethane (1%).

Figure 40 shows the UV-vis absorption and normalized fluorescence spectra of dyads **1b** and **2b**. If THF was used as a solvent, UV-vis spectra of both dyads **1b** and **2b** revealed the characteristic Q_y-band of ZnChl monomers ($\lambda_{\max} = 647$ and 646 nm respectively), since in this solvent metal coordination and hydrogen bonding between ZnChl units is prevented due to the ligation of THF as a fifth ligand at the zinc ion and its hydrogen bond acceptor ability. The absorption maxima of the respective NDI units are located in the “green gap” of the ZnChl absorption spectrum ($\lambda_{\max} = 550$ nm for **1b** and 607 nm for **2b**, respectively). Both the NDI absorption bands match the UV-vis spectra of the individual NDI chromophores **40** ($\lambda_{\max} = 547$ nm, THF) and **44** ($\lambda_{\max} = 614$ nm, THF), respectively, indicating that no ground state interactions between NDI and monomeric ZnChl units are existent. The fluorescence spectra of **1b** and **2b** monomers do not exhibit any NDI emission bands even though NDI reference components **40** and **44** are highly fluorescent ($\phi_{\text{Fl}} = 0.58$ and 0.39

respectively, THF). Likewise, the fluorescence quantum yields of dyad **1b** and **2b** monomers ($\phi_{\text{Fl}} = 0.12$ and 0.11 respectively), which were determined by selective excitation of the respective NDI S_0 - S_1 absorption band, are in the same range as the quantum yield of ZnChl **5b** monomers ($\phi_{\text{Fl}} = 0.19$, THF), suggesting almost complete quenching of NDI emission by efficient FRET.

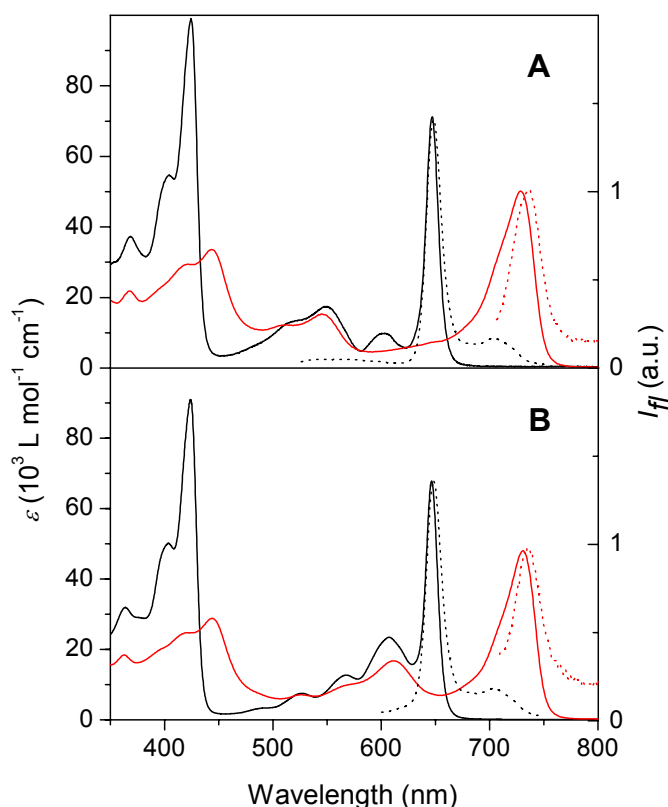


Figure 40. A) UV-vis (solid lines) and normalized fluorescence (dashed lines, $\lambda_{\text{ex}} = 510$ nm) spectra of **1b**. Monomers in THF (black); aggregates in cyclohexane/ tetrachloromethane (1%) at room temperature. B) UV-vis (solid lines) and normalized fluorescence (dashed lines, $\lambda_{\text{ex}} = 530$ nm) spectra of **2b**. Monomers in THF (black); aggregates in cyclohexane/ tetrachloromethane (1%) at room temperature.

A mixture of cyclohexane/ tetrachloromethane (1%) is a nonpolar aprotic solvent system in which good solubility of dyads **1b** and **2b** is provided despite the fact that the fifth coordination site of the zinc ion as well as the hydroxyl-functionality are not well solvated. As a consequence self-aggregation takes place in this solvent as revealed by a bathochromic shift of the ZnChl Q_y -band to 729 (**1b**) and 731 (**2b**) nm, respectively (Figure 40). It is noticed that the absorption spectra of NDI units in **1b** and **2b** aggregates ($\lambda_{\text{max}} = 545$ and 611 nm respectively) are only slightly hypsochromically shifted compared to those of the isolated NDI chromophores **40**

and **44** ($\lambda_{\max} = 540$ and 604 nm respectively, Table 1). This observation suggests that in aggregates of dyads **1b** and **2b** no excitonic coupling between NDI units at the periphery of the rod-like ZnChl rod aggregates occurs.

Another evidence for *J*-type excitonic coupling of ZnChl units of **1b** and **2b** in cyclohexane/ tetrachloromethane (1%) is provided by steady state fluorescence spectra (Figure 40). Aggregated species of **1b** and **2b** show the characteristically small Stokes shift of the ZnChl Q_y -band ($\Delta\lambda = 8$ and 6 nm respectively).¹²⁰ Furthermore, for aggregates of **1b** and **2b** complete quenching of the fluorescence of the respective NDI units is observed and the quantum yields of the emission from the ZnChl subunits have decreased to $\phi_{\text{Fl}} \leq 0.001$, indicating that not only the emission of the NDI units is quenched but also that the aggregated ZnChl species is poorly fluorescent. Such low fluorescence quantum yields are characteristic for ZnChl and BChl *c*, *d*, *e* aggregates, since efficient quenching processes originate from the presence of small amounts of oxidized chlorin,¹²⁵ which cannot be excluded for the present system. However, it has been demonstrated both for chlorosomes as well as artificial chlorin aggregates that their LH efficiencies are not adversely affected by these quenching processes if effective energy acceptors are present (see Chapters 2.2.2 and 2.3.1). For instance, in chlorosomes the excitation energy of the rod antennae is transferred efficiently to BChl *a* protein complexes in the baseplate,¹⁰⁶⁻¹¹⁵ while for artificial ZnChl LH systems co-aggregated BChl *a* functionalities act as efficient energy acceptors.¹²²⁻¹²⁶

3.2.3 Temperature-Dependent UV-vis Absorption and CD Spectroscopy of Zinc Chlorin-Naphthalene Diimide Dyads

To further elaborate the aggregation process of ZnChl-NDI dyads **1b** and **2b**, temperature-dependent UV-vis spectroscopic measurements were carried out in cyclohexane/ tetrachloromethane (1%). Figure 41 shows the absorption spectra of solutions of dyad **1b** at three different concentrations, which were first heated up to 65 °C. It was not possible to choose higher temperatures due to the boiling point of the solvent mixture. Preliminary tests had shown that at all temperatures a stationary state is reached after 30 min equilibration time. Thus, the measurements were started 1 h after the temperature change. The UV-vis spectra of **1b** at 65 °C revealed

not only a decreased aggregate absorption band at 729 nm but also an absorption maximum at 646 nm, indicating a risen amount of monomers in the equilibrium at this temperature (Figures 41A-C). Upon subsequent cooling of the samples from 65 °C to 25 °C in 10 °C intervals and an equilibration time of again 1 h, the Q_y -band of aggregates increases back to its initial intensity while the monomer band disappears completely confirming the reversibility of aggregate formation of **1b**.

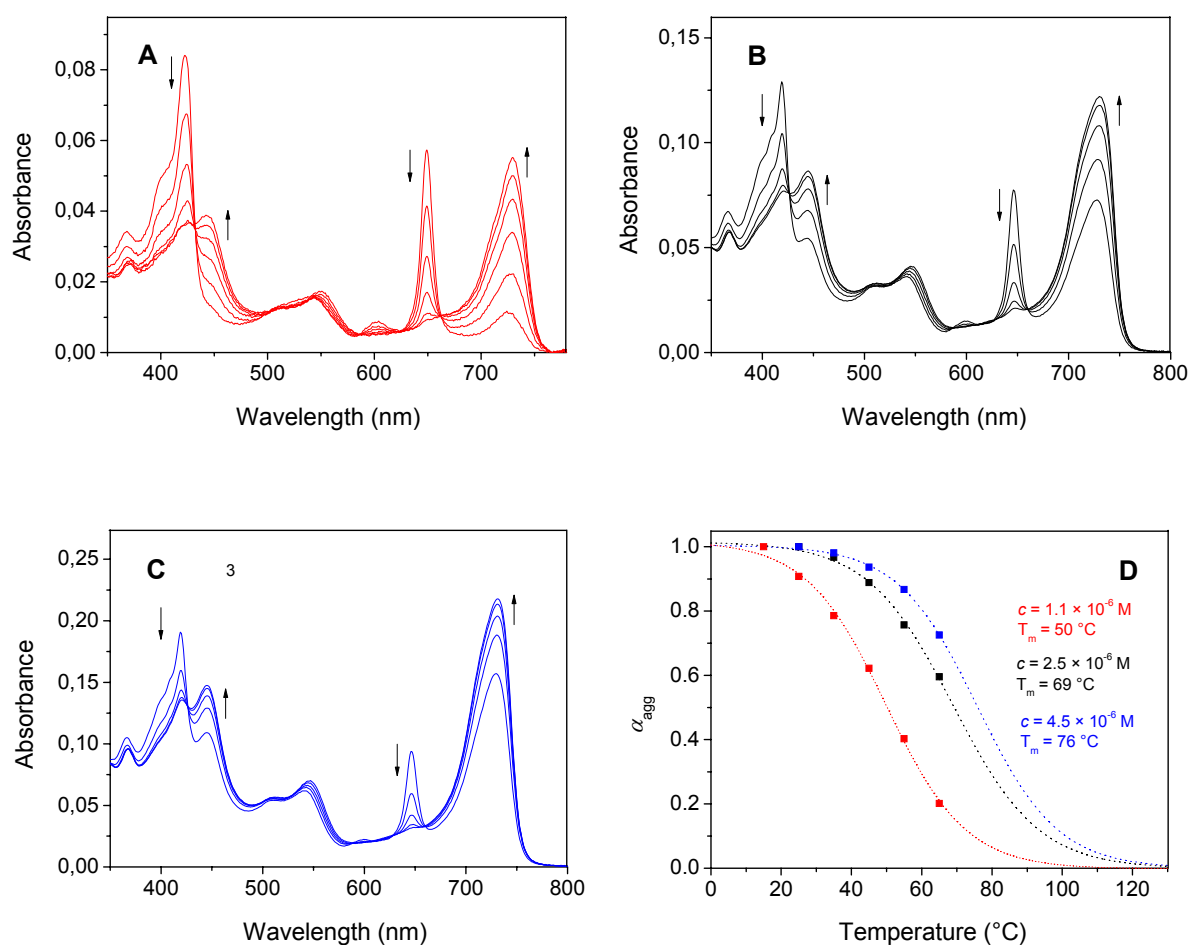


Figure 41. Temperature-dependent UV-vis spectra of ZnChI-NDI_{NO} **1b** in cyclohexane/tetrachloromethane (1%) at different concentrations of (A) $c = 1.2 \times 10^{-6}$ M, (B) $c = 2.5 \times 10^{-6}$ M, and (C) $c = 4.5 \times 10^{-6}$ M. The initial temperature of 65 °C was decreased successively in 10 °C steps down to 25 °C and at each temperature the solution was equilibrated for 1 h; the arrows indicate the changes upon decreasing temperature. (D) shows the data points for the decrease of α_{agg} at 729 nm upon increasing temperature. The data have been fitted with the Boltzmann distribution.

Because monomers of **1b** do not show any absorption in the range of the aggregate Q_y band maximum (Figure 40), the normalized absorption intensity of the aggregate at 729 nm can be plotted as a function of the temperature, giving a sigmoidal curve

(Figure 41D). The plot can be approximated with the Boltzmann distribution (eq 13) in which α_{agg} is the normalized fraction of aggregated molecules.¹⁵⁹

$$\alpha_{agg} = \frac{1}{1 + e^{\frac{T - T_m}{\Delta T}}} \quad (13)$$

The so-called “melting” temperature T_m is defined as the temperature at which $\alpha = 0.5$ and ΔT relates to the width of the curve. It was observed that an increasing concentration of **1b** aggregate solutions (1.1×10^{-6} - 4.5×10^{-6} M) goes along with an increase of the melting temperature ($50 \rightarrow 76$ °C) (Figure 41D). Absorption measurements of **2b**, which were conducted under the same conditions as for **1b** and at a concentration of $c = 2.2 \times 10^{-6}$ M revealed analogous temperature-dependence of the UV-vis spectra (Figure 42A). The maximum of the aggregate Q_y band at 731 nm was decreased after the initial heating going along with a rising monomer Q_y band at 647 nm. The cooling process showed a transition from the molecularly dissolved species back to the aggregated state. The melting temperature at this concentration was calculated to be 65 °C (Figure 42B). As a result, the temperature-dependence of monomer-aggregate equilibria of dyads **1b** and **2b** is very similar, confirming that aggregates of **1b** and **2b** exhibit comparable stability.

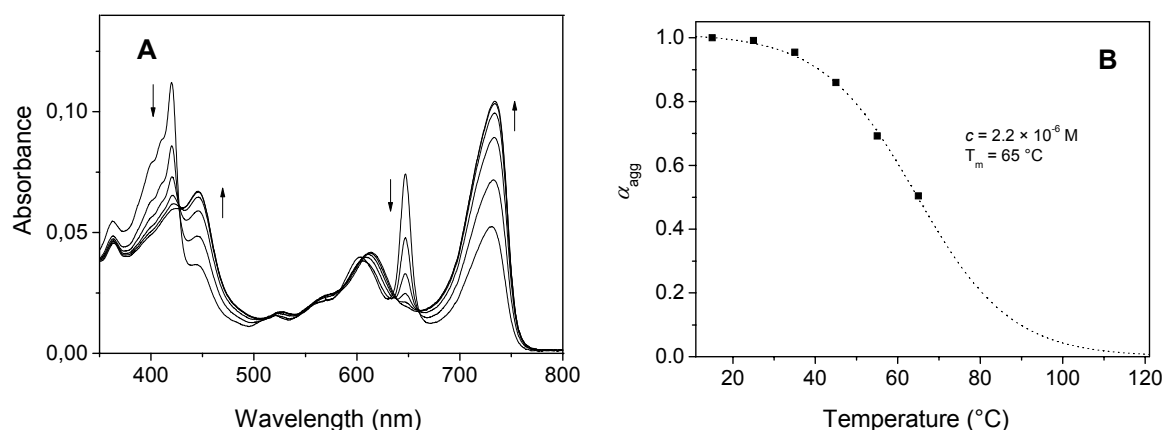


Figure 42. (A) Temperature-dependent UV-vis spectra of ZnChI-NDI_{11N} **2b** ($c = 2.2 \times 10^{-6}$ M) in cyclohexane/ tetrachloromethane (1%). The initial temperature of 65 °C was decreased successively in 10 °C steps down to 25 °C and at each temperature the solution was equilibrated for 1 h; the arrows indicate the changes upon decreasing temperature. (D) The data points for the decrease of α_{agg} at 731 nm upon increasing temperature and the related Boltzmann fit are shown.

The self-assembly process of ZnChl dyes such as ZnChls **5** into cylindrical nanorods goes along with an induced circular dichroism (CD) effect due to excitonic coupling, since the transition dipole moments are arranged in a helically chiral order.^{160,161} Examination of an aggregate solution of ZnChl-NDI_{NO} **1b** and **2b** in cyclohexane/tetrachloromethane (1%) by CD spectroscopy reveals a characteristic Cotton effect for the chlorin Q_y absorption band as well (Figure 43). The displayed effect consists of an exciton couplet whose shape resembles the signals observed previously for aggregates of the parent ZnChls **5**.¹⁵ By contrast, no Cotton effect of the peripheral NDI_{NO} units could be detected, indicating once more that these chromophores do not interact with each other in the self-assembled dyads **1b** and **2b**.

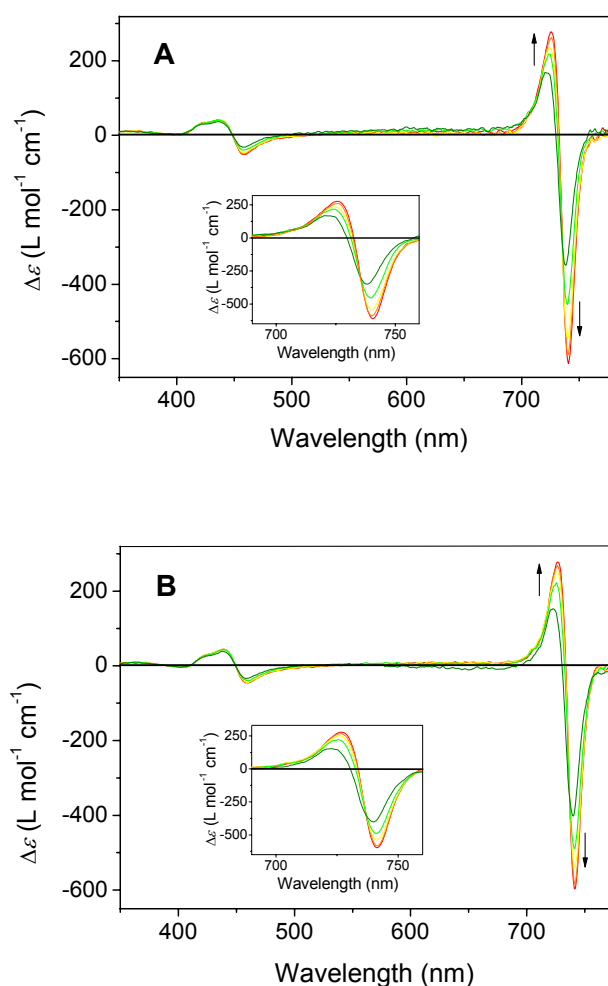


Figure 43. Temperature-dependent CD spectra of (A) ZnChl-NDI_{NO} **1b** ($c = 3.0 \times 10^{-6} \text{ M}$) and (B) ZnChl-NDI_{NN} **2b** ($c = 4.2 \times 10^{-6} \text{ M}$) in cyclohexane/ tetrachloromethane (1%). The initial temperature of 65 °C was decreased successively in 10 °C steps down to 25 °C and at each temperature the solution was equilibrated for 1 h; the arrows indicate the changes upon decreasing temperature. Inset in (A) and (B): magnification of the CD signals.

After increasing the temperature of the aggregate solution of **1b** to 65 °C and an equilibration time of 1 h, the intensity of the induced CD effect is diminished, indicating dissolution of the aggregated species into monomers. On stepwise decrease of the temperature to 25 °C in intervals of 10 °C and equilibration times of 1 h the amplitude of the exciton couplet arises again. This increase can be taken as a further evidence for the reversibility of the aggregation process of dyad **1b** in cyclohexane/ tetrachloromethane (1%).

3.2.4 UV-vis Absorption, Steady State Emission, and CD Properties of the ZnChl-NDI_{NN}-NDI_{NO} Triad **3**

The absorption spectrum of ZnChl-NDI_{NN}-NDI_{NO} **3** in THF exhibits the absorption maxima of the two different NDI components at 552 and 610 nm, respectively, along with the typical ZnChl monomer Q_y-band at 647 nm (Figure 44A). Thus, it is concluded that there are no ground state interactions between the different chromophore building blocks of triad **3**. In cyclohexane/ tetrachloromethane (1%) the characteristic bathochromic shift of the Q_y-band to 731 nm signifies J-type excitonic coupling of the ZnChl units in the same way as observed for dyads **1b** and **2b** ($\lambda_{\text{max}} = 729$ and 731 nm, respectively). Further, the “green gap” of ZnChl aggregates is now completely covered by the absorption bands of the NDI_{NO} and NDI_{NN} units whose absorption maxima ($\lambda_{\text{max}} = 551$ and 619 nm) are slightly shifted compared to the NDI_{NN}-NDI_{NO} component **52** ($\lambda_{\text{max}} = 543$ and 612 nm), indicating that there are no significant interactions between peripheral NDI chromophores within the self-assembled nanorod of triad **3**. This result is further supported by the CD spectrum of **3** aggregates (Figure 44B) which shows the characteristic bisignate Cotton effect resembling the exciton couplet of **1b** and **2b** aggregates (Figure 42), but lacks any signal originating from the NDI units.

Stationary fluorescence spectra of **3** monomers which have been measured at selective excitation of either the NDI_{NN} or NDI_{NO} unit, reveal only one emission band originating from the ZnChl moiety ($\lambda_{\text{max}} = 648$ and 704 nm), while the emission of both NDI chromophores is completely quenched. The fluorescence quantum yield of **3** monomers ($\phi_{\text{Fl}} = 0.11$) is independent of the excitation wavelength and resembles the values obtained for **1b**, **2b**, and **5a** monomers. This observation supports the

proposal that excitation of any NDI chromophore is followed by efficient intramolecular FRET to the ZnChl moiety. Emission spectra of triad **3** in cyclohexane/tetrachloromethane (1%) show the typically small Stokes shift ($\Delta\lambda = 4$ nm) of ZnChl aggregates. Self-assemblies of **3** are only slightly fluorescent, since the emission of both NDI units is quenched again by the ZnChl aggregate. The fluorescence quenching of excited NDI chromophores suggests energy transfer from the peripheral NDIs to the self-assembled ZnChl rod antenna. Such transfer processes will be discussed in detail in chapter 3.3.

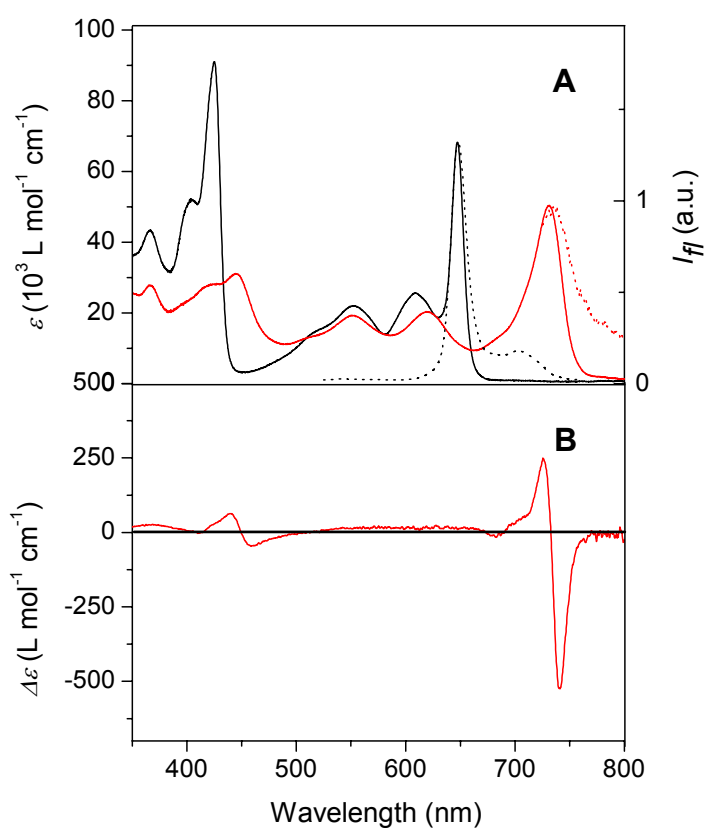


Figure 44. A) UV-vis spectra (solid lines) and normalized fluorescence spectra (dotted lines) of triad **3** monomers in THF (black, $\lambda_{\text{ex}} = 510$ nm) and of triad **3** aggregates (red, $\lambda_{\text{ex}} = 540$ nm) in cyclohexane/tetrachloromethane (1%). B) CD spectrum of triad **3** aggregates in cyclohexane/tetrachloromethane (1%) (red).

3.2.5 AFM Studies

Having established the spectral features of self-assemblies of NDI-functionalized ZnChls, also their structural features were addressed using atomic force microscopy (AFM). AFM is a widely used tool to investigate the topography of a surface. Images are generated by probing the surface with a sharp tip attached to the end of a flexible silicon cantilever. Small interaction forces between the sample and the tip produce a deflection of the cantilever that is detected and converted into height information. When the heights for each position of the tip over the sample are plotted, the topography of the sample can be reconstructed.¹⁶² During the measurement, the distance between tip and surface is kept constant.

For the examination of compound **2b** an aggregate solution in cyclohexane/ THF (1%) was prepared, which was spin-coated onto a highly ordered pyrolytic graphite (HOPG) substrate. The measurement revealed elongated objects of different lengths as shown in Figures 45A and 45B. Direct measurements of the contour lengths L of 362 rods gave a mean value of $L = 93 \pm 75$ nm. The longest observed aggregates exhibit contour lengths in the range of 300-380 nm and the longer rods (> 100 nm) are slightly curved. The elasticity of these bended objects can be characterized by the so-called persistence length P , i.e. the distance over which orientational correlations along the rod aggregate persist or, expressed differently, the decay length through which the memory of the initial orientation of the aggregate persists.^{163,164} The persistence length can be calculated for each elongated object using equation 14.

$$\langle R^2 \rangle_{2D} = 4PL \frac{1 - 2P}{L \left(1 - e^{-\frac{L}{2P}} \right)} \quad (14)$$

The respective contour lengths and end-to-end distances R are both determined by the experiment. Evaluation of the persistence length of curved rods has been estimated to be 200 ± 30 nm, indicating a pronounced stiffness of these assemblies.

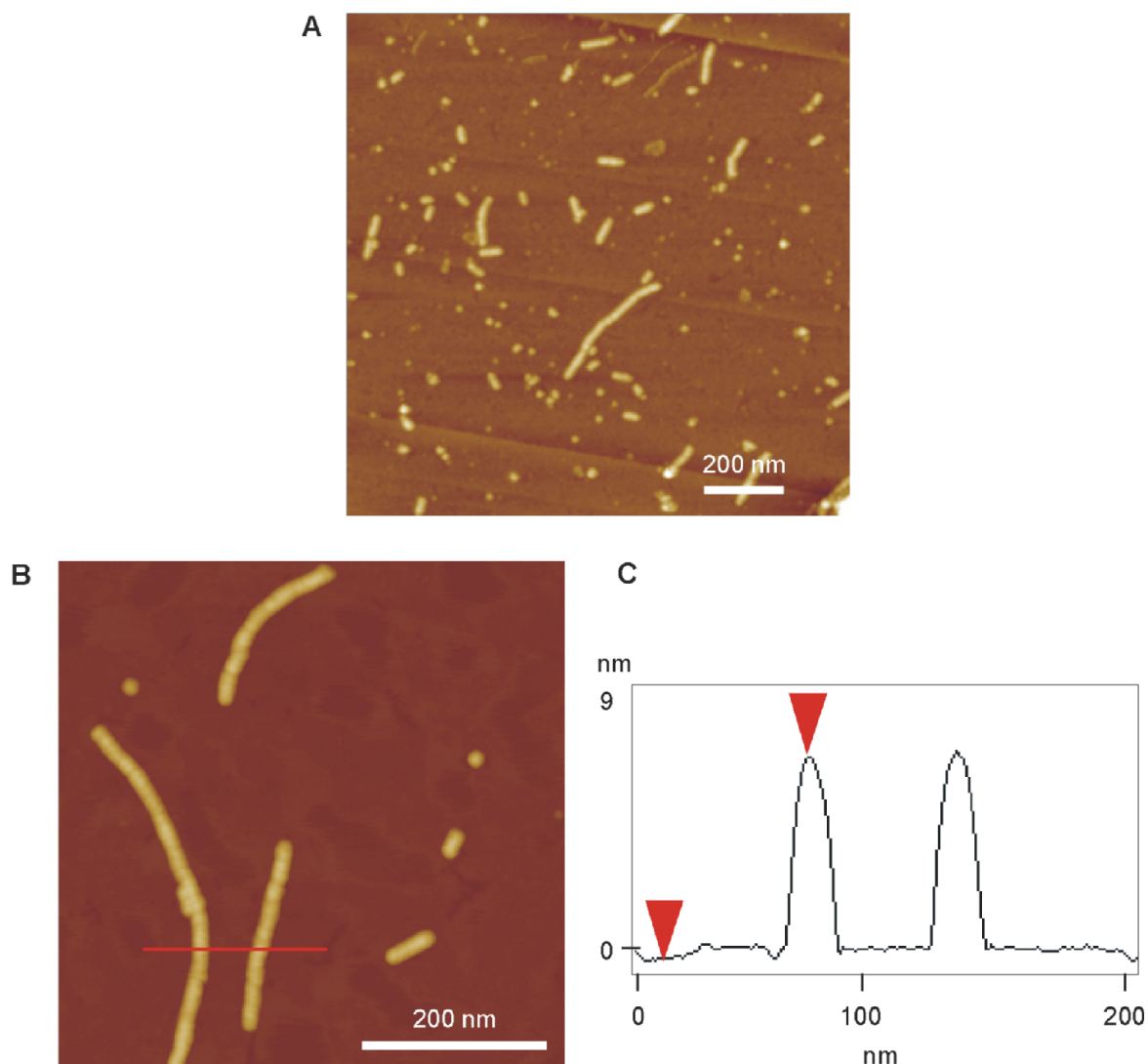


Figure 45. A) and B) Tapping mode AFM images of a ZnChl-NDI_{11N} **2b** sample which was prepared by spin-coating from a solution of **2b** ($c \sim 1 \times 10^{-5}$ M) in cyclohexane/ THF (1%) onto highly ordered pyrolytic graphite (HOPG) and measured under ambient conditions. C) Profile of the red line in (B), the vertical distance between the red triangles provides the height of the rod aggregate.

All objects possess a height of 7.3 ± 0.2 nm (Figure 45C) which is slightly higher than that observed previously for ZnChl rods of compound **5a** without additional NDI dyes using AFM (5.8 ± 0.4 nm)^{15,86} and than that measured for the rod-like BChl *c* aggregates in the chlorosomes of *Chloroflexus aurantiacus*.⁸⁵ It is concluded that this increase in the diameter of about 1.5 nm is due to the additional NDI chromophores at the periphery of the rod.

For aggregate solutions of dyad **1b** and triad **3** no rod structures were detected. Instead, AFM studies revealed worm-like objects showing smaller heights than **2b**

aggregates. Such objects might represent collapsed rod aggregates, which are formed by π - π interactions of the HOPG surface and ZnChl chromophores.

As a result from UV-vis absorption, steady state emission, and CD spectroscopy on compounds **1b**, **2b**, and **3** one can derive that the same type of ZnChl aggregates is formed in cyclohexane/ tetrachloromethane (1%) by ZnChl-NDI dyads as well as by the triad, even though the bulkier NDI_{NN}-NDI_{NO} functionality at the periphery of **3** aggregates should be more impedimental towards rod formation than the single NDI substituents at the circumference of **1b** and **2b** aggregates. The spectral and microscopic features of self-assemblies of **1b**, **2b**, and **3** are in good agreement with the data observed for unsubstituted ZnChl aggregates as formed by compounds **5a** and **5b** as well as with the BChl *c* aggregates in the chlorosomes of green filamentous bacteria. Thus, ZnChl self-assemblies which are functionalized by additional chromophores could be rationally designed without impeding the formation of a rod aggregate structure.

3.3 Investigation of Light-Harvesting Properties

The question if the LH capacity of **1-3** aggregates is improved by peripheral NDI chromophores depends on the efficiency of energy transfer from these NDI units to the ZnChl rod antenna. A first hint for such energy transfer processes in aggregates as well as in monomers has been obtained by stationary fluorescence spectroscopy, since upon excitation of NDI units in **1-3** aggregates and monomers complete fluorescence quenching of these chromophores takes place (vide supra). To get a detailed insight into the excited-state properties of compounds **1-3**, time-resolved fluorescence studies were carried out using the single photon timing (SPT) technique.ⁱⁱ This method is particularly advantageous for the examination of the fluorescence kinetics of ZnChl aggregates, since its high sensitivity facilitates that even low fluorescent samples can be detected clearly. Furthermore, the SPT technique allows resolution of decay times over a rather huge time range, i.e. from a few picoseconds to nanoseconds.

3.3.1 Time-Resolved Fluorescence Spectroscopy Measurements – Instrumentation and Analysis

SPT Technique Set-up

The principle of SPT measurements is based on the idea that the probability distribution for the photon emission of one single excited molecule in dependence of time resembles the fluorescence decay curve of a set of these molecules.¹⁶⁵ For the measurement of this probability distribution the sample is excited by a laser pulse and that point in time, at which the first photon is emitted, is recorded. The measuring set-up of an SPT apparatus is depicted in Figure 46.^{166,167} A beam splitter directs a fraction of the light beam to a photodiode (PD), whose electric pulse marks the reference time. The single photon which is emitted by the sample is detected by a

ⁱⁱ Time-resolved fluorescence data were measured at the Max Planck Institute for Bioinorganic Chemistry, Mülheim an der Ruhr, under the guidance of Prof. Dr. Alfred Holzwarth and in collaboration with his co-workers Yuliya Miloslavina and Dr. Marc G. Müller.

photomultiplier (PMT). The monochromator (MR) which is located between sample and photomultiplier, provides protection from scattered light and is used for the selection of the detection wavelength. Photodiode and photomultiplier both forward their electric pulse to a time-to-amplitude converter (TAC) serving as an electronic watch. This device generates a voltage pulse whose amplitude is proportional to the difference in the arrival times of photodiode pulse and photomultiplier pulse. An analog-to-digital converter transmits the value of the respective amplitude to the address of a channel of a multi-channel analyzer (MCA) in which the emission event is counted and stored. The addition of all detected emission events gives the probability distribution curve in dependence on time, exhibiting the shape of a histogram and, thus, describing the fluorescence decay of the sample.

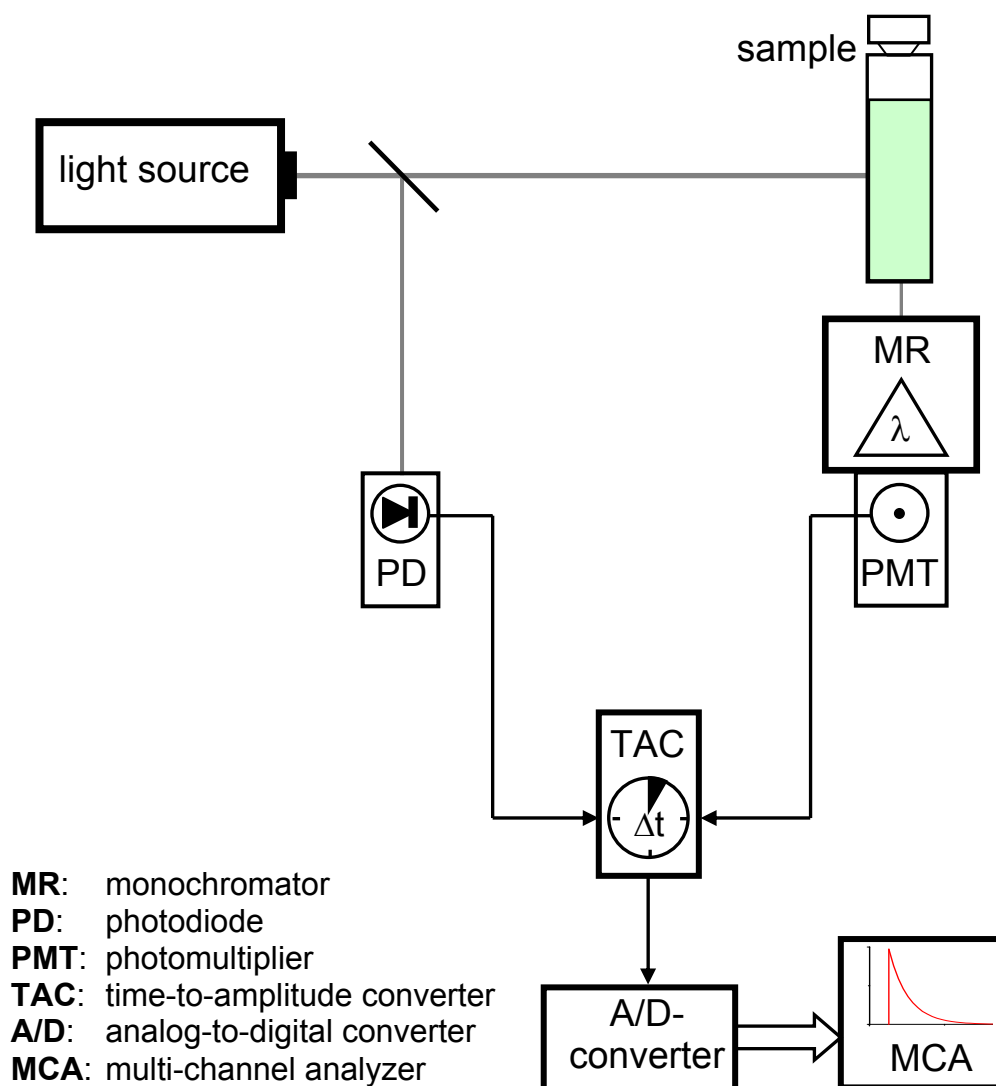


Figure 46. Block diagram of an SPT apparatus.¹⁶⁶

The SPT apparatus contains a picosecond dye laser system which consists of an mode-coupled argon ion laser (model 2030 with mode locker 342A and mode locker driver 452, Spectra Physics) and a synchronically coupled dye laser (model 375B, Spectra Physics) equipped with a cavity dumper (model 344S with cavity dumper driver 454, Spectra Physics). The excitation wavelength depends on the respective laser dye and can be tuned continuously within a range of about 100 nm per dye. For excitation at shorter wavelengths Rhodamin 110 (work space: $\lambda = 540\text{-}600$ nm) was applied and for excitation wavelengths of ~ 630 nm DCM ($\lambda = 610\text{-}760$ nm) was chosen. The measurements were performed using a “magic angle” set-up. This is essential to avoid the detection of decay components which arise from anisotropy relaxation during the rotation of molecules or aggregates while they are excited. The optical set-up of the SPT apparatus used for the measurements of time-resolved fluorescence spectroscopy has been described previously in detail in the literature.^{166,167}

Analysis of Time-Resolved Emission Data

The measured fluorescence decay function $Y(t)$ resembles a convolution of the pure fluorescence decay of the sample $D(t)$, the time-dependent profil of the laser pulse, and the response function of the detector system $P(t)$. At first, the form function of the laser pulse and the pure decay of the sample convolve. The resulting convolution product again convolves with the system response function, giving the measured fluorescence decay function (eq 15). The system response function can be recorded by exchange of the sample cuvette by a scattering, nonfluorescent suspension.

$$Y(t) = \int_0^t P(t) \cdot D(t - \tau) d\tau \quad (15)$$

The pure fluorescence decay $D(t)$ resembles a sum of exponential terms with the amplitudes a_k and the corresponding lifetimes τ_k (eq 16). Each term is attributed to a certain decay ($a > 0$) or rise ($a < 0$) process.

$$D(t) = \sum_{k=1}^n a_k e^{-\frac{t}{\tau_k}} \quad (16)$$

The measured fluorescence decay $Y(t)$ is analyzed in order to determine amplitudes and lifetimes by an iterative method. After the iterative procedure a theoretical decay curve $G(t)$ is observed whose deviation from the measured decay curve $Y(t)$ is assessed using χ^2 (eq 17).

$$\chi^2 = \frac{1}{N-P} \sum_{i=1}^N \left(\frac{Y(t_i) - G(t_i)}{\sqrt{Y(t_i)}} \right)^2 \quad (17)$$

N is the number of channels, by which the theoretical curve $G(t)$ and the measured curve $Y(t)$ are compared, P is the number of free parameters (lifetimes, amplitudes) in the theoretical curve, and t_i is the time of channel i . For an optimal modulation of lifetimes and amplitudes of the decay kinetics by the fit algorithm χ^2 should equal 1.0. If the decay curves are measured at different observation wavelengths, a so-called global analysis can be performed, assuming that lifetimes are independent of the observation wavelength. This condition is generally fulfilled for assemblies of photosynthetic pigments. Advantageously, when global analysis is performed the fit provided by the iterative method converges faster due to a reduced number of parameters compared to single decay analysis. Global analysis allows to determine the fluorescence decay kinetics more precisely than analysis of single decays.¹⁶⁸

3.3.2 Excited State Decay of Zinc Chlorins and Naphthalene Diimides

First the excited state lifetimes τ of NDI and ZnChl reference chromophores were evaluated (Table 2). A solution of the pink NDI_{NO} **40** in cyclohexane/tetrachloromethane (1%) was excited at 540 nm and decay curves were measured for eight different detection wavelengths in the range of 550-650 nm. Global analysis revealed monoexponential fluorescence decay of excited compound **40** with a lifetime of 12 ns. The decay of the blue NDI_{NN} **44** after excitation with 620 nm laser pulses was examined at nine observation wavelengths in the range of 625-700 nm, giving again monoexponential decay and a similar decay time ($\tau = 10$ ns).

Then the ZnChl reference chromophore ZnChl **5b** was investigated. A monomer solution of **5b** in 2-Me-THF/ methanol (1%) was excited at 640 nm and the decay curves were recorded at 650, 655, and 710 nm. As a result, nearly monoexponential

decay with a time constant of 4.3 ns was observed for **5b** monomers. ZnChl **5b** forms well soluble cylindrical self-assemblies in the solvent mixture *n*-hexane/ 2-Me-THF (1%). Such an aggregate solution of **5b** was irradiated with 720 nm laser pulses and the emission was detected at nine wavelengths in the range of 730-770 nm. Global analysis revealed multi-exponential decay of excited **5b** aggregates. The most dominant component shows a 13 ps lifetime, followed by a smaller 45 ps component and a slightly present 130 ps decay. Such multi-exponential decay behaviour is a typical feature of ZnChl and BChl *c* rod aggregates.^{94,125,126} As mentioned in Chapter 2.3.1, the shortest decay component ($\tau = 13$ ps) of isolated ZnChl aggregates is attributed to energy relaxation between different excitonic levels and the longer components are most likely due to quenching processes by small amounts of oxidized chlorin present in the aggregate.¹²⁵

Table 2. Fluorescence Lifetimes for Reference Chromophores NDI_{NO} **40**, NDI_{NN} **44**, and ZnChl **5b** Monomers and Aggregates.

Compound	λ_{ex} (nm)	τ_1	τ_2	τ_3
NDI _{NO} 40 ^a	540	12 ns	-	-
NDI _{NN} 44 ^a	620	10 ns	-	-
ZnChl 5b mon. ^b	640	4.3 ns	-	-
ZnChl 5b agg. ^c	720	13 ps	45 ps	130 ps

^a Cyclohexane/ tetrachloromethane (1%); ^b 2-Me-THF/ MeOH (1%); ^c *n*-hexane/ 2-Me-THF (1%).

3.3.3 Kinetics of Energy Transfer Processes in Dyad and Triad Monomers

To examine the excited-state decay behavior of **1b**, **2b**, and **3** monomers, solutions of these compounds in 2-Me-THF were prepared. Selective excitation of the NDI_{NO} moiety of dyad **1b** with 540 nm picosecond laser pulses and global analysis of the resulting emission decay curves in a multi-exponential model provided one major positive amplitude decay-associated component in the wavelength region of the NDI_{NO} emission ($\lambda \leq 635$ nm) (Figure 47A and Table 3). This component exhibits a lifetime of 25 ps, which reflects energy transfer from NDI_{NO} to the ZnChl unit, as evidenced by its large negative amplitude in the ZnChl emission band ($\lambda \geq 635$ nm). Moreover, a very small amplitude component with $\tau = 13$ ns reflects that the main

lifetime component of NDI_{NO} (reference compound NDI_{NO} **40**: $\tau \sim 12$ ns, Table 2) is almost absent, which also proves the quenching of the NDI_{NO} dye. The ZnChI emission region is dominated by a large positive amplitude component with the lifetime $\tau = 0.85$ ns and a minor amplitude with $\tau = 160$ ps; both of them can be assigned to the decay of ZnChI monomers (reference compound ZnChI **5b** monomers: $\tau \sim 4.3$ ns, Table 2). The shortening and the heterogeneity of the ZnChI lifetime versus the isolated ZnChI monomer alone must be due to some intramolecular or intermolecular quenching process.

Monomers of ZnChI- NDI_{NN} **2b** have been excited selectively with 620 nm picosecond laser pulses. The wavelength region of the NDI_{NN} chromophore ($\lambda \leq 635$ nm) is dominated by a positive amplitude component ($\tau = 7$ ps), which turns negative in the emission region of ZnChI monomers and can therefore be assigned to an intramolecular energy transfer process (Figure 47B). As observed for dyad **1b**, the amplitude component of residual NDI_{NN} emission is very small ($\tau = 12$ ns), while the long wavelength range is dominated by the amplitude components of the ZnChI monomer emission ($\tau = 140$ ps and $\tau = 75$ ps).

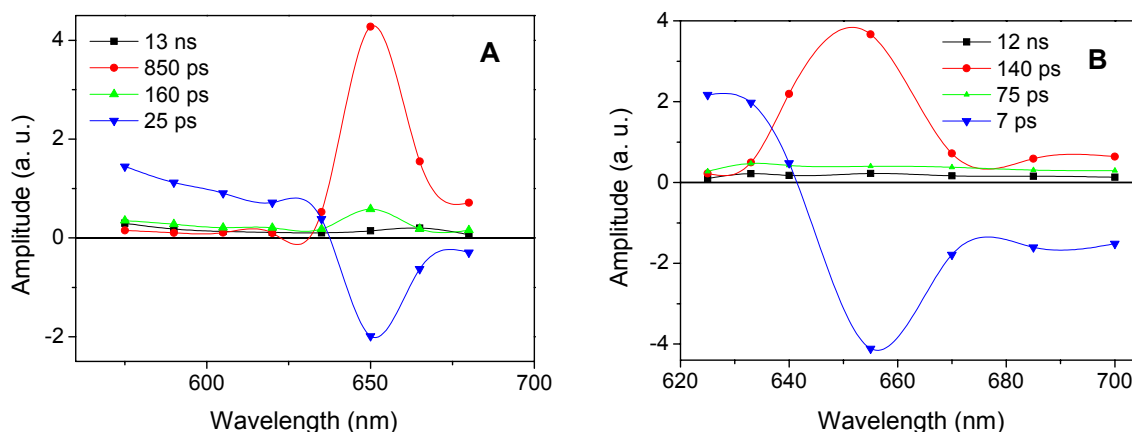


Figure 47. Fluorescence decay-associated spectra of (A) ZnChI- NDI_{NO} **1b** monomers ($\lambda_{\text{ex}} = 540$ nm; $c \sim 4.5 \times 10^{-6}$ M) and (B) ZnChI- NDI_{NN} **2b** monomers ($\lambda_{\text{ex}} = 620$ nm; $c \sim 2.4 \times 10^{-5}$ M) in 2-Me-THF.

Table 3. Fluorescence Lifetimes and Corresponding Amplitudes at Indicated Wavelengths for Monomers of Dyads **1b** and **2b** in 2-Me-THF.

ZnChl-NDI _{NO} 1b ($\lambda_{\text{ex}} = 540$ nm)			ZnChl-NDI _{NN} 2b ($\lambda_{\text{ex}} = 620$ nm)		
τ	Amplitudes ^a		τ	Amplitudes ^a	
	@ 575 nm	@ 650 nm		@ 625 nm	@ 655 nm
13 ns	0.30	0.14	12 ns	0.10	0.22
0.85 ns	0.15	4.3	0.14 ns	0.22	3.7
160 ps	0.35	0.58	75 ps	0.27	0.40
25 ps	1.4	-2.0	7 ps	2.2	-4.1

^a Negative amplitudes indicate rise components.

For the examination of excited state properties of triad **3** monomers, at first, predominantly the NDI_{NO} (and slightly the NDI_{NN}) units were excited with 540 nm picosecond laser pulses (Figure 48A and Table 4). Global analysis of the resulting decay data gave one dominant positive amplitude component with the lifetime $\tau = 22$ ps in the emission region of NDI_{NO}, while the contribution of the amplitude component of unquenched NDI_{NO} ($\tau = 8.0$ ns) is negligibly small. The 22 ps lifetime component exhibits negative amplitudes above 638 nm, indicating that the 2.0 ns species which shows the lifetime and the emission spectrum of the ZnChl moiety is populated by direct energy transfer from the NDI_{NO} unit.

In a further experiment 621 nm laser pulses were chosen to excite the NDI_{NN} chromophore (Figure 48B and Table 4). Again, the amplitude component of the NDI_{NN} emission ($\tau = 7.8$ ns, detection wavelengths $\lambda \leq 640$ nm) was negligibly small, indicating strong emission quenching. Instead, a considerable positive amplitude component could be observed in the long wavelength range which was assigned to the ZnChl monomer emission decay ($\tau = 2.0$ ns). In this region, additionally a strongly negative component ($\tau = 8$ ps) occurred showing that excitation energy of NDI_{NN} units was transmitted to the ZnChl chromophores by a fast energy transfer process.

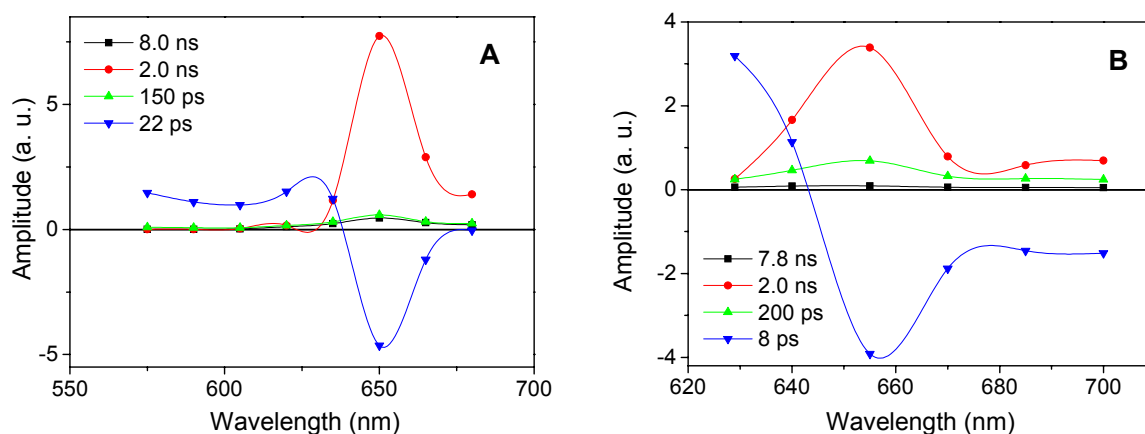


Figure 48. Fluorescence decay-associated spectra of ZnChI-NDI_{NN}-NDI_{NO} **3** monomers in 2-Me-THF. (A) $\lambda_{\text{ex}} = 540$ nm; $c \sim 5.1 \times 10^{-6}$ M; (B) $\lambda_{\text{ex}} = 621$ nm; $c \sim 5.1 \times 10^{-6}$ M.

Table 4. Fluorescence Lifetimes and Corresponding Amplitudes at Indicated Wavelengths for Monomers of Triad **3** in 2-Me-THF.

Triad 3 ($\lambda_{\text{ex}} = 540$ nm)			Triad 3 ($\lambda_{\text{ex}} = 621$ nm)		
τ	Amplitudes ^a		τ	Amplitudes ^a	
	@ 575 nm	@ 650 nm		@ 629 nm	@ 655 nm
8.0 ns	0	0.46	7.8 ns	0.06	0.09
2.0 ns	0.01	7.7	2.0 ns	0.26	3.4
150 ps	0.09	0.58	200 ps	0.25	0.69
22 ps	1.5	-4.6	8 ps	3.2	-3.9

^a Negative amplitudes indicate rise components.

To assess whether the latter energy transfer process proceeds sequentially via the middle NDI_{NN} chromophore or the energy is transmitted directly from the excited NDI_{NO} to the ZnChI unit, a solution of the NDI_{NN}-NDI_{NO} reference chromophore **52** in 2-Me-THF was investigated for comparison. Excitation of **52** at 540 nm provided a 29 ps lifetime component which turns from positive amplitude values in the wavelength range of the NDI_{NO} emission ($\lambda < 620$ nm) to negative amplitudes in the NDI_{NN} emission region ($\lambda > 620$ nm), indicating intramolecular energy transfer from NDI_{NO} to NDI_{NN} (Figure 49). Thus, the time constant of FRET between NDI_{NO} and NDI_{NN} in **52** ($\tau = 29$ ps) exceeds the time constant of the energy transfer observed for triad **3** ($\tau =$

22 ps). Accordingly, the excitation of NDI_{NO} units within triad **3** monomers is apparently followed by a direct energy transfer to the ZnChl dye.

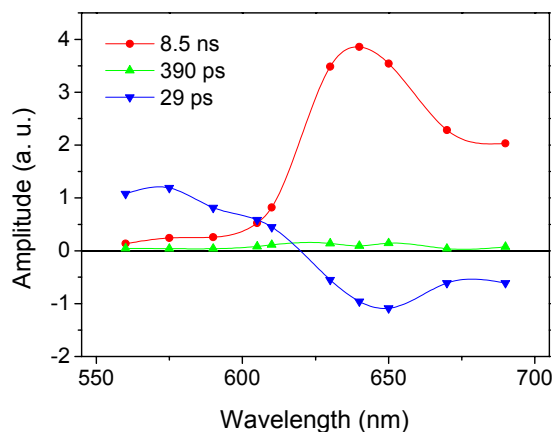


Figure 49. Fluorescence decay-associated spectra of reference chromophore NDI_{NN}-NDI_{NO} **52** ($\lambda_{\text{ex}} = 540$ nm; $c \sim 5.0 \times 10^{-6}$ M) in 2-Me-THF.

The energy level diagrams in Figure 50 show the de-excitation pathways which occur after irradiation of the respective NDI units in **1b**, **2b**, and **3** monomers. The energy levels resemble the S_0 - S_1 transitions. These energies have been calculated from the intersection point of the absorption spectra and normalized emission spectra of the reference chromophores NDI_{NO} **40** and NDI_{NN} **44**, respectively, in THF. For calculation of S_0 - S_1 transitions of the ZnChl moieties the absorption and emission spectra of **1b**, **2b**, and **3**, respectively, were employed. Figure 50 shows that the energy level diagram and the photophysical deactivation processes of triad **3** monomers resemble the sum of the diagrams of dyads **1b** and **2b**.

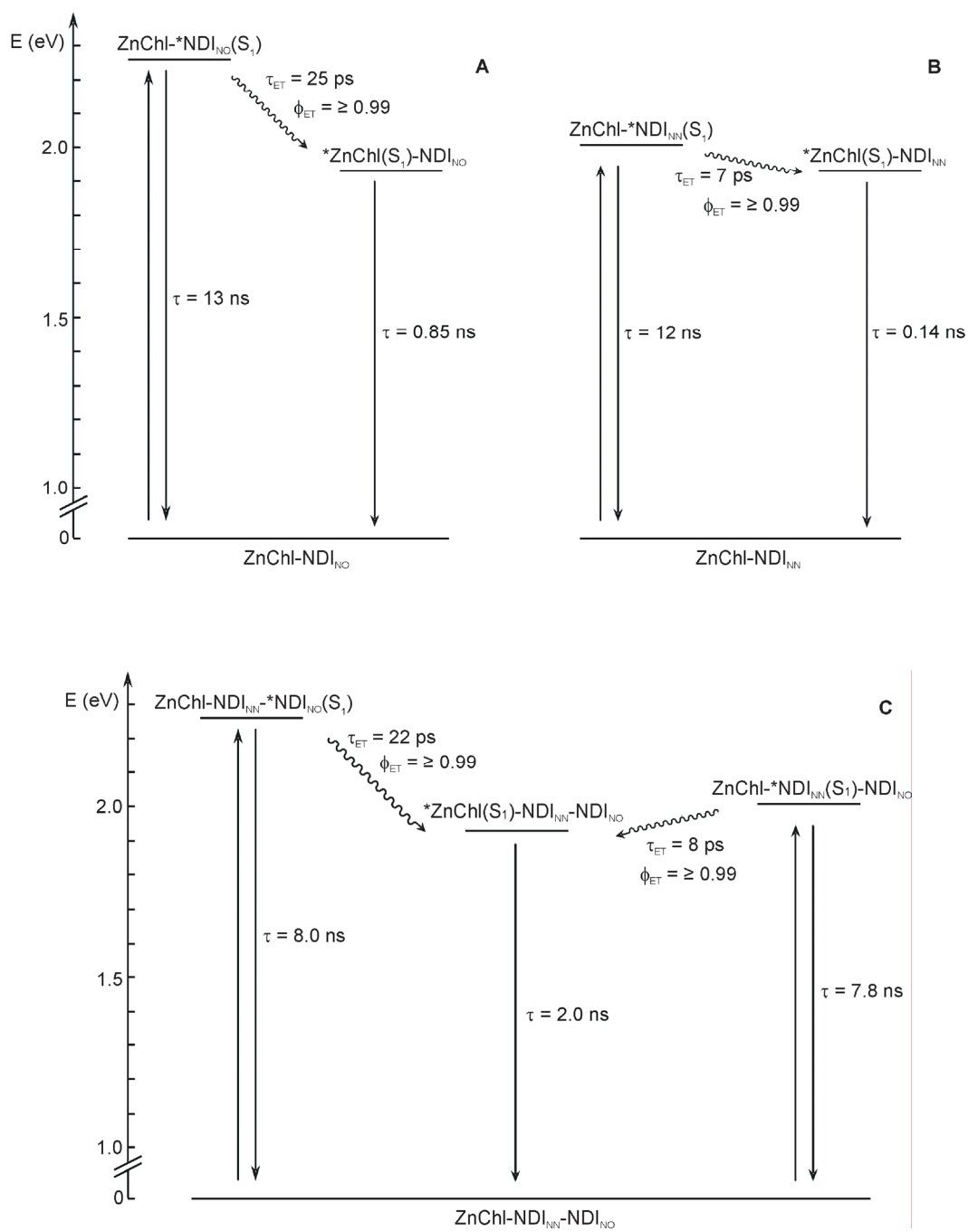


Figure 50. Energy level diagram and photophysical behaviour of monomers of (A) ZnChI-NDI_{NO} **1b**, (B) ZnChI-NDI_{NN} **2b**, and (C) ZnChI-NDI_{NN}-NDI_{NO} **3** in 2-Me-THF (1%).

3.3.4 Kinetics of Energy Transfer Processes in Self-Assembled Dyads and Triad

To investigate the energy transfer processes in self-assembled multichromophoric compounds **1b**, **2b**, and **3** time-resolved fluorescence measurements were conducted in cyclohexane/ tetrachloromethane (1%) solutions. The NDI_{NO} unit of dyad **1b** aggregates was excited by 540 nm laser pulses, which resulted in one dominant positive amplitude component with the lifetime $\tau = 6$ ps in the wavelength region of the NDI_{NO} emission ($\lambda < 640$ nm) (Figure 51A and Table 5). A minor amplitude component with $\tau = 10$ ns is attributed to the residual fluorescence of a marginal amount of unquenched NDI_{NO}. The 6 ps amplitude component turns strongly negative in the emission region of ZnChl aggregates ($\lambda > 700$ nm), demonstrating that an energy transfer from the NDI_{NO} chromophores to the self-assembled ZnChl aggregate takes place. Two positive amplitude components with the lifetimes $\tau = 87$ and 18 ps match the emission spectrum of the ZnChl **5b** aggregates (Table 2), reflecting the decay of those excited states that are generated by energy transfer from excited NDI_{NO} dyes. The fluorescence decay proceeds in a multi-exponential way, resembling the typical decay behaviour of ZnChl rod aggregates such as **5b**.^{125,126}

Furthermore, time-resolved fluorescence spectroscopic measurements have been performed on aggregates of ZnChl-NDI_{NN} **2b**. Upon illumination of the sample with 620 nm laser pulses the blue colored NDI_{NN} chromophores are excited selectively. The resulting DAS are shown in Figure 51B. As for dyad **1b**, nearly complete quenching of the excited NDI_{NN} chromophores ($\tau = 11$ ns) has been observed for **2b**. Furthermore, a small component with $\tau = 2.6$ ns occurs in the NDI_{NN} emission region. This component is apparently due to small amounts of residual **2b** monomer present in equilibrium with the aggregate. The dominant amplitude component ($\tau = 5$ ps) in the short wavelength region turns strongly negative in the emission region of ZnChl aggregates ($\lambda > 700$ nm), indicating fast energy transfer. The lifetimes of the multi-exponential ZnChl aggregate decay (18, 88, and 710 ps) match the decay characteristics of **1b** aggregates.

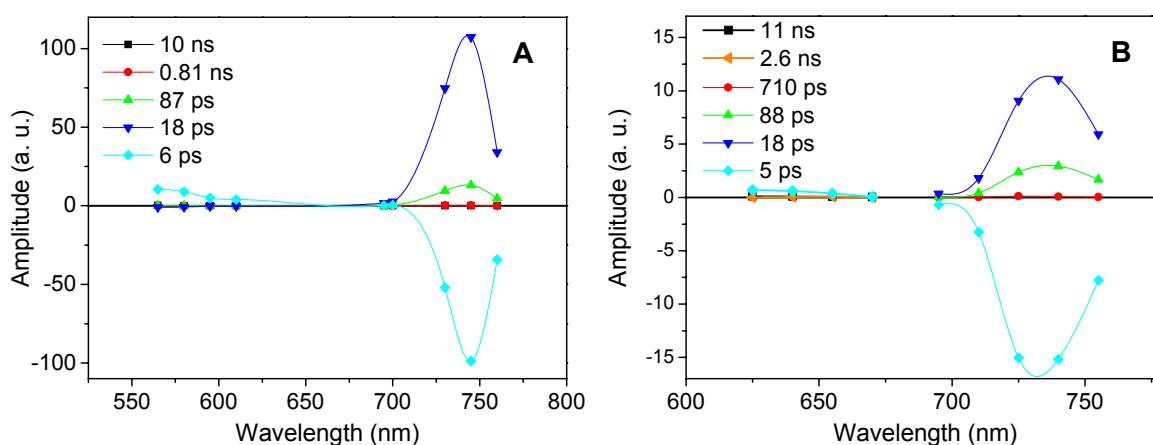


Figure 51. Fluorescence decay-associated spectra of aggregates of (A) ZnChI-NDI_{NO} **1b** ($\lambda_{\text{ex}} = 540$ nm; $c \sim 7.5 \times 10^{-6}$ M) and (B) ZnChI-NDI_{NO} **2b** ($\lambda_{\text{ex}} = 620$ nm; $c \sim 7.6 \times 10^{-6}$ M) in cyclohexane/tetrachloromethane (1%).

Table 5. Fluorescence Lifetimes and Corresponding Amplitudes at Indicated Wavelengths for Aggregates of ZnChI-NDI **1b** and **2b** in Cyclohexane/ Tetrachloromethane (1%).

ZnChI-NDI _{NO} 1b ($\lambda_{\text{ex}} = 540$ nm)			ZnChI-NDI _{NN} 2b ($\lambda_{\text{ex}} = 620$ nm)		
τ	Amplitudes ^a		τ	Amplitudes ^a	
	@ 560 nm	@ 745 nm		@ 625 nm	@ 740 nm
10 ns	0.15	0.01	11 ns	0.09	0
87 ps	0.03	13	88 ps	0	2.9
18 ps	-0.86	108	18 ps	0	11
6 ps	11	-99	5 ps	0.69	-15

^a Negative amplitudes indicate rise components.

Prior to investigating the photophysical processes in triad **3** aggregates, a solution of the NDI_{NN}-NDI_{NO} reference compound **52** in cyclohexane/ tetrachloromethane (1%) was examined. A clear evidence for FRET from the excited NDI_{NO} chromophore to the NDI_{NN} unit in this solvent system has already been obtained from the steady state emission spectrum of **52**, as only an NDI_{NN} emission band has been detected (Figure 38B). To gain insight into the kinetics of this process, NDI_{NN}-NDI_{NO} **52** was irradiated with 540 nm laser pulses and the fluorescence decay was recorded at eight wavelengths in the range of 575-680 nm (Figure 52). Global analysis revealed a 15 ps lifetime component, which turns from positive amplitudes in wavelength region of the NDI_{NO} emission region ($\lambda < 615$ nm) to negative amplitudes in the NDI_{NN}

emission region. This lifetime component is attributed to an energy transfer from NDI_{NO} to the blue NDI_{NN} dye. In the NDI_{NN} emission region a dominant positive 11 ns amplitude component for the NDI_{NN} emission decay is observed. The additional small 980 ps component might be due to some intramolecular or intermolecular quenching process.

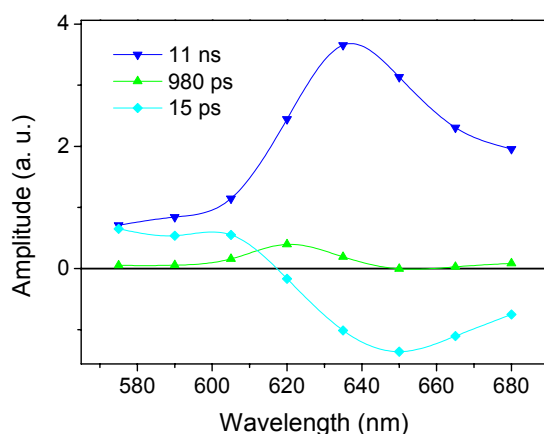


Figure 52. Fluorescence decay-associated spectra of reference chromophore NDI_{NN}-NDI_{NO} **52** ($\lambda_{\text{ex}} = 540$ nm; $c \sim 6.9 \times 10^{-6}$ M) in cyclohexane/ tetrachloromethane (1%).

The excited state properties of triad **3** aggregates in cyclohexane/ tetrachloromethane (1%) have been first investigated by exciting mainly the NDI_{NO} (and slightly NDI_{NN}) units with at 540 nm. The resulting DAS are depicted in Figure 53A and the amplitude components and their lifetimes are collected in Table 6. As observed for dyad **1b**, the amplitude component of the NDI_{NO} emission ($\lambda_{\text{max}} = 558$ nm) with the lifetime $\tau = 10$ ns is very small compared to the amplitude component with the lifetime $\tau = 6$ ps in the short wavelength range ($\lambda \leq 700$ nm). The latter turns strongly negative in the region of ZnChl aggregate emission ($\lambda_{\text{max}} = 738$ nm) and is therefore attributed to an energy transfer process from NDI_{NO} to the ZnChl antenna. The time constant of 6 ps for this process is smaller than that observed for the energy transfer from NDI_{NO} to NDI_{NN} in reference compound **52** ($\tau = 15$ ps). Thus, it is more likely that upon excitation of NDI_{NO} in triad **3** the excitation energy is directly transmitted to the ZnChl antenna rather than being transferred along a cascade via the NDI_{NN} unit. The decay of excited ZnChl aggregate, which is generated by this energy transfer, shows the characteristic multi-exponential behavior with a major 14 ps and a minor 76 ps amplitude component.

In a further experiment 621 nm laser pulses were chosen to excite the NDI_{NN} unit (Figure 53B and Table 6). Again, the amplitude component which could be attributed to NDI_{NN} emission ($\tau = 10$ ns, detection wavelengths $\lambda \leq 670$ nm) was negligibly small owing to strong emission quenching. A larger positive amplitude component ($\tau = 4$ ps) occurs in the same wavelength region. This component turns strongly negative in the ZnChl aggregate emission ($\lambda \geq 710$ nm) region and can, therefore, be assigned to a fast energy transfer process from NDI_{NN} chromophores to the ZnChl rod antenna. The multi-exponential decay of ZnChl aggregates is dominated by a 12 ps lifetime component and a few additional longer wavelength components with much smaller amplitudes.

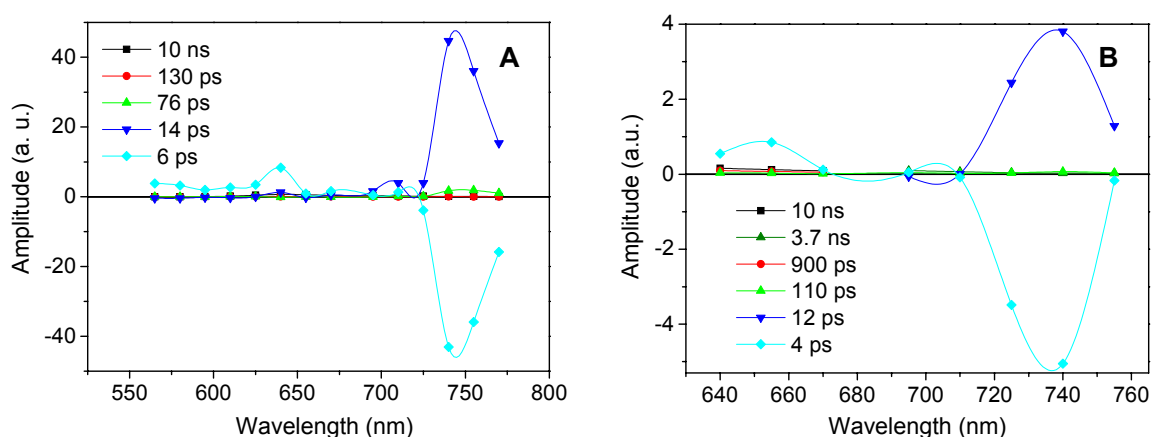


Figure 53. Fluorescence decay-associated spectra of aggregates of triad **3** in cyclohexane/tetrachloromethane (1%). (A) $\lambda_{\text{ex}} = 540$ nm; $c \sim 6.9 \times 10^{-6}$ M; (B) $\lambda_{\text{ex}} = 621$ nm; $c \sim 7.9 \times 10^{-6}$ M.

Table 6. Fluorescence Lifetimes and Corresponding Amplitudes at Indicated Wavelengths for Aggregates of Triad **3** in Cyclohexane/ Tetrachloromethane (1%).

Triad 3 ($\lambda_{\text{ex}} = 540$ nm)			Triad 3 ($\lambda_{\text{ex}} = 621$ nm)			
τ	Amplitudes ^a			τ	Amplitudes ^a	
	@ 565 nm	@ 640 nm	@ 740 nm		@ 640 nm	@ 740 nm
10 ns	0.02	0.69	0.12	10 ns	0.14	0
76 ps	0.02	-0.10	1.8	110 ps	0.03	0.06
14 ps	-0.39	1.3	47	12 ps	0	3.4
6 ps	3.8	8.4	-43	4 ps	0.49	-4.5

^a Negative amplitudes indicate rise components.

The decay pathway followed after excitation of the respective NDI units in **1b**, **2b**, and **3** aggregates are illustrated in the energy level diagrams shown in Figure 54. The energy level diagram and photophysical processes of triad **3** aggregates nearly resemble the sum of the diagrams of dyads **1b** and **2b**. The most remarkable feature of triad **3** is the ultrafast energy transfer, directly from the outer pink NDI unit to the central ZnChl rod aggregate.

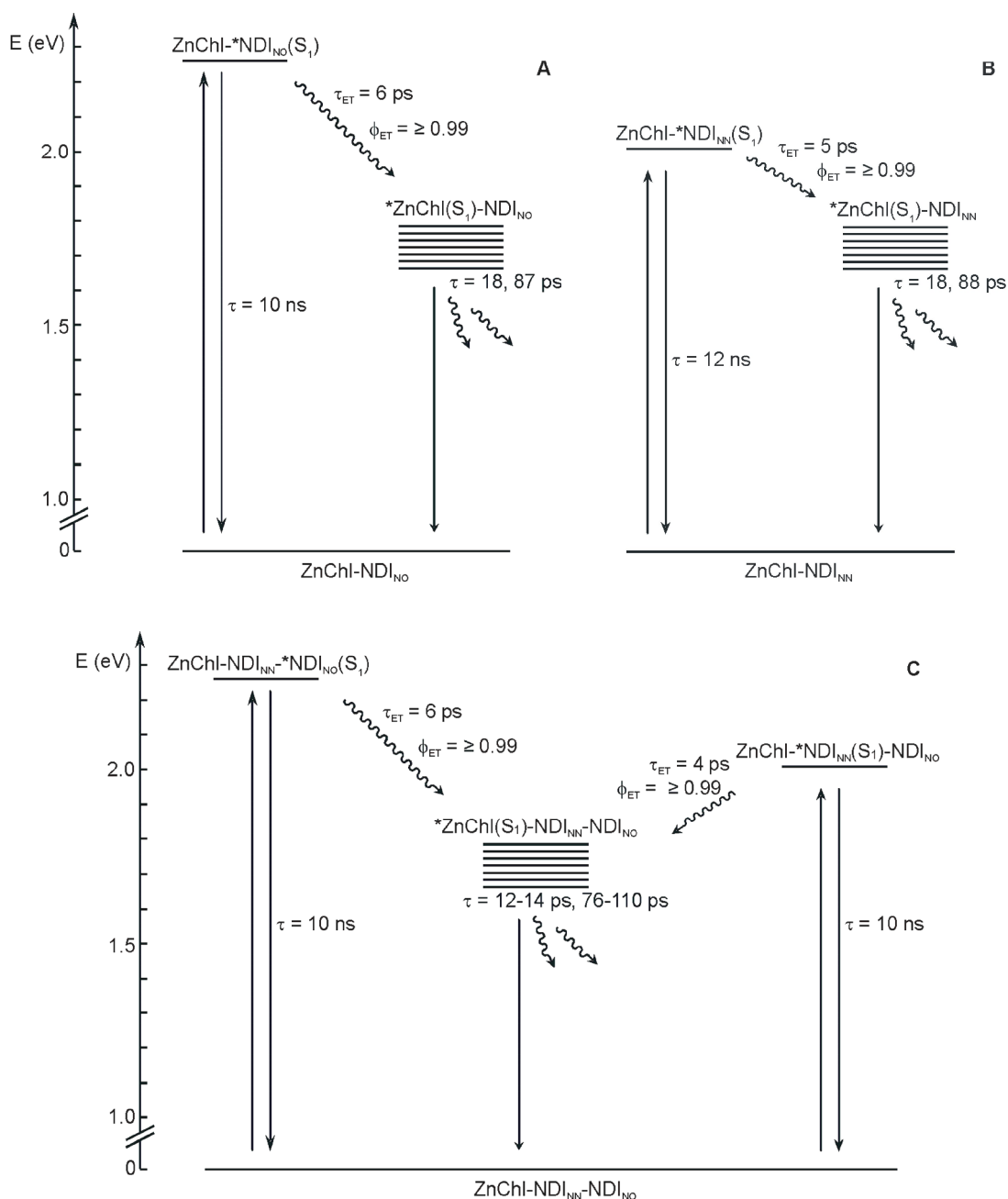


Figure 54. Energy level diagram and photophysical behaviour of aggregates of (A) ZnChl-NDI_{NO} **1b**, (B) ZnChl-NDI_{NN} **2b**, and (C) ZnChl-NDI_{NN}-NDI_{NO} **3** in cyclohexane/ tetrachloromethane (1%).

The energy transfer rates k_{ET} and decay rates k_D of the donor emission can be easily calculated from the time-resolved fluorescence results. For monomers of compounds **1b**, **2b**, and **3**, the energy transfer rates have been calculated to be in the range of $4.0\text{-}4.5\times 10^{10} \text{ s}^{-1}$, if NDI_{NO} was acting as an energy donor, and $1.3\text{-}1.4\times 10^{11} \text{ s}^{-1}$ with NDI_{NN} as donor unit (Table 7). Energy transfer rates from peripheral NDI chromophores to the ZnChl rod aggregate are even larger showing values of $1.7\times 10^{11} \text{ s}^{-1}$ at excitation of the NDI_{NO} chromophore and $2.0\text{-}2.5\times 10^{11} \text{ s}^{-1}$, if NDI_{NN} units were excited (Table 8).

According to the Förster theory, the values of energy transfer rates depend on the extent of the overlap integral $J(\lambda)$ of the normalized emission spectrum of the NDI energy donor and the absorption spectrum of the ZnChl monomer or aggregate, respectively (eq 6 and eq 7). Thus, the overlap integrals $J(\lambda)$ of **1b**, **2b**, and **3** monomers and aggregates have been calculated using equation 8 (Chapter 2.1.3). The overlap integrals of NDI_{NN} and ZnChl dyes of **2b** and **3** monomers ($J(\lambda) = 2.21\times 10^{15} \text{ M}^{-1} \text{ cm}^{-1} \text{ nm}^4$) exceed the overlap integrals of the pink NDI_{NO} and the ZnChl moiety of **1b** and **3** monomers ($J(\lambda) = 1.02\times 10^{15} \text{ M}^{-1} \text{ cm}^{-1} \text{ nm}^4$) (Table 7). This result is in good agreement with the observation, that the energy transfer processes from NDI_{NN} donors are slightly faster than those from NDI_{NO} units for **1b**, **2b**, and **3** monomers.

Table 7. Energy Transfer Rates Derived from Time-Resolved Emission Data and Overlap Integrals of **1b**, **2b**, and **3** Monomers in 2-Me-THF.

Compound	k_D		$k_{ET} (\text{s}^{-1})$	$J(\lambda) (\text{M}^{-1} \text{ cm}^{-1} \text{ nm}^4)$
	$\text{NDI}_{\text{NO}} (\text{s}^{-1})$	$\text{NDI}_{\text{NN}} (\text{s}^{-1})$		
1b	7.7×10^7		4.0×10^{10}	1.02×10^{15}
2b		8.3×10^7	1.4×10^{11}	2.21×10^{15}
3	1.3×10^8		4.5×10^{10}	1.02×10^{15}
3		1.2×10^8	1.3×10^{11}	2.21×10^{15}

Accordingly, the overlap integrals of NDI_{NN} and ZnChl chromophores of **2b** and **3** aggregates ($J(\lambda) = 1.69 \times 10^{15} \text{ M}^{-1} \text{ cm}^{-1} \text{ nm}^4$) exceed the overlap integrals of NDI_{NO} and ZnChl dyes of **1b** and **3** aggregates ($J(\lambda) = 5.64 \times 10^{14} \text{ M}^{-1} \text{ cm}^{-1} \text{ nm}^4$), resulting in slightly faster energy transfer processes for NDI_{NN} donors than for NDI_{NO} donors (Table 8).

Table 8. Energy Transfer Rates Derived from Time-Resolved Emission Data and Overlap Integrals of **1b**, **2b**, and **3** Aggregates in Cyclohexane/ Tetrachloromethane (1%).

Compound	k_D		$k_{ET} (\text{s}^{-1})$	$J(\lambda) (\text{M}^{-1} \text{ cm}^{-1} \text{ nm}^4)$
	NDI _{NO} (s^{-1})	NDI _{NN} (s^{-1})		
1b	1.0×10^8		1.7×10^{11}	5.64×10^{14}
2b		9.1×10^7	2.0×10^{11}	1.69×10^{15}
3	1.0×10^8		1.7×10^{11}	5.64×10^{14}
3		1.0×10^8	2.5×10^{11}	1.69×10^{15}

However, the overlap integrals of **1b**, **2b**, and **3** aggregates are lower than those of the respective monomers (Tables 7 and 8), although, for aggregates, larger energy transfer rates have been observed. Thus, there must be a different explanation for the fast energy transfers in **1b**, **2b**, and **3** aggregates.

A reason for the large transfer rates in **1b**, **2b**, and **3** aggregates could be an increase in the transition dipole moment $|\bar{\mu}|$ of the ZnChl aggregate Q_y-band in comparison to the monomer Q_y-transition, leading to larger Coulombic interaction energies between energy donors and acceptors. Thus, the transition dipole moment of the Q_y band of ZnChl **5a** monomers (wavelength range: 580-715 nm) in THF and that of **5a** in cyclohexane (98.9%)/ tetrachloromethane (1%)/ THF (0.1%) (wavelength range: 625-770 nm) have been calculated using equations 4 and 5. For monomers, the transition dipole moment of the Q_y band equals 4.7 D, while for aggregates an increased transition dipole moment of 5.6 D has been observed.

A second explanation for the fast energy transfer in **1b**, **2b**, and **3** aggregates could be the tight arrangement of ZnChl chromophores, which provides the NDI energy donors with a wide choice of potential energy acceptors.

3.3.5 Calculation of Energy Transfer Efficiencies

The singlet-singlet excitation energy transfer efficiency from NDI to ZnChl chromophores in **1b**, **2b**, and **3** monomers and ZnChl rod aggregates can in principle be estimated either from steady state or from time-resolved fluorescence data. To calculate energy transfer efficiencies from steady state spectroscopic measurements, it is necessary to record excitation spectra at an acceptor emission wavelength which is separated from the donor emission region. However, for monomers of **1b**, **2b**, and **3** it was not possible to find an appropriate detection wavelength, since the broad S_0 - S_1 emission band of NDI_{NO} and NDI_{NN}, respectively, overlap with the rather narrow emission band of the ZnChl monomer. Therefore, all recorded excitation spectra of **1b**, **2b**, and **3** monomers did not exactly match with the respective absorption spectrum, but showed a too large contribution of the NDI band. On the other hand, the fluorescence intensities of **1b**, **2b**, and **3** aggregates are too low to get excitation spectra of these species, which would be smooth enough for a quantitative analysis. Hence it was decided to calculate energy transfer efficiencies ϕ_{ET} from time-resolved data only using eq 11 (Chapter 2.3.1). Due to the high energy transfer rates on the picosecond time scale (Table 7 and Table 8), energy transfer efficiencies for monomers as well as for aggregates of compounds **1b**, **2b**, and **3** of $\phi_{ET} \geq 99\%$ were obtained.

3.3.6 Calculation of Light-Harvesting Efficiencies

Since it has been shown that all excited NDI units transfer their energy directly and completely to the ZnChl rod, the increase of the LH capacity of the multi-chromophoric LH systems **1b**, **2b**, and **3** compared to monochromophoric aggregates of ZnChl **5a** can be calculated from the ratio of the respective cross sections of terrestrial solar light absorption. The absorption cross section of a particular molecule refers to its ability to absorb a photon of a particular wavelength. The cross sections σ for solar light absorption of aggregates of dyads **1b**, **2b**, and **3** ($\sigma_{1b,2b,3}$) and ZnChl **5a** (σ_{5a}) can be calculated by integration of the products of the respective absorption spectra $A(\lambda)$ and the terrestrial solar spectral irradiance $W(\lambda)$ (Figure 3, blue curve) in the range of 350-800 nm ($\Delta\lambda = 1$ nm):

$$\sigma_{\mathbf{1b},\mathbf{2b},\mathbf{3}} = \int_{350nm}^{800nm} (A_{\mathbf{1b},\mathbf{2b},\mathbf{3}}(\lambda) \cdot W(\lambda)) d\lambda \quad (18)$$

$$\sigma_{\mathbf{5a}} = \int_{350nm}^{800nm} (A_{\mathbf{5a}}(\lambda) \cdot W(\lambda)) d\lambda \quad (19)$$

The ratio between the absorption cross sections of **1b** aggregates and ZnChl aggregates is calculated to be 1.36, implying an increase of 36% in the total LH efficiency of ZnChl-NDI_{NO} **1b** aggregates emanated from the appended NDI_{NO} chromophores:

$$\frac{\sigma_{\mathbf{1b}}}{\sigma_{\mathbf{5a}}} = 1.36 \rightarrow 36\% \text{ increase.}$$

For ZnChl-NDI_{NN} **2b**, an improvement of 26% was reached due to energy transfer from the blue NDI_{NN} and best results were obtained for triad **3**, showing an increase of 63% of the total LH efficiency.

Chapter 4: Summary

Supramolecular, excitonically coupled dye aggregates are of high interest for the development of new electronic materials on the nanoscale.^{169,170} They serve as efficient light-harvesting and exciton transport systems due to the high density and the defined geometrical arrangement of chromophores. However, such systems can only exploit the terrestrial sunlight sufficiently if they cover the whole range of the spectral solar irradiance by a variety of antenna chromophores.

The present work deals with the extension of the cross section for solar light absorption of the self-assembled zinc chlorin rod antenna, which is the artificial counterpart for the natural protein-free bacteriochlorophyll *c* light-harvesting system in bacterial chlorosomes. In artificial zinc chlorin as well as natural bacteriochlorophyll *c* self-assemblies excitation energy is delocalized over several excitonically coupled chromophores and it can be transported over large distances along the cylinder. Yet both systems do not make use of the most intensive wavelength range of solar irradiance, i.e. the so-called “green gap”. Thus, in the first part of this work supporting light-harvesting chromophores were covalently linked to supramolecular zinc chlorin building blocks. Target molecules **1-3** bear either one or two additional naphthalene diimides which absorb light in the desired wavelength region. The additional dyes were attached in the 17³ position of zinc chlorins in order to avoid an interference of the naphthalene diimides on the rod formation. The chlorin building blocks of compounds **1-3** were synthesized by a multi-stage procedure starting from chlorophyll *a* and core-substituted naphthalene diimide chromophores were prepared by successive transformation of pyrene. Subsequently, the single components of multi-chromophores **1-3** were linked to each other by esterification or amidation reactions, respectively, followed by functionalization of the chlorin moieties with the 3¹-hydroxy group and the central zinc ion. UV-vis spectroscopic measurements in THF revealed that in monomers of compounds **1-3** the respective chromophoric building blocks do not interact with each other in the ground state.

The next challenge was to find a nonpolar aprotic solvent system, which supports the self-assembly process of **1-3** multichromophores into well-soluble cylindrical aggregates. Cyclohexane turned out to be an appropriate solvent for compounds **1b**, **2b**, and **3** bearing long alkyl side chains, while compounds **1a** and **2a** precipitate.

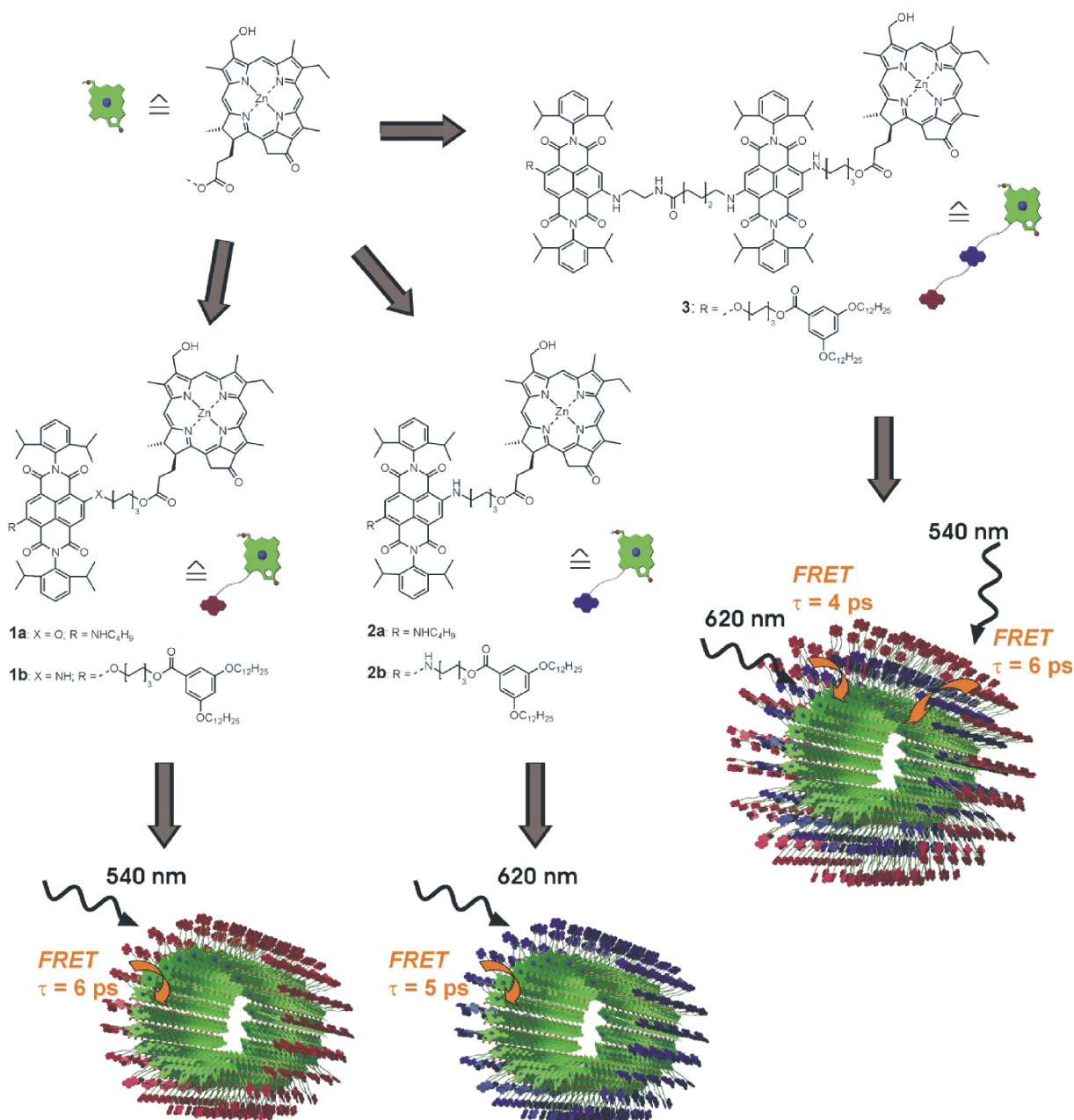


Figure 55. Zinc chlorin-naphthalene diimide dyads **1,2** and triad **3** synthesized in this work, schematic illustration of the self-assembled aggregate structures, and time constants of FRET (fluorescence resonance energy transfer) processes within the light-harvesting systems upon illumination.

UV-vis, CD, and steady state fluorescence spectroscopy of compounds **1b**, **2b**, and **3** in cyclohexane revealed that these derivatives form *J*-aggregates, since similarly

large red-shifts of the chlorin Q_y band from 646-647 nm (monomers) to 729-731 nm (aggregates) as for parent bacteriochlorophyll *c* aggregates were detected. These results indicate a close analogy of the short-range arrangement of zinc chlorin chromophores in aggregates of **1b**, **2b**, and **3** to that in bacteriochlorophyll *c* and zinc chlorin aggregates without additional chromophores. Self-assembly of the zinc chlorin units into rod-type extended aggregate structures was further evidenced by the pronounced bisignate CD signal in the range of the Q_y band which arises from a helical arrangement of transition dipole moments. On the other hand, naphthalene diimide absorption bands were only slightly influenced by the choice of the solvent and CD spectra of **1b**, **2b**, and **3** solutions in cyclohexane did not reveal any Cotton effect for these chromophores. Thus, it was concluded that naphthalene diimide chromophores do not interact with each other at the periphery of the self-assembled zinc chlorin rod. Temperature-dependent UV-vis and CD spectroscopic studies of dyads **1b** and **2b** showed that the self-assembly process is reversible. Moreover, atomic force microscopy of aggregates of dyad **2b** provided evidence for their rod-shaped structure and indicated a pronounced stiffness of the elongated objects. The increase of the diameter of **2b** aggregates compared to zinc chlorin rods which are unsubstituted at their periphery was caused by the enveloping naphthalene diimide layer.

The photophysical behaviour of naphthalene diimide and zinc chlorin reference chromophores and of **1b**, **2b**, and **3** monomer and aggregate solutions was investigated by time-resolved fluorescence experiments. Upon selective excitation of blue or pink naphthalene diimide units of **1b**, **2b**, and **3** monomers their excitation energy is quantitatively conveyed to the zinc chlorin chromophore within the picosecond time scale (7-25 ps). For aggregates of **1b**, **2b**, and **3** energy transfer processes from peripheral naphthalene diimides to the inner green zinc chlorin rod antenna were observed, showing even faster energy transfer time constants (5-6 ps). Therefore, the “green gap” was bridged by the attached naphthalene diimide antenna chromophores, giving dye aggregates whose light-harvesting efficiency for the absorption of terrestrial sunlight is increased by up to 63% compared to the parent zinc chlorin or natural bacteriochlorophyll *c* rod aggregates. The present systems represent a highly efficient example of a self-organized, matrix-free, multichromophoric antenna.

Chapter 5: Zusammenfassung

Supramolekulare, exzitonisch gekoppelte Farbstoffaggregate sind für die Entwicklung neuer elektronischer Nanomaterialien von großem Interesse.^{169,170} Aufgrund der dichten Packung an Chromophoren und deren definierter gegenseitiger Ausrichtung dienen sie als effiziente Lichtsammel- und Exzitonentransport-Systeme. Allerdings kann das terrestrische Sonnenlicht nur dann zur Genüge genutzt werden, wenn für dessen gesamten intensiven sichtbaren Spektralbereich eine Vielfalt verschieden farbiger Lichtsammel-Chromophore zur Verfügung steht.

Das Ziel der vorliegenden Arbeit war die Erweiterung des Absorptionsquerschnitts von selbstorganisierten Zinkchlorin-Stabantennen für eine optimierte Ausschöpfung der solaren Strahlung. Zinkchlorin-Aggregate sind hervorragende Modellsysteme für die natürlichen Bakteriochlorophyll *c*-Antennen bakterieller Chlorosomen, deren zylindrische Struktur gänzlich ohne eine stabilisierende Protein-Matrix besteht. In beiden Systemen ist die Anregungsenergie über mehrere exzitonisch gekoppelte Farbstoff-Moleküle delokalisiert und kann durch schnellen Energietransfer über weite Strecken entlang der Zylinderachse transportiert werden. Indes sind weder Modell noch bakterielles Original in der Lage, im intensivsten Wellenlängen-Bereich des Sonnenlichts, der sogenannte „Grüne Lücke“, zu absorbieren. Aus diesem Grund wurden im ersten Teil dieser Arbeit supramolekulare Zinkchlorin-Bausteine kovalent mit zusätzlichen Lichtsammel-Chromophoren verknüpft.

Die Zielmoleküle **1-3** sind mit einem bzw. zwei zusätzlichen Naphthalindiimiden funktionalisiert, deren Absorptionsbande im gewünschten Bereich liegt. Für die Anknüpfung der zusätzlichen Farbstoffe wurde die 17³-Position des Zinkchlorin-Bausteins ausgewählt, um möglichst einen negativen Einfluss des Naphthalindiimids auf die Stabaggregatbildung zu unterbinden. Die Chlorinbausteine der Verbindungen **1-3** wurden in einem mehrstufigen Verfahren ausgehend von Chlorophyll *a* hergestellt und die Synthese der Kern-funktionalisierten Naphthalindiimide erfolgte durch sukzessive Umwandlung von Pyren. Die einzelnen Bausteine der Multichromophore **1-3** wurden daraufhin durch Veresterungs- oder Amidierungs-

Reaktionen miteinander verknüpft und zuletzt wurden die jeweiligen Chlorin-Einheiten mit der für die Selbstorganisation notwendigen 3¹-Hydroxy-Gruppe und dem zentralen Zink-Ion funktionalisiert. UV-vis-spektroskopische Messungen in THF ergaben, dass innerhalb der Monomere der Verbindungen **1-3** keine elektronischen Wechselwirkungen zwischen den jeweiligen Chromophor-Bausteinen auftreten.

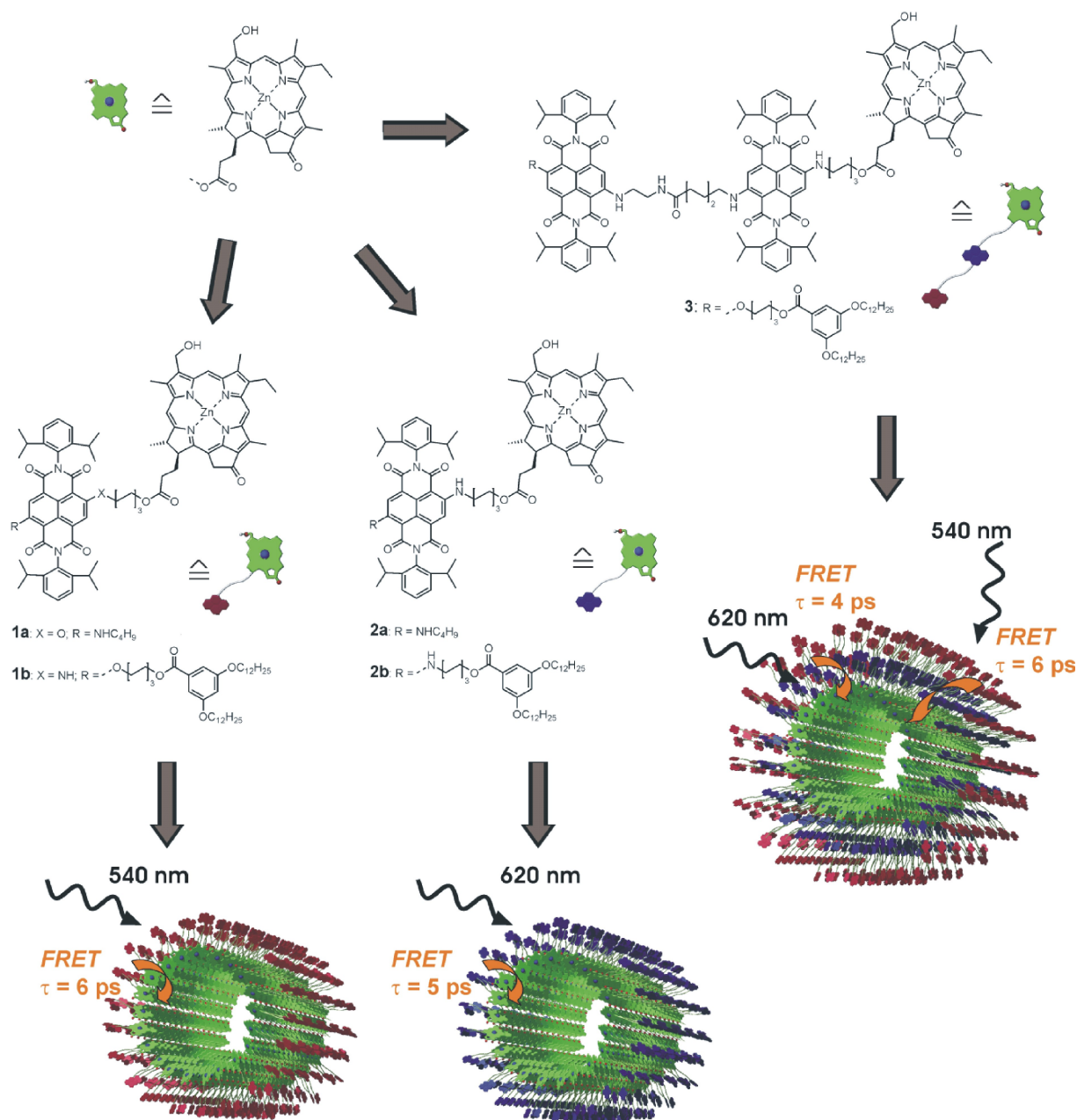


Figure 56. Zinkchlorin-Naphthalendiimid-Dyaden **1,2** und Triade **3**, die in der vorliegenden Arbeit synthetisiert wurden. Schematische Darstellung der Aggregatstrukturen sowie Zeitkonstanten der FRET-Prozesse (Fluoreszenz-Resonanz-Energietransfer) innerhalb der Lichtsammelsysteme, die bei Bestrahlung beobachtet wurden.

Im nächsten Schritt musste ein unpolares aprotisches Lösungsmittel-System gefunden werden, das die Selbstorganisation der Multi-Chromophore **1-3** zu gut löslichen, zylindrischen Aggregatstrukturen ermöglicht. Cyclohexan erwies sich als geeignetes Solvens für die mit langen Alkyl-Seitenketten funktionalisierten Verbindungen **1b**, **2b** und **3**, wohingegen die Dyaden **1a** und **2a** präzipitierten. Mittels UV-vis-, CD- und stationärer fluoreszenzspektroskopischer Untersuchungen der Verbindungen **1b**, **2b** und **3** in Cyclohexan konnte gezeigt werden, dass alle drei Zinkchlorin-Derivate *J*-Aggregate ausbilden, für die ähnliche Rotverschiebungen der Chlorin- Q_y -Banden von 646-647 nm (Monomere) zu 729-731 nm (Aggregate) detektiert wurden. Diese Ergebnisse deuten darauf hin, dass in den Selbstorganisations dieser Verbindungen eine ähnliche Nahordnung der Zinkchlorine wie bei unsubstituierten Bakteriochlorophyll *c*- und Zinkchlorin-Aggregaten vorliegt. Die Selbstorganisation von Zinkchlorinen zu stabförmigen Strukturen wurde weiterhin durch ein ausgeprägtes bisignantes CD-Signal im Bereich der Q_y -Bande belegt, welches durch eine helikale Anordnung der Übergangsdipolmomente hervorgerufen wird. Im Gegensatz dazu wurden die Absorptionsbanden der Naphthalindiimid-Komponenten kaum durch die Wahl des Lösungsmittels beeinflusst, und in den CD-Spektren der Cyclohexan-basierten Lösungen von **1b**, **2b** und **3** war kein Cotton-Effekt zu finden, der den Naphthalindiimiden hätte zugeordnet werden können. Dies steht in Einklang mit der Vorstellung, dass die Naphthalindiimid-Chromophore an der Peripherie der Stabaggregate keine Wechselwirkungen untereinander ausbilden. Temperatur-abhängige UV-vis- und CD-spektroskopische Studien der Dyaden **1b** und **2b** belegten die Reversibilität des Selbstorganisations-Prozesses. Ein weiterer Nachweis für das Vorliegen von Stabaggregaten wurde durch rasterkraftmikroskopische Aufnahmen von Verbindung **2b** erbracht, für die längliche Objekte ($L = 93 \pm 75$ nm) mit beachtlicher Persistenzlänge detektiert werden konnten. Eine Vergrößerung des Durchmessers der Aggregate von **2b** im Vergleich zu an der Peripherie unsubstituierten Zinkchlorin-Stäben wurde auf die umhüllende Naphthalindiimid-Schicht zurückgeführt.

Die photophysikalischen Charakteristika von Naphthalindiimid- und Zinkchlorin-Referenzchromophoren sowie der Monomer- und Aggregatlösungen der Multi-Chromophore **1b**, **2b** und **3** wurden mittels zeitaufgelöster Fluoreszenz-Experimente untersucht. Bei einer selektiven Anregung der blau- oder pinkfarbenen Naphthalindiimid-Einheiten der Monomere wurde ermittelt, dass die

Anregungsenergie in allen Fällen innerhalb von wenigen Pikosekunden (7-25 ps) zum Zinkchlorin-Baustein überführt wird. Innerhalb der multichromophoren Aggregate von **1b**, **2b** und **3** finden hoch effiziente Energietransfer-Prozesse von den peripheren Naphthalindiimiden zum inneren Zinkchlorin-Kern statt, deren Zeitkonstanten die der Monomere sogar noch unterschreiten (5-6 ps). Somit konnte die „Grüne Lücke“ der Zinkchlorin-Aggregate durch die Anknüpfung von Naphthalindiimiden als zusätzliche Antennenfarbstoffe überbrückt und die Effizienz für die Absorption von terrestrischem Sonnenlicht um bis zu 63% im Vergleich zum originalen System gesteigert werden. Die vorliegenden Aggregate repräsentieren somit ein hocheffizientes Beispiel eines selbst-organisierten, matrix-freien, multichromophoren Lichtsammelsystems.

Chapter 6: Experimental Section

6.1 Materials and Methods

Thin Layer Chromatography (TLC)

TLC experiments were performed on aluminium foils, which were coated with silica gel 60 F₂₅₄ and a concentration zone, purchased from Merck KGaA (Hohenbrunn, Germany).

Column Chromatography

Flash and normal pressure column chromatography were done using silica gel Si60 (mesh size 0.032-0.063 mm) from Merck KGaA (Hohenbrunn, Germany) as stationary phase. The eluents are mentioned in the respective procedures. Column chromatography of chlorin derivatives was carried out in a darkened hood.

High Performance Liquid Chromatography (HPLC)

Analytical HPLC was performed on a pump system (PU-2080 PLUS) with a multi-wavelength photodiode array detector (MD-2015 PLUS) from JASCO GmbH (Groß-Umstadt, Germany), equipped with a ternary gradient unit (LG-2080-02) and line-degasser (DG-2080-53). Preparative HPLC was carried out on a system (PU-2080 PLUS) with a four-wavelength photodiode array detector (UV-2077 PLUS). HPLC grade solvents (Rectapur) from VWR GmbH (Darmstadt, Germany) were used. Reversed-phase HPLC columns from Macherey-Nagel GmbH & Co. KG (Düren, Germany) were used (analytical column, Ø = 4.6 mm: EC 250/4.6 NUCLEODUR 100-5 C18 ec, analytical pre-column: CC 8/4 NUCLEODUR 100-5 C18 ec; semi-preparative column, Ø = 21 mm: SP 250/21 NUCLEODUR 100-7 C18 ec, semi-preparative pre-column: SP 50/21 NUCLEODUR 100-7 C18 ec).

NMR Spectroscopy

¹H NMR spectra were recorded at 25 °C on a Bruker Advance 400 spectrometer (Bruker GmbH, Ettlingen, Germany) and ¹H,¹H-COSY NMR spectra were measured at 600 MHz on a Bruker DMX600 spectrometer. Chemical shifts δ were calibrated

against the respective residual solvent peak and are given in parts per million (ppm). For NMR spectroscopy, deuterated solvents from Sigma-Aldrich Chemie GmbH (Munich, Germany) were used. Coupling constants (J) were rounded off to one decimal and are given in Hertz (Hz). The assignment of protons at the positions 5, 10, 20 and 2¹, 7¹, 12¹ of chlorin derivatives was done by comparison with literature data.^{121,171} ¹H, ¹H-COSY NMR spectra were measured for compounds **1a**, **2a**, **2b**, **3**, and **45b** facilitating exact assignment of all protons. The data obtained for these compounds were used for the interpretation of ¹H NMR spectra of related substrates.

Mass Spectrometry (MS)

MALDI-TOF mass spectrometry was performed on a Bruker Autoflex II spectrometer (Bruker Daltronics GmbH, Bremen, Germany). EI and FAB mass spectrometry was performed on a Finnigan MAT 90 spectrometer using 3-nitrobenzylalcohol as a matrix for sample preparation. High resolution mass spectra (HRMS) were recorded on an ESI MicroTOF Focus from Bruker Daltronics.

Melting Points

Melting points were determined using a Olympus Bx41 polarization microscope (Olympus GmbH, Hamburg, Germany) equipped with a heating stage (THMS 600, Linkam, Great Britain) and are uncorrected.

Elemental Analysis

Elemental analysis was performed on a CHNS 932 analyzer (Leco Instruments GmbH, Mönchengladbach, Germany) in the Analysis Division of the Institute of Inorganic Chemistry, University of Würzburg. Compounds with high content (> 20%) of chlorine or bromine were analyzed at the Institute of Organic Chemistry, University of Stuttgart.

UV-vis Absorption Spectroscopy

For all measurements, spectroscopic grade solvents (Uvasol[®]) from Merck were used. UV-vis spectra were measured in quartz glass cuvettes under ambient conditions unless otherwise stated. The measurements were performed on a PE 950 or a PE Lambda 40P spectrometer (both Perkin Elmer GmbH, Rodgau, Germany). For temperature-dependent UV-vis spectroscopy, a Peltier system was used as temperature controller. Molar extinction coefficients ϵ were calculated from Lambert-Beer's law. Extinction coefficients of aggregate solutions are given in relation to the respective monomer concentrations.

Steady State Fluorescence Spectroscopy

The steady state fluorescence spectra were measured under ambient conditions on a PTI QM4/2003 spectrofluorometer in right angle set-up and are corrected against photomultiplier and lamp intensity. A long wavelength range emission corrected photomultiplier R928 was used. Fluorescence quantum yields were determined as the average value for three different excitation wavelengths by applying high dilution conditions ($A < 0.05$) using *N,N'*-bis-(2,6-diisopropylphenyl)-1,6,7,12-tetraphenoxyperylene-3,4:9,10-tetracarboxylic acid diimide ($\phi_{em} = 0.96$ in CHCl_3)^{172,173} or nileblue a as reference ($\phi_{em} = 27\%$ in ethanol).¹⁷⁴

CD Spectroscopy

For all CD measurements spectroscopic grade solvents (Uvasol[®]) from Merck and quartz glass cuvettes were used. CD spectra were recorded with a JASCO J-810 spectrometer, equipped with a CDF-242 Peltier element.

Time-Resolved Fluorescence Spectroscopy

The experimental set-up of the single photon counting (SPT) technique is described in Chapter 3.3.1 and in more detail in the literature.^{166,167} Solutions for time-resolved fluorescence spectroscopy were prepared from substances, which were stored under argon and exclusion of light immediately after purification by HPLC. Spectroscopic grade solvents (Uvasol[®]) from Merck were used that were dried according to standard procedures and kept under argon.¹⁷⁵ Tiny amounts of sodium dithionite were added to every solvent flask in order to achieve reducing conditions. The samples were prepared and transferred to 1 cm quartz cuvettes in a glove box under an argon atmosphere.

Atomic Force Microscopy (AFM)

Atomic force microscopy was performed on a Nanoscope IV controller Veeco Multi Mode AFM (Veeco Instruments Inc., Santa Barbara, US) using silicon tips (Olympus, OMCL-AC160TS) with a resonance frequency of 300 kHz. The measurements were done under ambient conditions in the Tapping Mode. The samples were prepared by spin-coating (5000 rpm) of an aggregate solution on highly ordered pyrolytic graphite (HOPG), purchased from NanoTechnology Instruments.

Reagents and Solvents

DPTS and 3,5-bis(dodecyloxy)benzoic acid were synthesized according to literature.^{176,177} The cyanobacterium *Spirulina Platensis* which was used for the

extraction of chlorophyll *a* was obtained from the firm Dr. Winfried Behr (Bonn, Germany) and imported from China. All other reagents and solvents were obtained from commercial sources, i.e., Merck, Acros, Aldrich, or Fluka. Reagents were used without further purification, unless otherwise stated. Solvents were purified and dried according to standard procedures.¹⁷⁵

6.2 Synthesis and Analytical Data of Intermediates and Target Molecules

The synthetic procedures and analytical data of intermediate products and target molecules are given in the same order as presented in Chapter 3.1. All reactions of chlorin derivatives were carried out under an argon atmosphere in the absence of light. Chlorin derivative **29**, which is used as a precursor for all NDI-functionalized ZnChls, has been prepared by a semi-synthetic route starting with the extraction of the cyanobacterium *Spirulina Platensis*. The extraction procedure and the subsequent steps to **29** had been described previously in the literature, but some alterations have been undertaken.^{156,157,122} Furthermore, the literature-known stepwise transformation of pyrene into 2,6-dichloro-1,4,5,8-naphthalene-tetracarboxylic acid dianhydride (**33**) has been slightly modified.¹⁵⁸ The amended procedures are also presented in this section.

13²-Demethoxycarbonyl-pheophorbide a methylester (phea a, 27). (COR001 and COR003)

The synthesis of phea *a* was started with the Soxhlet extraction of the cyanobacterium *Spirulina Platensis* (400 g) with acetone (1.5 L). After 48 h, the solvent was evaporated from the extract and the remaining dark-green, strongly viscous residue was placed into a 500 mL round-bottomed flask. 2,4,6-Trimethylpyridine (300 mL) was added and the reaction mixture was refluxed for 6 h at 160 °C. Immediately after removal of the solvent by distillation in vacuo, methanol (50 mL) was added. Then a pre-prepared mixture of methanol (250 mL) and conc. sulfuric acid (10 mL) was poured into the solution and stirred for 16 h at room temperature. During this time the color changed from dark green to bluish green. Then saturated aqueous NaHCO₃ solution (500 mL) and diethyl ether (500 mL) were mixed in a 3 L beaker and the reaction mixture was added carefully to it. The pH was adjusted to 6-7 by the addition of solid NaHCO₃, followed by extraction of the aqueous phase with diethyl ether (4 × 700 mL). The combined organic phases were washed with water (2 × 1 L), dried over anhydrous sodium sulfate and the solvent was evaporated. The remaining highly viscous residue was subjected to column

chromatography first using *n*-pentane/diethyl ether 5:1 as an eluent to remove the unpolar carotenoids and lipids. Subsequently, the fraction of diethyl ether was increased stepwise and at the end, pure diethyl ether was used to elute pheo *a* (**27**). Since pheo *a* molecules are prone to aggregation, some precipitation on the top of the column as a dark blue solid could not be avoided. After finishing the column chromatography, this residue was collected by a spatula and washed out from the silica with THF. From 800 g *Spirulina Platensis* yielded ~4 g of pure pheo *a* (**27**) were obtained and the latter was characterized according to the literature.¹⁵⁶

3-Devinyl-3-formyl-13²-demethoxycarbonyl-pheophorbide *a* methylester (28**). (COR005)**

Pheo *a* (**27**) (500 mg, 0.911 mmol) was dissolved in THF (120 mL) and to the solution conc. acetic acid (1.5 mL), water (1.5 mL), and osmium tetroxide (1.0 mg, 0.0039 mmol) were added. The reaction mixture was stirred at room temperature for 30 min and after that, the formation of dihydroxylated intermediate could be detected by TLC as a bluish grey spot. After stirring for additional 30 min, saturated aqueous sodium periodate (NaIO₄) solution (25 mL) was added slowly by means of a syringe pump (flow: 10 mL/h). Subsequently, another portion of NaIO₄ solution (25 mL) was added and stirring was continued for 1 h. Then water (300 mL) was added and the aqueous phase was extracted with diethyl ether (3 × 300 mL). The combined organic phases were washed successively with saturated aqueous NaHCO₃ solution (200 mL) and water (300 mL) and dried over anhydrous sodium sulphate. The solvent was removed under reduced pressure and the crude product was subjected to column chromatography (*n*-pentane/ diethyl ether 1:1) to afford the pure aldehyde **28** (476 mg, 95%) as a brown solid. Compound **28** was characterized according to the literature.¹⁵⁸

3-Devinyl-3-formyl-13²-demethoxycarbonyl-pheophorbide *a* carboxylic acid (29**). (COR012)**

To a solution of compound **28** (300 mg, 0.545 mmol) in THF (30 mL), conc. hydrochloric acid (20 mL) was added. The reaction mixture was stirred at room temperature for 3 h. Then saturated aqueous NaHCO₃ solution (200 mL) was poured into the solution carefully and the aqueous phase was extracted with CHCl₃ (3 × 200 mL). The combined organic phases were dried over anhydrous sodium sulphate and

the solvent was evaporated. Purification by column chromatography (CHCl₃/MeOH 19:1) yielded compound **29** as a dark brown solid (237 mg, 0.441 mmol, 81%). The characterization data of compound **29** are in agreement with those reported in the literature.¹²²

1,2,3,5,6,7,8,10-Octachloro-1,2,6,7-tetrahydropyrene (30). (COR100)

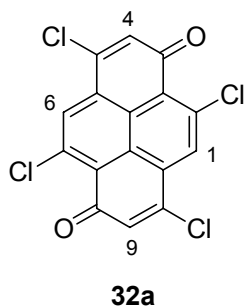
In a 2-L 3-necked round bottom flask, equipped with a mechanical stirrer, a gas inlet tube and an outlet tube, pyrene (100 g, 0.494 mol) and iodine (3.0 g) were dissolved in 1,2,4-trichlorobenzene (1 L) to result in a violet solution. Then chlorine gas was bubbled through the solution continuously. After 45 min, the reaction flask was heated up to 50 °C by an oil bath and the formation of a light green solid was observed. After an additional 45 min, the temperature was increased to 110 °C and after 2.5 h at this temperature, the solid dissolved again. After additional 2 h, addition of chlorine was stopped, the heating was turned off, and the reaction mixture was cooled to room temperature gradually. A white solid precipitated which was separated by filtration, washed with toluene (2 × 200 mL) and dried in vacuo. Yield: 89.0 g (38%). Mp: 290 °C. MS (EI): m/z (%) calcd for C₁₆H₆Cl₈ [M]⁺: 481.9, found: 481.9 (13). Anal. calcd for C₁₆H₆Cl₈: C, 39.88; H, 1.26. Found: C, 40.03; H, 1.50. Due to its extremely low solubility in common organic solvents, no NMR spectrum could be recorded for **30**.

1,3,5,6,8,10-Hexachloropyrene (31a) and 1,3,5,7,8,10-hexachloropyrene (31b) regioisomers. (COR101)

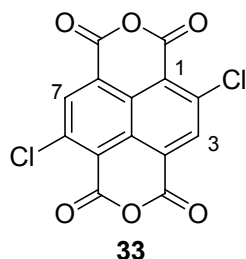
Compound **30** (89.0 g, 0.186 mol) and ethanol (700 mL) were placed in a 3-L 3-necked flask equipped with a mechanical stirrer and a condenser. Afterwards potassium hydroxide (64.4 g, 1.12 mol) was added slowly. The suspension was refluxed for 5 h and the resultant yellow solid was separated by filtration and washed with boiling water (500 mL) to obtain 73.6 g (97%) of an isomeric mixture of **31a** and **31b**. Mp: > 350 °C. MS (EI): m/z (%) calcd for C₁₆H₄Cl₆ [M]⁺: 407.9, found: 407.9 (100). Anal. calcd for C₁₆H₄Cl₆: C, 47.00; H, 0.99; Cl, 52.02. Found: C, 46.68; H, 1.25; Cl, 52.22. Due to their extremely low solubility in common organic solvents, no NMR spectrum could be obtained for **31a** and **31b**.

2,5,7,10-Tetrachloropyrene-3,8-quinone (32a). (VW046a)

In a 100-mL 3-necked round bottom flask equipped with a thermometer, fuming nitric acid (24 mL) was cooled with an ice bath. A portion of the regioisomeric mixture of **31a** and **31b** (8.18 g, 20.0 mmol) was added slowly to maintain the temperature between 0 and +5 °C. The cooled reaction mixture was stirred for further 15 min. During the reaction, regioisomer **32a** precipitated as an orange solid. The precipitate was separated by filtration with a G3 frit and washed with acetic acid (5 × 20 mL) and water (2 × 20 mL). The crude product was purified by sublimation (1 mbar, 240-280 °C) to obtain 3.33 g (45%) of **32a** in analytically pure form. Mp: 320-325 °C. ¹H NMR (D₂SO₄, 400 MHz): δ 7.96 (s, 2H, H1, H6), 6.75 (s, 2H, H4, H9). MS (EI): m/z (%) calcd for C₁₆H₄Cl₄O₂ [M]⁺: 369.9, found: 369.9 (100). Anal. calcd for C₁₆H₄Cl₄O₂: C, 51.94; H, 1.09. Found: C, 51.38; H, 1.10.

**2,6-Dichloro-1,4,5,8-naphthalenetetracarboxylic acid dianhydride (33). (VW046b)**

In a 100-mL 3-necked round bottom flask equipped with a thermometer and a condenser, 2.02 g (5.46 mmol) of **32a** were dissolved in conc. sulfuric acid (28 mL). The solution was heated with an oil bath at 100 °C under stirring for 10 min. Then fuming nitric acid (3.1 mL) was added slowly by a syringe, whereupon the reaction temperature increased to 130 °C and a yellow solid precipitated. The oil bath was removed and the reaction mixture was cooled down to 70 °C and poured into a portion of ice. The precipitated solid was separated by filtration with a frit (G3) and dried in vacuo. Recrystallization with acetic acid provided 0.908 g (49%) of compound **33**. Mp: > 350 °C. ¹H NMR (d₈-THF, 400 MHz): δ 8.79 (s, 2H, H3, H7). MS (EI): m/z (%) calcd for C₁₄H₂Cl₂O₆ [M]⁺: 336.1, found: 336.1 (70); calcd for C₁₃H₂Cl₂O₄ [M-CO₂]⁺: 291.9, found: 292.0 (100). Anal. calcd for C₁₄H₂Cl₂O₆: C, 49.89; H, 0.60. Found: C, 49.90; H, 0.68.



***N,N'*-Bis-(2',6'-diisopropylphenyl)-2,6-dichloro-1,4,5,8-naphthalenetetracarboxylic acid diimide (34). (COR074)**

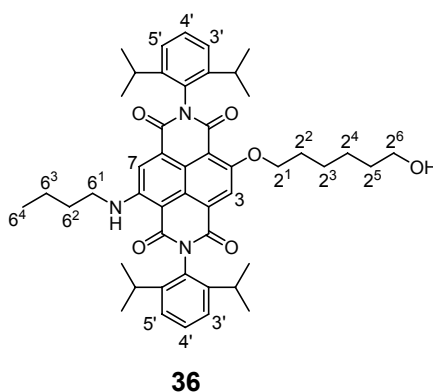
This compound was synthesized and characterized according to literature.²¹

***N,N'*-Bis-(2',6'-diisopropylphenyl)-2-chloro-6-butylamino-1,4,5,8-naphthalenetetracarboxylic acid diimide (35). (COR082)**

This compound was synthesized and characterized according to literature.²¹

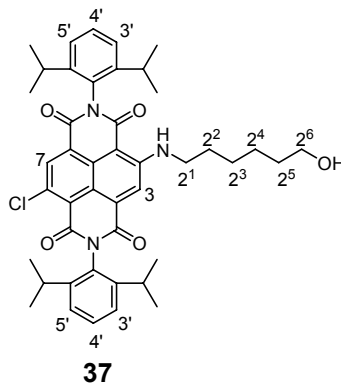
***N,N'*-Bis-(2',6'-diisopropylphenyl)-2-(6'-hydroxyhexyloxy)-6-butylamino-1,4,5,8-naphthalenetetracarboxylic acid diimide (36). (COR092)**

NDI **35** (50 mg, 0.076 mmol) was dissolved in CH₂Cl₂ (10 mL) and 1,6-hexanediol (3 g) and potassium carbonate (50 mg, 0.36 mmol) were added. Then CH₂Cl₂ was removed at the rotary evaporator and the reaction mixture was stirred at 120 °C for 4 h. Afterwards, CHCl₃ (50 mL) and 1N HCl (50 mL) were added, and the organic layer was separated, washed with water (50 mL) and dried over anhydrous Na₂SO₄. After removal of the solvent, the residue was objected to HPLC (methanol/CH₂Cl₂ 3:1) to obtain compound **36** as a pink solid. Yield 24 mg (42%). Mp: 275 °C. ¹H NMR (CDCl₃, 400 MHz): δ 9.79 (t, *J* = 5.2 Hz, 1H, NH), 8.44 (s, 1H, H3), 8.36 (s, 1H, H7), 7.50 (m, 2H, H4'), 7.35 (m, 4H, H3', H5'), 4.36 (t, *J* = 6.4 Hz, 2H, H2¹), 3.57 (m, 4H, H6¹, H2⁶), 2.73 and 2.69 (both sept, *J* = 6.9 Hz, 4H, *i*Pr-*H*), 1.93, 1.74, and 1.48 (m, 13H, H2²-H2⁵, H6², H6³, OH), 1.17 (m, 24H, *i*Pr-CH₃), 0.95 (t, *J* = 7.4 Hz, 3H, H6⁴). UV-vis (THF): λ_{max} (ε) = 547 (18100), 368 (11600), 350 nm (11100 M⁻¹ cm⁻¹). Fluorescence (THF, 293 K): λ_{max} = 575 nm (λ_{ex} = 525 nm), quantum yield φ_{Fl} = 0.71. HRMS (ESI): *m/z* calcd for C₄₈H₆₀N₃O₆ [M+H]⁺: 774.4482, found: 774.4477. Anal. calcd for C₄₆H₅₉N₃O₆ × 0.5 H₂O: C, 73.63; H, 7.72; N, 5.37. Found: C, 73.38; H, 7.65; N, 5.27.



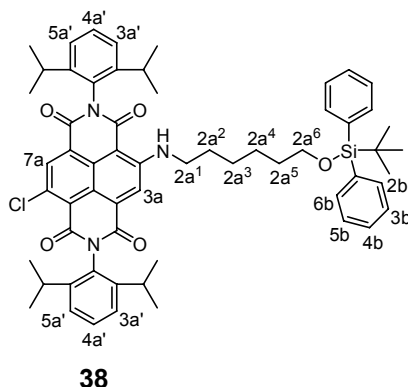
***N,N'*-Bis-(2',6'-diisopropylphenyl)-2-(6'-hydroxyhexyloxy)-6-chloro-1,4,5,8-naphthalenetetracarboxylic acid diimide (37). (COR108)**

N,N'-Bis-(2',6'-diisopropylphenyl)-2,6-dichloronaphthalene-1,4,5,8-tetracarboxylic acid dimide (**34**) (400 mg, 0.610 mmol) and 6-aminohexanol (1.43 mg, 12.2 mmol) were dissolved in CHCl_3 (40 mL) and stirred for 5 h at room temperature prior to addition of 1N HCl (40 mL). Then the organic layer was separated, washed with water (2 × 20 mL), dried over anhydrous Na_2SO_4 and the solvent was removed by rotary evaporation. The residue was first purified by column chromatography with CHCl_3 and subsequently by HPLC (methanol/ CH_2Cl_2 9:1) to afford a red solid. Yield 400 mg (89%). Mp: 295-296 °C. ^1H NMR (CDCl_3 , 400 MHz): δ 10.06 (t, $J = 5.2$ Hz, 1H, NH), 8.78 (s, 1H, H7), 8.40 (s, 1H, H3), 7.52 (t, $J = 7.8$ Hz, 1H, H4'), 7.50 (t, $J = 7.8$ Hz, 1H, H4'), 7.37 (d, $J = 7.8$ Hz, 2H, H3', H5'), 7.34 (d, $J = 7.8$ Hz, 2H, H3', H5'), 3.61 (m, 4H, H2¹, H2⁶), 2.68 (sept, $J = 6.8$ Hz, 4H, *iPr-H*), 1.80 and 1.50 (m, 8H, H2²-H2⁵), 1.17 (m, 24H, *iPr-CH*₃), OH could not be detected. MS (FAB, 3-nitrobenzylalcohol): m/z calcd for $\text{C}_{44}\text{H}_{51}\text{ClN}_3\text{O}_7$ [$\text{M}+\text{H}$]⁺: 736.4, found: 736.5. Anal. calcd for $\text{C}_{44}\text{H}_{50}\text{ClN}_3\text{O}_7$: C, 71.77; H, 6.84; N, 5.71. Found: C, 71.63; H, 6.78; N, 5.51.



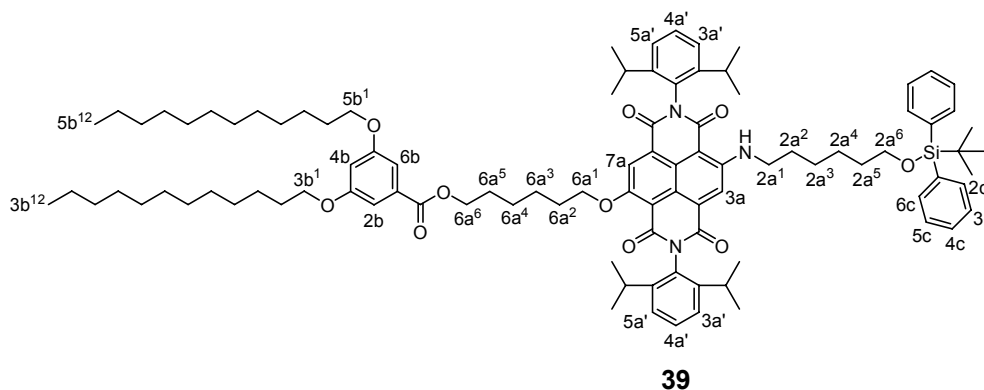
Compound 38. (COR154)

A mixture of NDI **37** (530 mg, 0.720 mmol), imidazol (98 mg, 1.4 mmol), DMAP (176 mg, 1.44 mmol), and *tert*-butyldiphenylsilyl chloride (396 mg, 1.44 mmol) in dry CH₂Cl₂ (100 mL) was stirred for 30 min at room temperature under an argon gas atmosphere. Then the organic phase was washed with water (3 × 100 mL) and dried over anhydrous Na₂SO₄. Evaporation of the solvent gave compound **38** as a red solid. Yield 700 mg (>99%). Mp: 130-133 °C. ¹H NMR (CDCl₃, 400 MHz): δ 9.96 (t, *J* = 5.2 Hz, 1H, NH), 8.71 (s, 1H, H7a), 8.31 (s, 1H, H3a), 7.56 (m, 4H, H2b, H6b), 7.43 (m, 2H, H4a'), 7.27 (m, 10H, H3a', H5a', H3b-H5b), 3.56 and 3.48 (m, 4H, H2a¹, H2a⁶), 2.60 (m, 4H, *i*Pr-*H*), 1.79-1.39 (m, 8H, H2a²-H2a⁵), 1.09 (m, 24H, *i*Pr-CH₃), 0.95 (s, 9H, *t*Bu-CH₃). UV-vis (THF): λ_{max} (ε) = 530 (13300), 498 (11300), 365 nm (11600 M⁻¹ cm⁻¹). HRMS (ESI): *m/z* calcd for C₆₀H₆₉N₃O₅Si [M+H]⁺: 974.4695, found: 974.4686. Anal. calcd for C₆₀H₆₈N₃O₅Si × 0.5 H₂O: C, 73.26; H, 7.07; N, 4.27. Found: C, 73.20; H, 7.07; N, 3.94.

**Compound 39. (COR158)**

NDI **38** (700 mg, 0.718 mmol) was dissolved in CH₂Cl₂ (20 mL) and 1,6-hexanediol (10 g) and potassium carbonate (992 mg, 7.18 mmol) were added to this solution. Then CH₂Cl₂ was removed at the rotary evaporator, and the reaction mixture was stirred at 100 °C for 12 h; during this time the color of the mixture turned pink. Then CHCl₃ (100 mL) and 1N HCl (100 mL) were added and the organic layer was separated, washed with water (100 mL) and dried over anhydrous Na₂SO₄. After removal of the solvent, the residue was subjected to column chromatography (CHCl₃). A pink solid (670 mg) was isolated, which was then dissolved in CH₂Cl₂ (100 mL). To this solution, 3,5-bisdodecyloxybenzoic acid (567 mg, 0.951 mmol), DCC (654 mg, 3.17 mmol), DMAP (232 mg, 1.90 mmol), and DPTS (671 mg, 1.90 mmol) were added and the reaction mixture was stirred at room temperature for 3 h. The

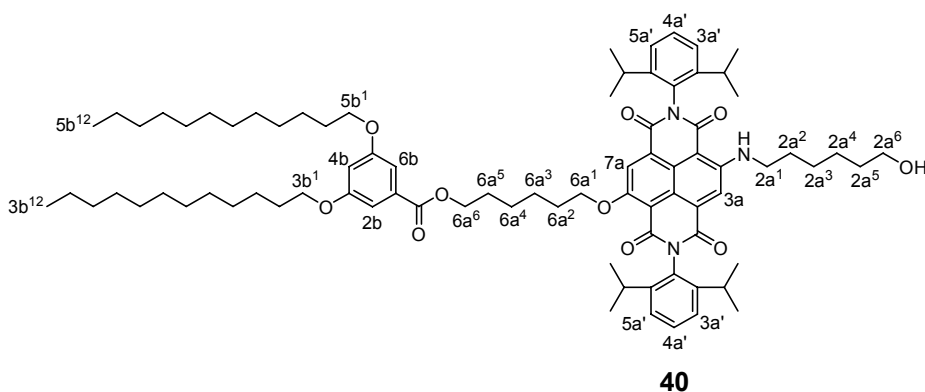
CH₂Cl₂ phase was washed with water (2 × 50 mL), dried over anhydrous Na₂SO₄, and the solvent was removed under reduced pressure. The crude product was purified by column chromatography (CH₂Cl₂) to give 747 mg (68%) of NDI **39**. Mp: not detectable due to the pasty consistence of **39** at room temperature. ¹H NMR (CDCl₃, 400 MHz): δ 9.70 (t, *J* = 5.0 Hz, 1H, NH), 8.37 (s, 1H, H7a), 8.28 (s, 1H, H3a), 7.56 (m, 4H, H2c, H6c), 7.41 (m, 2H, H4a'), 7.27 (m, 10H, H3a', H5a', H3c-H5c), 7.06 (d, *J* = 2.3 Hz, 2H, H2b, H6b), 6.55 (t, *J* = 2.3 Hz, 1H, H4b), 4.29 (t, *J* = 6.3 Hz, 2H, H6a¹), 4.18 (t, *J* = 6.7 Hz, 2H, H6a⁶), 3.88 (m, 4H, H3b¹, H5b¹), 3.56 and 3.45 (m, 4H, H2a¹, H2a⁶), 2.64 (m, 4H, *i*Pr-*H*), 1.86 (m, 2H, H6a²), 1.74-1.19 (m, 54H, H2a²-H2a⁵, H6a³-H6a⁵, H3b²-H3b¹¹, H5b²-H5b¹¹), 1.09 (m, 24H, *i*Pr-CH₃), 0.94 (s, 9H, *t*Bu-CH₃), 0.81 (t, *J* = 6.9 Hz, 6H, H3b¹², H5b¹²). HRMS (ESI): *m/z* calcd for C₉₇H₁₃₄N₃O₁₀Si [M+H]⁺: 1528.9828, found: 1528.9835.



NDI_{NO} **40**. (COR161)

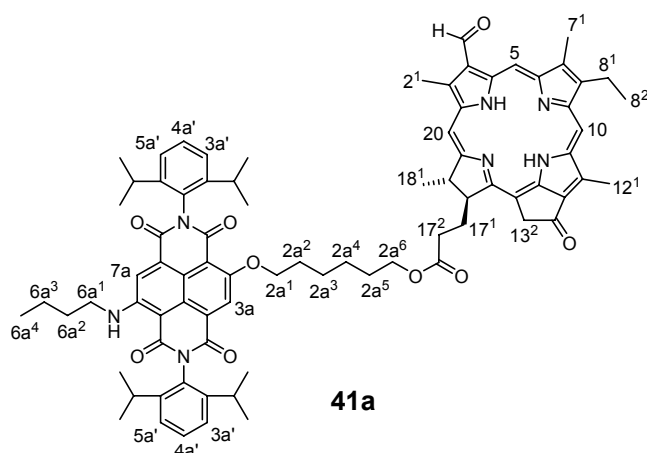
A solution of compound **39** (450 mg, 0.295 mmol) and tetra-*n*-butylammonium fluoride (771 mg, 2.95 mmol) in dry THF (100 mL) was stirred for 4 h at room temperature under an argon gas atmosphere. Then CH₂Cl₂ (200 mL) was added and the organic solution was washed with water (3 × 200 mL) and dried over anhydrous Na₂SO₄. After removal of solvent, further purification by column chromatography (CHCl₃) yielded the pink compound **40**. Yield 244 mg (64%). Mp: not detectable due to the pasty consistence of **40** at room temperature. ¹H NMR (CDCl₃, 400 MHz): δ 9.80 (t, *J* = 5.3 Hz, 1H, NH), 8.44 (s, 1H, H7a), 8.36 (s, 1H, H3a), 7.48 (m, 2H, H4a'), 7.33 (m, 4H, H3a', H5a'), 7.13 (d, *J* = 2.3 Hz, 2H, H2b, H6b), 6.61 (t, *J* = 2.3 Hz, 1H, H4b), 4.36 (t, *J* = 6.3 Hz, 2H, H6a¹), 4.25 (t, *J* = 6.7 Hz, 2H, H6a⁶), 3.95 (m, 4H, H3b¹, H5b¹), 3.63-3.55 (m, 4H, H2a¹, H2a⁶), 2.70 (m, 4H, *i*Pr-*H*), 1.94 (m, 2H, H6a²), 1.85-1.26 (m, 54H, H2a²-H2a⁵, H6a³-H6a⁵, H3b²-H3b¹¹, H5b²-H5b¹¹), 1.16 (m, 24H, *i*Pr-CH₃), 0.88 (t, *J* = 6.9 Hz, 6H, H3b¹², H5b¹²), OH could not be detected. UV-vis (THF):

λ_{\max} (ϵ) = 547 (17100), 367 nm ($12100 \text{ M}^{-1} \text{ cm}^{-1}$); UV-vis (cyclohexane/ 1% CCl_4): λ_{\max} (ϵ) = 540 (17100), 507 (12600), 364 nm ($12900 \text{ M}^{-1} \text{ cm}^{-1}$). Fluorescence (THF, 293 K): λ_{\max} = 575 nm (λ_{ex} = 525 nm), quantum yield ϕ_{Fl} = 0.58; fluorescence (cyclohexane/ 1% CCl_4 , 293 K): λ_{\max} = 558 nm (λ_{ex} = 510 nm), quantum yield ϕ_{Fl} = 0.67. HRMS (ESI): m/z calcd for $\text{C}_{81}\text{H}_{115}\text{NaN}_3\text{O}_{10}$ $[\text{M}+\text{Na}]^+$: 1312.8479, found: 1312.8482.



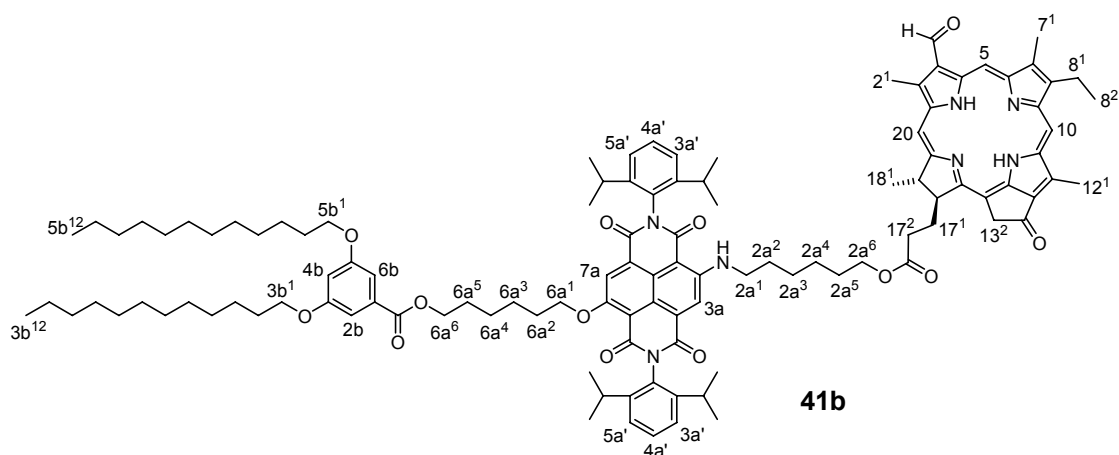
Compound 41a. (COR093)

A mixture of chlorin derivative **29** (100 mg, 0.186 mmol), NDI **36** (159 mg, 0.205 mmol), DCC (219 mg, 1.03 mmol), DMAP (50 mg, 0.41 mmol), DPTS (121 mg, 0.410 mmol), and *N*-ethyldiisopropylamine (500 μL) in dry CH_2Cl_2 (10 mL) was stirred for 24 h at room temperature. Then CH_2Cl_2 (100 mL) was added and the organic phase was washed with 1N HCl (100 mL) and water (100 mL), dried over anhydrous Na_2SO_4 , and solvent was removed by rotary evaporation. Purification of the crude product by HPLC (methanol/ CH_2Cl_2 13:7) afforded dyad **41a** as a red-brown solid. Yield 95 mg (40%). Mp: 201 $^\circ\text{C}$. ^1H NMR (CDCl_3 , 400 MHz): δ 11.57 (s, 1H, CHO), 10.34 (s, 1H, H10), 9.77 (t, J = 5.2 Hz, 1H, NH), 9.64 (s, 1H, H5), 8.85 (s, 1H, H20), 8.39 and 8.34 (both s, 2H, H3a, H7a), 7.50-7.22 (m, 6H, H3a', H4a', H5a'), 5.34 (d, J = 19.9 Hz, 1H, H13²), 5.18 (d, J = 19.9 Hz, 1H, H13²), 4.58 (dq, J = 7.3 Hz, J = 2.0 Hz, 1H, H18), 4.38 (td, J = 8.2 Hz, J = 2.0 Hz, 1H, H17), 4.27 (t, J = 6.2 Hz, 2H, H2a⁶), 3.94 (m, 2H, H2a¹), 3.78 (s, 3H, H12¹), 3.75 (q, J = 7.7 Hz, 2H, H8¹), 3.73 (s, 3H, H2¹), 3.55 (m, 2H, H6a¹), 3.34 (s, 3H, H7¹), 2.73-2.53 and 2.35-2.26 (m, 10H, H17¹, H17², *iPr*-H, H2a²), 1.84 (d, J = 7.3 Hz, 3H, H18¹), 1.74 (t, J = 7.7, 3H, H8²), 1.84-1.71 (m, 10H, H2a³-2a⁵, H6a², H6a³), 1.12 (m, 24H, *iPr*-CH₃), 0.94 (t, J = 7.3 Hz, 3H, H6a⁴), -0.10 (s, 1H, NH), -2.03 (s, 1H, NH). HRMS (ESI): m/z calcd for $\text{C}_{80}\text{H}_{90}\text{N}_7\text{O}_9$ $[\text{M}+\text{H}]^+$: 1292.6799, found: 1292.6799.



Compound 41b. (COR165)

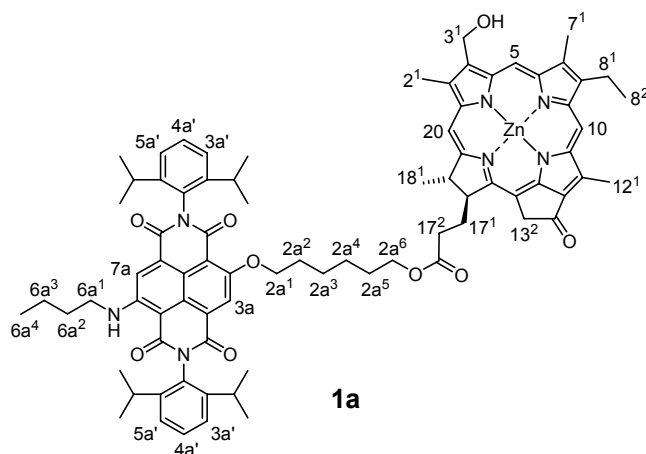
A mixture of chlorin derivative **29** (101 mg, 0.189 mmol), NDI_{NO} **40** (244 mg, 0.189 mmol), DCC (117 mg, 0.567 mmol), DMAP (69 mg, 0.57 mmol), DPTS (167 mg, 0.567 mmol), and *N*-ethyldiisopropylamine (500 μ L) in dry CH₂Cl₂ (10 mL) was stirred for 24 h at room temperature. CHCl₃ (100 mL) was added and the organic phase was washed with 1N HCl (100 mL) and water (100 mL), dried over anhydrous Na₂SO₄, and solvent was removed by rotary evaporation. Purification of the crude product by column chromatography (CHCl₃) and subsequent semi-preparative HPLC (methanol/CH₂Cl₂ 11:9) afforded dyad **41b** as a red-brown solid. Yield 133 mg (39%). Mp: 93-97 °C. ¹H NMR (CDCl₃, 400 MHz): δ 11.57 (s, 1H, CHO), 10.55 (s, 1H, H10), 9.81 (s, 1H, H5), 9.73 (m, 1H, NH), 9.01 (s, 1H, H20), 8.43 (s, 1H, H7a), 8.31 (s, 1H, H3a), 7.45 (m, 2H, H4a'), 7.30 (m, 4H, H3a', H5a'), 7.13 (d, *J* = 2.4 Hz, 2H, H2b, H6b), 6.61 (t, *J* = 2.4 Hz, 1H, H4b), 5.38 (d, *J* = 19.9 Hz, 1H, H13²), 5.18 (d, *J* = 19.9 Hz, 1H, H13²), 4.64 (m, 1H, H18), 4.44 (m, 1H, H17), 4.35 (t, *J* = 6.2 Hz, 2H, H6a¹), 4.25 (t, *J* = 6.8 Hz, 2H, H6a⁶), 3.99 (m, 2H, H2a⁶), 3.95 (t, *J* = 6.6 Hz, 4H, H3b¹, H5b¹), 3.81 (m, 2H, H8¹), 3.80 (s, 3H, H12¹), 3.75 (s, 3H, H2¹), 3.49 (m, 2H, H2a¹), 3.38 (s, 3H, H7¹), 2.70-2.31 (m, 8H, *i*Pr-H, H17¹, H17²), 1.92 (m, 2H, H6a²), 1.88 (d, *J* = 7.3 Hz, 3H, H18¹), 1.85-1.26 (m, 57H, H8², H2a²-H2a⁵, H6a³-H6a⁵, H3b²-H3b¹¹, H5b²-H5b¹¹), 1.12 (m, 24H, *i*Pr-CH₃), 0.87 (t, *J* = 6.9 Hz, 6H, H3b¹², H5b¹²), -0.11 (*br* s, 1H, NH), -2.04 (*br* s, 1H, NH). UV-vis (THF): λ_{max} (ϵ) = 691 (50800), 630 (4900), 550 (22600), 520 (19300), 425 (63100), 385 nm (51000 M⁻¹ cm⁻¹). HRMS (ESI): *m/z* calcd for C₁₁₃H₁₄₆N₇O₁₃ [M+H]⁺: 1809.0973, found: 1809.0943.



ZnChI-NDI_{NO} **1a**. (COR097)

BH₃(*t*-BuNH₂) (10 mg, 0.11 mmol) was added to an ice-cooled solution of aldehyde **41a** (71 mg, 0.055 mmol) in dry CH₂Cl₂ (30 mL) and the reaction mixture was stirred at 0 °C for 4 h. Then 1N HCl (30 mL) was poured into the mixture, followed by vigorous stirring for additional 30 min. The organic layer was separated, washed successively with water (2 × 50 mL), saturated aqueous NaHCO₃ solution (50 mL), and water again (50 mL), and dried over anhydrous Na₂SO₄. After removal of the solvent, the residual solid was subjected to HPLC (MeOH/CH₂Cl₂ 7:3) to provide the pure at C-3¹ position hydroxy-functionalized ChI-NDI_{NO} dyad (63 mg, 90%) This product (45 mg, 0.035 mmol) was dissolved in THF (10 mL) and a saturated methanolic zinc acetate dihydrate solution (20 mL) was added to it. After stirring for 2 h at room temperature, diethylether (50 mL) was added. The solution was washed with water (3 × 20 mL) and saturated aqueous NaHCO₃ solution (1 × 20 mL) and dried over Na₂SO₄. Removal of the solvent by rotary evaporation and purification of the crude product by HPLC (methanol/CH₂Cl₂ 4:1) afforded Zn(II)-containing dyad **1a** as a dark violet solid. Yield 29 mg (55% with respect to **41a**). Mp: 203 °C. ¹H NMR (d₈-THF, 400 MHz): δ 9.84 (t, *J* = 5.1 Hz, 1H, NH), 9.62 (s, 1H, H10), 9.50 (s, 1H, H5), 8.49 (s, 1H, H20), 8.42 and 8.37 (both s, 2H, H3a, H7a), 7.40 (m, 2H, H4a'), 7.30-7.17 (m, 4H, H3a', H5a'), 5.73 (d, *J* = 5.7 Hz, 2H, H3¹), 5.10 (d, *J* = 19.6 Hz, 1H, H13²), 4.95 (d, *J* = 19.6 Hz, 1H, H13²), 4.51 (m, 1H, H18), 4.45 (t, *J* = 5.7 Hz, 1H, OH), 4.30 (m, 3H, H17, H2a¹), 3.95-3.78 (m, 4H, H2a⁶, H8¹), 3.61 (m, 5H, H12¹, H6a¹), 3.31 (m, 6H, H2¹, H7¹), 2.69 (m, 4H, *i*Pr-H), 2.31, 2.18, and 2.05 (m, 4H, H17¹, H17²), 1.78, 1.47, and 1.28 (m, 16H, H8², H18¹, H6a², H6a³, H2a²-H2a⁴), 1.07 (m, 24H, *i*Pr-CH₃), 0.96 (t, *J* = 7.4 Hz, 3H, H6a⁴). UV-vis (THF): λ_{max} = 648, 602, 550,

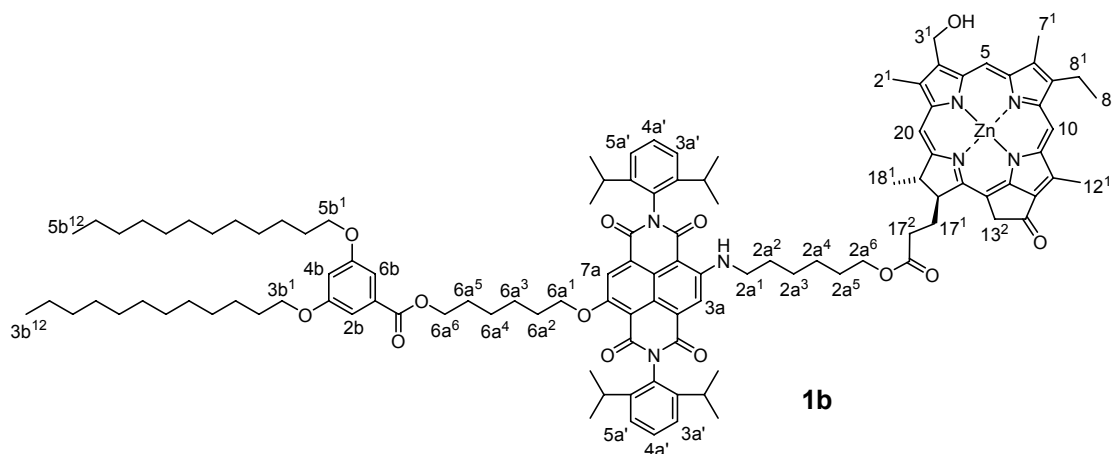
425, 405, 369 nm. HRMS (ESI): calcd for $C_{80}H_{87}N_7O_8Zn$ $[M-OH]^+$: 1338.5985, found: 1338.5985.



ZnChl-NDI₁₀ **1b**. (COR166)

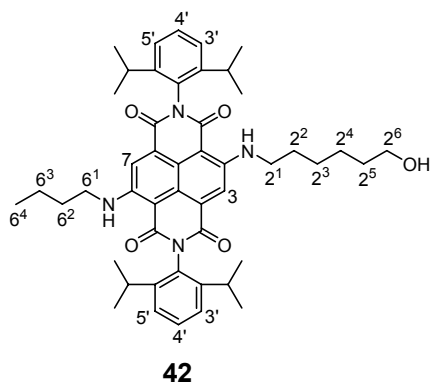
$BH_3(t-BuNH_2)$ (5 mg, 0.058 mmol) was added to an ice-cooled solution of aldehyde **41b** (100 mg, 0.0553 mmol) in dry CH_2Cl_2 (40 mL) and the reaction mixture was stirred at 0 °C for 3 h under an argon gas atmosphere. Then 1N HCl (20 mL) was poured into the mixture, followed by vigorous stirring for additional 15 min. The organic layer was separated, washed successively with water (2 × 100 mL), saturated aqueous $NaHCO_3$ solution (100 mL), and water again (100 mL), dried over anhydrous Na_2SO_4 . After removal of solvent, the residual solid was dissolved in THF (5 mL) and a saturated methanolic zinc acetate dihydrate solution (20 mL) was added. After stirring for 5 h at room temperature, diethylether (100 mL) was added. The solution was washed with water (3 × 100 mL) and saturated aqueous $NaHCO_3$ solution (1 × 100 mL) and dried over Na_2SO_4 . Removal of solvent by rotary evaporation and purification of the crude product by HPLC (methanol/THF 7:3) afforded compound **1b** as a dark violet solid. Yield 54 mg (0.029 mmol, 50%). Mp: 227-229 °C. 1H NMR (d_8 -THF, 400 MHz): δ 9.80 (t, J = 5.7 Hz, 1H, NH), 9.62 (s, 1H, H10), 9.50 (s, 1H, H5), 8.49 (s, 1H, H20), 8.45 (s, 1H, H7a), 8.35 (s, 1H, H3a), 7.39-7.22 (m, 6H, H3a'-H5a'), 7.09 (d, J = 2.4 Hz, 2H, H2b, H6b), 6.64 (t, J = 2.4 Hz, 1H, H4b), 5.72 (d, J = 5.7 Hz, 2H, H3¹), 5.10 (d, J = 19.5 Hz, 1H, H13²), 4.95 (d, J = 19.5 Hz, 1H, H13²), 4.51 (m, 1H, H18), 4.45 (t, J = 5.7 Hz, 1H, OH), 4.36 (t, J = 6.1 Hz, 2H, H6a¹), 4.30 (m, 1H, H17), 4.22 (t, J = 6.8 Hz, 2H, H6a⁶), 3.95 (t, J = 6.4 Hz, 4H, H3b¹, H5b¹), 3.91 (m, 2H, H2a⁶), 3.80 (m, 2H, H8¹), 3.60 (s, 3H, H12¹), 3.55 (m, 2H, H2a¹), 3.31 (s, 3H, H2¹), 3.30 (s, 3H, H7¹), 2.75-2.67 (m, 4H, *i*Pr-H), 2.62-2.15 (m, 4H, H17¹, H17²), 1.92 (m, 2H, H6a²), 1.79 (d, J = 7.4 Hz, 3H, H18¹), 1.66-1.29 (m,

57H, H8², H2a²-H2a⁵, H6a³-H6a⁵, H3b²-H3b¹¹, H5b²-H5b¹¹), 1.13-1.05 (m, 24H, *i*Pr-CH₃), 0.88 (t, *J* = 6.8 Hz, 6H, H3b¹², H5b¹²). UV-vis (THF): λ_{\max} (ϵ) = 647 (71200), 603 (9900), 549 (17400), 425 (98700), 404 (54700), 369 nm (37300 M⁻¹ cm⁻¹); UV-vis (cyclohexane/ 1% CCl₄): λ_{\max} (ϵ) = 729 (50100), 545 (15300), 512 (12300), 443 (33600), 421 (29500), 368 nm (21800 M⁻¹ cm⁻¹). Fluorescence (THF, 293 K): λ_{\max} = 648, 703 nm (λ_{ex} = 510 nm), quantum yield ϕ_{Fl} = 0.12; fluorescence (cyclohexane/ 1% CCl₄, 293 K): λ_{\max} = 737 nm (λ_{ex} = 515 nm), quantum yield $\phi_{\text{Fl}} \leq 0.001$. HRMS (ESI): *m/z* calcd for C₁₁₃H₁₄₅N₇NaO₁₃Zn [M+Na]⁺: 1895.0244, found: 1895.0068.

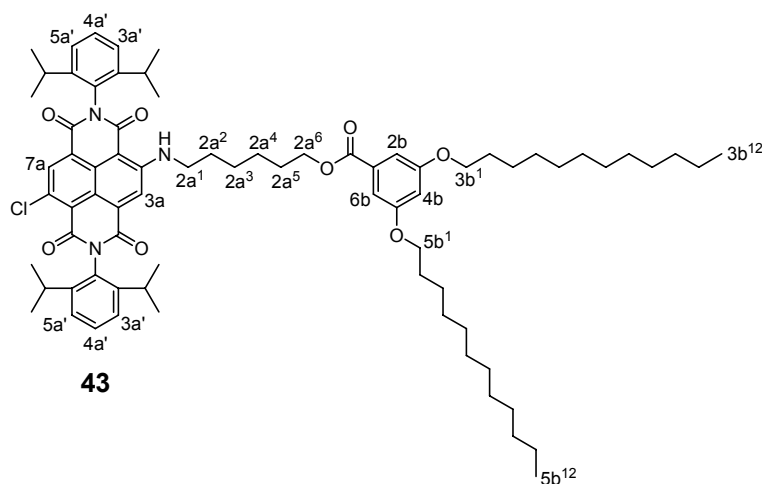


***N,N'*-Bis-(2',6'-diisopropylphenyl)-2-(6'-hydroxyhexylamino)-6-butylamino-1,4,5,8-naphthalenetetracarboxylic acid diimide (42). (COR094)**

NDI **37** (450 mg, 0.650 mmol) was dissolved in molten 6-aminohexanol (5 mL). The solution was stirred at 80 °C for 2 h; during this time the color of the solution turned blue. Then CHCl₃ (100 mL) and 1N HCl (100 mL) were added and the organic layer was separated, washed with water (2 × 50 mL) and dried over Na₂SO₄. The CHCl₃ solution was evaporated under vacuum to give a blue solid, which was purified by column chromatography (CHCl₃). Yield: 344 mg (66%). Mp: 294 °C. ¹H NMR (CDCl₃, 400 MHz): δ 9.34 (m, 2H, NH), 8.26 (m, 1H, H3, H7), 7.50 (t, *J* = 7.6 Hz, 2H, H4'), 7.35 (d, *J* = 7.6 Hz, 4H, H3', H5'), 3.62 (t, *J* = 6.5 Hz, 2H, H2⁶), 3.51 (m, 4H, H2¹, H6¹), 2.70 (sept, *J* = 6.8 Hz, 4H, *i*Pr-H), 1.74 and 1.45 (m, 13H, H2²-H2⁵, H6², H6³, OH), 1.17 (m, 24 H, *i*Pr-CH₃), 0.94 (t, *J* = 7.3 Hz, 3H, H6⁴). UV-vis (THF): λ_{\max} (ϵ) = 613 (23300), 363 (15000), 346 nm (12100 M⁻¹ cm⁻¹). Fluorescence (THF, 293 K): λ_{\max} = 639 nm (λ_{ex} = 525 nm), quantum yield ϕ_{Fl} = 0.49. HRMS (ESI): calcd for C₄₈H₆₀N₄O₅ [M]⁺: 772.4563, found: 772.4572. Anal. calcd for C₄₈H₆₀N₄O₅ × 0.5 H₂O: C, 73.72; H, 7.86; N, 7.16. Found: C, 73.39; H, 7.88; N, 6.97.

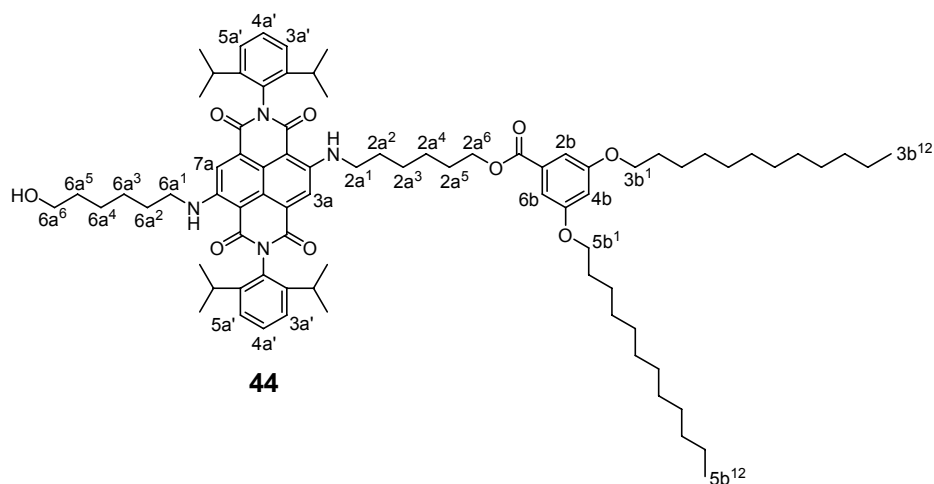
**Compound 43. (COR109)**

NDI **37** (360 mg, 0.489 mmol) was dissolved in CH_2Cl_2 (36 mL) and 3,5-bis(dodecyloxy)benzoic acid (264 mg, 0.538 mmol), DCC (506 mg, 2.45 mmol), DMAP (180 mg, 1.47 mmol) and DPTS (433 mg, 1.47 mmol) were added. The reaction mixture was stirred at room temperature for 2 h and then poured into 1N HCl (40 mL). The organic layer was separated, washed with water (2 \times 20 mL), dried over Na_2SO_4 and the solvent was removed by rotary evaporation. Successive purification of the crude product by column chromatography (CHCl_3/n -pentane 1:1) and HPLC (methanol/ CH_2Cl_2 3:2) gave compound **43** as a pink solid. Yield: 320 mg (54%). Mp: 54-56 $^\circ\text{C}$. ^1H NMR (CDCl_3 , 400 MHz): δ 10.06 (t, $J = 5.1$ Hz, 1H, NH), 8.78 (s, 1H, H7a), 8.39 (s, 1H, H3a), 7.50 (m, 2H, H4a'), 7.35 (m, 4H, H3a', H5a'), 7.13 (d, $J = 2.4$ Hz, 2H, H2b, H6b), 6.62 (t, $J = 2.4$ Hz, 1H, H4b), 4.27 (t, $J = 6.6$ Hz, 2H, H2a⁶), 3.95 (t, $J = 6.6$ Hz, 4H, H3b¹, H5b¹), 3.61 (m, 2H, H2a¹), 2.68 (sept, $J = 6.8$ Hz, 4H, *i*Pr-H), 1.76 (m, 6H, H2a², H3b², H5b²), 1.45 (m, 6H, H2a³-H2a⁵), 1.30 (m, 36H, H3b³-H3b¹¹, H5b³-H5b¹¹), 1.17 (m, 24H, *i*Pr- CH_3), 0.88 (t, $J = 6.9$ Hz, 6H, H3b¹², H5b¹²). HRMS (ESI): m/z calcd for $\text{C}_{75}\text{H}_{102}\text{ClN}_3\text{NaO}_8$ [$\text{M}+\text{Na}$]⁺: 1230.7252, found: 1230.7246. Anal. calcd for $\text{C}_{75}\text{H}_{102}\text{ClN}_3\text{O}_8$: C, 74.50; H, 8.50; N, 3.48. Found: C, 74.60; H, 8.75; N, 3.46.



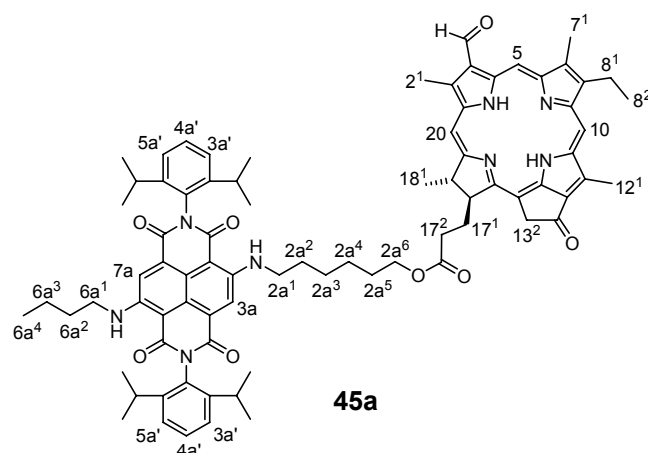
Compound 44. (COR110)

NDI **43** (240 mg, 0.198 mmol) was dissolved in molten 6-aminohexanol (10 mL). The solution was stirred at 90 °C for 2 h; during this time the color of the solution turned blue. Then CHCl₃ (100 mL) and 1N HCl (40 mL) were added and the organic layer was separated, washed with water (2 × 20 mL) and dried over Na₂SO₄. The CHCl₃ solution was evaporated under vacuum to give a blue solid which was purified by column chromatography (CHCl₃) and HPLC (methanol/CH₂Cl₂ 13:7). Yield: 204 mg (80%). Mp: 146-148 °C. ¹H NMR (CDCl₃, 400 MHz): δ 9.36 (m, 2H, NH), 8.26 (s, 1H, H3a), 8.26 (s, 1H, H7a), 7.50 (m, 2H, H4a'), 7.35 (m, 4H, H3a', H5a'), 7.13 (d, *J* = 2.4 Hz, 2H, H2b, H6b), 6.62 (t, *J* = 2.4 Hz, 1H, H4b), 4.26 (t, *J* = 6.7 Hz, 2H, H2a⁶), 3.95 (t, *J* = 6.6 Hz, 4H, H3b¹, H5b¹), 3.61 and 3.51 (m, 6H, H2a¹, H6a¹, H6a⁶), 2.70 (sept, *J* = 6.8 Hz, 4H, *iPr-H*), 1.76 (m, 8H, H2a², H6a², H3b², H5b²), 1.48 (m, 12H, H2a³-H2a⁵, H6a³-H6a⁵), 1.30 (m, 36H, H3b³-H3b¹¹, H5b³-H5b¹¹), 1.17 (m, 24H, *iPr-CH*₃), 0.88 (t, *J* = 6.9 Hz, 6H, H3b¹², H5b¹²), OH could not be detected. UV-vis (THF): λ_{max} (ε) = 614 (23700), 362 (14200), 346 nm (12100 M⁻¹ cm⁻¹); UV-vis (cyclohexane/ 1% CCl₄): λ_{max} (ε) = 604 (23500), 564 (11600), 360 nm (12300 M⁻¹ cm⁻¹). Fluorescence (THF, 293 K): λ_{max} = 637 nm (λ_{ex} = 575 nm), quantum yield φ_{F1} = 0.50; fluorescence (cyclohexane, 293 K) λ_{max} = 622 nm (λ_{ex} = 575 nm), quantum yield φ_{F1} = 0.70. HRMS (ESI): *m/z* calcd for C₈₁H₁₁₆N₄NaO₉ [M+Na]⁺: 1311.8640, found: 1311.8638. Anal. calcd for C₈₁H₁₁₆N₄O₉: C, 75.43; H, 9.06; N, 4.34. Found: C, 75.21; H, 9.00; N, 4.31.



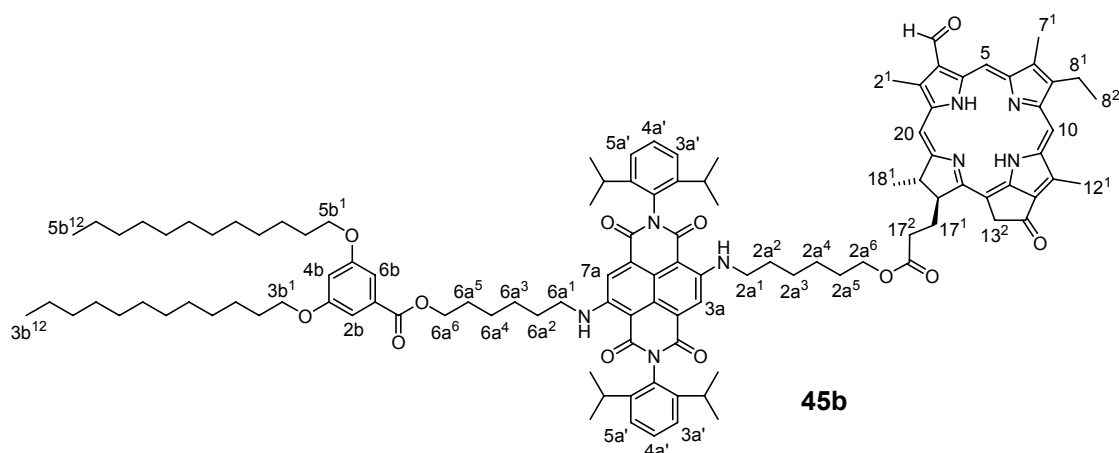
Compound 45a. (COR095)

A mixture of chlorin derivative **29** (113 mg, 0.211 mmol), NDI **42** (179 mg, 0.232 mmol), DCC (435 mg, 2.11 mmol), DMAP (130 mg, 1.06 mmol), DPTS (312 mg, 1.06 mmol), and *N*-ethyl-diisopropylamine (500 μ L) in dry CH_2Cl_2 (10 mL) was stirred for 24 h at room temperature. Then CH_2Cl_2 (100 mL) was added and the organic phase was washed with 1 N HCl (100 mL) and water (100 mL), dried over anhydrous Na_2SO_4 , and the solvent was removed by rotary evaporation. Purification of the crude product by HPLC (methanol/ CH_2Cl_2 13:7) afforded dyad **45a** as a turquoise-blue solid. Yield: 117 mg (43%). Mp: 157 $^\circ\text{C}$. ^1H NMR (CDCl_3 , 600 MHz): δ 11.48 (s, 1H, CHO), 10.42 (s, 1H, H10), 9.70 (s, 1H, H5), 9.26 (t, $J = 5.1$ Hz, 1H, NH), 9.19 (t, $J = 5.0$ Hz, 1H, NH), 8.91 (s, 1H, H20), 8.18 and 8.14 (both s, 2H, H3a, H7a), 7.38 (m, 2H, H4a'), 7.26-7.20 (m, 4H, H3a', H5a'), 5.31 (d, $J = 20.0$ Hz, 1H, H13²), 5.13 (d, $J = 20.0$ Hz, 1H, H13²), 4.56 (m, 1H, H18), 4.35 (m, 1H, H17), 3.90 (m, 2H, H2a⁶), 3.72 (s, 3H, H12¹), 3.69 (m, 2H, H8¹), 3.67 (s, 3H, H2¹), 3.42 (m, 2H, H6a¹), 3.37 (m, 2H, H2a¹), 3.29 (s, 3H, H7¹), 2.60 (m, 4H, *i*Pr-H), 2.68-2.51 and 2.26 (m, 4H, H17¹, H17²), 1.80 (d, $J = 7.4$ Hz, 3H, H18¹), 1.66 (t, $J = 7.6$ Hz, 3H, H8²), 1.65-1.55 (m, 4H, H2a², H6a²), 1.42-1.25 (m, 8H, H2a³-H2a⁵, H6a³), 1.04 (m, 24H, *i*Pr- CH_3), 0.87 (t, $J = 7.4$ Hz, 3H, H6a⁴), -0.48 (s, 1H, NH), -2.04 (s, 1H, NH). UV-vis (THF): $\lambda_{\text{max}} = 693$ (51800), 615 (27700), 554 (19500), 521 (14800), 426 (73200), 387 (63400), 365 nm (49800 $\text{M}^{-1} \text{cm}^{-1}$). HRMS (ESI): m/z calcd for $\text{C}_{80}\text{H}_{91}\text{N}_8\text{O}_8$ $[\text{M}+\text{H}]^+$: 1291.6958, found: 1291.6953.



Compound 45b. (COR111)

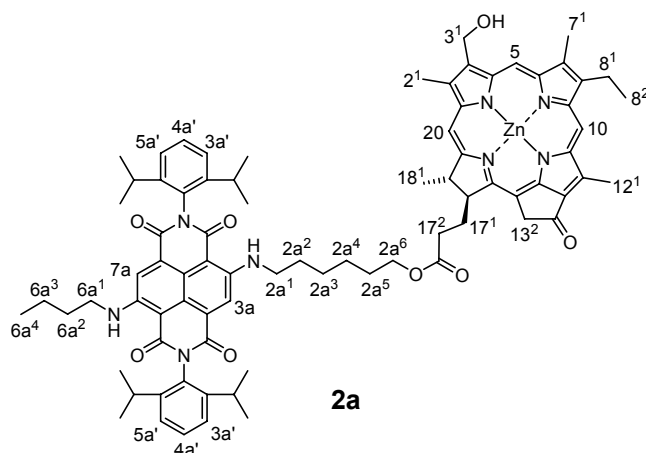
Chlorin derivative **29** (75 mg, 0.14 mmol) and naphthalene diimide **44** (181 mg, 0.140 mmol) were dissolved in CH_2Cl_2 (5 mL), and DCC (144 mg, 0.70 mmol), DMAP (51 mg, 0.42 mmol), DPTS (124 mg, 0.42 mmol) and *N*-ethyldiisopropylamine (500 μL) were added at room temperature. The reaction mixture was stirred for 24 h and CHCl_3 (20 mL) was added. The mixture was washed with 1N HCl (1 \times 20 mL) and water (2 \times 20 mL), dried over anhydrous Na_2SO_4 and the solvent was removed by rotary evaporation. Successive purification of the crude product by column chromatography (CHCl_3/n -pentane 4:1) and HPLC (methanol/ CH_2Cl_2 11:9) afforded a turquoise-blue solid. Yield: 108 mg (43%). Mp: 103-106 $^\circ\text{C}$. ^1H NMR (CDCl_3 , 600 MHz): δ 11.48 (s, 1H, CHO), 10.73 (s, 1H, H10), 9.96 (s, 1H, H5), 9.28 (m, 1H, NH), 9.23 (m, 1H, NH), 9.11 (s, 1H, H20), 8.17 and 8.16 (2s, 2H, H3a, H7a), 7.40 (m, 2H, H4a'), 7.29-7.24 (m, 4H, H3a', H5a'), 7.05 (d, $J = 3.6$ Hz, 2H, H2b, H6b), 6.54 (t, $J = 3.6$ Hz, 1H, H4b), 5.38 (d, $J = 19.2$ Hz, 1H, H13²), 5.18 (d, $J = 19.2$ Hz, 1H, H13²), 4.64 (m, 1H, H18), 4.43 (m, 1H, H17), 4.26 (t, $J = 6.6$ Hz, 2H, H6a⁶), 4.03 (m, 2H, H2a⁶), 3.95 (t, $J = 6.5$ Hz, 4H, H3b¹, H5b¹), 3.87 (m, 2H, H8¹), 3.75 (s, 3H, H12¹), 3.72 (s, 3H, H2¹), 3.51 (m, 2H, H6a¹), 3.49 (s, 3H, H7¹), 3.46 (m, 2H, H2a¹), 2.87-2.82, 2.70-2.64, and 2.44-2.35 (m, 4H, H17¹, H17²), 2.60 (m, 4H, *iPr-H*), 1.86 (d, $J = 7.5$ Hz, 3H, H18¹), 1.78-1.68 (m, 9H, H8², H6a², H3b², H5b²), 1.58-1.23 (m, 50H, H2a²-H2a⁵, H6a³-H6a⁵, H3b³-H3b¹¹, H5b³-H5b¹¹), 1.06 (m, 24H, *iPr-CH*₃), 0.87 (t, $J = 7.0$ Hz, 6H, H3b¹², H5b¹²), chlorin NH protons could not be detected. HRMS (ESI): m/z calcd for $\text{C}_{113}\text{H}_{147}\text{N}_8\text{O}_{12}$ [$\text{M}+\text{H}$]⁺: 1808.1138, found: 1808.1133.



ZnChI-NDI_{11N} 2a. (COR099)

BH₃(*t*-BuNH₂) (34 mg, 0.39 mmol) was added into an ice-cooled solution of aldehyde **45a** (100 mg, 0.0774 mmol) in CH₂Cl₂ (30 mL) and the reaction mixture was stirred at 0 °C for 2 h. Then 1N HCl (30 mL) was added and the mixture was stirred vigorously for additional 30 min. The organic layer was separated, washed with water (2 × 20 mL), dried over anhydrous Na₂SO₄ and the solvent was evaporated under vacuum. The residual solid was subjected to HPLC (MeOH/CH₂Cl₂ 7:3) to provide at C-3¹ position hydroxy-functionalized intermediate product (90 mg, 90%). This product (70 mg, 0.054 mmol) was dissolved in THF (14 mL) and a saturated methanolic zinc acetate dihydrate solution (20 mL) was added. After stirring for 2 h at room temperature, diethylether (50 mL) was added to it. The solution was washed with water (3 × 20 mL) and saturated aqueous NaHCO₃ solution (1 × 20 mL) and dried over Na₂SO₄. Removal of the solvent by rotary evaporation and purification of the crude product by HPLC (methanol/CH₂Cl₂ 4:1) afforded dyad **2a** as a turquoise-green solid. Yield: 47 mg (59% with respect to **45a**). Mp: 255-256 °C. ¹H NMR (d₈-THF, 400 MHz): δ 9.62 (s, 1H, H₁₀), 9.51 (s, 1H, H₅), 9.41 (t, *J* = 5.2 Hz, 1H, NH), 9.36 (t, *J* = 5.0 Hz, 1H, NH), 8.49 (s, 1H, H₂₀), 8.26 and 8.24 (both s, 2H, H_{3a}, H_{7a}), 7.40-7.22 (m, 6H, H_{3a'}, H_{4a'}, H_{5a'}), 5.73 (d, *J* = 5.7 Hz, 2H, H_{3¹}), 5.10 (d, *J* = 19.6 Hz, 1H, H_{13²}), 4.95 (d, *J* = 19.4 Hz, 1H, H_{13²}), 4.52 (dq, *J* = 7.2 Hz, *J* = 2.1 Hz, 1H, H₁₈), 4.18 (t, *J* = 5.7 Hz, 1H, OH), 4.30 (td, *J* = 8.5 Hz, *J* = 2.8 Hz, 1H, H₁₇), 3.90 (m, 2H, H_{2a⁶}), 3.81 (m, 2H, H_{8¹}), 3.60 (s, 3H, H_{12¹}), 3.53 (m, 2H, H_{6a¹}), 3.47 (m, 2H, H_{2a¹}), 3.32 (s, 3H, H_{2¹}), 3.30 (s, 3H, H_{7¹}), 2.70 (m, 4H, *iPr-H*), 2.51, 2.32, and 2.20 (m, 4H, H_{17¹}, H_{17²}), 1.79 (d, *J* = 7.3 Hz, 3H, H_{8²}), 1.65 (m, 5H, H_{18¹}, H_{6a²}), 1.52-1.22 (m, 10H, H_{2a²}-H_{2a⁵}, H_{6a³}), 1.08 (m, 24H, *iPr-CH*₃), 0.96 (t, *J* = 7.4 Hz, 3H, H_{6a⁴}). UV-vis

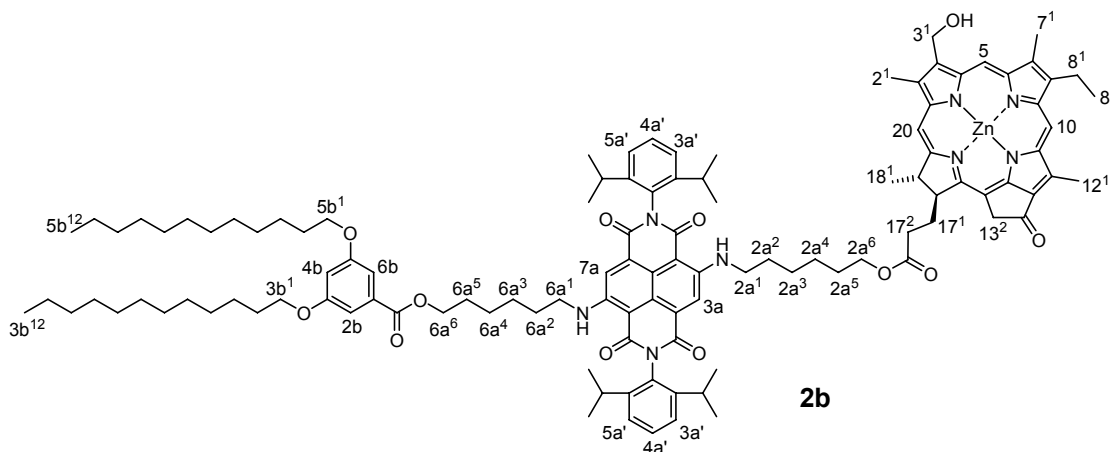
(THF): λ_{\max} = 647, 608, 569, 425, 404, 365 nm. HRMS (ESI): calcd for $C_{80}H_{89}N_8O_7Zn$ $[M-OH]^+$: 1337.6145, found: 1337.6101.



ZnChl-NDI_{NN} **2b**. (COR118)

$BH_3(t-BuNH_2)$ (10 mg, 0.12 mmol) was added into an ice-cooled solution of aldehyde **45b** (107 mg, 0.059 mmol) in CH_2Cl_2 (20 mL) and the reaction mixture was stirred at 0 °C for 4 h under an argon gas atmosphere. Then 1N HCl (30 mL) was added and the mixture was stirred vigorously for additional 30 min. The organic layer was separated, washed with water (2 × 20 mL), dried over anhydrous Na_2SO_4 , and the solvent was evaporated under vacuum. The residual solid was dissolved in THF (10 mL) and a saturated methanolic zinc acetate dihydrate solution (30 mL) was added. After stirring for 6 h at room temperature, diethylether (50 mL) was added. The solution was washed with water (3 × 20 mL) and saturated aqueous $NaHCO_3$ solution (1 × 20 mL) and dried over Na_2SO_4 . Removal of the solvent by rotary evaporation and purification of the crude product by HPLC (methanol/ CH_2Cl_2 4:1) afforded dyad **2b** as a turquoise-green solid. Yield: 66 mg (59%). Mp: 251-253 °C. 1H NMR (d_8 -THF, 400 MHz): δ 9.62 (s, 1H, H10), 9.50 (s, 1H, H5), 9.43 (t, J = 5.2 Hz, 1H, NH), 9.36 (t, J = 5.0 Hz, 1H, NH), 8.49 (s, 1H, H20), 8.26 and 8.24 (both s, 2H, H3a, H7a), 7.40-7.22 (m, 6H, H4a'-H6a'), 7.09 (d, J = 2.3 Hz, 2H, H2b, H6b), 6.64 (t, J = 2.3 Hz, 1H, H4b), 5.72 (d, J = 5.7 Hz, 2H, H3¹), 5.10 (d, J = 19.4 Hz, 1H, H13²), 4.95 (d, J = 19.4 Hz, 1H, H13²), 4.51 (dq, J = 7.2 Hz, J = 2.3 Hz, 1H, H18), 4.43 (t, J = 5.7 Hz, 1H, OH), 4.30 (m, 1H, H17), 4.24 (t, J = 6.7 Hz, 2H, H6a⁶), 3.95 (t, J = 6.4 Hz, 4H, H3b¹, H5b¹), 3.89 (m, 2H, H2a⁶), 3.81 (m, 2H, H8¹), 3.60 (s, 3H, H12¹), 3.56 (m, 2H, H6a¹), 3.47 (m, 2H, H2a¹), 3.31 (s, 3H, H2¹), 3.30 (s, 3H, H7¹), 2.70 (m, 4H, *i*Pr-H), 2.62, 2.51, 2.32, and 2.20 (m, 4H, H17¹, H17²), 1.78, 1.65, 1.52, 1.45, and 1.29 (m, 62H, H8², H18¹, H2a²-H2a⁵, H6a²-H6a⁵, H3b²-H3b¹¹, H5b²-H5b¹¹), 1.12-

1.05 (m, 24H, *i*Pr-CH₃), 0.88 (t, *J* = 6.8 Hz, 6H, H3b¹², H5b¹²). UV-vis (THF): λ_{\max} (ϵ) = 646 (67800), 607 (23500), 569 (12600), 527 (7510), 424 (91000), 404 (50100), 364 nm (31900 M⁻¹ cm⁻¹); UV-vis (cyclohexane/ 1% CCl₄): λ_{\max} (ϵ) = 731 (48000), 611 (16800), 444 (28800), 420 (24700), 363 nm (18400 M⁻¹ cm⁻¹). HRMS (ESI): *m/z* calcd for C₁₁₃H₁₄₆N₈NaO₁₂Zn [M+Na]⁺: 1894.0244, found: 1894.0212.

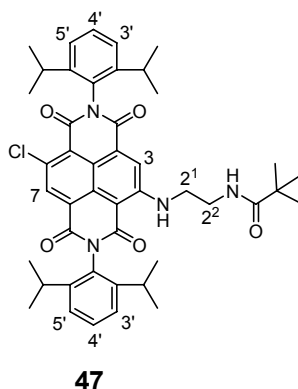


***N,N'*-Bis-(2',6'-diisopropylphenyl)-2-(2'-aminoethylamino)-6-chloro-1,4,5,8-naphthalenetetracarboxylic acid diimide (46). (VW016)**

Synthesis and characterization was made according to literature.²¹

Compound 47. (VW019)

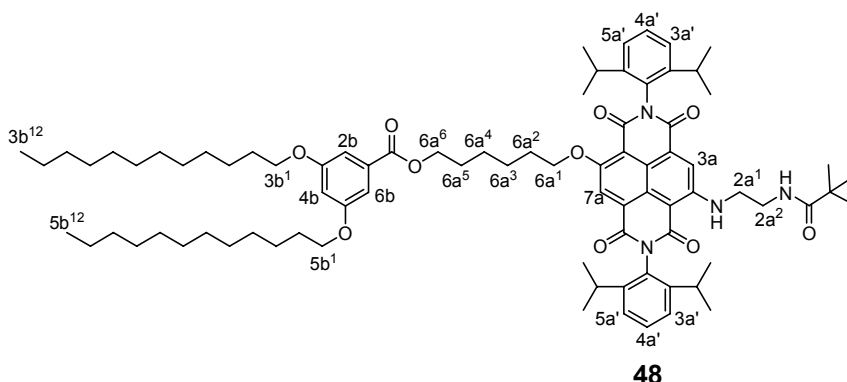
A solution of di-*tert*-butyl dicarbonate (BOC₂O; 2.95 g, 13.5 mmol) in dry CH₂Cl₂ (10 mL) was added dropwise to a solution of *N,N'*-bis-(2,6-diisopropylphenyl)-2-(2'-aminoethylamino)-6-chloro-1,4,5,8-naphthalenetetracarboxylic acid diimide (**46**) (920 mg, 1.35 mmol) in dry CH₂Cl₂ (30 mL) at room temperature. After 30 min, the CH₂Cl₂ phase was washed with water (2 × 30 mL) and the solvent was removed at the rotary evaporator. Column chromatography (Et₂O/*n*-pentane 1:1) afforded compound **47** as a red solid. Yield: 910 mg (87%). Mp: 185-187 °C. ¹H NMR (CDCl₃, 400 MHz): δ 10.13 (t, *J* = 5.4 Hz, 1H, NH), 8.79 (s, 1H, H7), 8.39 (s, 1H, H3), 7.50 (m, 2H, H4'), 7.37 (d, *J* = 7.8 Hz, 2H, H3', H5'), 7.34 (d, *J* = 7.8 Hz, 2H, H3', H5'), 4.80 (s, 1H, NHCO), 3.75 (m, 2H, H2¹), 3.49 (m, 2H, H2²), 2.67 (m, 4H, *i*Pr-H), 1.37 (s, 9H, *t*Bu-CH₃), 1.70 (m, 24H, *i*Pr-CH₃). UV-vis (THF): λ_{\max} (ϵ) = 528 (14000), 365 nm (12200 M⁻¹ cm⁻¹). HRMS (ESI): *m/z* calcd for C₄₅H₅₂ClN₄O₆ [M+H]⁺: 779.3570, found: 779.3563. Anal. calcd for C₄₅H₅₁ClN₄O₆: C, 69.35; H, 6.60; N, 7.19; Cl, 4.55. Found: C, 68.91; H, 6.77; N, 6.75; Cl, 4.42.



Compound 48. (VW021)

NDI **47** (870 mg, 1.12 mmol) was dissolved in CH_2Cl_2 (20 mL) and 1,6-hexanediol (8.30 g, 70.2 mmol) and potassium carbonate (829 mg, 6.00 mmol) were added. Then CH_2Cl_2 was removed at the rotary evaporator, and the reaction mixture was stirred at 80 °C for 6 h; during this time the color of the mixture turned pink. Afterwards, CHCl_3 (100 mL) and 1N HCl (100 mL) were added and the organic layer was separated, washed with water (100 mL) and dried over Na_2SO_4 . After removal of solvent, the residue was subjected to column chromatography (methanol/ CH_2Cl_2 1:99). A pink solid (675 mg) was obtained, which was then dissolved in CH_2Cl_2 (80 mL) and 3,5-bis(dodecyloxy)benzoic acid (560 mg, 1.14 mmol), DCC (784 mg, 3.80 mmol), DMAP (279 mg, 2.28 mmol), DPTS (671 mg, 2.28 mmol) and *N*-ethyl-diisopropylamine (500 μL) were added. The reaction mixture was stirred at room temperature for 3 h. The CH_2Cl_2 phase was washed with water (2 \times 50 mL), and the solvent was removed under reduced pressure. Purification of the crude product was achieved by column chromatography (CH_2Cl_2), giving compound **48** in analytically pure form. Yield: 761 mg (55%). Mp: 82-84 °C. ^1H NMR (CDCl_3 , 400 MHz): δ 9.87 (t, J = 5.5 Hz, 1H, NH), 8.46 (s, 1H, H7a), 8.35 (s, 1H, H3a), 7.49 (m, 2H, H4a'), 7.36 (d, J = 7.7 Hz, 2H, H3a', H5a'), 7.32 (d, J = 7.7 Hz, 2H, H3a', H5a'), 7.13 (d, J = 2.3 Hz, 2H, H2b, H6b), 6.62 (t, J = 2.3 Hz, 1H, H4b), 4.78 (s, 1H, NHCO), 4.37 (t, J = 6.3 Hz, 2H, H6a¹), 4.26 (t, J = 6.7 Hz, 2H, H6a⁶), 3.94 (m, 4H, H3b¹, H5b¹), 3.71 (m, 2H, H2a¹), 3.47 (m, 2H, H2a²), 2.70 (m, 4H, *i*Pr-H), 1.93 (m, 2H, H6a²), 1.76, 1.57, and 1.45 (m, 14H, H6a³-H6a⁵, H3b², H3b³, H5b², H5b³), 1.37 (s, 9H, *t*Bu- CH_3), 1.26 (m, 32H, H3b⁴-H3b¹¹, H5b⁴-H5b¹¹), 1.17 (m, 24H, *i*Pr- CH_3), 0.88 (t, J = 6.9 Hz, 6H, H3b¹², H5b¹²). UV-vis (THF): λ_{max} (ϵ) = 544 (16900), 367 nm (12000 $\text{M}^{-1} \text{cm}^{-1}$). HRMS

(ESI): m/z calcd for $C_{82}H_{117}N_4O_{11}$ $[M+H]^+$: 1333.8713, found: 1333.8712. Anal. calcd for $C_{82}H_{116}N_4O_{11}$: C, 73.84; H, 8.77; N, 4.20. Found: C, 73.78; H, 8.72; N, 4.06.



Compound 49. (COR177)

To a solution of NDI **48** (730 mg, 0.547 mmol) in CH_2Cl_2 (25 mL), CF_3COOH (3 mL) was added. The reaction mixture was stirred at room temperature for 30 min under an argon gas atmosphere and then washed with water (3×50 mL). Evaporation of the solvent gave the corresponding BOC-protected product **49** as a pink solid (645 mg, 96% of crude product), which was used for the following reaction without further purification and characterization.

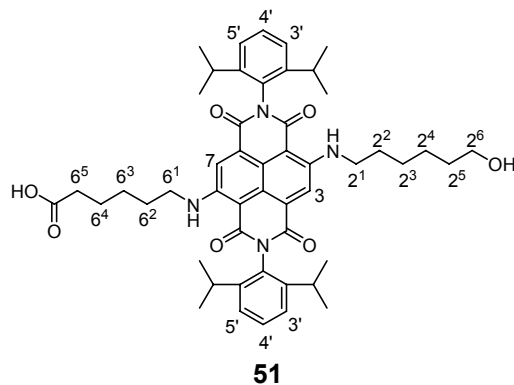
***N,N'*-Bis-(2',6'-diisopropylphenyl)-2-chloro-6-(6'-carboxy-*n*-hexylamino)-1,4,5,8-naphthalenetetracarboxylic acid diimide (50). (COR211b)**

NDI **50** was prepared from NDI **49** according to literature procedure and the characterization data of **50** were in agreement with those reported in literature.²¹

***N,N'*-Bis-(2',6'-diisopropylphenyl)-2-(6'-hydroxyhexylamino)-6-(6'-carboxyhexylamino)-1,4,5,8-naphthalenetetracarboxylic acid diimide (51). (DB015, COR211c)**

NDI **50** (80 mg, 0.11 mmol) was dissolved in molten 6-aminohexanol (5 mL). The solution was stirred at 80 °C for 2 h; during this time the color of the solution turned blue. Then $CHCl_3$ (100 mL) and 1N HCl (100 mL) were added and the organic layer was separated, washed with 1N HCl (2×100 mL) and dried over Na_2SO_4 . The $CHCl_3$ solution was evaporated under vacuum to give NDI **51** as a blue solid, which was purified by column chromatography (methanol/ $CHCl_3$ 5:95-7:93). Yield: 84 mg (91%). Mp: 311-312 °C. 1H NMR ($CDCl_3$, 400 MHz): δ 9.36 (m, 2H, NH), 8.26 and 8.25 (s,

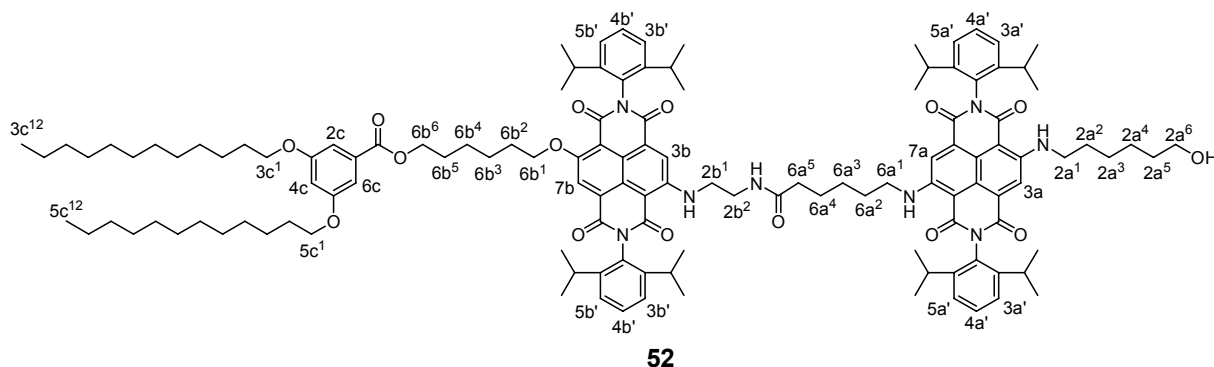
2H, H3, H7), 7.50 (t, $J = 7.7$ Hz, 2H, H4'), 7.35 (d, $J = 7.7$ Hz, 4H, H3', H5'), 3.61 (t, $J = 6.4$ Hz, 2H, H2⁶), 3.51 (m, 4H, H2¹, H6¹), 2.68 (m, 4H, *iPr-H*), 2.33 (t, $J = 7.3$ Hz, 2H, H6⁵), 1.76-1.50 (m, 14H, H2²-H2⁵, H6²-H6⁴), 1.15 (m, 24H, *iPr-CH*₃), *OH* and *COOH* could not be detected. UV-vis (THF): $\lambda_{\text{max}} = 612, 361$ nm. HRMS (ESI): m/z calcd for C₅₀H₆₂N₄O₇ [M+H]⁺: 831.4696, found: 831.4691.



Compound 52. (VW027)

HATU (114 mg, 0.30 mmol) and *N*-ethyldiisopropylamine (250 μ L) were added into a solution of NDI **51** (84 mg, 0.10 mmol) in CH₂Cl₂ (15 mL), and the reaction mixture was stirred at room temperature for 5 min under an argon gas atmosphere. NDI **49** (123 mg, 0.10 mmol) was added and the mixture was stirred for additional 5 min. Then the mixture was poured into CH₂Cl₂ (100 mL), washed with water (2 \times 100 mL), and dried over anhydrous Na₂SO₄. The CH₂Cl₂ solution was evaporated under vacuum to give NDI-NDI **52** as a violet solid which was purified by column chromatography (methanol/CH₂Cl₂ 1:99). Yield: 127 mg (62%). Mp: 123-126 $^{\circ}$ C. ¹H NMR (CDCl₃, 400 MHz): δ 9.79 (m, 1H, *NH*), 9.34 (m, 2H, *NH*), 8.45 (s, 1H, H7b), 8.30, 8.26, and 8.23 (s, 3H, H3a, H7a, H3b), 7.52-7.42 (m, 4H, H4a', H4b'), 7.35-7.30 (m, 8H, H3a', H5a', H3b', H5b'), 7.13 (d, $J = 2.3$ Hz, 2H, H2c, H6c), 6.62 (t, $J = 2.3$ Hz, 1H, H4c), 6.21 (m, 1H, *NHCO*), 4.36 (t, $J = 6.2$ Hz, 2H, H6b¹), 4.26 (t, $J = 6.8$ Hz, 2H, H6b⁶), 3.96 (t, $J = 6.6$ Hz, 4H, H3c¹, H5c¹), 3.61 (t, $J = 6.4$ Hz, 2H, H2a⁶), 3.54-3.40 (m, 8H, H2a¹, H6a¹, H2b¹, H2b²), 2.69 (m, 8H, *iPr-H*), 2.14 (m, 2H, H6a⁵), 1.94 (m, 2H, *CH*₂), 1.79-1.68 (m, 12H, *CH*₂), 1.60-1.53 (m, 4H, *CH*₂), 1.44 (m, 12H, *CH*₂), 1.26 (m, 32H, H3c⁴-H3c¹¹, H5c⁴-H5c¹¹), 1.15 (m, 48H, *iPr-CH*₃), 0.88 (t, $J = 6.9$ Hz, 6H, H3c¹², H5c¹²), *OH* could not be detected. UV-vis (THF): $\lambda_{\text{max}} (\epsilon) = 613 (20900), 548 (23900), 364 \text{ nm} (23300 \text{ M}^{-1} \text{ cm}^{-1})$; UV-vis (cyclohexane/ 1% CCl₄): $\lambda_{\text{max}} (\epsilon) = 612 (22100), 543 (22000), 363 \text{ nm} (24100 \text{ M}^{-1} \text{ cm}^{-1})$. Fluorescence (THF, 293 K): $\lambda_{\text{max}} =$

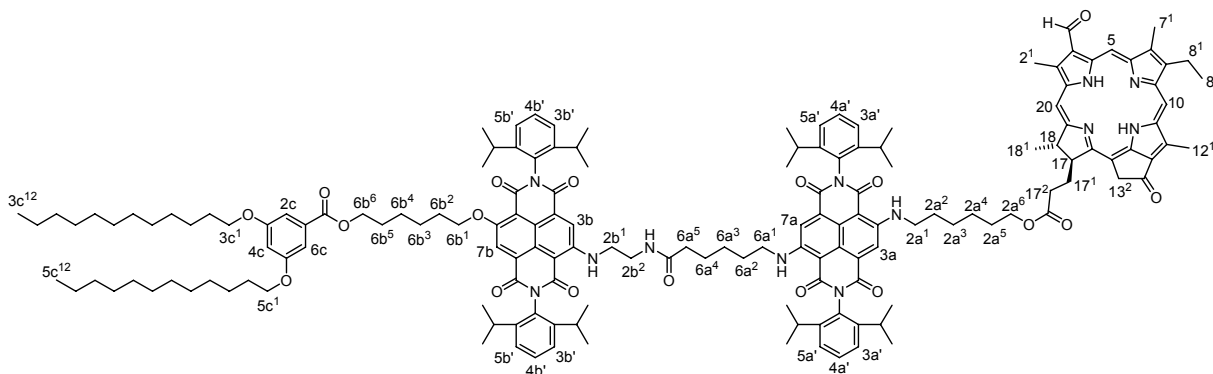
638 nm ($\lambda_{\text{ex}} = 525$ nm), quantum yield $\phi_{\text{Fl}} = 0.39$; fluorescence (cyclohexane, 1% CCl_4 , 293 K): $\lambda_{\text{max}} = 634$ nm ($\lambda_{\text{ex}} = 520$ nm), quantum yield $\phi_{\text{Fl}} = 0.51$. HRMS (ESI): m/z calcd for $\text{C}_{127}\text{H}_{169}\text{N}_8\text{O}_{15}$ $[\text{M}+\text{H}]^+$: 2046.2707, found: 2046.2715.



Compound 53. (COR217)

A mixture of chlorin derivative **29** (33 mg, 0.062 mmol), $\text{NDI}_{\text{NN}}\text{-NDI}_{\text{NO}}$ **52** (127 mg, 0.062 mmol), DCC (38 mg, 0.19 mmol), DMAP (23 mg, 0.19 mmol), DPTS (55 mg, 0.19 mmol), and *N*-ethyldiisopropylamine (250 μL) in CH_2Cl_2 (3 mL) was stirred for 24 h at 35 $^\circ\text{C}$. CHCl_3 (50 mL) was added and the organic phase was washed successively with 1N HCl (1 \times 30 mL) and water (30 mL), dried over anhydrous Na_2SO_4 , and solvent was removed by rotary evaporation. Purification of the crude product by column chromatography (CHCl_3) and subsequent semi-preparative HPLC (methanol/ CH_2Cl_2 3:2) afforded dyad **53** as a brownish black solid. Yield: 41 mg (26%). Mp: 107-109 $^\circ\text{C}$. ^1H NMR (CDCl_3 , 400 MHz): δ 11.57 (s, 1H, CHO), 10.33 (s, 1H, H10), 9.79 (t, $J = 5.1$ Hz, 1H, NH), 9.63 (s, 1H, H5), 9.33 (t, $J = 5.4$ Hz, 1H, NH), 9.26 (t, $J = 4.9$ Hz, 1H, NH), 8.84 (s, 1H, H20), 8.45 (s, 1H, H7b), 8.30 (s, 1H, H3b), 8.21 (m, 2H, H3a, H7a), 7.49-7.44, 7.39-7.36, 7.33-7.30, and 7.24 (m, 12H, H3a'-H5a', H3b'-H5b'), 7.13 (d, $J = 2.3$ Hz, 2H, H2c, H6c), 6.62 (t, $J = 2.3$ Hz, 1H, H4c), 6.18 (t, $J = 5.5$ Hz, 1H, NHCO), 5.34 (d, $J = 20.0$ Hz, 1H, H13²), 5.17 (d, $J = 20.0$ Hz, 1H, H13²), 4.57 (m, 1H, H18), 4.37 (m, 3H, H17, H6b¹), 4.26 (t, $J = 6.8$ Hz, 2H, H6b⁶), 3.99-3.86 (m, 6H, H2a⁶, H3c¹, H5c¹), 3.77-3.72 (m, 8H, H8¹, H12¹, H2¹), 3.47-3.39 (m, 8H, H2b¹, H2b², H2a¹, H6a¹), 3.33 (s, 3H, H7¹), 2.75-2.52 and 2.36-2.24 (m, 12H, *iPr*-H, H17¹, H17²), 2.12 (m, 2H, H6a⁵), 1.94 (m, 2H, H6b²), 1.83 (d, $J = 7.3$ Hz, 3H, H18¹), 1.73-1.62 (m, 17H, H3c², H5c², H8², H6b⁵, H6b³, H6a², H2a², H6a⁴), 1.47-1.40 (m, 10H, H3c³, H5c³, H6b⁴, H2a⁵, H6a³), 1.26 (m, 36H, H3c⁴-H3c¹¹, H5c⁴-H5c¹¹, H2a³, H2a⁴), 1.17-1.07 (m, 48H, *iPr*-CH₃), 0.87 (t, $J = 6.9$ Hz, 6H, H3c¹², H5c¹²).

-0.12 (*br s*, 1H, *NH*), -2.04 (*br s*, 1H, *NH*). UV-vis (THF): λ_{max} (ϵ) = 691 (51700), 617 (21700), 551 (29800), 521 (22700), 425 (65700), 385 (54400), 367 nm (50700 M⁻¹ cm⁻¹). HRMS (ESI): calcd for C₁₅₉H₁₉₈N₁₂NaO₁₈ [M+Na]⁺: 2586.4844, found: 2586.4869.

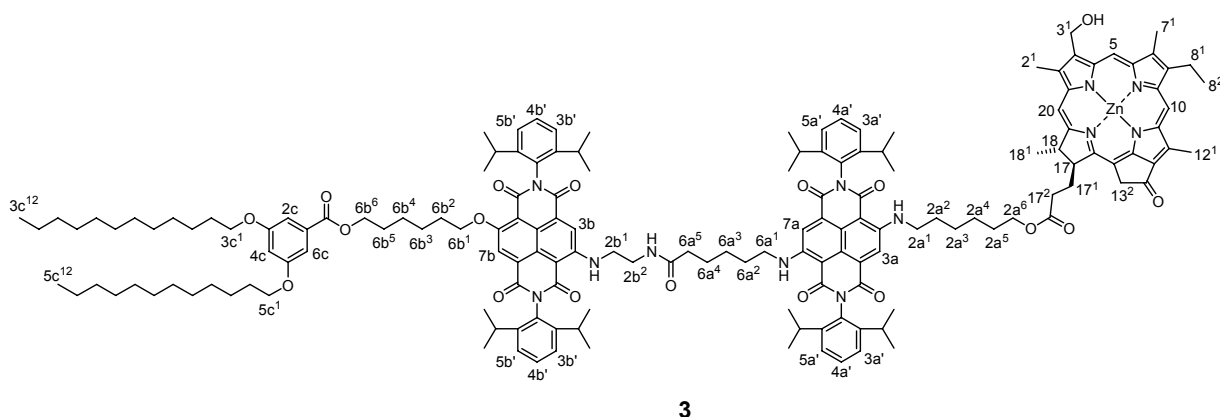


53

ZnChI-NDI_{IN}-NDI_{NO} 3. (COR218)

BH₃(*t*-BuNH₂) (5 mg, 0.058 mmol) was added to an ice-cooled solution of aldehyde **53** (15 mg, 0.0058 mmol) in CH₂Cl₂ (20 mL), and the reaction mixture was stirred at 0 °C for 3 h under an argon gas atmosphere. Then 1N HCl (20 mL) was poured into the mixture, followed by vigorous stirring for additional 15 min. The organic layer was separated, washed successively with water (2 × 30 mL), saturated aqueous NaHCO₃ solution (20 mL), and water again (30 mL), dried over anhydrous Na₂SO₄ and the solvent was evaporated under vacuum. The residual solid was dissolved in THF (10 mL) and a saturated methanolic zinc acetate dihydrate solution (50 mL) was added. After stirring for 16 h at room temperature, diethylether (100 mL) was added. The solution was washed with water (3 × 100 mL) and saturated aqueous NaHCO₃ solution (1 × 100 mL) and dried over anhydrous Na₂SO₄. Removal of the solvent by rotary evaporation and purification of the crude product by HPLC (methanol/THF 7:3) afforded triad **3** as a bluish black solid. Yield: 10 mg (66%). Mp: 213-214 °C. ¹H NMR (d₈-THF, 600 MHz, ¹H, ¹H-COSY): δ 9.93 (t, *J* = 5.7 Hz, 1H, *NH*), 9.63 (s, 1H, H10), 9.51 (s, 1H, H5), 9.37 (m, 2H, *NH*), 8.50 (s, 1H, H20), 8.47 (s, 1H, H7b), 8.40 (s, 1H, H3b), 8.24 (m, 2H, H3a, H7a), 7.40, 7.34, 7.28, and 7.24 (m, 12H, H3a'-H5a', H3b'-H5b'), 7.10 (d, *J* = 2.4 Hz, 2H, H2c, H6c), 6.92 (*br s*, 1H, *NHCO*), 6.65 (t, *J* = 2.4 Hz, 1H, H4c), 5.73 (d, *J* = 5.8 Hz, 2H, H3¹), 5.11 (d, *J* = 18.9 Hz, 1H, H13²), 4.96 (d, *J* = 18.9 Hz, 1H, H13²), 4.52 (m, 1H, H18), 4.49 (t, *J* = 5.8 Hz, 1H, *OH*), 4.38 (t, *J* = 6.2 Hz, 2H, H6b¹), 4.31 (td, *J* = 8.9 Hz, *J* = 2.5 Hz, 1H, H17), 4.23 (t, *J* = 6.8 Hz, 2H,

H6b⁶), 3.96 (t, $J = 6.5$ Hz, 4H, H3c¹, H5c¹), 3.91 (m, 2H, H2a⁶), 3.82 (q, $J = 7.7$ Hz, 2H, H8¹), 3.67 (m, 2H, H2b¹), 3.61 (s, 3H, H12¹), 3.50-3.41 (m, 6H, H2b², H2a¹, H6a¹), 3.32 (s, 3H, H2¹), 3.31 (s, 3H, H7¹), 2.79-2.67 (m, 8H, *iPr-H*), 2.63, 2.52, 2.32, and 2.20 (m, 4H, H17¹, H17²), 2.05 (t, $J = 7.4$ Hz, 2H, H6a⁵), 1.92 (m, 2H, H6b²), 1.79 (d, $J = 7.4$ Hz, 3H, H18¹), 1.76 (m, 4H, H3c², H5c²), 1.73-1.71 (m, 5H, H8², H6b⁵), 1.68-1.62 (m, 6H, H6b³, H6a², H2a²), 1.60 (m, 2H, H6a⁴), 1.52-1.43 (m, 10H, H3c³, H5c³, H6b⁴, H2a⁵, H6a³), 1.38-1.28 (m, 36H, H3c⁴-H3c¹¹, H5c⁴-H5c¹¹, H2a³, H2a⁴), 1.15-1.05 (m, 48H, *iPr-CH*₃), 0.89 (t, $J = 7.0$ Hz, 6H, H3c¹², H5c¹²). UV-vis (THF): $\lambda_{\max} (\epsilon) = 647$ (68200), 610 (25700), 552 (22000), 425 (91000), 403 (52300), 366 (43500 M⁻¹ cm⁻¹); UV-vis (cyclohexane/ 1% CCl₄): $\lambda_{\max} (\epsilon) = 731$ (50400), 619 (19300), 551 (19300), 444 (31000), 367 nm (27700 M⁻¹ cm⁻¹). Fluorescence (THF, 293 K): $\lambda_{\max} = 648$, 704 nm ($\lambda_{\text{ex}} = 510$ nm), quantum yield $\phi_{\text{Fl}} = 0.11$; fluorescence (cyclohexane/ 1% CCl₄, 293 K): $\lambda_{\max} = 738$ nm ($\lambda_{\text{ex}} = 540$ nm). MS (Maldi-TOF): calcd for C₁₅₉H₁₉₈N₁₂O₁₈Zn [M]⁺: 2627.4, found: 2627.4. HRMS (ESI): *m/z* calcd for C₁₅₉H₁₉₈N₁₂NaO₁₈Zn [M+Na]⁺: 2650.4136, found: 2650.4152.



References

- (1) <http://www.erin.utoronto.ca/~w3env100y/oldstuff/Murck.Resources.htm>
 - (2) Estimated by the US Energy Information Administration; <http://www.eia.doe.gov/>
 - (3) Huber, R. *Angew. Chem.* **1989**, *101*, 849-871; *Angew. Chem., Int. Ed.* **1989**, *28*, 849-869.
 - (4) Katz, J. J. *Photosynth. Res.* **1990**, *26*, 143-160.
 - (5) Van Grondelle, R.; Dekker, J. P.; Gillbro, T.; Sundström, V. *Biochim. Biophys. Acta* **1994**, *1187*, 1-65.
 - (6) Schulten, K. In *Simplicity and Complexity in Proteins and Nucleic Acids*; Frauenfelder, H., Deisenhofer, J., Wolynes, P. G., Eds.; Dahlem University Press: Berlin, 1999, pp. 227-253.
 - (7) Cogdell, R. J.; Lindsay, J. G. *New Phytol.* **2000**, *145*, 167-196.
 - (8) Law, C. J.; Roszak, A. W.; Southall, J.; Gardiner, A. T.; Isaacs, N. W.; Cogdell, R. J. *Mol. Membr. Biol.* **2004**, *21*, 183-191.
 - (9) Holzwarth, A. R. In *Series on Photoconversion of Solar Energy*; Archer, M. D., Barber, J., Eds.; Imperial College Press: London, UK, 2002; pp 43-115.
 - (10) Scholes, G. D.; Fleming, G. R. *Adv. Chem. Phys.* **2006**, *132*, 57-129.
 - (11) Balaban, T. S.; Tamiaki, H.; Holzwarth, A. R. *Top. Curr. Chem.* **2005**, *258*, 1-38.
 - (12) Olson, J. M. *Photochem. Photobiol.* **1998**, *67*, 61-75.
 - (13) Manske, A. K.; Glaeser, J.; Kuypers, M. M. M.; Overmann, J. *Appl. Environ. Microbiol.* **2005**, *71*, 8049-8060.
 - (14) Scholes, G. D.; Rumbles, G. *Nature* **2006**, *5*, 683-696.
 - (15) Huber, V.; Katterle, M.; Lysetska, M.; Würthner, F. *Angew. Chem.* **2005**, *117*, 3208-3212; *Angew. Chem., Int. Ed.* **2005**, *44*, 3147-3151.
- For reviews on supramolecular LH systems, see refs. 16-20:
- (16) Balzani, V.; Ceroni, P.; Maestri, M.; Vicinelli, V. *Curr. Opin. Chem. Biol.* **2003**, *7*, 657-665.
 - (17) Fréchet, J. M. J. *J. Polym. Sci. Pol. Chem.* **2003**, *41*, 3713-3725.
 - (18) Würthner, F. *Chem. Commun.* **2004**, 1564-1579.
 - (19) Hoeben, F. J. M.; Jonkheim, P.; Meijer, E. W.; Schenning, A. P. H. J. *Chem. Rev.* **2005**, *105*, 1491-1546.

-
- (20) Wasielewski, M. R. *J. Org. Chem.* **2006**, *71*, 5051-5066.
- (21) Würthner, F.; Ahmed, S.; Thalacker, C.; Debaerdemaeker, T. *Chem. Eur. J.* **2002**, *8*, 4742-4750.
- (22) Thalacker, C.; Miura, A.; De Feyter, S.; De Schryver, F. C.; Würthner, F. *Org. Biomol. Chem.* **2005**, *3*, 414-422.
- (23) Thalacker, C.; Röger, C.; Würthner, F. *J. Org. Chem.* **2006**, *71*, 8098-8105.
- (24) Emerson, R.; Arnold, W. *Gen. Physiol.* **1932**, *16*, 191-205.
- (25) *Photosynthese*; Häder, D.-P., Ed., Georg Thieme Verlag: Stuttgart, 1999.
- (26) Grosmann, A. R. *Photosynth. Res.* **2003**, *76*, 207-215.
- (27) Scheer, H. In *Chlorophylls*; Scheer, H., Ed.; CRC Press: Boca Raton, US, 1991; pp 3-30.
- (28) Dorough, G. D.; Miller, J. R.; Huennekens, F. M. *J. Am. Chem. Soc.* **1951**, *73*, 4315-4320.
- (29) Dorough, G. D.; Huennekens, F. M. *J. Am. Chem. Soc.* **1952**, *74*, 3974-3976.
- (30) Gouterman, M.; Wagnière, G. H.; Snyder, L. C. *J. Mol. Spectrosc.* **1963**, *11*, 108-127.
- (31) Simpson, W. T. *J. Chem. Phys.* **1949**, *17*, 1218-1221.
- (32) Longuet-Higgins, H. C.; Rector, C. W.; Platt, J. R. *J. Chem. Phys.* **1950**, *18*, 1174-1181.
- (33) Gouterman, M. *J. Chem. Phys.* **1959**, *30*, 1139-1161.
- (34) Gouterman, M. *J. Mol. Spectrosc.* **1961**, *6*, 138-163.
- (35) Hoff, A. J.; Amesz, J. In *Chlorophylls*; Scheer, H., Ed.; CRC Press: Boca Raton, US, 1991; pp 723-738.
- (36) Bogorad, L. *Ann. Rev. Plant Physiol.* **1975**, *26*, 369-401.
- (37) Brown, S. B.; Houghton, J. D.; Vernon, D. I. *J. Photochem. Photobiol. B* **1990**, *5*, 3-23.
- (38) Glazer, A. N. *J. Appl. Phycol.* **1994**, *6*, 105-112.
- (39) Cole, W. J.; Chapman, D. J.; Siegelman, H. W. *J. Am. Chem. Soc.* **1967**, *89*, 3643-3645.
- (40) Cole, W. J.; Chapman, D. J.; Siegelman, H. W. *J. Am. Chem. Soc.* **1967**, *89*, 5976-5977.
- (41) Meyer, K. *Chem. unserer Zeit* **2002**, *36*, 178-192.
- (42) Frank, H. A.; Chynwat, V.; Desamero, R. Z. B.; Farhoosh, R.; Erickson, J.; Bautista, J. *Pure Appl. Chem.* **1997**, *69*, 2117-2124.

-
- (43) Fraser, N. J.; Hashimoto, H.; Cogdell, R. J. *Photosynth. Res.* **2001**, *70*, 249-256.
- (44) Polívka, T.; Sundström, V. *Chem. Rev.* **2004**, *104*, 2021-2071.
- (45) Vaswani, H. M.; Holt, N. E.; Fleming, G. R. *Pure Appl. Chem.* **2005**, *77*, 925-945.
- (46) Griffiths, M.; Sistrom, W. R.; Cohenbazire, G.; Stanier, R. Y. *Nature* **1995**, *176*, 1211-1214.
- (47) Edge, R.; Truscott, T. G. In *Photochemistry of Carotenoids*; Frank, H. A., Young, A. J., Britton, G., Cogdell, R. J., Eds.; Kluwer Academic Publishers: Dordrecht, The Netherlands, 1999.
- (48) Horton, P.; Ruban, A. V.; Walters, R. G. *Annu. Rev. Plant Physiol. Plant Mol. Biol.* **1996**, *47*, 655-684.
- (49) Holt, N. E.; Fleming, G. R.; Niyogi, K. K. *Biochemistry* **2004**, *43*, 8281-8289.
- (50) Holt, N. E.; Zigmantas, D.; Valkunas, L.; Li, X.-P.; Niyogi, K. K.; Fleming, G. R. *Science* **2005**, *307*, 433-436.
- (51) Berera, R.; Herrero, C.; van Stokkum, I. H. M.; Vengris, M.; Kodis, G.; Palacios, R. E.; van Amerongen, H.; van Grondelle, R.; Gust, D.; Moore, T. A.; Moore, A. L.; Kennis, J. T. M. *Proc. Natl. Acad. Sci. USA* **2006**, *103*, 5343-5348.
- (52) Lang, H. P.; Hunter, C. N. *Biochem. J.* **1994**, *298*, 197-205.
- (53) Frank, H. A.; Josue, J. S.; Bautista, J. A.; van der Hoef, I.; Jansen, F. J.; Lugtenburg, J.; Wiederrecht, G.; Christensen, R. L. *J. Phys. Chem. B* **2002**, *106*, 2083-2092.
- (54) Ricci, M.; Bradforth, S. E.; Jimenez, R.; Fleming, G. R. *Chem. Phys. Lett.* **1996**, *259*, 381-390.
- (55) Bensasson, R. V.; Land, E. J.; Moore, A. L.; Crouch, R. L.; Dirks, G.; Moore, T. A.; Gust, D. *Nature* **1981**, *290*, 329-332.
- (56) Wasielewski, M. R.; Lidell, P. A.; Barrett, D.; Moore, T. A.; Gust, D. *Nature* **1986**, *322*, 570-572.
- (57) Osuka, A.; Yamada, H.; Maruyama, K.; Mataga, N.; Asahi, T.; Ohkouchi, M.; Okada, T.; Yamazaki, I.; Nishimura, Y. *J. Am. Chem. Soc.* **1993**, *115*, 9439-9452.
- (58) Debreczeny, M. P.; Wasielewski, M. R.; Shinoda, S.; Osuka, A. *J. Am. Chem. Soc.* **1997**, *119*, 6407-6414.

-
- (59) The graphic has been modified from Campbell, N. A. In *Biologie*; Markl, J., Ed.; Spektrum Akademischer Verlag: Heidelberg, Berlin, Oxford, 1997, p. 209.
- (60) Kasha, M. *Rad. Res.* **1963**, *20*, 55-71.
- (61) Kasha, M.; Rawls, H. R.; Ashraf El-Bayoumi, M. *Pure Appl. Chem.* **1965**, *11*, 371-392.
- (62) *Molekülphysik und Quantenchemie*; Haken, H., Wolf, H.-C. Eds.; 3rd ed., Springer-Verlag: Berlin, Heidelberg, New York, 1998, pp. 297-299.
- (63) *Theory of Molecular Excitons*; Davydov, A. S., Ed., Plenum Press: New York, 1971.
- (64) Fidler, H.; Knoester, J.; Wiersma, D. A. *J. Chem. Phys.* **1991**, *95*, 7880-7890.
- (65) *Modern Molecular Photochemistry*; Turro, N. J., Ed., University Science Books: Sausalito, California, 1991, pp. 296-361.
- (66) *Molecular Fluorescence Principles and Application*; Valeur, B., Ed., Wiley-VCH: Weinheim, 2002, p. 120.
- (67) Beatty, J. T.; Overmann, J.; Lince, M. T.; Manske, A. K.; Lang, A. S.; Blankenship; R. E.; Van Dover, C. L.; Martinson, T. A.; Plumley, F. G. *Proc. Natl. Acad. Sci. USA* **2005**, *102*, 9306-9310.
- (68) McDermott, G.; Prince, S. M.; Freer, A. A.; Hawthornthwaite-Lawless, A. M.; Papiz, M. Z.; Cogdell, R. J.; Isaacs, N. W. *Nature (London)* **1995**, *374*, 517-521.
- (69) Koepke, J.; Hu, X.; Muenke, C.; Schulten, K.; Michel, H. *Structure (London)* **1996**, *4*, 581-597.
- (70) <http://www.gla.ac.uk/ibls/BMB/rjc/index.html>
- (71) Freer, A.; Prince, S.; Sauer, K.; Papiz, M.; Hawthornthwaite-Lawless, A.; McDermott, G.; Cogdell, R. J.; Isaacs, N. W. *Structure (London)* **1996**, *4*, 449-462.
- (72) Hu, X.; Damjanović, A.; Ritz, T.; Schulten, K. *Proc. Natl. Acad. Sci. USA* **1998**, *95*, 5935-5941.
- (73) Damjanović, A.; Kosztin, I.; Kleinekathöfer, U.; Schulten, K. *Phys. Rev. E* **2002**, *65*, 031919.
- (74) Gall, A.; Fowler, G. J. S.; Hunter, C. N.; Robert, B. *Biochemistry* **1997**, *36*, 16282-16287.
- (75) Sturgis, J. N.; Robert, B. *Photosynth. Res.* **1996**, *50*, 5-10.

-
- (76) Staehelin, L. A.; Golecki, J. R.; Fuller, R. C.; Drews, G. *Arch. Microbiol.* **1978**, *119*, 269-277.
- (77) Zhu, Y.; Ramakrishna, B. L.; van Noort, P. I.; Blankenship, R. E. *Biochim. Biophys. Acta* **1995**, *1232*, 197-207.
- (78) Oelze, J.; Golecki, J. R. In *Anoxygenic Photosynthetic Bacteria*; Blankenship, R. E., Madigan, M. T., Bauer, C. E., Eds.; Kluwer: Dordrecht, 1995, pp. 259-278.
- (79) Staehelin, L. A.; Golecki, J. R.; Drews, G. *Biochim. Biophys. Acta* **1980**, *589*, 30-45.
- (80) Frigaard, N.-U., Chew, A. G. M.; Li, H.; Maresca, J. A.; Bryant, D. A. *Photosynth. Res.* **2003**, *78*, 93-117.
- (81) Bystrova, M. I.; Mal'gosheva, I. N.; Krasnovskii, A. A. *Mol. Biol.* **1979**, *13*, 440-451.
- (82) Smith, K. M.; Kehres, L. A., Fajer, J. *J. Am. Chem. Soc.* **1983**, *105*, 1387-1389.
- (83) Griebenow, K.; Holzwarth, A. R. *Biochim. Biophys. Acta* **1989**, *973*, 235-240.
- (84) Golecki, J. R.; Oelze, J. *Arch. Microbiol.* **1987**, *148*, 236-241.
- (85) Sprague, S. G.; Staehelin, L. A.; DiBartolomeis, M. J.; Fuller, R. C. *J. Bacteriol.* **1981**, *147*, 1021-1031.
- (86) Huber, V.; *Dissertation*; Universität Würzburg, 2007.
- (87) Holzwarth, A. R.; Griebenow, K.; Schaffner, K. *J. Photochem. Photobiol. A* **1992**, *65*, 61-71.
- (88) Balaban, T. S.; Holzwarth, A. R.; Schaffner, K.; Boender, G.-J., de Groot, H. J. M. *Biochemistry* **1995**, *34*, 15259-15266.
- (89) Hildebrandt, P.; Griebenow, K.; Holzwarth, A. R.; Schaffner, K. *Z. Naturforsch.* **1991**, *46c*, 228-232.
- (90) Hildebrandt, P.; Tamiaki, H.; Holzwarth, A. R.; Schaffner, K. *J. Phys. Chem.* **1994**, *98*, 2192-2197.
- (91) Lutz, M.; van Brakel, G. In *Green Photosynthetic Bacteria*; Olson, J. M., Ormerod, J. G., Amesz, J., Stackebrandt, E., Trüper, H. G., Eds.; Plenum Press: New York, 1988, p. 23.
- (92) Worcester, D. L.; Michalski, T. J.; Katz, J. J. *Proc. Natl. Acad. Sci. USA* **1986**, *83*, 3791-3795.
- (93) Holzwarth, A. R.; Schaffner, K. *Photosynth. Res.* **1994**, *41*, 225-233.

-
- (94) Prokhorenko, V. I.; Steensgaard, D. B.; Holzwarth, A. R. *Biophys. J.* **2000**, *79*, 2105-2120.
- (95) Griebenow, K.; Holzwarth, A. R.; Van Mourik, F.; Van Grondelle, R. *Biochim. Biophys. Acta* **1991**, *1058*, 194-202.
- (96) Van Dorssen, R. J.; Vasmel, H.; Amesz, J. *Photosynth. Res.* **1986**, *9*, 33-45.
- (97) Van Amerongen, H.; van Haeringen, B.; van Gorp, M.; van Grondelle, R. *Biophys. J.* **1991**, *59*, 992-1001.
- (98) Prokhorenko, V. I.; Steensgaard, D. B.; Holzwarth, A. R. *Biophys. J.* **2001**, *85*, 3173-3186.
- (99) Steensgaard, D. B.; Wackerbarth, H.; Hildebrandt, P.; Holzwarth, A. R. *J. Phys. Chem. B* **2000**, *104*, 10379-10386.
- (100) Van Rossum, B.-J.; Steensgaard, D. B.; Mulder, F. M.; Boender, G. J.; Schaffner, K.; Holzwarth, de Groot, H. J. M. *Biochemistry* **2001**, *40*, 1587-1595.
- (101) Hirota, M.; Moriyama, T.; Shimada, K.; Miller, M.; Olson, J. M.; Matsuura, K. *Biochim. Biophys. Acta* **1992**, *1099*, 271-274.
- (102) Brune, D. C.; Nozawa, T.; Blankenship, R. E. *Biochemistry* **1987**, *26*, 8644-8652.
- (103) Miller, M.; Gillbro, T.; Olson, J. M. *Photochem. Photobiol.* **1993**, *57*, 98-102.
- (104) Brune, D. C.; Gerola, P. D.; Olson, J. M. *Photosynth. Res.* **1990**, *24*, 253-263.
- (105) Tamiaki, H. *Coord. Chem. Rev.* **1996**, *148*, 183-197.
- (106) Brune, D. C.; King, G. H.; Infosino, A.; Steiner, T.; Thewalt, M. L. W.; Blankenship, R. E. *Biochemistry* **1987**, *26*, 8652-8658.
- (107) Müller, M. G.; Griebenow, K.; Holzwarth, A. R. In *Current Research in Photosynthesis*; Baltscheffsky, M., Ed.; Kluwer: Dordrecht, 1990; Vol. II, pp. 177-180.
- (108) Causgrove, T. P.; Brune, D. C.; Wang, J.; Wittmershaus, B. P.; Blankenship, R. E. *Photosynth. Res.* **1990**, *26*, 39-48.
- (109) Miller, M.; Cox, R. P.; Gillbro, T. *Biochim. Biophys. Acta* **1991**, *1057*, 187-194.
- (110) Müller, M. G.; Griebenow, K.; Holzwarth, A. R. *Biochim. Biophys. Acta* **1993**, *1144*, 161-169.
- (111) Holzwarth, A. R.; Müller, M. G.; Griebenow, K. *J. Photochem. Photobiol. B* **1990**, *5*, 457-465.

-
- (112) Savikhin, S.; Zhu, Y.; Blankenship, R. E.; Struve, W. S. *J. Phys. Chem.* **1994**, *98*, 10322-10334.
- (113) Savikhin, S.; Zhu, Y.; Blankenship, R. E.; Struve, W. S. *J. Phys. Chem.* **1996**, *100*, 3320-3322.
- (114) Savikhin, S.; Zhu, Y.; Blankenship, R. E.; Struve, W. S. *J. Phys. Chem.* **1996**, *100*, 17978-17980.
- (115) Saga, Y.; Tamiaki, H.; Shibata, Y.; Itoh, S. *Chem. Phys. Lett.* **2005**, *409*, 34-37.
- (116) Montaña, G. A.; Wu, H.-M.; Lin, S.; Brune, D. C.; Blankenship, R. E. *Biochemistry* **2003**, *42*, 10246-10251.
- (117) Montaña, G. A.; Xin, Y.; Lin, S.; Blankenship, R. E. *J. Phys. Chem. B* **2004**, *108*, 10607-10611.
- (118) Griebenow, K.; Müller, M. G.; Holzwarth, A. R. *Biochim. Biophys. Acta* **1991**, *1059*, 226-232.
- (119) Tamiaki, H.; Holzwarth, A. R.; Schaffner, K. *J. Photochem. Photobiol. B* **1992**, *15*, 355-360.
- (120) Cheng, P.; Lidell, P. A.; Ma, S. X. C.; Blankenship, R. E. *Photochem. Photobiol.* **1993**, *58*, 290-295.
- (121) Tamiaki, H.; Amakawa, M.; Shimono, Y.; Tanikaga, R.; Holzwarth, A. R.; Schaffner, K. *Photochem. Photobiol.* **1996**, *63*, 92-99.
- (122) Miyatake, T.; Tamiaki, H.; Holzwarth, A. R.; Schaffner, K. *Photochem. Photobiol.* **1999**, *69*, 448-456.
- (123) Tamiaki, H.; Miyatake, T.; Tanikaga, R.; Holzwarth, A. R.; Schaffner, K. *Angew. Chem.* **1996**, *108*, 810-812; *Angew. Chem., Int. Ed.* **1996**, *35*, 772-774.
- (124) Miyatake, T.; Tamiaki, H.; Holzwarth, A. R.; Schaffner, K. *Helv. Chim. Acta* **1999**, *82*, 797-810.
- (125) Prokhorenko, V. I.; Holzwarth, A. R.; Müller, M. G.; Schaffner, K.; Miyatake, T.; Tamiaki, H. *J. Phys. Chem. B* **2002**, *106*, 5761-5768.
- (126) Prokhorenko, V. I.; Katterle, M.; Holzwarth, A. R.; Schaffner, K.; Miyatake, T.; Tamiaki, H. In *Femtochemistry and Femtobiology – Ultrafast Dynamics in Molecular Science*; Douhal, A., Santamaria, J., Eds.; World Scientific: New Jersey, London, Singapore, Hong Kong, 2001, pp. 782-788.

- (127) Frigaard, N.-U.; Tokita, S.; Matsuura, K. *Biochim. Biophys. Acta* **1999**, *1413*, 108-116.
- (128) Van Patten, P. G.; Shreve, A. P.; Lindsey, J. S.; Donohoe, R. J. *J. Phys. Chem B* **1998**, *102*, 4209-4216.
- (129) Choi, M.-S.; Yamazaki, T.; Yamazaki, I.; Aida, T. *Angew. Chem.* **2004**, *116*, 152-160; *Angew. Chem., Int. Ed.* **2004**, *43*, 150-158.
- (130) Kobuke, Y. *Eur. J. Inorg. Chem.* **2006**, 2333-2351.
- (131) Nakamura, Y.; Aratani, N.; Osuka, A. *Chem. Soc. Rev.* **2007**, *36*, 831-845.
- (132) Anderson, S.; Anderson, H. L.; Bashall, A.; McPartlin, M.; Sanders, J. K. M. *Angew. Chem.* **1995**, *107*, 1196-1200; *Angew. Chem., Int. Ed.* **1995**, *34*, 1096-1099.
- (133) Li, J.; Ambroise, A.; Yang, S. I.; Diers, J. R.; Seth, J.; Wack, C. R.; Bocian, D. F.; Holten, D.; Lindsey, J. S. *J. Am. Chem. Soc.* **1999**, *121*, 8927-8940.
- (134) Ambroise, A.; Li, J.; Yu, L.; Lindsey, J. S. *Org. Lett.* **2000**, *17*, 2563-2566.
- (135) Yu, L.; Lindsey, J. S. *J. Org. Chem.* **2001**, *66*, 7402-7419.
- (136) Tomizaki, K.-y.; Yu, L.; Wei, L.; Bocian, D. F.; Lindsey, J. S. *J. Org. Chem.* **2003**, *68*, 8199-8207.
- (137) Song, H.-e.; Kirmaier, C.; Schwartz, J. K.; Hindin, E.; Yu, L.; Bocian, D. F.; Lindsey, J. S.; Holten, D. *J. Phys. Chem. B* **2006**, *110*, 19131-19139.
- (138) Kim, D.; Osuka, A. *Acc. Chem. Res.* **2004**, *37*, 735-745.
- (139) Hori, T.; Aratani, N.; Takagi, A.; Matsumoto, T.; Kawai, T.; Yoon, M.-C.; Yoon, Z. S.; Cho, S.; Kim, D.; Osuka, A. *Chem. Eur. J.* **2006**, *12*, 1319-1327.
- (140) Park, M.; Yoon, M.-C.; Yoon, Z. S.; Hori, T.; Peng, X.; Aratani, N.; Hotta, J.-i.; Uji-i, H.; Sliwa, M.; Hofkens, J.; Osuka, A.; Kim, D. *J. Am. Chem. Soc.* **2007**, *129*, 3539-3544.
- (141) Hori, T.; Nakamura, Y.; Aratani, N.; Osuka, A. *J. Organomet. Chem.* **2007**, *692*, 148-155.
- (142) Lee, S. J.; Hupp, J. T. *Coord. Chem. Rev.* **2006**, *250*, 1710-1723.
- (143) Slone, R. V.; Hupp, J. T. *Inorg. Chem.* **1997**, *36*, 5422-5423.
- (144) Haycock, R. A.; Hunter, C. A.; James, D. A.; Michelsen, U.; Sutton, L. R. *Org. Lett.* **2000**, *2*, 2435-2438.
- (145) Takahashi, R.; Kobuke, Y. *J. Am. Chem. Soc.* **2003**, *125*, 2372-2373.

-
- (146) Hwang, I.-W.; Park, M.; Ahn, T. K.; Yoon, Z. S.; Ko, D. M.; Kim, D.; Ito, F.; Ishibashi, Y.; Khan, S. R.; Nagasawa, Y.; Miyasaka, H.; Ikeda, C.; Takahashi, R.; Ogawa, K.; Satake, A.; Kobuke, Y. *Chem. Eur. J.* **2005**, *11*, 3753-3761.
- (147) Hajjaj, F.; Yoon, Z. S.; Yoon, M.-C.; Park, J.; Satake, A.; Kim, D.; Kobuke, Y. *J. Am. Chem. Soc.* **2006**, *128*, 4612-4623.
- (148) Kuramochi, Y.; Satake, A.; Kobuke, Y. *J. Am. Chem. Soc.* **2004**, *126*, 8668-8669.
- (149) Kobuke, Y., personal information.
- (150) Wang, Z.; Medforth, C. J.; Shelnut, J. A. *J. Am. Chem. Soc.* **2004**, *126*, 15954-15955.
- (151) Dähne, S. *Bunsen-Magazin* **2002**, *4*, 81-92.
- (152) Spitz, C.; Knoester, J.; Quart, A.; Daehne, S. *Chem. Phys.* **2002**, *275*, 271-284.
- (153) Kirstein, S.; von Berlepsch, H.; Boettcher, C.; Burger, C.; Quart, A.; Reck, G.; Daehne, S. *ChemPhysChem* **2000**, *1*, 146-150.
- (154) Bendarz, M.; Knoester, J. *J. Phys. Chem. B* **2001**, *105*, 12913-12923.
- (155) Lampoura, S. S.; Spitz, C.; Dähne, S.; Knoester, J.; Duppen, K. *J. Phys. Chem. B* **2002**, *106*, 3103-3111.
- (156) Smith, K. M.; Goff, D. A.; Simpson, D. J. *J. Am. Chem. Soc.* **1985**, *107*, 4946-4954.
- (157) Johnson, D. G.; Svec, W. A.; Wasielewski, M. R. *Isr. J. Chem.* **1988**, *28*, 193-203.
- (158) Vollmann, H.; Becker, H.; Corell, M.; Streeck, H. *Justus Liebigs Ann.* **1937**, *531*, 1-159.
- (159) Apperloo, J. J.; Janssen, R. A. J.; Malenfant, P. R. L.; Fréchet, J. M. J. *Macromolecules* **2000**, *33*, 7038-7043.
- (160) Berova, N.; Nakanishi, K. In *Circular Dichroism: Principles and Applications*, Berova, N.; Nakanishi, K.; Woody, R., Eds.; VCH: New York, US, 2000; pp. 337-368.
- (161) Prokhorenko, V. I.; Steensgaard, D. B.; Holzwarth, A. R. *Biophys. J.* **2003**, *85*, 3173-3186.
- (162) Bustamante, C.; Keller, D.; Yang, G. *Curr. Opin. Struct. Biol.* **1993**, *3*, 363-372.
- (163) Rivetti, C.; Guthold, M.; Bustamante, C. *J. Mol. Biol.* **1996**, *264*, 919-932.

-
- (164) Lysetska, M.; Knoll, A.; Boehringer, D.; Hey, T.; Krauss, G.; Krausch, G. *Nucl. Acids Res.* **2002**, *30*, 2686-2691.
- (165) O'Connor, D. V.; Phillips, D. *Time-correlated single photon counting*; Academic Press: London, 1988.
- (166) Müller, M. G.; *Dissertation*; Universität Düsseldorf, 1991.
- (167) Müller, M. G.; Griebenow, K.; Holzwarth, A. R. *Biochim. Biophys. Acta* **1991**, *1098*, 1-12.
- (168) Knutson, J. R.; Beechem, J. M.; Brand, L. *Chem. Phys. Lett.* **1983**, *102*, 501-507.
- (169) Schenning, A. P. H. J.; Meijer, E. W. *Chem. Commun.* **2005**, 3245-3258.
- (170) Gregg, B. A. *J. Phys. Chem. B.* **2003**, *107*, 4688-4698.
- (171) Cheng, P.; Liddell, P. A.; Ma, S. X. C.; Blankenship, R. E. *Photochem. Photobiol.* **1993**, *58*, 290-295.
- (172) Gvishi, R.; Reisfeld, R.; Burshtein, Z. *Chem. Phys. Lett.* **1993**, *213*, 338-344.
- (173) Seybold, G.; Wagenblast, G. *Dyes Pigm.* **1989**, *11*, 303-317.
- (174) Sens, R.; Drexhage, K. H. *J. Luminesc.* **1981**, *24*, 709-712.
- (175) Perrin, D. D.; Amarego, W. L.; Perrin, D. R. *Purification of Laboratory Chemicals*; Pergamon Press Ltd.: Oxford, 1980.
- (176) Messmore, B. W.; Hulvat, J. F.; Sone, E. D.; Stupp, S. I. *J. Am. Chem. Soc.* **2004**, *126*, 14452-14458.
- (177) Metzger, R. M.; Wisner, D. C.; Laidlaw, R. K.; Takassi, M. A.; Mattern, D. L.; Panetta, C. A. *Langmuir* **1990**, *6*, 350-357.

Curriculum Vitae

Cornelia Röger

Date of birth: June 23rd 1979

Nationality: German

Education

- Since 11/2003 PhD thesis at the University of Würzburg, Institute of Organic Chemistry, under the supervision of Prof. Dr. F. Würthner
- 11/1998-09/2003 Studies of Chemistry, University of Würzburg
- 09/2003 Diploma in Chemistry
- 02/2003-09/2003 Diploma thesis under the supervision Prof. Dr. F. Würthner
Title: *“Synthese eines Carotinoid-funktionalisierten, selbstorganisationsfähigen Chlorophylls“*
- 03-07/2002 Organic-chemical research practical at the Heriot-Watt-University in Edinburgh as a Sokrates exchange student
- 1998 Abitur, Gymnasium bei St. Michael, Schwäbisch Hall

Awards

- 07/2004-06/2006 Dissertation scholarship, “Degussa Stiftung”
- 15/05/2004 “Matthias-Manger-Preis” of the University of Würzburg for the diploma examination

List of Publications

“Core-Tetrasubstituted Naphthalene Diimides: Synthesis, Optical Properties, and Redox Characteristics.”

Röger, C.; Würthner, F. *J. Org. Chem.* **2007**, *72*, 8070-8075.

“Synthesis and Optical Properties of Fluorescent Naphthalene Diimide Dyes Bearing Three Core Substituents.”

Röger, C.; Ahmed, S.; Würthner, F. *Synthesis* **2007**, 1872-1876.

“Efficient Energy Transfer from Peripheral Chromophores to the Self-Assembled Zinc Chlorin Rod Antenna: A Bioinspired Light-Harvesting System to Bridge the ‘Green Gap’.”

Röger, C.; Müller, M. G.; Lysetska, M.; Miloslavina, Y.; Holzwarth, A. R.; Würthner, F. *J. Am. Chem. Soc.* **2006**, *128*, 6542-6543.

“Synthesis and Optical and Redox Properties of Core-Substituted Naphthalene Diimide Dyes.”

Thalacker, C.; Röger, C.; Würthner, F. *J. Org. Chem.* **2006**, *71*, 8098-8105.

“Photoproduction of Proton Gradients with π -Stacked Fluorophore Scaffolds in Lipid Bilayers.”

Bhosale, S.; Sisson, A. L.; Talukdar, P.; Fürstenberg, A.; Banerji, N.; Vauthey, E.; Bollot, G.; Mareda, J.; Röger, C.; Würthner, F.; Sakai, N.; Matile, S. *Science* **2006**, *313*, 84-86.

“A New Type of Chainlike Tetranuclear Rhodium Complexes with PR_3 and $AsMe_3$ as Bridging Ligands.”

Pechmann, T.; Brandt, C. D.; Röger, C.; Werner, H. *Angew. Chem.* **2002**, *114*, 2398-2401; *Angew. Chem., Int. Ed.* **2002**, *41*, 2301-2303.